Universität Potsdam

Institut für Biochemie und Biologie
Institut für Physik und Astronomie
Biologische Physik & Pflanzenphysiologie

Dissertation zur Erlangung des akademischen Grades
doctor rerum naturalium (Dr. rer. nat.)

A study on Coronin-A and Aip1 function in motility of *Dictyostelium discoideum* and on Aip1 interchangeability between *Dictyostelium discoideum* and *Arabidopsis thaliana*

Maike Stange

1. Reviewer Prof. Dr. Carsten Beta
Institut für Physik und Astronomie
Universität Potsdam

2. Reviewer Prof. Dr. Markus Grebe
Institut für Biochemie und Biologie
Universität Potsdam

3. Reviewer Prof. Dr. Martin Hülskamp
Institut für Pflanzenwissenschaften
Universität zu Köln

February 26, 2024

Maike Stange
A study on Coronin-A and Aip1 function in motility of Dictyostelium discoideum and on Aip1 interchangeability between Dictyostelium discoideum and Arabidopsis thaliana
Dissertation zur Erlangung des akademischen Grades *doctor rerum naturalium* (Dr. rer. nat.)
February 26, 2024
Reviewers: Prof. Dr. Carsten Beta, Prof. Dr. Markus Grebe and Prof. Dr. Martin Hülskamp
Supervisors: Prof. Dr. Carsten Beta and Prof. Dr. Markus Grebe

Universität Potsdam
Biologische Physik & Pflanzenphysiologie
Institut für Physik und Astronomie
Institut für Biochemie und Biologie
Karl-Liebknecht-Straße 24/25
14469 Potsdam

Published online on the
Publication Server of the University of Potsdam:
https://doi.org/10.25932/publishup-62856
https://nbn-resolving.org/urn:nbn:de:kobv:517-opus4-628569

Abstract

Actin is one of the most highly conserved proteins in eukaryotes and distinct actin-related proteins with filament-forming properties are even found in prokaryotes. Due to these commonalities, actin-modulating proteins of many species share similar structural properties and proposed functions. The polymerization and depolymerization of actin are critical processes for a cell as they can contribute to shape changes to adapt to its environment and to move and distribute nutrients and cellular components within the cell. However, to what extent functions of actin-binding proteins are conserved between distantly related species, has only been addressed in a few cases. In this work, functions of Coronin-A (CorA) and Actin-interacting protein 1 (Aip1), two proteins involved in actin dynamics, were characterized. In addition, the interchangeability and function of Aip1 were investigated in two phylogenetically distant model organisms. The flowering plant *Arabidopsis thaliana* (encoding two homologs, AIP1-1 and AIP1-2) and in the amoeba *Dictyostelium discoideum* (encoding one homolog, DdAip1) were chosen because the functions of their actin cytoskeletons may differ in many aspects. Functional analyses between species were conducted for AIP1 homologs as flowering plants do not harbor a CorA gene.

In the first part of the study, the effect of four different mutation methods on the function of Coronin-A protein and the resulting phenotype in *D. discoideum* was revealed in two genetic knockouts, one RNAi knockdown and a sudden loss-of-function mutant created by chemical-induced dislocation (CID). The advantages and disadvantages of the different mutation methods on the motility, appearance and development of the amoebae were investigated, and the results showed that not all observed properties were affected with the same intensity. Remarkably, a new combination of Selection-Linked Integration and CID could be established.

In the second and third parts of the thesis, the exchange of Aip1 between plant and amoeba was carried out. For *A. thaliana*, the two homologs (*AIP1-1* and *AIP1-2*) were analyzed for functionality as well as in *D. discoideum*. In the Aip1-deficient amoeba, rescue with AIP1-1 was more effective than with AIP1-2. The main results in the plant showed that in the *aip1-2* mutant background, reintroduced AIP1-2 displayed the most efficient rescue and *A. thaliana AIP1-1* rescued better than DdAip1. The choice of the tagging site was important for the function of Aip1 as steric hindrance is a problem. The DdAip1 was less effective when tagged at the C-terminus, while the plant AIP1s showed mixed results depending on the tag position. In conclusion, the foreign proteins partially rescued phenotypes of mutant plants and mutant amoebae, despite the organisms only being very distantly related in evolutionary terms.

Zusammenfassung

Actin ist eines der am stärksten konservierten Proteine in Eukaryoten und sogar Prokaryoten weisen Aktin-ähnliche Proteine mit filamentbildenden Eigenschaften auf. Aufgrund dieser Gemeinsamkeiten teilen Aktin-modulierte Proteine vieler Arten ähnliche strukturelle Eigenschaften und vermutlich auch Funktionen. Die Polymerisierung und Depolymerisation von Aktin sind kritische Prozesse für eine Zelle, da sie zu Zellformänderungen beitragen können, um sich an die Umgebung anzupassen und Nährstoffe sowie zelluläre Komponenten innerhalb der Zelle zu bewegen und zu verteilen. Inwieweit die Funktionen von Aktin-bindenden Proteinen zwischen entfernt verwandten Arten funktionell konserviert sind, wurde jedoch nur in wenigen Fällen untersucht. In dieser Arbeit wurden Funktionen von Coronin-A (CorA) und Actin-interagierendem Protein 1 (AIP1), zweier an der Aktindynamik beteiligter Proteine, charakterisiert. Darüber hinaus wurde die Austauschbarkeit und Funktion von AIP1 in zwei phylogenetisch entfernten Modellorganismen untersucht. Die Blütenpflanze *Arabidopsis thaliana* (kodiert für zwei Homologe: AIP1-1 und AIP1-2) und die Amöbe *Dictyostelium discoideum* (kodiert für ein Homolog: DdAip1) wurden ausgewählt, weil die Funktionen ihrer Aktin-Zytoskelette in mehreren Aspekten verschieden sein könnten. Funktionelle Analysen zwischen Arten wurden für *AIP1*-Homologe durchgeführt, da Blütenpflanzen kein *CorA* Gen tragen.

Im ersten Teil der Arbeit wurde die Wirkung von vier verschiedenen Mutationsmethoden auf die Funktion des CorA-Proteins und des resultierenden Phänotyps in *D. discoideum* in zwei genetischen Knockouts, einem RNAi Knockdown und einem durch chemisch induzierte Delokalisierung (CID) erzeugten Mutanten geprüft. Die Vor- und Nachteile der Methoden zur Motilität, des Aussehens und der Entwicklung der Amöben wurden untersucht. Die Ergebnisse zeigten, dass nicht alle beobachteten Eigenschaften mit der gleichen Intensität beeinflusst wurden. Hierbei wurde eine neue Methodenkombination aus selektionsgebundener Integration und CID etabliert.

Im zweiten und im dritten Teil der Arbeit wurde der Austausch von *AIP1* zwischen Pflanze und Amöben durchgeführt. Die zwei *A. thaliana*-Homologe *AIP1-1* und *AIP1-2* wurden auf Funktionalität in *D. discoideum* geprüft. In Aip1-defizienten Amöben war die Rettung mit AIP1-1 effektiver als bei AIP1-2. Die Hauptergebnisse der Arbeit wiesen darauf hin, dass AIP1-2 im *aip1.2-1 act7* Mutantenhintergrund die effizienteste Rettung zeigte, während *A. thaliana AIP1-1* effizienter rettete als DdAip1. Die Auswahl der Tagging-Site war für die AIP1-Funktion bedeutend, da sterische Hinderung eine Rolle spielen könnte. DdAip1 war weniger effektiv, wenn es am C-Terminus fusioniert war, während die Proteinfusionen der *A. thaliana* AIP1s je nach Position der „tags“ unterschiedliche Ergebnisse zeigten. Zusammenfassend retteten die fremden Proteine teilweise Phänotypen von mutierten Pflanzen und mutierten Amöben, obwohl die Organismen evolutionär weit entfernt verwandt sind.

Acknowledgement

This work is dedicated to my father, who passed away during the time of my Ph.D., but ever supported my work and way of life.

First and foremost I want to thank my first supervisor Carsten Beta and my second supervisor Markus Grebe for the fantastic opportunity to work in their labs and supervise my experimental and written work. Both of you supported my work a lot even when times got rough. Thank you again for always being willing to fund my work much longer than expected.

I also want to thank Ralph Gräf, Marianne Grafe, and Irene Meyer for support in experimental design and setup and for very beneficial discussions on *Dictyostelium discoideum* and RNAi. The RNAi plasmid was kindly provided by Irene Meyer.

Especially, I want to thank Günther Gerisch and Maria Ecke for providing the aip1-null#9.1 mutant and the corA-null HG1556 mutant as well as the combined double mutant.

In particular, I want to thank Sven Flemming for kindly introducing me to the SLI technique and for the brilliant discussions and help on the project. Likewise, I thank Robert Großmann, who did all the marvelous programming of the analysis tools in MATLAB, in which I would have been lost. In addition, I want to thank Andrés Eduardo Rodriguez Cubillos for his excellent support in plant physiology and Western blotting and Anke Koch, who already retired but was introducing the plant work to me in a great manner and with lots of patience.

Of course I also want to thank Carola Kuhn and Kirsten Sachse for their technical support in the labs and their help in the cultivation of plants or cells and further collection of experimental data.

I want to thank Matija Stanic for being a fantastic colleague and friend to me. With deep gratitude, I want to thank René Schneider, Anja Schleicher (GFZ, Potsdam), and Marta Sośnicka (GFZ, Potsdam) for motivating me to finish this work.

All the members of the Biological Physics department and Plant Physiology department I did not directly address in my acknowledgments, I would also thank you for helping me to make it through this tough time and making the coffee breaks and lunchtimes so enjoyable: I love you all.

Last but not least I want to mention some people who were capitally part of my scientific career: Claudia Fournier (GSI, Darmstadt), Julia Wiedemann (Universitair Medisch Centrum, Groningen) and Robert Niedl (inventicsDx, Berlin). I am glad that all of you made my life so fantastic.

NIV Bible; Ecclesiastes 7:8
The end of a matter is better than its beginning, and patience is better than pride.

Contents

1 Introduction and Theoretical Background

1.1 *Dictyostelium discoideum*

The amoeba *Dictyostelium discoideum* is widely used as a model organism for amoeboid movement as well as to investigate and characterize intracellular processes (Williams, 2010). While higher eukaryotic amoeboid moving cells like neutrophil leucocytes are comparatively difficult to culture in the laboratory, *D. discoideum* is simple to handle and relies on easily implementable living conditions, although still sharing most biochemical and biological processes with diverse eukaryotic cells. It was first isolated from forest soil, where it lives as a single-celled organism and predatory hunts bacteria by engulfing and taking them up by phagocytosis. Usually, it has a haploid genome and it proliferates by mitotic division (Ashworth et al., 1970), but there is also a sexual proliferation cycle known (Kessin et al., 2001). It is about 10 μm in diameter and crawls through the environment using adhesion points, which connect the environment to the cytoskeleton. The cell body is pulled over the substrate by reorganizing the cytoskeleton, which results in intracellular pushing or pulling forces. The earliest isolated *D. discoideum* strains could only be cultured in laboratories on a bacterial layer (Sussman, 1966). In 1967, the first *D. discoideum* cells could be cultured axenically in media and usually were abbreviated as 'AX' (Sussman et al., 1967). Regardless if axenic or not, when nutrients in the environment run low, starving cells start to periodically secrete cyclic adenosine monophosphate (cAMP) into their vicinity (Saran et al., 2002). These pulses of cAMP act as a chemoattractant for other *D. discoideum* cells and finally lead to the differentiation of cells and the formation of aggregates and fruiting bodies, which contain the spores (see Figure 1.1). Like spores of other organisms, *D. discoideum* spores are units of unsexual reproduction. Due to their resistance to environmental stress, they preserve the survival of the amoeba colony for longer times. The full cycle of morphogenesis is reviewed in Chisholm et al., 2004. As only the cells differentiating into spores are part of the next generation, stalk-building cells are altruistically dying for the survival of the colony and that is why it was also called a 'social' amoeba. The multicellular development of *D. discoideum* was first described in 1935 (Raper, 1935) and since then has often been reported and been the subject of many studies (Williams, 2010).

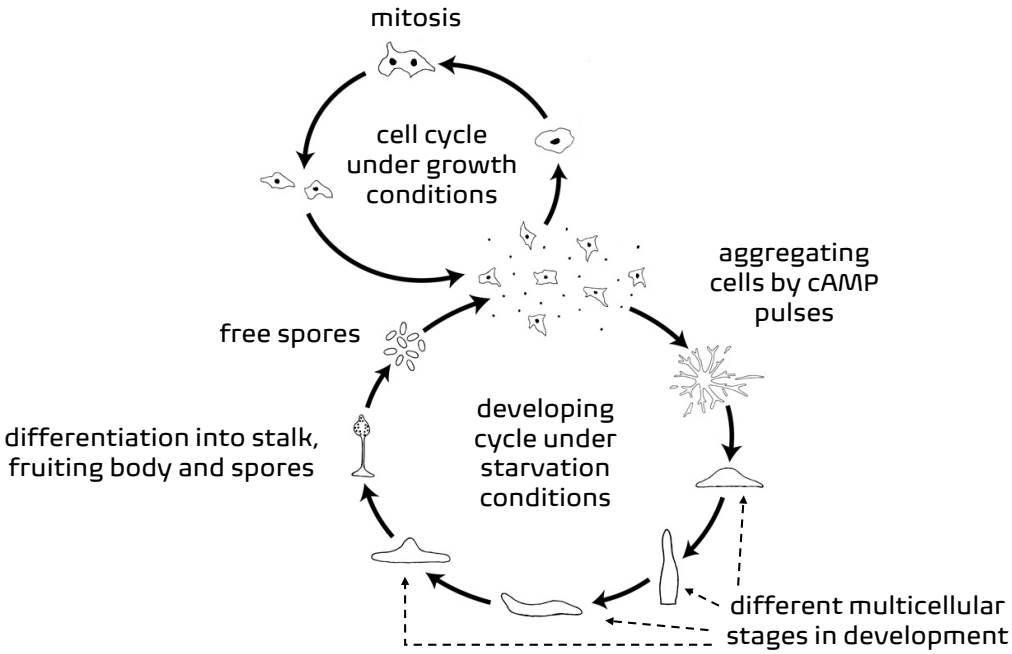

Fig. 1.1: **Unicellular cell cycle and multicellular developmental cycle of *D. discoideum*;** under growth conditions cells undergo a mitotic cell division cycle of around 6-8 hours (upper left); under starvation conditions cells start to pulse cAMP in their vicinity and form aggregates; during development, spore containing fruiting bodies are formed to preserve the survival of the colony (∼approximately 24 hours); Not drawn to scale. Adapted and simplified from David Brown & Joan E. Strassmann; licensed by CC Creative Commons Attribution - Share Alike 3.0; (Brown et al., 2022).

The detection of cAMP and the ability to sense and follow up a cAMP gradient gave rise to a multitude of studies addressing chemotaxis, cell motility, and cell polarization in the past and a still ongoing field of research. During the starvation process, the *D. discoideum* cell polarizes towards the gradient and keeps this polarization, which results in a leading edge and rear of the cell with specifically dedicated proteins involved (King et al., 2009; Ridley, 2011; Iglesias, 2012; Goehring et al., 2013). This fast and complete change in its proteome and cellular appearance and function is another ongoing research topic and still drives a lot of investigations.

1.2 *Arabidopsis thaliana*

Arabidopsis thaliana is a model organism in plant biology and is commonly known as mouse-ear or thale cress. It is native to Europe, Asia, and Africa and can be found by the side of the road or in dry and disturbed fields. The first descriptions of its appearance are already found in the 16th century in Germany and to honor its finder, Johannes Thal (1542–1583), it was named "thal"-iana. It is a winter annual weed,

Fig. 1.2: **Photo of an adult *A. thaliana* Col-0 wildtype plant**; approx. height around 30 cm; lower to upper: typical central stem with additional side stems and rosette-forming leaves; siliques containing the seeds on the upper part of the stems and open white flowers as well as flower buds.

with a short life cycle of around six weeks. After germination from a seed of about 0.3 mm size, the pair of embryonic leaves termed cotyledons that later also nourish the early seedling emerges at the apical end of the hypocotyl and enclose the shoot apical meristem. The first leaves emerge crosswise from the center. At the basal end of the hypocotyl, the primary root provides the first energy and nutrients. The primary and subsequent true leaves are formed from the actively dividing shoot apical meristem which harbors the apical stem cell population. The leaves form a rosette from where the central stem emerges, after which some side stems follow. The full plant grows up to around 25 cm when growing in the environment, but is even larger under greenhouse conditions. The flowers are only 3 mm small. After self-pollinating, the pistils are building up siliques each containing up to 50 seeds for Col-0 accession (see Figure 1.2). (Jiang et al., 2020; Krämer, 2015; Huala et al., 2001) The fast growth and its undemanding nature concerning required nutrients and sunlight

have made it a perfect candidate for scientific research on flowering plants. In 2000 the full genome was sequenced (Arabidopsis Genome Initiative, 2000). An easy transformation and mutation method by using *Agrobacterium tumefaciens* is also available (Clough et al., 1998). The community working on *A. thaliana* has strongly grown since the 1960's and a large number of plant and mutant lines is now available on stock (TAIR, www.arabidopsis.org, Berardini et al., 2015). No other plant has ever been this intensively examined regarding genetic studies, biochemical and physiological processes, protein characterization, influences of light and dark, and finally the more recent approach to finding genes and factors involved in resistance against parasites, heat, and drought (Provart et al., 2016; Rasul et al., 2021).

1.3 Differences in Cellular Structure and Comparison of Amoeboid and Plant Cells

Plant cells like those of *A. thaliana* are strong and stiff structures. Their cell wall is made up of cellulose microfibrils, cross-linking hemicellulose, and pectins and encloses the cellular membrane. The cell wall has a strong connection to the wall of the neighboring cells through the middle lamella (see Figure 1.3 top). The cytoplasmic connections between two neighboring cells are formed by plasmodesmata. These are openings in the cell wall with adjacent plasma membrane harboring a cytoplasmic channel through which the endoplasmic reticulum in the form of a desmotubule runs. Plasmodesmata are thus symplastic (cytoplasm-dependent) connections for intercellular communication (Benitez-Alfonso, 2014). Symplastic and apoplastic (cell wall-dependent) routes are essential for the transfer of information in a multicellular plant with highly differentiated cell types.

In contrast, the composition of the structure of unicellular *D. discoideum* cells is similar to the one of mammalian cells (Müller-Taubenberger et al., 2013). They are not surrounded by a cell wall. Only the double lipid layer plasma membrane with various integrated proteins defines the border of the cell (see Figure 1.3 bottom). This allows a quick and reversible deformation of the cell. For *D. discoideum* this is essential while hunting bacteria in the ground (King et al., 2009), as the soil is a mixture of differently-sized rocks, minerals, liquids, and air-filled cavities as well as organic compounds. Other amoeboid-moving cells like leucocytes have to leave the blood vessels through a process called diapedesis and crawl through the tight surrounding tissue until they reach their destined target area (Muller, 2013).

Plants and amoeba still share most of their intracellular structures and organelles. A sketch of a plant and an animal cell is shown in Figure 1.3. Both are eukaryotic and carry a nucleus surrounded by an outer and inner nuclear membrane and which

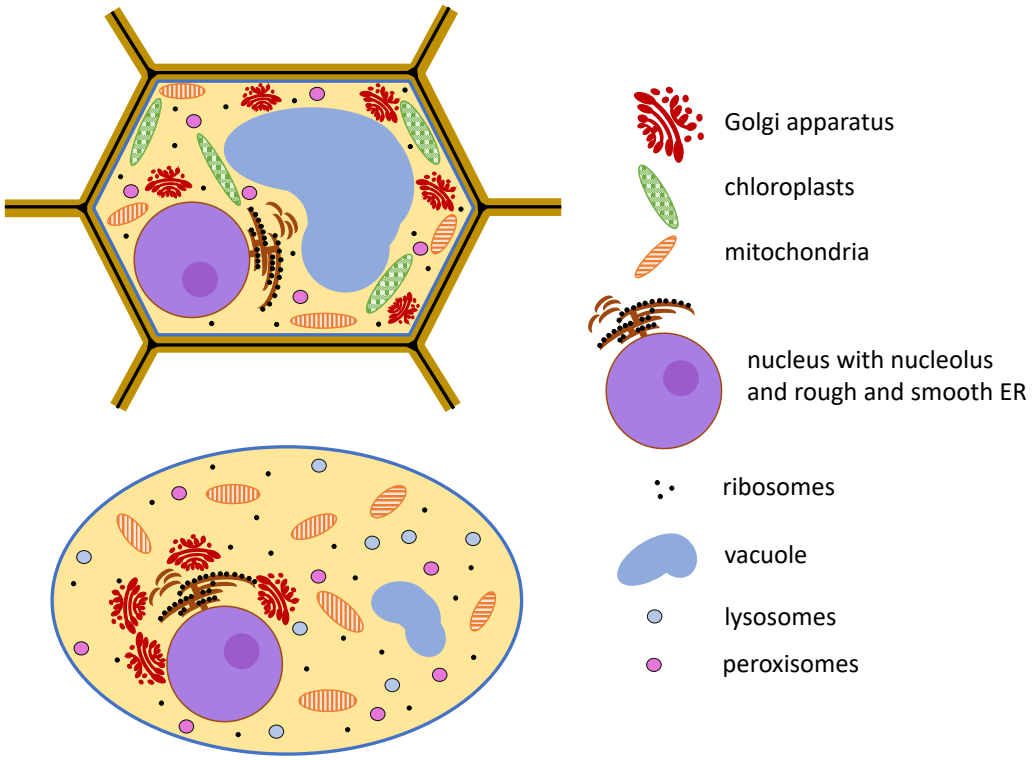

Fig. 1.3: Illustration of a plant cell (top) and an animal cell (bottom) for visualization of differences in structure and composition; static plant cell with cell wall (light brown) and strong connection to neighboring cells (black: middle lamella between the cells); dark blue: deformable double lipid layered plasma membrane with embedded proteins enclosing the cytoplasm and all organelles; ER: endoplasmic reticulum; not drawn to scale.

includes at least one nucleolus. They have a Golgi system as well as smooth and rough endoplasmic reticulum (Griffing, 1991). Ribosomes and peroxisomes are shared as well. Whereas mammalian and also *D. discoideum* cells can only produce energy in the form of ATP in the mitochondria, green plants in addition have chloroplasts in which photosynthesis takes place and in which energy is also saved in starch grains. Mitochondria and chloroplasts both have their own genome. It is an overall excepted hypothesis, that they have arisen as organelles by endosymbiosis of solitary living bacterial-like organisms into an eukaryotic cell. That is why they are coated by a double lipid layer in contrast to most other organelles. The most prominent difference in plant cells is the huge tonoplast with the vacuole (see Figure 1.3) which can nearly fill up the cellular volume. Although this term might be misleading, it is not empty space but filled up with water and nutrients and functions for conserving the turgor pressure during osmotic stress in the cell (summarized out of Munk et al., 2009, Alberts, 2008 and Taiz et al., 2018).

Both cell types are perfectly adjusted to their function. The cells of *A. thaliana* plants are building up tight tissue and form a stationary multicellular organism in which intercellular communication affects every cell's fate. Proliferation and differentiation are highly synchronized or scheduled by phytohormones like auxin (Goldsmith, 1993). Solitary living amoeboid cells all have their own fate and need to move from one nutrient source to another to survive. Therefore, the fast reorganization of the cytoskeleton is needed to maintain the structural integrity under the deformation of the cell body and thus prevent the cell from ruptures. For amoeboid movement and other cell shape-changing processes, the actin structures have to be reorganized quickly and a perfect homeostasis between degradation and polymerization has to take place. When persistently moving in one direction, the cell forms a front and a back. In the front, the actin network is polymerized and modified (explained in more detail in the next Section). In the back, the contraction of the actin fibers by myosin-II-driven processes leads to a targeted movement. This treadmilling also takes place in plants, whereby the bundling of actin plays a bigger role than the network building in amoeba. The function of the actin cytoskeleton in plants is more in pathogen perception, signaling, and immunity (Porter et al., 2016) than in stabilizing and shaping the cell.

1.4 The Cytoskeleton and Actin Dynamics

Cytoskeleton is a general expression for the different fibrous structures, which are essential for preserving the shape and stability of a cell. This includes microtubules, intermediate filaments (IF), and the actin network (see Figure 1.4). All three components of the cytoskeleton are also linked to each other by a high number of connecting proteins (Pollard, 2016; Hohmann et al., 2019; McCurdy et al., 2001). Intermediate filaments are polymers of elongated monomers, which connect in a coiled-coil structure and form fibrils. In plants, an intermediate filament-like system was found to form between and along microtubules (Yang et al., 1992). In contrast to microtubules and the actin network, IFs are not involved in vesicular transport and do not undergo a constant growing and shrinking process. Microtubules and actin filaments are both polar polymers built up from active globular dimers or monomers and each of them is bound to a nucleoside diphosphate or triphosphate. Strikingly, the actin cytoskeleton and the microtubule system have an interchanged function in plant and animal cells. While in animal cells microtubules are mainly involved in providing a platform for the transport of vesicles, as well as in the correct distribution of chromosomes to the daughter cells during cell division, in plant cells they function as the main player in structural integrity and are essential for shape and stability of a plant cell as the so-called cortical microtubules and self-organize in parallel orientation along the long axis of the cell (for a review on

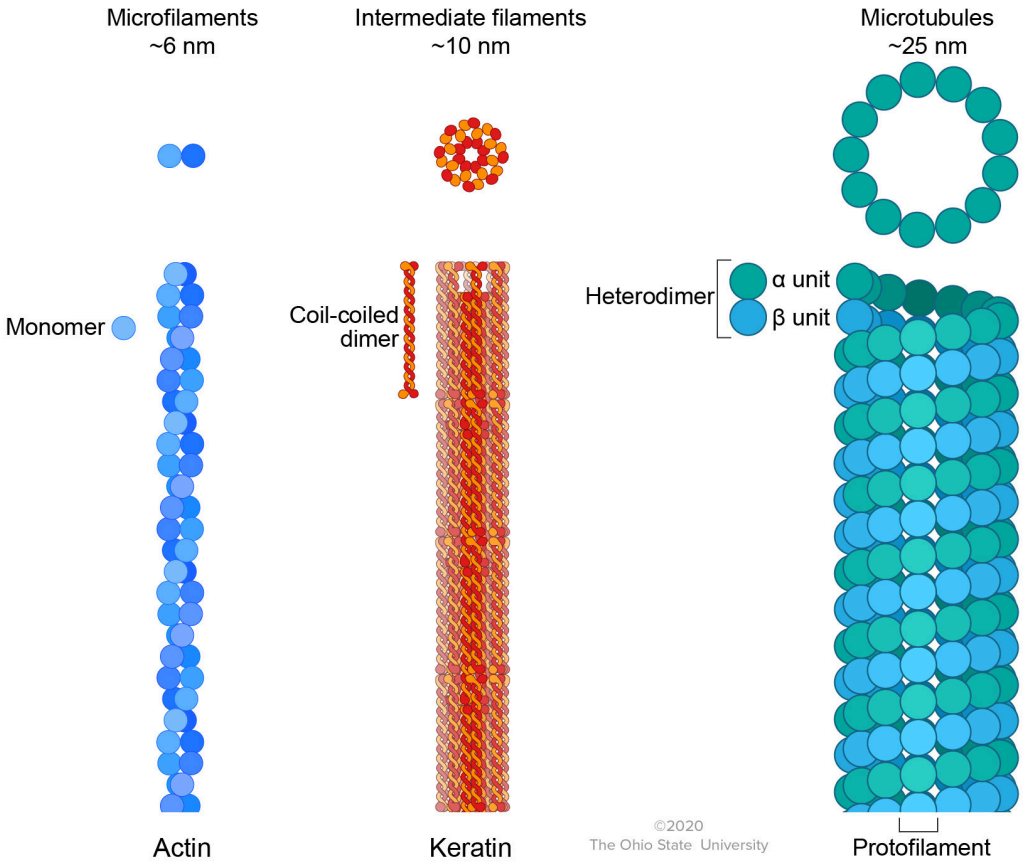

Fig. 1.4: Illustration of the three general components of the cytoskeleton: microfilaments as twisted fibers, intermediate filaments as filled rods, and microtubules as hollow rods; top: specific diameter in nm; middle: cross-section; lower: longitudinal view with smallest elements of the fibers (monomer, coil-coiled dimer, and heterodimer); bottom: examples for the three types of fibers. Licensed under a Creative Commons Attribution-NonCommercial 4.0 International License (Premanandan et al., 2017).

plant cells see Vaughn et al., 1998). Only during cell division microtubules form a spindle array. In plants, microtubules are nucleated from different sites along the plasmalemma and the nuclear envelope (see Murata et al., 2007 for review). In animal cells, microtubules emerge radially from one to two microtubule-organizing centers involving centrioles. Centrioles could only be found in lower plants like ferns and mosses (Murata et al., 2007). Microtubules form hollow cylinders. In contrast to this, the actin network is a highly branched structure in animal cells, which consists of twisted actin filaments. In these cells, actin structures are responsible for preserving the cell shape by building up in a network directly under the cortex and around the nucleus. In plant cells, actin is mostly involved in cell polarity formation, positioning of organelles and cytoplasmic streaming, the guiding of the cell wall synthesis in cell division and response to pathogens as well as in many more functions (reviewed in McCurdy et al., 2001). Actin filaments are there mostly

organized in bundles under the cortex or net-axial fine bundles of actin filaments at the tip of growing root hairs (McCurdy et al., 2001).

In contrast to stable intermediate filaments, microtubules undergo dynamic instability (Horio et al., 2014), and actin filaments undergo the so-called treadmilling. It is a process, where less active ADP-bound monomers are removed from the end of the structure and recycled to be used on the polymerizing site (Wegner, 1976; Porter et al., 2016). Actin monomers are also called globular actin or G-actin and are bound to adenosine nucleotides. Active monomers carry an ATP and can form non-covalently bound polymers. This leads to actin filaments, also called filamentous (F-) actin. Polymerization takes place at the barbed (or +) end of the fiber. Along the fiber, the ATP is hydrolyzed to the lower energy ADP and free phosphate. At the pointed (or -) end of the fiber, only the more unstable ADP-bound actins are present and this part depolymerizes easily by dissociation, thereby providing monomers for reuse (see Figure 1.5).

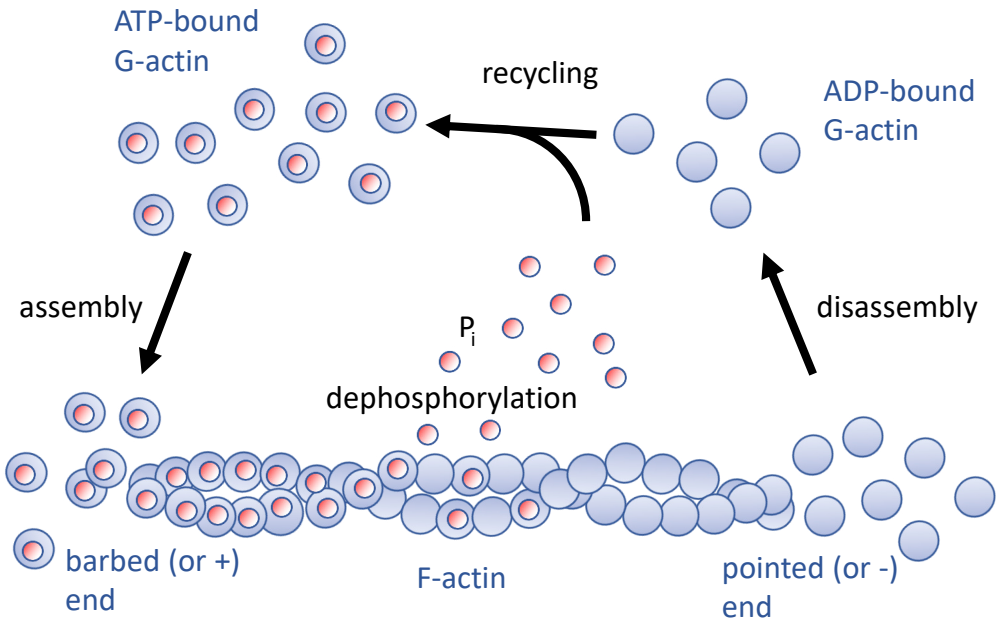

Fig. 1.5: Simplified chart of actin filament treadmilling; ATP-bound globular (G-) actin is assembled at the plus end of the filamentous (F-) actin; during aging, the ATP is dephosphorylated into ADP and free phosphate (P_i); ADP-bound actin is less stable and disassembles at the minus end of the fiber; free G-actin is then reactivated with ATP.

The actin cytoskeleton in amoeba cells can be classified into cortical actin, branched actin, stress fibers, focal adhesions, and uropods. The cortical actin is more disordered in comparison to the others and is used to distribute forces throughout the cell. It is the main structural component for maintaining the cell's shape. Branched actin forms a network that can generate pushing forces towards the plasma membrane

Fig. 1.6: Comparison of *A. thaliana* ACTIN-7 (upper row) and *D. discoideum* Major actin (lower row) amino acid sequence by Clustal Omega Algorithm (McWilliam et al., 2013); Amino acid sequence identity is 91% (*); 96% are positives (*/.:); left: reference numbers and UniProt name (Consortium, 2021); middle: Amino acid sequence in 1 letter code, colors for identification of similar properties; right: position in the amino acid chain.

or contract the cells back at the uropod. On the one hand, actin bundles can be used as stress fibers. Their function is to distribute forces over the cell while being connected to the outer matrix by adhesion points and transmembrane structures. On the other hand, these bundles can form filopodia, enabling the cell to investigate its surrounding (explained in more detail in Section 1.6). (reviewed in Hohmann et al., 2019 and Carlier et al., 2015). As already mentioned above, in contrast to animal cells, actin bundles in plant cells are important for the intracellular transport, and positioning of organelles and important for polarity formation. To summarize, the fast reorganization of actin filaments in the cell is therefore essential for migration, nutrition uptake, rearrangement of the intracellular organelles, and growth. All these functions are crucial for all living cells, so the structure and sequence of actin have been highly conserved throughout all living kingdoms.

Interestingly, 41 genes are coding for actin or actin-related proteins in *D. discoideum*. The most abundant sequence is of Actin-8, and therefore 17 of these gene products are called 'major actin' (Joseph et al., 2008). *A. thaliana* holds only eight different genes for actin (Šlajcherová et al., 2012). Two more are discussed to code for it as well. So the number of genes does not seem to be proportional to the complexity of an organism. By alignment of actin amino acid sequences from *D. discoideum* and *A. thaliana* using Clustal Omega Algorithm (McWilliam et al., 2013), sequence

identity of 91% is given and 5% more amino acids are positives, which share the same properties (see also Figure 1.6)

1.5 Actin-associated Proteins and WD40-repeat Proteins

Actin polymerization and depolymerization are based on a critical concentration of actin monomers in a cell, at which a steady state of both operations can be achieved. The limit of this treadmilling is influenced by the off-rate of ADP-actin monomers. As the turnover rate of actin filaments *in vivo* is much higher than this off-rate, other promoting or inhibiting factors had to be found (Theriot, 1997). Until now, lots of proteins are known to interact with actin structures. Some of them are actively using actin filaments for guided transport of vesicles and are moving on the fibers. Some proteins bind to the fibers to initiate actin branching or built up a connection to other structures. Others bind to the pointed or barbed end of the fiber to prevent or enhance actin reorganization. Finally, there are proteins interacting with the actin monomers to add or remove phosphates, carry the G-actin to the site of action, or inhibit polymerization. An overview of important actin-binding proteins (ABPs) and actin-associated proteins is given in table 1.1. They are grouped according to their function. In 2016 Pollard reviewed and updated his findings from 1986 (Pollard et al., 1986; Pollard, 2016). Additional actin-associated proteins can be found in Hohmann et al., 2019, McCurdy et al., 2001, and Porter et al., 2016.
All these proteins usually act as participants in a cascade, after being initiated by external cues. These signaling cascades lead to the fast reorganization of the cytoskeleton. Most widely known is the regulation of actin through the signaling pathways based on transmembrane proteins. Some essential signal transduction pathways involving G-protein coupled receptors (GPCRs) are initiated by the GPCR cAMP-receptor (cAR1) or phosphatidylinositol (PIP) in *D. discoideum*. The function of GPCR in plants is still controversially discussed (Millner et al., 1996; Trusov et al., 2016). Receptor tyrosine kinases (RTKs) in animal cells respond to polypeptides like cytokines, growth factors, or hormones. In plants, receptor-like kinases (RLK) are found to have the same function but differ at the site of phosphorylation (Jose et al., 2020). The RLK FERONIA and Leucine-Rich Repeat Extensins are known to link the plasma membrane to the cell wall and act as a kind of cell wall rigidity sensor (Dünser et al., 2019). Integrins link the extracellular matrix components to the cell and the cytoskeleton or are involved in cell-cell interaction. In plants, again similar proteins could be found and are called Integrin-like proteins (Swatzell et al., 1999). In animal cells, they activate Rho guanine nucleotide exchange factors (Rho-GEFs), which then again activate small GTPases like Rho, Rac, and Cdc42. In plants, those homologs are collectively called Rho of Plants (ROP), which are disabled by ROP

GTPase-activating proteins (ROP-GAPs) and enabled by ROP guanine nucleotide exchange factors (ROP-GEFs) (Gu et al., 2006). Subsequently, WAVE or SCAR protein complexes, WASP protein, or formin proteins directly interact with Arp2/3 or other regulating complexes and influence actin polymerization. Rho is also able to regulate other parts of the cytoskeleton by interacting with downstream kinases (see Figure 1.7).

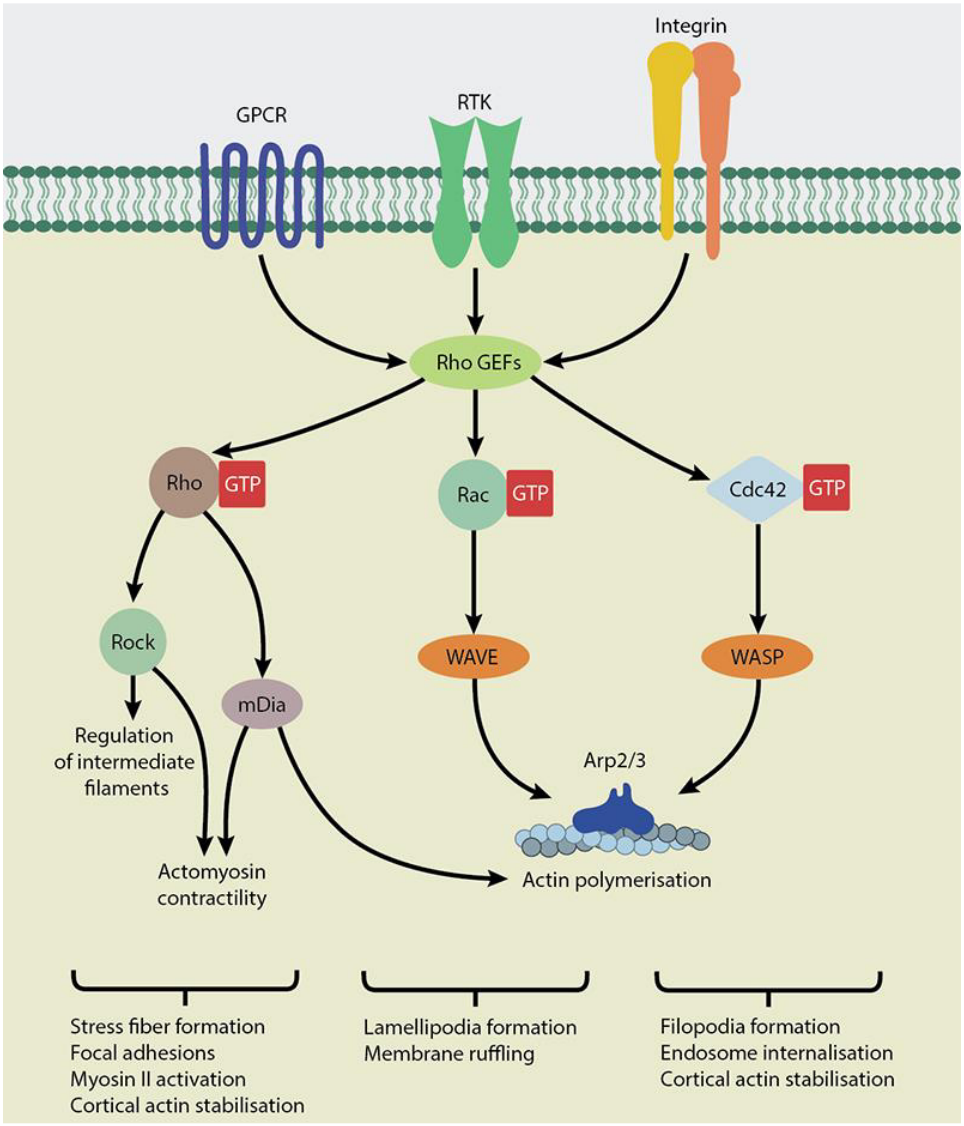

Fig. 1.7: **Overview of general inducible actin dynamics**; Activation of GPCRs, RTKs, or integrins activates downstream RhoGEFs. This results in the activation of various Rho-family GTPases. The differential activation of Rho-GTPases leads to transformation in actin localization, actomyosin contraction, and treadmilling, causing shifts in the cell's shape, morphology, and/or motility; for specific function see Table 1.1; modified from "What are Rho GTPases?" MBInfo © 2018 National University of Singapore; MBInfo, 2018.

Tab. 1.1: **Actin binding proteins (ABPs) grouped according to their function with examples** based on Pollard et al., 1986; Pollard, 2016, Hohmann et al., 2019, Staiger et al., 1987, Yanagisawa et al., 2013, Porter et al., 2016, McCurdy et al., 2001 and Ruijter et al., 1999. Bold: proteins found in plant and animal cells

Function	Example
Actin monomer binding proteins	**Profilins** DNase-I Vitamin-D Binding Protein
Capping proteins	**Gelsolin** **Spectrin** Acumentin Fragmin
Severing proteins	**Actin depolymerizing factor (ADF) / Cofilin** **Gelsolin** **Formins (FH2 domain)** **Actin-interacting protein (Aip1)**
Nucleation proteins	**Arp2/3** Coronin mDia1 mDia2 **Ena/VASP** FMNL2
Polymerases	**Profilins** **Ena/VASP**
Cross-linking proteins	**Fimbrin** Spectrin Fascin Filamin Paladin
Signaling molecules	Cdc42 **Rac1** **RhoA/ROP** ROCK **WASP/WAVE** **LIMK**
Membrane-cortex linker	Ezrin Radixin Moesin

To fluorescently label actin treadmilling sites for imaging, the G- or F-actin itself is usually not tagged anymore, because a sterical hindering occurs when the large fluorescent dye is tagged to the protein monomers. Its influences on the turnover rate of actin treadmilling should not be underestimated.

Several small markers are binding to the actin polymerization site, which are commonly used to visualize actin in *D. discoideum* cells. The widely used ones are LifeAct peptide (corresponds to the trademark of ibidi® GmbH, München, Germany) (Riedl et al., 2008) and LimE protein. LimE or LIM domain-containing protein E is a small zinc-binding protein, which is part of the actin regulation pathway induced by small GTPases and a typical marker for actin polymerization sites (Prassler et al., 1998, Bretschneider et al., 2004, Papuga et al., 2010). Its major function is the connection of the microtubule system to the cortical actin network. LimE is usually found at high concentration in the pseudopodia of moving *D. discoideum* cells (Westphal et al., 1997). Two LimE family proteins have also been found to cross-link actin bundles in a vegetative and reproductive pattern in *A. thaliana* (Papuga et al., 2010). But another common and reliable marker for actin cytoskeleton network in plants is GFP-ABD2-GFP, a fluorescently double-tagged version of the actin-binding domain of fimbrin (Wang et al., 2008). In contrast to this huge construct, LifeAct only consists of the first 17 amino acids of the Actin-binding protein (ABP) 120 from the yeast *Saccharomyces cerevisiae* and therefore is extremely small in comparison to other actin-binding proteins. Its advantage is, that it does not compete with the cell's orthologous proteins and therefore does not influence the homeostasis of the cells. Unfortunately, more recent studies have shown, that the fluorescently labeled LifeAct stabilizes the actin filaments which leads to artifacts in the cells and alters stress fibers and network architecture (Flores et al., 2019). Conclusively, one should be advised to not take LifeAct as an actin marker, when the focus of an experiment lies on the actin network or motility.

WD40 repeat proteins are one huge family of proteins interacting with actin and are ubiquitously used in all species. They are named after the repetitive tryptophan (W) and aspartic acid (D) motif after every forty amino acids. Most commonly, they have a seven-bladed propeller-like structure linked to another subunit of the protein (reviewed in Jain et al., 2018). Two important members of this family (Actin-interacting protein 1 and Coronin-A) are the subjects of this work and are described in more detail in the following two paragraphs.

1.5.1 Actin-interacting Protein 1

Actin-interacting protein 1 (Aip1 or AIP1) plays a major role in actin treadmilling. It was first found to be an actin-binding partner in 1995 when David Amberg found the

homolog Aip1p in yeast (Amberg et al., 1995). Since then, more and more homologs in all different kingdoms of life, as well as their function, have been discovered (e.g. Ketelaar et al., 2004, Ren et al., 2007). The structure of all Aip1 homologs has been highly conserved throughout evolution (see Figure 1.8), although the amino acid sequence in the beta sheets of the blades has been altered during evolution (see SI 10.1, Figure 10.1). It is a 64 kDa sized dual β-propeller-like protein made of WD-repeats and by this forming an open clam shell structure. It has an actin degrading function itself, but shows high affinity to cofilin (Ono, 2003), which it enhances in its activity to sever actin filaments by 5 to 10-fold (Nadkarni et al., 2014).

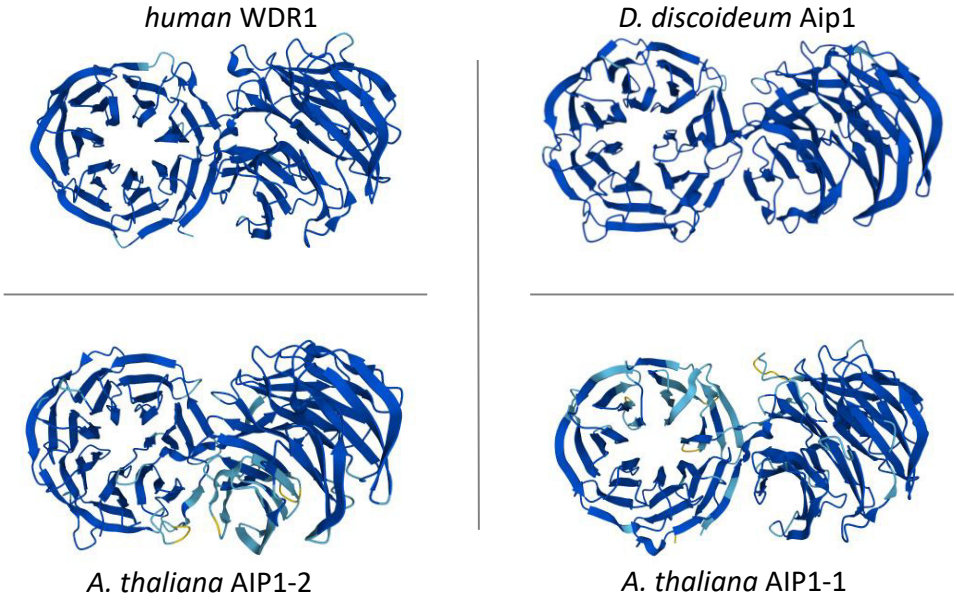

Fig. 1.8: 3D-structure prediction of Aip from different species; (taken from UniProt Consortium, 2021 Ref.No.: AtAIP1-1:Q9ZU34, AtAIP1-2:Q9LV35, WDR1: O75083, DdAip1:P54686); clearly visible structural similarities are shown.

Cofilin (also referred to as actin-depolymerizing factor (ADF) as another isoform) interacts with Aip1 as its most important interaction partner by being inserted into the groove of the two subdomains of Aip1 (Clark, 2006). It has been shown in the past, that Aip1 binds to older ADP-bound F-actin and destabilizes the binding of actin monomers in the fiber (Nadkarni et al., 2014). Cofilin/ADF binds in high affinity to older ADP-bound actin and the additional binding of Aip1 to the cofilin/ADF decorated actin filament, leads to an even enhanced depolymerization (Kueh et al., 2008). Since the 1980s cofilin/ADF are known to be involved in actin depolymerization and severing of actin filaments. Cofilin/ADF is also able to de-branch older actin networks and act as Arp2/3 antagonists. It has been found, that they are phosphorylation- and pH-regulated and also involved in stress response and apoptosis, as well as in additional actin-dependant processes like plant cell

elongation and root hair growth (for reviews on ADF/cofilin see Kanellos et al., 2016; Inada, 2017).

In mammals, Aip1 is encoded by the WD-repeat protein 1 (WDR1) gene. Studies on homozygous human Aip1 mutants showed an extremely shortened life span mostly ending before adolescence due to a high risk of severe infections (Kuhns et al., 2016) because of none-functional leukocytes (Etzioni et al., 2020). Heart function as well as all non-skeletal myocyte-depending processes are affected. WDR1-hypomorph mice exhibited thrombocytopenia (Kile et al., 2007) and a decreased rate of vessel wound healing (Dasgupta et al., 2016). Leukocytes are amoeboid moving cells as well. Therefore, the effects of lacking Aip1 in much lower complex systems like *D. discoideum* have already been the subject of many studies in the past (reviewed in Ono, 2003). In Aip1 loss-of-function mutants speed is decelerated when measured in small intervals (Konzok et al., 1999, Ishikawa-Ankerhold et al., 2010). Mitosis is affected as well as the fluid uptake by phagocytosis. The growth rate is lowered and multinuclear cells appear more frequently in these mutants (Konzok et al., 1999). In addition, actin rods are formed in the nucleus (Ishikawa-Ankerhold et al., 2017), which are also associated with neuronal diseases in mammals. The phenotype is only expressed in homozygous individuals, as the mutation is autosomal recessive in humans (Kuhns et al., 2016) and *C. elegans* (Ono et al., 2011) and also heterozygous plants do not show a phenotype. While only one gene for Aip1 exists in *D. discoideum*, two genes are known to code for AIP1 in *A. thaliana* (Allwood et al., 2002). This plant and the worm *C. elegans* (Ono et al., 2011) are so far the only organisms in which two different AIP genes were found. The evolutionary relationship between both *Arabidopsis* AIPs and the *Dictyostelium* Aip is shown in a well-elaborated phylogenetic tree (see Figure 1.9) of all in 2002 known Aips by Ellen Allwood (Allwood et al., 2002).

The gene products of the three genes of interest taken from *D. discoideum* and *A. thaliana* also vary in their size: DdAip1 is 597 aa long and has a molar weight of 64.0 kDa. 609 aa and a resulting molar weight of 66.0 kDa are expressed from *AIP1-2*. AIP1-1 is 611 aa long and 66.4 kDa in weight (Consortium, 2021). In *A. thaliana*, the two proteins are active in different parts of the plant. While AIP1-1 is pollen-specific, AIP1-2 is expressed in the major part of the plant. In root cells, AIP1-2 expression is restricted to root hair cells (Kiefer et al., 2015). In this context, AIP1-2 was found to be the phylogenetic older isoform of Aip1 (Allwood et al., 2002). At a certain point in evolution a doubling of the AIP1 gene had taken place and the AIP1-1 homolog was specifically expressed in pollen, while the AIP1-2 gene is expressed in most organs. Overall, not all angiosperm plants seem to have two AIP1 coding genes. In the rice *Oryza sativa*, although being an angiosperm plant, only one gene coding for Aip1 could be found, as in lower plants like ferns and mosses (Shi et al., 2013). In *Physcomitrella patens* for example also only one AIP1 gene

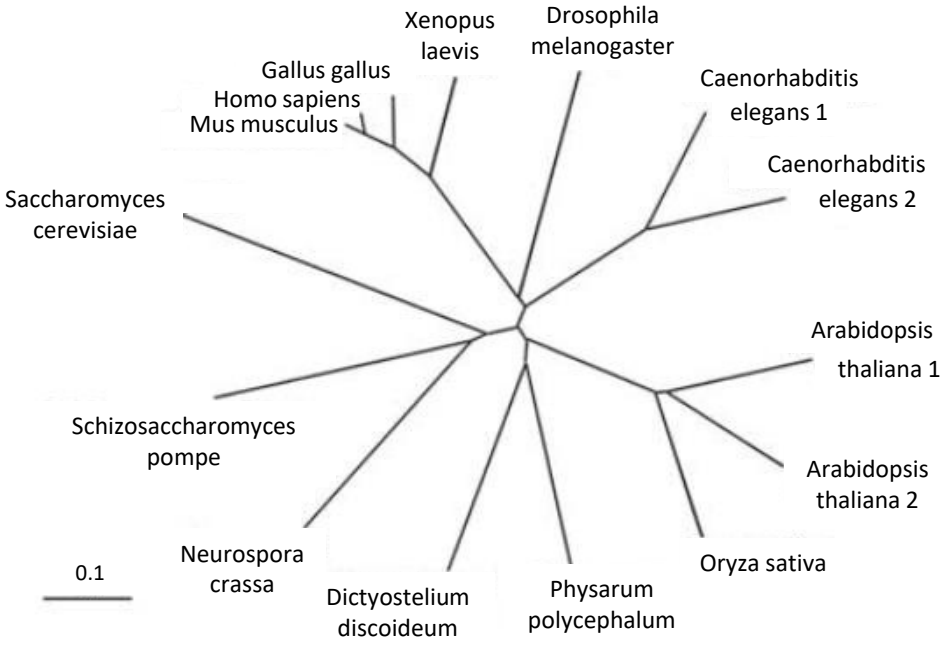

Fig. 1.9: Phylogenetic tree of all in 2002 known Aips from different kingdoms of life (Allwood et al., 2002); Aip1 of *D. discoideum* in lower left; *A. thaliana* AIPs in the middle right; in contrast to evolutionary strong differing human WDR1 in upper left; scale bar: the amount of genetic change in bp per 100 bp.

could be found (Augustine et al., 2011). AIP1-2 and AIP1-1 still share an amino acid sequence homology of 67%. Interestingly, the amino acid sequence of AIP1-2 is more similar to the Aip1 in *D. discoideum*. They share a sequence identity of 40% with 59% positives while in comparison AIP1-1 only shares 37% identity and 57% positives (see SI 10.1). So after initiating the sexual reproduction in plants, the *AIP1* gene was more altered in the pollen than the one in the rest of the plant, which seems to have been less adapted.

By knocking out AIP1-1 plants are delayed in the production of pollen and pollen tubes and therefore are said to be close to non-fertile. AIP1-1 is also a major player in correct vesicle transport in pollen tips to support the pollen growth and when being knocked out, pollen tubes do not show their unique apical actin structure (reviewed by Diao et al., 2020). Both AIP1 mutants alone show a minor phenotype and are hardly distinguishable from the wildtype. But alcohol inducible RNAi on a conserved sequence of both AIP1 leading to a double knockdown of *AIP1-1* and *AIP1-2* results in strong phenotypic changes (Ketelaar et al., 2004). Although the effects were strongly varying between the different plant lines, an unusual appearance of actin cables in the root hairs and strong effects on growth could be shown. The plants failed to flower, had shorter shoots, and showed strong signs of stress response, as well as 5-fold shorter and fewer root hairs. Cells in the leaves were overall smaller. The

strongest phenotypes manifested even in failed bolting. Interestingly, overexpression of the N-terminally HA-tagged AIP1-1 in all plant cells under a strong viral 35S promoter did not lead to significant changes in the aerial parts of the plants, but root hairs were 8-times shorter and much thicker and exhibited bulbs at the tip (Ketelaar et al., 2007). Additional to the effect on the root hair appearance, the actin bundles in the root hair cells were finer and less aligned to the axis of the hair. In yeast, the interaction of Aip1 and actin could be shown initially (Amberg et al., 1995). In AIP1-2 mutants, strong interaction with actins could be shown. Double knockouts of AIP1-2 and ACT7 show a strong phenotype in stem and silique growth when germinating at all. Only around 14% of the *aip1.2-1act7-6* double mutant are vital and show twisted stem and reduced growth (Kiefer et al., 2015).

1.5.2 *Aip1* based double mutants in *D. discoideum* and *A. thaliana*

It has been shown, that there is proof of the cooperative function of Aip and Coronin (Ishikawa-Ankerhold et al., 2010) as well as *in vitro* studies of Coronin, Aip, and cofilin (Kueh et al., 2008). In a *D. discoideum aip1* and *corA* double mutant, development, and growth are even more reduced than in one of the single mutants. Furthermore, the total actin level was increased and the actin network was shown to be stabilized in clusters under the cortex, although cofilin levels were upregulated 4-fold (Ishikawa-Ankerhold et al., 2010). This led to reduced phagocytosis and additionally, double mutants were rarely able to produce even small fruiting bodies. These cells also showed multinuclearity and huge vesicles.

As Coronin is not present for comparison in *A. thaliana*, the previously described double mutant *aip1-2.1 act7-6* was used instead, as it had been shown to also exhibit a stronger phenotype in comparison to the *aip1-2* mutant alone. *Actin* mutations seem to behave synergistically with *aip1* knockouts. Only in root hair positioning an epistatic relationship was observed. The germination rate of single mutants is very close to the wildtype, but the double mutant has a highly impaired germination rate of only around 10%. Roots are shortened and the main stem is not straight but appears to be zigzagging. Siliques are smaller and twisted, as well as the smaller leaves at the stems. The planar polarity in root hair cells is highly impaired, which can be shown by the wrong positioning of ROP and the resulting more apical root hair emerging site (Kiefer et al., 2015).

1.5.3 Coronin and the Coronin Family of Proteins

Coronin-A is another WD (Trp-Asp)-repeat protein involved in actin treadmilling. It is a 49 kDa large single β-propeller-like subunit connected to a C-terminal coiled-coil domain (Uetrecht et al., 2006). In comparison to Aip1, it has an F-actin building and an F-actin depolymerization function, depending on to which protein it is bound (Gandhi et al., 2009). When Coronin synergistically interacts with cofilin, it destabilizes ADP-bound actin filaments just as Aip1 does (Kanellos et al., 2016). On the opposite, it has a strong binding affinity to freshly formed ATP-rich F-actin when cooperating with the Arp2/3 complex and therefore initializes and promotes actin branching and cross-linking (Goode et al., 1999; Humphries et al., 2002). In older actin networks, Coronin can replace the Arp2/3 complex and start debranching the network, by providing more pointed ends where depolymerization with recruited cofilin can take place. Overall, a direct interaction of Coronin-A with actins could not be found, but its influence on the actin structures via other proteins and probably as a signaling molecule as well seems to be very important as the phenotypes of mutants lacking Coronin-A are severe (Fabrice et al., 2020).

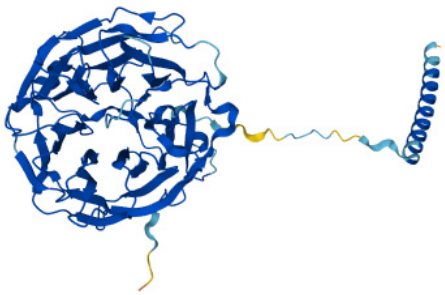

Fig. 1.10: 3D-structure of *D. discoideum* Coronin-A; typical structure of type 1 short Coronin with an N-terminal seven-bladed β-propeller and a C-terminal coiled-coil domain connected by a linker; both N-terminus (bottom) and c- terminus (right) are easy to access for interaction partners; from Uniprot (Consortium, 2021, Ref.No.: P27133).

Coronin was first named after the high abundance of the protein in crown-shaped actin-rich protrusions in developing *D. discoideum* cells (Hostos et al., 1991). Coronin proteins have been found in all animal cells, protists, and fungi as well, but could never be shown to exist in plants (Eckert et al., 2011). Until now, a large number of Coronin-like proteins is known, and therefore these proteins were summed up in their own protein family. In *D. discoideum* two major Coronins are present: Coronin-A and Coronin-B. In contrast to Coronin-A, Coronin-B consists of two β-propeller-like subunits connected by a long linker containing a large proportion of polar amino acids (see Figure 1.10 and Figure 1.11)(Shina et al., 2010). Due to this major difference in structure, all Coronins are grouped into short (class 1 and 2) and long (class 3 and 4) Coronins (reviewed in Uetrecht et al., 2006 and Eckert et al.,

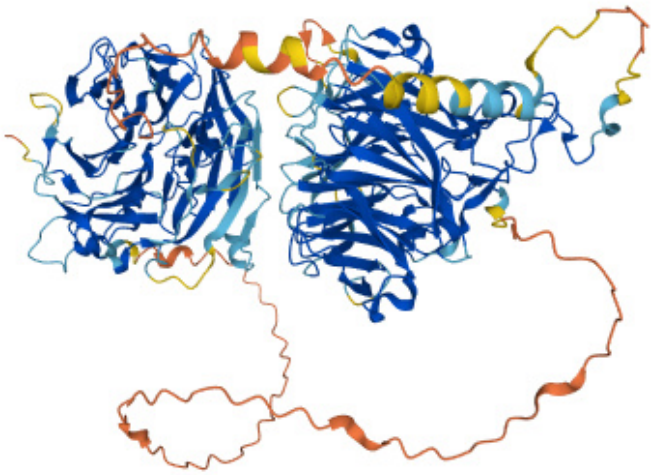

Fig. 1.11: 3D-structure of *D. discoideum* Coronin B; double seven-bladed β-propeller structure of type 3 long Coronins with the characteristical extended linker; most probably evolved by gene duplication of type 1 or 2 Coronin; from Uniprot (Consortium, 2021, Ref.No.: Q55E54).

2011). Comparisons of all subunits gave the hint, that during evolution the short Coronin gene was duplicated and spacial proximity and further mutations led to the rise of long Coronins. Interestingly, class 4 Coronins are only found in lower eukaryotic cells like amoebozoa, other amoeboid-moving unicellular organisms, and also in fungi and are hypothesized to be lost during evolution (Eckert et al., 2011). Coronin is said to be an even more important protein in actin treadmilling than Aip1. Loss of Coronin activity for example by loss-of-function mutation leads to strong phenotypes including aberrant protrusion formation, cell motility, and chemotaxis (Cai et al., 2007). In *D. discoideum* these cells are nearly non-motile, show aberrant cell morphology, insufficient mitosis, and deformation of the nuclei, which leads to a large number of multinucleated cells (Hostos et al., 1993). All actin-dependent processes are highly influenced, including phagocytosis (Maniak et al., 1995) which results in a decreased uptake of nutrients, causing a slow growth rate. The defense response to gram-positive intracellular parasites like mycobacteria is inhibited, so Coronin-lacking cells are an easy target for invaders. In other species, Coronin is an important actin regulator as well. In the mutant of the fruitfly *Drosophila melanogaster* the percentage of surviving embryos is low and adult animals have strong defects in leg and wing formation. *Caenorhapditis elegans* worm embryos are impaired in building up a dorsal axis due to dysfunctional vesicle transport. (Uetrecht et al., 2006, Gandhi et al., 2008)

1.6 Amoeboid Movement versus Plant Root Hair Growth

The rearrangement of the actin cytoskeleton is one of the major processes in a cell to change its shape and still preserve its function in a particular manner while acting together in a tissue or solitary living. The response to extracellular signaling is important for all actin-depending processes, reaching from a change in shape, building up cellular protrusions, movement, and even more essential capabilities. This can be cell division, uptake of nutrients or secretion of signaling substances, and finally also cell growth (Fletcher et al., 2010; Vantard et al., 2002). In *D. discoideum* as well as in *A. thaliana* both cellular growth and cell division are the most important processes. Differences occur when comparing the motility and stiffness of the cells. In amoeboid cells, the change in cell shape is more important than the stiffness of the structure in comparison to plant cells. Root cells in the plant are essential for nutrition and water uptake and the cell division and elongation in the root in addition to forming root hairs is crucial for root growth, which in turn leads to retarded growth of the aerial parts (Takatsuka et al., 2014). In *D. discoideum* the formation of pseudopodia, filopodia as well as lamellipodia takes place to remodel the cell. A not actin-driven cell deforming mechanism is blebbing (Welch, 2015; Yoshida et al., 2006). As already mentioned above (see Section 1.4) filopodia are actin bundle-driven hair-like structures, while pseudopodia and uropods are based on local pushing or contractile forces of cortical and branched actin. Lamellipodia are formed when the whole front of a cell is being pushed forward like a wave by network-forming actin (Blanchoin et al., 2014). All these expansions of the cell enable the movement of *D. discoideum* cells (see Figure 1.12).

Plant root cells are radially arranged and form a well-organized tissue with alternating root non-hair and root hair cells in the epidermal layer. They are made by asymmetric division and growth and differentiation of meristematic stem cells in the root tip. The cells divide by forming a cell plate at the division zone in the equatorial plane in the meristem zone, undergo a phase change in the transition zone and elongate in the elongation zone of the root tip (Takatsuka et al., 2014). When cells with root hair fate are almost fully elongated, the root hair cells are starting to produce a protrusion at the basal end of the cell, which emerges and forms the root hair. This is done in two steps: The initiation step of the root hair by a disk-shaped area in which the cell wall loosens and the tip growth step, when directed secretion leads to an elongation of the hair (Grierson et al., 2014). The positioning of the root hair is coordinated by the concentration of ROPs (Molendijk, 2001, reviewed in Grierson et al., 2014), which are highly influenced by auxin (Fischer et al., 2006; Ikeda et al., 2009), the most important phytohormone and plant growth-regulator

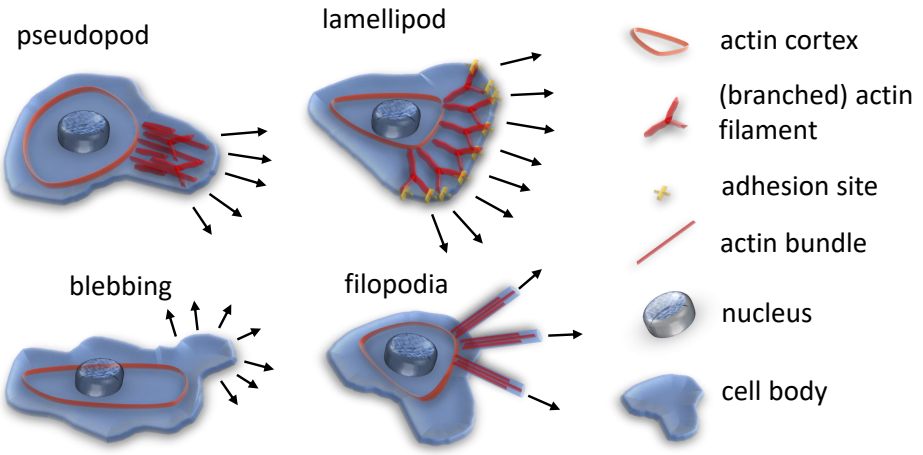

Fig. 1.12: **Movement modes of *D. discoideum***; pseudopods are formed by actin network forces pushing the membrane locally outward; lamellipodia appear less frequent, they are formed when the pushing forces spread over a huge front of the cell; filopodia are string like extensions driven by actin bundles; blebbing occurs, when the cellular membrane is no longer linked to the actin cortex.

for planar polarity as well as by the receptor-like kinase FERONIA (Duan et al., 2010; Wang et al., 2022). The tip of the root hair is then growing outward by a large number of exocytosis events (Ketelaar et al., 2008). This process is only briefly interrupted when the cell nucleus is transported into the root hair (see Figure 1.13) by actin bundles. Then the growth of the tip continues.

A comparison between the process of root hair growth in *A. thaliana* and the fast reorganization of the cytoskeleton in non-starved *D. discoideum* is only suitable because the movement of the non-polarized amoeba in media is exactly as fast as the root hair tip growth: 1 μm/min (Bosgraaf et al., 2009; Grierson et al., 2014). As the timescales are comparable, differences in the growth of a protrusion can be compared and it has already been shown, that Aip1 is involved in this (Konzok et al., 1999; Ketelaar et al., 2004).

1.7 Selection-linked Integration - SLI

Most classical and widely used gene mutation methods are based on the integration of a resistance cassette into a gene, which leads to the expression of a nonfunctional N-terminal part of the protein (see Figure 1.14). Therefore, this mutation method is known to create so-called 'loss-of-function' or 'null' mutants. The resistance cassette has its own promoter and terminator and is usually integrated in the opposite direction of the gene's reading frame.

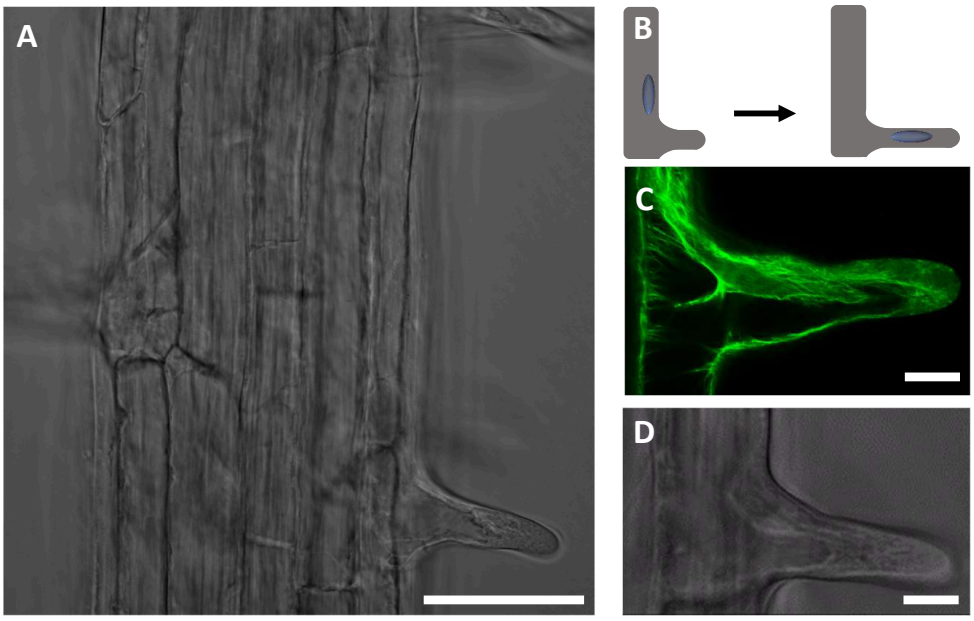

Fig. 1.13: **Root and root hair of *A. thaliana***; A: brightfield image of a root with emerging hair from the basal end of a root hair cell; B: a sketch of root hair cell and repositioning of the nucleus during root hair growth (see also Nakamura et al., 2018a); C: the confocal image of the strong actin bundles (visualized by GFP-ABD2-GFP) in the cell and the emerging root hair; in the root hair tip the bundles are not as distinct, because the turnover in actin is high and the expansion of the root hair membrane takes place there; D: brightfield image of a short emerging hair with a nucleus in the transition zone between the cell body and hair; scale bar A: 50 μm; scale bar C+D: 10 μm.

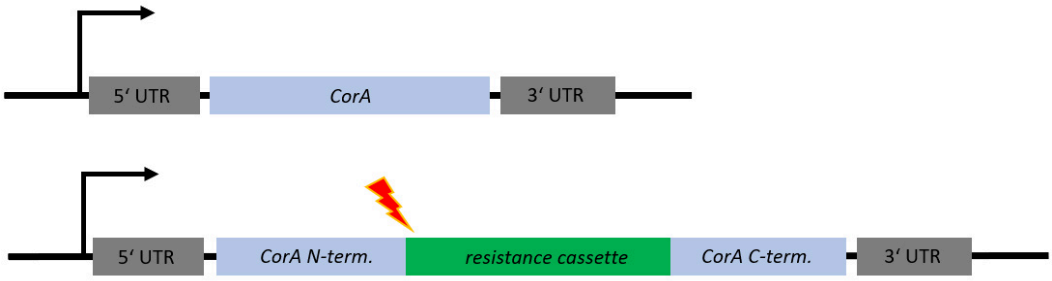

Fig. 1.14: **Classical loss-of-function mutant creation by integration of a resistance cassette and the resulting disruption of the CorA gene**; upper: endogenous gene locus; lower: modified gene locus; Flash: the first part of the protein is expressed until reaching the resistance cassette.

Selection-linked integration (SLI) is a homologous recombination-based method, where a full plasmid is integrated at a predefined specific position into the host

genome, which results in a knockout of the gene. SLI has been adapted for use in *D. discoideum* (Sven Flemming, personal communication) after successful application to the pathogenic protozoan *Plasmodium falciparum* which causes malaria tropica (Birnbaum et al., 2017). A similar method was also used before to express a tagged protein by replacing the endogenous gene (Daunderer et al., 2002). To knock out a gene, the first 700 bp of the gene of interest (GOI) are cloned into a vector, including an additional stop codon before the actual beginning. This 700 bp long sequence is the part, where the homologous sequence is recognized and recombined into the gene. This is followed by a 2A skip peptide (Kim et al., 2011, Wang et al., 2015), which is causing an intermitting translation and allows separated multi-gene expression from one mRNA strand. The attached resistance gene does not have its own promoter and is therefore expressed under the same endogenous promoter as the no longer functional GOI (Lai et al., 2010). This allows to select for cells, which have already integrated the plasmid into the genome. The additional stop codon leads to the safe termination of translation and thus to the non-expression of the endogenous protein. The plasmid also carries a resistance cassette in its backbone to ensure the selection of transformed cells carrying the plasmid (e.g. Figure 1.15).

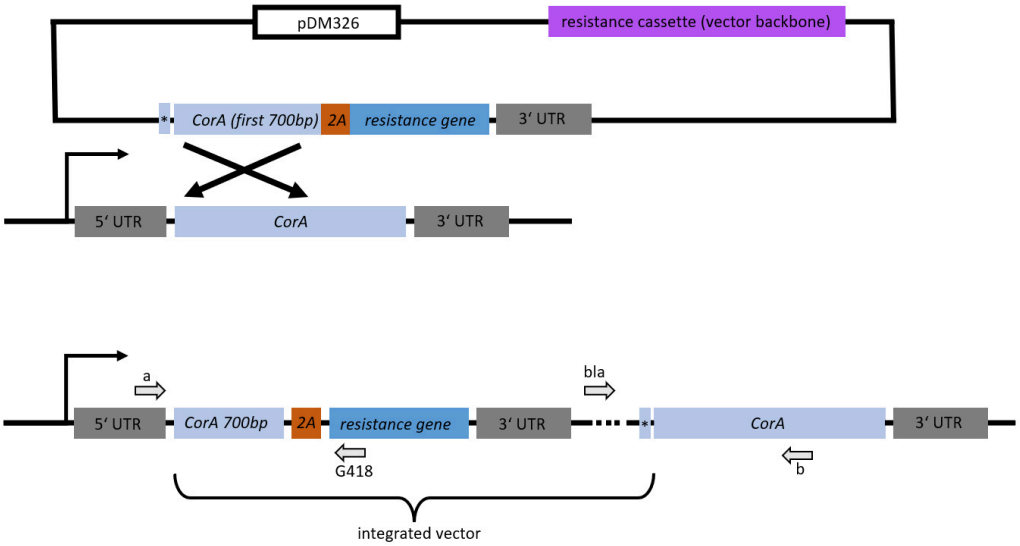

Fig. 1.15: Knockout creation by using selection-linked integration (SLI) of a plasmid into the CorA gene; upper: plasmid with first 700 bp of the GOI with an additional stop (*) codon prior to the homologous recombination site; 2A skip peptide for multi-gene expression; resistance gene with no own promoter to ensure selection of only genetically-modified cells; lower: modified gene locus; Arrows: primer binding sites for integration check by PCR on genomic DNA.

SLI can also be used to express a gene for a tagged protein under its natural promoter. This advantage is also used for the creation of so-called knock sideway mutants (see Figure 1.16). Knock sideway is also called chemical-induced dislocation (CID)

and has also already been used in HeLa cells and other cell types to create sudden loss-of-function mutants (Robinson et al., 2010). Different forms of CID are known since 1997 (Graef et al., 1997) with several studies employing rapamycin or photo uncaging as induction methods (DeRose et al., 2013). Rapamycin is a macrolide compound produced by the bacterium *Streptomyces hygroscopicus* and was found to have an immunosuppressant function in mammals and antiproliferative function in amoeba (Wullschleger et al., 2006; Swer et al., 2014). In mammals, it down-regulates the reaction of B cells and T cells of the adaptive immune system to interleukin-2, a pro-inflammatory cytokine (Kuo et al., 1992). In *D. discoideum* it induces the transition from single-cell to multicellular differentiation by influencing the actin polymerization, the pseudopodia formation, and the phagocytosis via mTORC protein complexes (Jaiswal et al., 2019; Rosel et al., 2012). CID based on rapamycin has extensively been used in the Peter N. Devreotes Lab since 2017 (Miao et al., 2017) in *D. discoideum*. The mechanism behind this is based on the reversible dimerization of two protein domains by a small linking molecule, in this case, rapamycin. A protein of interest is tagged with a fluorescent protein and an additional monomer with high affinity to a specific substance. Another protein stationary localized in the membrane or an organelle of the cell carries another peptide with high affinity to the same substance. The protein of interest (POI) should not be influenced by the tags too much and should localize to its natural site of action. When the substance is added, both high-affinity domains bind to the chemical and therefore form a heterodimer. So the POI is caught by the substance and bound to the membrane or organelle which carries the anchor (method reviewed in Putyrski et al., 2012 and DeRose et al., 2013). As this happens on a second-to-minute timescale, the cell can not adapt as quickly as necessary and the effects of the now-lacking protein should be more severe than in a genetic knockout.

The advantages of expressing a knock sideway protein under its endogenous promoter are enormous and exceed the possibilities to express the POI together with the knock sideway tag from a plasmid after having knocked out the endogenous gene. Complementation from plasmids usually alters the equilibrium in the cell. The procedure is the same as the creation of a knockout, but in contrast to the SLI knockout method, for knock sideway construction, the last 800 bp of the GOI are acting as the homologous region. The 3' end of the gene in the plasmid is lacking the stop codon, but is linked to a fluorescent protein gene and again linked to one of the dimerization domains. Here, we use FKBP12 (linkage of two times FK506 binding domain), which is known to bind to rapamycin (Putyrski et al., 2012). The FKBP12–rapamycin complex binds to the FRB (FKBP and rapamycin binding) domain of TOR kinase, which can be expressed linked to a protein of the outer mitochondrial membrane or linked to a mitochondrial targeting sequence (MTS) of the yeast's N-terminal signal domain of *S. cerevisiae* Tom70p protein (Robinson et al., 2010). So if rapamycin is added to the cell culture, the POI dislocates to the

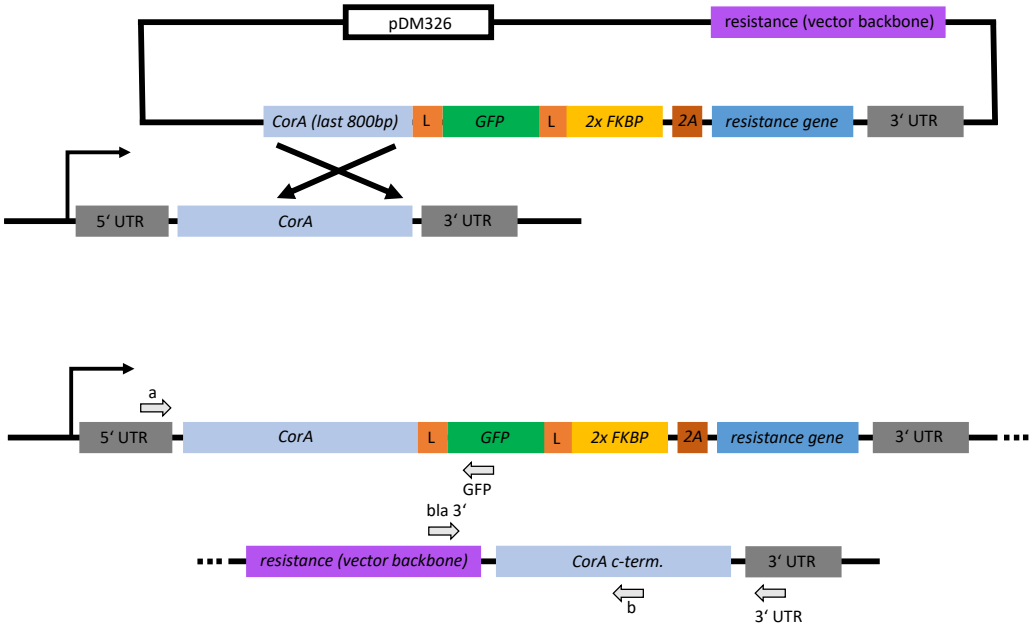

Fig. 1.16: knock sideway (CID) creation by using selection-linked integration of a plasmid into the CorA gene locus; upper: plasmid with last 800bp of the GOI with lacking stop codon as homologous recombination site; L: linker to the fluorescent tag (GFP); additional linker to the dual-FKBP-domain; 2A skip peptide for multi-gene expression; resistance gene with no own promoter to ensure selection of only genetic modified gene-containing cells; lower: modified gene locus; Arrows: primer binding sites for integration check by PCR on genomic DNA.

mitochondria and is no longer available at its normal site of action, resulting in a sudden loss of function (see Figure 1.17).

1.8 Aim of the Study

Studies on the function of Aip1 have been conducted in many different species before (see 1.5.1). This work focuses on the possibility to interchange Aip1 between evolutionarily distant species: The plant *A. thaliana* and the social amoeba *D. discoideum* (see Figure 1.9). Therefore Aip1 lacking or loss-of-function mutants of both species were characterized according to their phenotype and behavior. In *D. discoideum* the investigation on the Aip1-null mutant is referring to the already known changes in motility, cell shape, and growth. In *A. thaliana* the germination rate, root hair positioning, and root hair growth in an *aip1* single mutant and an *aip1 act7* double mutant have been observed. A complementation assay is conducted with endogenous as well as foreign Aip1. In *A. thaliana* also the possible rescue of *AIP1-2* with its homolog *AIP1-1* is analyzed. Regarding the huge differences in codon

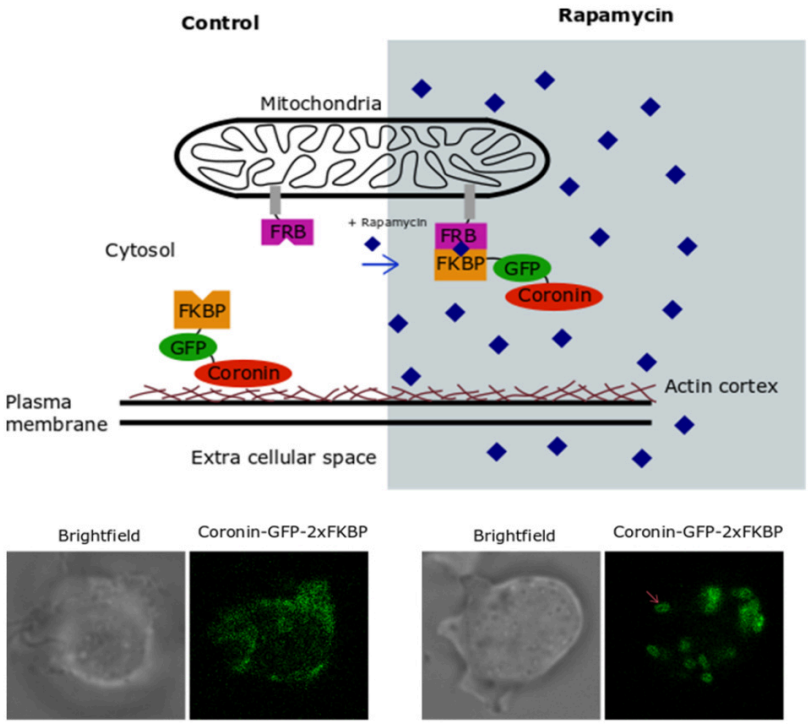

Fig. 1.17: **Principle of the knock sideway (CID) method**; upper: Illustration of the localization of the protein of interest in the control cell and its dislocation in the rapamycin-treated cell; lower: corresponding LSM images in brightfield and fluorescent channel; by Sven Flemming

usage in plants and amoeba, the foreign coding sequence (cds) was codon-optimized for use in the designated host.

As the *aip1* or *aip1-1* and *aip1-2* single mutants in amoeba or plants, respectively, do not show a strong phenotype, not only the Aip1 single mutants but also double mutant combinations were investigated. It has already been shown, that Aip1 interacts with Coronin-A in *D. discoideum*, and when both proteins are non-functional the mutant exhibits a strong phenotype regarding cell size, multinuclearity, motility, and growth. The previously, commonly used loss-of-function double mutant created by Ishikawa-Ankerhold et al., 2010 and the corresponding single mutant lacking Coronin-A (Hostos et al., 1993) display a clear disadvantage: The neomycin resistance cassette is inserted in the center of the *corA* gene for gene disruption. Frequently and after some days of cultivation, the gene's function is reverted and the resistance cassette integrates somewhere else in the genome. This leads to a still neomycin-resistant but heterogenous mix of cells in the culture, as it is not clear in which region the resistance cassette has re-integrated and which genes are affected by that. The first part of this study aims to create a stable single and double mutant of *corA* with Aip1-null in comparison to the already existing mutants.

This is accomplished in three different ways of influencing Coronin-A or its expression. First, a stable knockout mutant should be created using the new homologous recombination-based cloning method SLI. Second, RNAi strains are created, to knock down Coronin-A at the mRNA level. Last, the possibility to create a sudden loss-of-function mutant using selection-linked integration (SLI) and chemical-induced dislocation (CID) or knock sideway is investigated.

As Coronin is not present in plants, the previously described *aip1-2.1 act7-6* double loss-of-function mutant, defective in the major actin isoform ACT7 and the vegetatively expressed AIP1-2 (Kiefer et al., 2015) is chosen. This double mutant also shows a strong phenotype in comparison to the single mutants (Kiefer et al., 2015) and complementation back to the *act7-6* single mutant phenotype is accomplished here. T-DNA insertion rescue lines expressing AIP1-2-mCherry under control of the *AIP1-2* genomic 5' and 3' sequences had already been established (Kiefer et al., 2015). By employing the same approach also *AIP1-1* as well as *Ddaip1* are expressed in *A. thaliana* under the same promoter to approximately reach similar levels to the levels of the endogenous AIP1-2 protein in the *aip1-2.1* and *aip1-2.1 act7-6* mutant backgrounds. The aim of the second and third part of the study is to investigate if foreign Aip1 could also function in another distantly phylogenetically related host species and still interact with the highly conserved actin structures. Therefore the structural conserved Aip1 are interchanged and expressed in the flowering plant model organism *A. thaliana* and the amoeba *D. discoideum* as a model for moving animal cells, as their functions of the actin cytoskeleton differ widely.

2 Material and Methods

2.1 Material

2.1.1 Buffers and Solutions

Tab. 2.1: Sørensen buffer; pH 6.0

KH_2PO_4	14.6 mM
$Na_2HPO_4 \cdot 2H_2O$	2 mM

Tab. 2.2: Plant Protein Extraction buffer

Tris-HCl pH7.8	25 mM
$MgCl_2$	10 mM
EGTA	5 mM
Glycerol	10% (v/v)
NaCl	75 mM
Igepal CA-630	0.20% (v/v)
Na_3VO_4	0.1 mM
β - Glycerophosphate	60 mM
DTT	2 mM
Benzamidine	1 mM
Protein Inhibitor Cocktail (Sigma P9599)	1% (v/v)

Tab. 2.3: SDS sample buffer - cracking buffer (v/v)

SDS	6%
Glycerol	15%
Tris 0.5 M pH 6,8	30%
Bromophenol blue	ca. 5%
β-Mercaptoethanol (before use)	7,5%

Tab. 2.4: SDS-PAGE buffer

Tris	25 mM
Glycine	190 mM
SDS	0.01% (v/v)

Tab. 2.5: Towbin (Electrotransfer) buffer

Tris	50 mM
Glycine	150 mM
Methanol	20% (v/v)
SDS	0.020% (v/v)

Tab. 2.6: Tris Buffered Saline Tween-20 (TBST) buffer

Tris-HCl pH7.5	20 mM
NaCl	170 mM
Tween-20	0.05%

2.1.2 Antibodies

Tab. 2.7: Primary Antibodies

Antibody	Company	Dilution
anti-mCherry AB167453	abcam (Cambridge, UK)	1:1000
anti-Bip AS09 481	Agrisera (Vännäs, Sweden)	1:2000
anti-Coronin AB_10571321 / 176-3-6 (26 μg/ml)	DSHB (Iowa City, USA)	1:5000
anti-Actin AS13 2640	Agrisera (Vännäs, Sweden)	1:3000

Tab. 2.8: **HRP-conjugated Secondary Antibodies and Chemicals**

Antibody	Company	Dilution
goat-anti-rabbit AP307T	Merck (Darmstadt, Germany)	1:13000
goat-anti-mouse AS10 1189	Agrisera AB (Vännäs, Sweden)	1:10000
streptavidin-HRP conjugate RPN1231 *	Merck (Darmstadt, Germany)	1:5000

* Streptavidin-HRP conjugate was used to detect the highly biotinylated mitochondrial marker protein MCCC1 (3-methylcrotonyl-CoA carboxylase α) as an additional loading control to actin (Davidson et al., 2013), which might have been influenced by varying levels of Coronin-A and Aip1.

2.1.3 Antibiotics

Tab. 2.9: **Antibiotics**

Substance	Company	Final Concentration
Blasticidin S (hydrochloride)	Cayman Chemical (Ann Arbor, USA)	10 μg/ml
G418-Disulfat (Geneticin)	Amresco (Solon, USA)	10 μg/ml
Hygromycin B Gold	InvivoGen (San Diego, USA)	50 μg/ml
Penicillin/Streptomycin 10X	Biological Industries (Beit HaEmek, Israel)	Penicillin G Sodium Salt 100 U/ml Streptomycin Sulfate 100 μg/ml
Ampicillin	AppliChem (Darmstadt,Germany)	50 μg/ml (H_2O)
Kanamycin sulfate	Roth (Karlsruhe,Germany)	25 μg/ml (H_2O)
Tetracycline hydrochloride	Sigma-Aldrich (St.Louis, USA)	20 μg/ml (EtOH)
Gentamycine	Sigma-Aldrich (St.Louis,USA)	25 μg/ml mM (H_2O)
Rifampicine	Sigma-Aldrich (St.Louis,USA)	100 μg/ml (DMSO)
BASTA (Phosphinotricine)	Bayer (Leverkusen,Germany)	0.25 g/l (spray on plants)

2.1.4 Restriction Enzymes for Cloning

All restriction enzymes used for *D. discoideum* cloning were bought at New England Biolabs®Inc. (Ipswich, US) and in High-Fidelity (HF®) version if not specified elsewhere. Restriction enzymes for *A. thaliana* cloning were bought at Thermo Fisher Scientific (Waltham, USA) in FastDigest Quality. All enzymes were used according to the company's recommended protocol.

2.1.5 Kits for Molecular Biology

Tab. 2.10: Used kits for molecular biology

Application	Kit and Company
Purification of PCR product	NucleoSpin®Gel and PCR Clean-up MACHEREY-NAGEL GmbH & Co. KG (Düren, Germany)
Extraction of plasmids from *E. coli*	NucleoSpin®Plasmid MACHEREY-NAGEL GmbH & Co. KG (Düren, Germany)
PCR reaction (genotyping)	5X FIREPol® Master Mix Ready to load, 12.5 mM MgCl2 Solis BioDyne (Tartu, Estonia)
Substrate for HRP-conjugated antibodies/chemicals	SERVALight Polaris CL HRP WB Substrate Kit SERVA Electrophoresis GmbH (Heidelberg, Germany)

2.2 Methods used for *D. discoideum* and *A. thaliana*

2.2.1 Transformation of *Escherichia coli* for Cloning

Chemically competent *E. coli* strain DH5α was thawed on ice (see Untergasser, 2008 for protocol). After adding the plasmid and incubating for 30 min on ice, cells were heat shocked at 42°C for 35 sec. For recovery, the vial was placed on ice for another 5 min. 2 mm glass beads were used to spread the cell suspension on LB agar plates containing the appropriate antibiotic (ampicillin 50 μg/ml or kanamycin 25 μg/ml).

2.2.2 Immunoblotting and Protein Detection (Western blot)

The transfer was either run overnight at 15 V or for 1.2 h at 100 V in an ice bath. The transfer was done in Towbin buffer with a nitrocellulose membrane (Amersham Protran 0.45, GE Healthcare Europe GmbH, Freiburg, Germany). The membrane was then directly stained in 0.25% (w/v) Ponceau S (Sigma) in 1% (v/v) acetic acid. Images were taken with an HPScanjet G4050 scanner and VueScan software. After washing twice with deionized water, the blot was blocked with 5% (w/v) milk powder in TBST for 1 hour and additional with 5% (w/v) BSA in TBST for another hour. Primary antibody staining was performed overnight at 4°C or for 1-2 h at room temperature. If not specified elsewhere, all antibodies were diluted in 5% (w/v) BSA in TBST according to their recommended concentration (cf. Section 2.1.2). After washing the blot with TBST (1x, 2 times; 3x, 3 times; 1x, 2 times) for 10 min each, the appropriate HRP-conjugated secondary antibody was diluted in 5% (w/v) BSA in TBST, and the membrane incubated for 1-2 h at room temperature. After removing the unbound antibody by three additional washing steps with TBST, the substrate solution was added to the blot, and the emitted light was detected using a Fujifilm Intelligent Dark Box employing an Atik 460 EX camera in exposure times ranging from 5 seconds to 15 minutes.

2.3 Methods used for *Dictyostelium discoideum*

2.3.1 Cell Culture and Media

All *D. discoideum* cells were derived from the AX2-214 strain and were axenically cultured at 20°C in untreated cell culture flasks with an area of 75 cm^2 or in 25 ml shaking culture at 180 rpm in HL-5 media including glucose supplemented with vitamins and micro-elements (Formedium, UK) with the appropriate selection markers. Cells were pelleted, washed twice in Sørensen buffer for preservation and long time storage, and plated on Sørensen agar plates including 1.2% agar. After 3 days, spores were harvested and frozen in Sørensen buffer for storage at -80°C. Cell lines that did not produce spores were pelleted, chilled on ice for 5 min, and resuspended in HL-5 including 10% (v/v) DMSO. After incubation on ice for 10 more min, vials were transferred to a cryo container providing a cooling rate of -1°C per min. Tubes were then kept at -80°C.

2.3.2 Strains and Plasmids

All plasmids were constructed using restriction enzyme cleavage of double-strand DNA and homologous recombination-based Gibson Assembly with overlapping primers between 25 bp and 30 bp. The plasmid backbones of the two small expression vectors pDM326 for SLI constructs or pDM358 for cytosolic expression (Veltman et al., 2009) were used. Both carry an actin-15 promoter and an actin-8 3'UTR. The correct sequence of all constructs was confirmed by Sanger sequencing which was commercially done at LGC Genomics (Berlin, Germany). To better visualize the interaction between actin and Aip1 dynamics, another cell line expressing GFP-LimEΔ kindly provided by Prof. Dr. Günther Gerisch's laboratory (see also Ishikawa-Ankerhold et al., 2010) was transformed with N-terminal mCherry-tagged DdAip1.

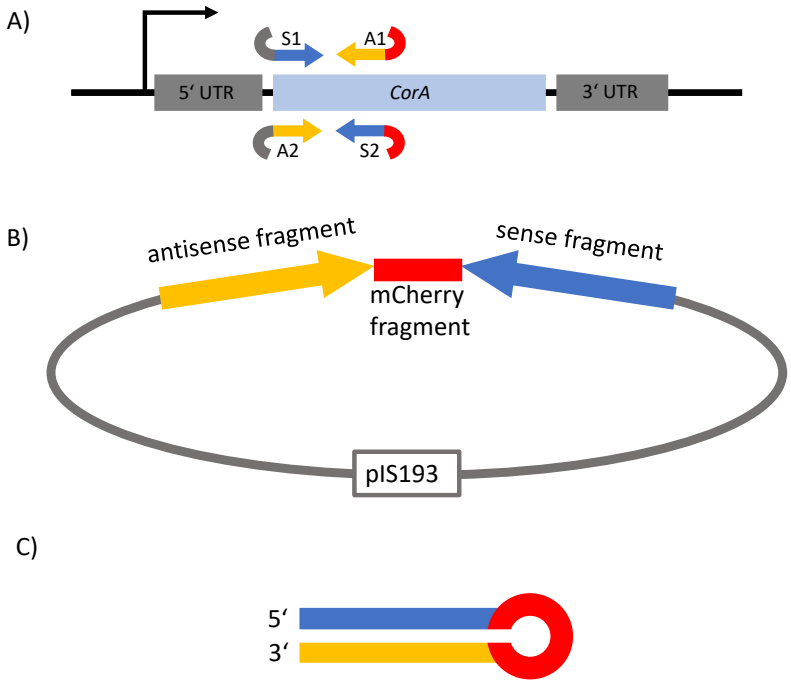

Fig. 2.1: **RNAi plasmid construction for CorA gene knockdown in *D. discoideum***; A): the creation of the sense and antisense fragment of the first 500 bp of the CorA gene by PCR; Expression cassette of the gene in grey and blue; Arrows: a primer with flanking Gibson Assembly overlap to the vector backbone or mCherry; A1 and A2: a primer for antisense fragment; S1 and S2: a primer for sense fragment; B: Illustration of the 5' CorA sense and antisense fragment with linking 190 bp of mCherry cloned into the pIS193 backbone (Samereier et al., 2011); C): resulting RNA viral-like hairpin structure after transcription.

RNAi plasmid construction was based on the strategy of Martens et al., 2002. The formation of a hairpin structure of the transcribed RNA mimics a typical viral RNA double-strand structure and is therefore degraded. The same hairpin sequence is then recognized in the mRNA of the transcribed gene of interest and most of its mRNA is also degraded before reaching the ribosome. RNAi is a form of translational silencing. Therefore a knockdown of the GOI can be realized. The needed hairpin structure can only form when two complementary sequences are separated by a linker. The plasmid backbone of pIS193 is used in this work and has been kindly provided by Prof. Dr. Ralph Gräf and Dr. Irene Meyer (Department of Cell Biology, University of Potsdam, Germany; see also Samereier et al., 2011). One part of its mCherry coding sequence between the NheI and AflII restriction sites in the plasmid was replaced by 500 bp of the antisense sequence of the 5' part of the CorA gene. In the second step, the sense fragment of the same gene section was inserted between SalI and BamHI restriction sites. 190 bp of mCherry coding sequence were kept in between to act as the linker and enable the binding of sense and antisense strands thereby forming a loop (see also Figure 2.1). Finally, the backbone resistance gene was changed from geneticin to hygromycin. After the Tth111I restriction site, the more frequently used restriction site ApaI was integrated. At the 3' end of the resistance gene, an EcoRI restriction site was added in 5'-position to the BstBI restriction site (see Figure 2.2). This was done to facilitate the future exchange of the resistance gene cassette.

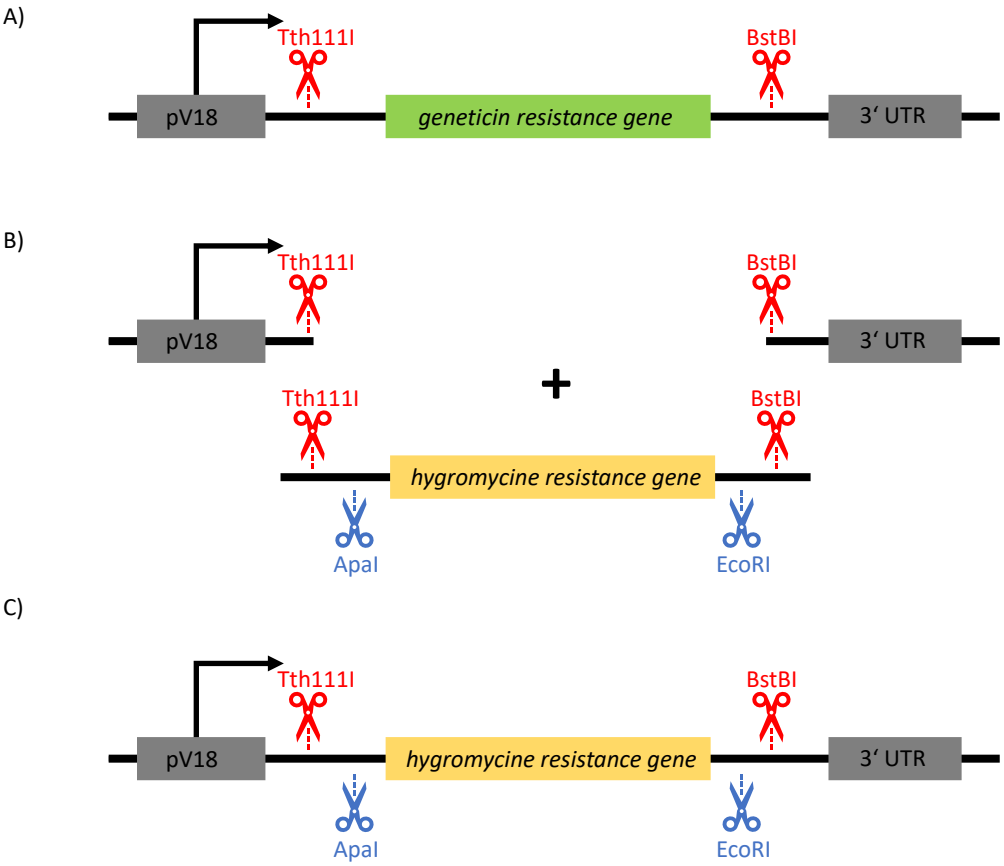

Fig. 2.2: Sketch of the substitution of geneticin resistance gene with hygromycin resistance gene and additional introduction of more frequently used restriction enzyme sites; pV18: ribosomal V18 promoter; A): Backbone resistance gene in pIS193 (see Samereier et al., 2011) with attached restriction enzyme cutting sites; B) cut vector backbone and Gibson Assembly fragment of hygromycin resistance gene with additional flanking restriction sites for frequently used restriction enzymes; C): final construct in the vector backbone carrying the new resistance gene.

Tab. 2.11: Strains for Coronin mutant characterization

Strain name	Function	Strain descriptor (official)
AX2	control	wildtype
Aip1-null#9.1 (DAip1-, DBS0252637)	classic *aip1* knockout	*aip1-*, bsR (loss-of-function, Konzok et al., 1999)
CorA-null HG1569#1 (DBS0236171)	classic *corA* knockout	*corA-*, neoR (loss-of-function, Hostos et al., 1993)
CorA/Aip1 **double-null** (DBS0350851)	classic double knockout	*aip1-/corA-*, bsR, neoR (loss-of-function double mutant, Ishikawa-Ankerhold et al., 2010)
***corA*-SLI**	new SLI *corA* knockout	*corA*-[SLI], neoR
double-KO: Aip1-null#9.1/*corA*-SLI	new SLI *corA* knockout in classic *aip1* knockout	*aip1-*, *corA*-[SLI], bsR, neoR
CorA-RNAi	*corA* knockdown	*corA*-[RNAi], hygR
Aip1-null#9.1/**CorA-RNAi**	*corA* knockdown in classic *aip1* knockout	*aip1-/corA*-[RNAi], bsR, hygR
CorA-null HG1569#1 **/CorA-RNAi**	classic *corA* knockout with RNAi knockdown plasmid to remove the N-terminal piece of the protein	*corA-*, *corA*-[RNAi], neoR, hygR
***corA*-SLI/CorA-RNAi**	new SLI *corA* knockout with RNAi knockdown plasmid for comparison to the CorA-null mutant	*corA*-[SLI]/*corA*-[RNAi], neoR, hygR
CorA-KS (+ MTS-L-FRB + mRFPmars-LimE)	new SLI *corA* knock sideway	*corA[SLI], [corA/corA-GFP-2xfkbp], [act15/mts:frb:2a:mRFPmars-limE]*, neoR, bsR
double-KS: Aip1-null#9.1 + CorA-KS (+ MTS-L-FRB + mRFPmars-LimE)	*corA* knock sideway in classic *aip1* knockout	*aip1-/corA[SLI], [corA/corA-GFP-2xfkbp], [act15/mts:frb:2a:mRFPmars-limE]*, bsR, neoR, hygR
CorA-OX (+ MTS-L-FRB + mRFPmars-LimE)	AX cells expressing additional knock sideway CorA and mitochondrial anchor	*[act15/ corA-GFP-2xfkbp], [act15/mts:frb:2a:mRFPmars-limE]*, bsR, hygR

Tab. 2.12: **Strains for interspecies interchange of Aip1**

Strain name	Function	Strain descriptor (official)
AX2	control	wildtype
Aip1-null#9.1 (DAip1-, DBS0252637)	classic *aip1* knockout	*aip1*-, bsR loss-of-function (Konzok et al., 1999)
***corA*-SLI**	new SLI *corA* knockout	*corA*-[SLI], neoR
double-KO: Aip1-null#9.1/ *corA*- SLI	new SLI *corA* knockout in classic *aip1* knockout	*aip1*-, *corA*-[SLI], bsR, neoR
Aip1-null#9.1 / **mC-DdAip1**	classic *aip1* knockout expressing endogenous Aip1 N-terminally tagged with mCherry	*aip1-,[act15/mCherry-aip1]*, bsR, hygR
Aip1-null#9.1 / **mC-AIP1-2**	classic *aip1* knockout expressing *A.t.* AIP1-2 N-terminally tagged with mCherry	*aip1-,[act15/mCherry-A.t.AIP1-2]*, bsR, hygR
Aip1-null#9.1 / **mC-AIP1-1**	classic *aip1* knockout expressing *A.t.* AIP1-1 N-terminally tagged with mCherry	*aip1-,[act15/mCherry-A.t.AIP1-1]*, bsR, hygR
Aip1-null#9.1 / **AIP1-2-mC**	classic *aip1* knockout expressing *A.t.* AIP1-2 C-terminally tagged with mCherry	*aip1-,[act15/A.t.AIP1-2-mCherry]*, bsR, hygR
Aip1-null#9.1 / **AIP1-1-mC**	classic *aip1* knockout expressing *A.t.* AIP1-1 C-terminally tagged with mCherry	*aip1-,[act15/A.t.AIP1-1-mCherry]*, bsR, hygR

double-KO / mC-DdAip1	double-KO expressing DdAip1 N-terminally tagged with mCherry	*aip1-*, *corA*-[SLI], [*act15/mCherry-aip1*], bsR, neoR, hygR
double-KO / mC-AIP1-2	double-KO expressing *A.t.* AIP1-2 N-terminally tagged with mCherry	*aip1-*, *corA*-[SLI], [*act15/mCherry-A.t.AIP1-2*], bsR, neoR, hygR
double-KO / mC-AIP1-1	double-KO expressing *A.t.* AIP1-1 N-terminally tagged with mCherry	*aip1-*, *corA*-[SLI], [*act15/mCherry-A.t.AIP1-1*], bsR, neoR, hygR
double-KO / AIP1-2-mC	double-KO expressing *A.t.* AIP1-2 C-terminally tagged with mCherry	*aip1-*, *corA*-[SLI], [*act15/A.t.AIP1-2-mCherry*], bsR, neoR, hygR
double-KO / AIP1-1-mC	double-KO expressing *A.t.* AIP1-1 C-terminally tagged with mCherry	*aip1-*, *corA*-[SLI], [*act15/A.t.AIP1-1-mCherry*], bsR, neoR, hygR

2.3.3 Transformation of *Dictyostelium discoideum* by Electroporation

Cells of the *D. discoideum* AX2 wildtype strain or the desired mutant background strains were grown overnight in a shaking culture in HL-5 media and at 180 rpm. After centrifugation at 500g for 5 min, the pellet was washed twice in cold H-50 buffer (4.76 g/l HEPES, 3.73 g/l KCl, 0.58 g/l NaCl, 0.12 g/l $MgSO_4$, 0.42 g/l $NaHCO_3$, 0.156 g/l NaH_2PO_4; pH 7.0) then resuspended to a concentration of 1 x 10^8 cells/ml and chilled on ice for 5 min. 100 μl of cell suspension and 10 μg of plasmid were transferred to an electroporation cuvette with a 2 mm gap and 3 pulses of 0.5 kV for 0.3 ms in 5-sec interval were applied. The cuvette was immediately put on ice for another 5 min and the cells were then transferred to a culture flask. 4 h after transformation the selection marker was added. Cells carrying an SLI integration plasmid were first selected by their plasmid backbone resistance. After being nearly confluent the cell cultures were split and one flask was treated with the integration selection marker, while the other was kept as a backup.

2.3.4 Genomic DNA Extraction with Protein K Method and PCR

To confirm the integration of the plasmid and to verify the genetic background, 1 mL of a dense *D. discoideum* culture (3-5 x 10^6 cells) was centrifuged for 5 min at 500g. The pellet was washed in 1 ml Sørensen buffer and then resuspended in 200 μl lysis buffer (1x PCR buffer; 1% NP40 (v/v); 50 μg/ml Proteinase K). After transfer to a 200 μl vial, the sample was incubated at 56° C for 45 min and subsequently at 95°C for 10 min. The resulting crude extract could be stored at -20°C or directly be used in a PCR reaction (primer design e.g. in Figure 2.3).

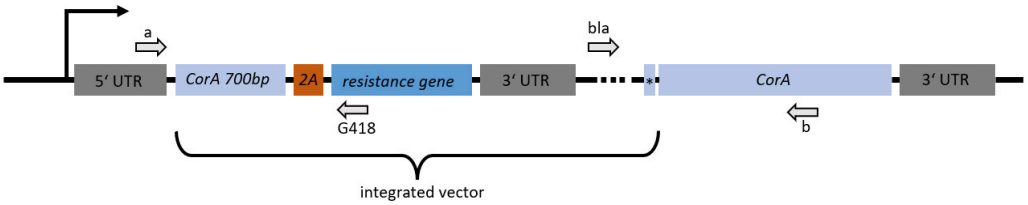

Fig. 2.3: Primer pairs and binding sites in *D. discoideum corA*$^-$ knockout mutants; Primer pairs were designed to facilitate detection of the integration of the plasmid into the *corA* gene locus; a: forward primer binding to the 5'UTR of the gene; G418: reverse primer binding to the integrated resistance gene sequence; bla: forward primer binding in the backbone resistance gene sequence; b: reverse primer binding to the C-terminal part of the *corA* gene, located 3' of the homologous recombination site.

2.3.5 Protein extracts from *D. discoideum* and SDS-PAGE

2 Million cells per strain were centrifuged for 5 min at 500g. After removal of the supernatant, the pellet was resuspended in 50 μl lysis buffer (9 M Urea, 10% (w/v) SDS, 5% (v/v) β-Mercaptoethanol, 0,2% (w/v) Bromophenol blue) and incubated for 5 min at 70°C. The derived crude protein extract was immediately placed on ice and stored at -20°C. Discontinuous SDS-PAGE was performed using a Biorad mini-gel system chamber. 12.5% polyacrylamide gel with a depth of 1 mm was run for 1.5 h at 120 V. A molecular weight standard (Thermo Scientific; PageRuler Prestained Protein Ladder; #26616) was run together with 25 μl of each sample. After the run, the gel was used for immunoblotting and protein detection (described in 2.2.2).

2.3.6 Growth Curves

Cells were grown in an overnight shaking culture and diluted to a density of 1 x 10^5 cells/ml. The number of cells/ml was manually counted every 8 h throughout 2 d

using a Neubauer counting chamber. Each strain was tested in duplicates with (+) and without rapamycin at a final concentration of 10 μM. The generation time was determined by averaging the growth over 2 days and calculating the time period in which the number of individuals in a population doubled.

2.3.7 Streaming and Fruiting Body Formation

After harvesting cells from a culture flask, the cell suspension was centrifuged at 500g for 5 min and washed twice in Sørensen buffer. The pellet was resuspended in 200 μl buffer and spread on Sørensen agar plates, containing 1.2% agar. Pictures were taken after 0, 24, 48, and 72 h using an Olympus CKX41 inverse microscope (LCAch N 40x/0.55na php or CAch N 10x/0.25na php objective) and a Thorlabs DCC1645C camera. The viability of the spores was not quantified but visually checked and estimated in comparison to the wildtype.

2.3.8 Morphology and Cell Size

To investigate the morphology and cell size of all strains, adherent cells were harvested and seeded with a density of 2 x 10^4 cells/cm^2. After 4 h brightfield microscopy pictures were taken using an Olympus CKX41 inverse microscope with a LCAch N 40x/0.55na php objective and a Thorlabs DCC1645C camera. A minimum of 1000 cell outlines per strain were marked manually in red in these images using an Apple Pencil™(2.Gen) on an Apple iPad Pro (11")™. Cell size and morphology were determined by using a MATLAB® (2019b, MathWorks, Natick, MA, USA) program (see below).

2.3.9 Image Processing for Morphology and Cell Size

The manually marked cell outlines in the brightfield images of at least 1000 cells were processed in MATLAB® (2019b, MathWorks, Natick, MA, USA) 2019b. Therefore the manually tagged cell outlines were read out from the red channel of the marked images and the resulting images were binarized (MATLAB routine: imbinarize) and resulting outlines were filled with a morphological filling method (MATLAB routine: imfill with the option 'holes'). Afterward, the binarized picture was segmented (MATLAB routine: bwconncomp identifying connected components). For each coherent set of pixels, the centroid, area and circularity was calculated (MATLAB routine: regionsprops with the options 'Centroid', 'Area' and 'Circularity'). The

connected pixel count of the objects was converted to the cell size according to the used magnification factor. Circularity C is defined as

$$C = \frac{4\pi A}{P^2} \tag{2.1}$$

with the area A and the perimeter P, such that for a perfect circle, where $A = \pi r^2$ and $P = 2\pi r$, the circularity is $C = 1$. For all other shapes $C < 1$.

2.3.10 Motility Assay

Cells were harvested and seeded in a 24-well glass bottom plate (1.9 cm^2/well) at a density of 1.5 x 10^4 cells/well. Each line was tested with DMSO as solvent mock-treated control and with rapamycin dissolved in DMSO to a final concentration of 10 μM rapamycin. Cells were allowed to settle for 20 min for induction of the drug effect. Pictures were taken every 30 sec by using confocal laser scanning microscopy (Zeiss LSM780, Plan-Apochromat 20x/0.8 M27 air objective, with 561 nm laser at 1% intensity and ZEN software). The transmitted light detector (TPMT channel) was used to create brightfield images, which were later segmented and cells were tracked by a MATLAB® (2019b, MathWorks, Natick, MA, USA) program (see below). Experiments were performed on at least six different days and pooled.

2.3.11 Image Processing and Analysis for Motility Assay

Images taken with a confocal LSM (see 2.3.10) were exported from ZEN software in tagged image file format and cells were segmented by using MATLAB® (2019b, MathWorks, Natick, MA, USA) object edge detection with the Sobel method (MATLAB routine: edge with option 'sobel'). An order-statistic filter was applied (MATLAB routine: ordfilt2), replacing each pixel by the 8th value of its sorted 3x3 neighborhood and the resulting image was smoothed with a Gaussian filter (MATLAB routine: imgaussfilt with a standard deviation of 1.8 pixels). After normalization, the images were binarized using Otsu's method (MATLAB routine: imbinarize with option 'global'), holes were filled (MATLAB routine: imfill with option 'holes') and the objects were eroded (MATLAB routine: imerode using a disk of radius one pixel as the morphological structuring element) to achieve a correct depiction of the cells. The centroid of each cell area was determined and the position of each cell was tracked based on Crocker et al., 1996 from image to image over the full image sequence of 240 frames (2 h, 30 sec time interval). Finally, around 100 tracks per strain (see Supplementary 10.4 for detailed numbers) were saved and plotted as an overlay on the brightfield images. In the last step, the numbered tracks in each

measurement were manually checked for floating cells or dead cells. These tracks were then removed from the tracklist.

For each trajectory $\mathbf{r}_j(t)$ with a track index j and the time t, the time-averaged mean squared displacement (TAMSD) was calculated as follows:

$$\delta_j^2(\tau) = \frac{1}{T-\tau} \int_0^{T-\tau} dt \, |\mathbf{r}_j(t+\tau) - \mathbf{r}_j(t)|^2 \,. \tag{2.2}$$

Then this value $\delta_j^2(\tau)$ is averaged using the arithmetic mean over all cells (track indices j) measured on the same day (<TAMSD>) as also previously described (Cherstvy et al., 2018). The mean of the <TAMSD> of the different days was then calculated and plotted in a log-log plot. The standard error was determined and plotted to give an indication of the reproducibility of the results between different days.

In addition, for each cell j the mean of the displacements $|\mathbf{r}_j(t+\tau) - \mathbf{r}_j(t)|$ within a given lag time τ was calculated and illustrated in a violin plot showing a histogram of those values. The prominent bigger points indicate the median of the distribution, which is more statistically robust to outlying values than the mean.

2.3.12 Confocal LSM Image Acquisition with Airyscan

To verify the expression of the desired rescue construct of Aip1 in mutant *D. discoideum* cells, fluorescent images of transformed cell lines were taken using the ZEN software on a ZEISS confocal LSM 880 with Airyscan mode and Plan-Apochromat 63x/1.4 Oil DIC M27 objective to obtain better quality images. The 488 nm laser line was used at 4-6% laser power for GFP excitation and the 561 nm laser with 4% laser power for mCherry excitation to visualize GFP-tagged Coronin-A and mCherry-tagged Aips in all rescue lines and mRFPmars-LimE in knock sideway lines.

2.4 Methods used for *Arabidopsis thaliana*

2.4.1 Growth Conditions and Media

The *A. thaliana* wildtype background employed in this study was Col-0 (Col-0). The *aip1.2-1*, *act7-6* single as well as the *aip1.2-1 act7-6* double mutant lines were originally generated in the Col-0 background (Kiefer et al., 2015). Col-0 was used as the wildtype control in all experiments. For all plant lines see also Table 2.13. Murashige-Skoog (MS) medium agar plates (4.3 g/l MS salt; 10 g/l sucrose; 0.5 g/l

MES hydrate; 8 g/l plant agar; pH 5.7) were used in all experiments. Seeds were sterilized using 70% (v/v) ethanol with 0.05% (v/v) Triton-X-100. After 1 min the solution was replaced by 3% (v/v) sodium hypochlorite solution and incubated for 12 min. Seeds were washed twice with distilled water and stratified in water at 4°C in the dark for 3-4 days. After plating the seeds on freshly prepared MS medium agar plates, the plates were sealed and put straight upright into a plant growth chamber (long day conditions: 16 h light at 22°C and 8 h darkness at 18°C). For direct growth on soil, seeds were sprinkled on pre-wet soil in small plastic pots with 7x7x8 cm dimensions and placed at 4°C for 3-4 days. Pots were then transferred to a 22°C temperature- and 70% humidity-controlled plant growth room with long-day conditions as in the growth chambers. After silique production had terminated, the plants were bagged and dried. Seeds were collected using a sieve with 425 μm pore size.

2.4.2 Plant Lines and Plasmids

All plasmids were derived from pGreenII0229 T-DNA vector (Hellens et al., 2000) carrying a kanamycin resistance cassette and an additional phosphinotricin acetyl-transferase resistance cassette enabling a resistance against the BASTA herbicide. Pre-existing plasmids, kindly provided by Christian Kiefer (Kiefer et al., 2015) were used for additional transgene cloning by restriction endonucleases (see below) and ligases. The coding sequence (cds) of *D. discoideum* Aip1 was commercially codon-optimized for usage in *A. thaliana* by BioCat (Heidelberg, Germany) with appropriate cloning sites attached and delivered in a pUC57 plasmid.

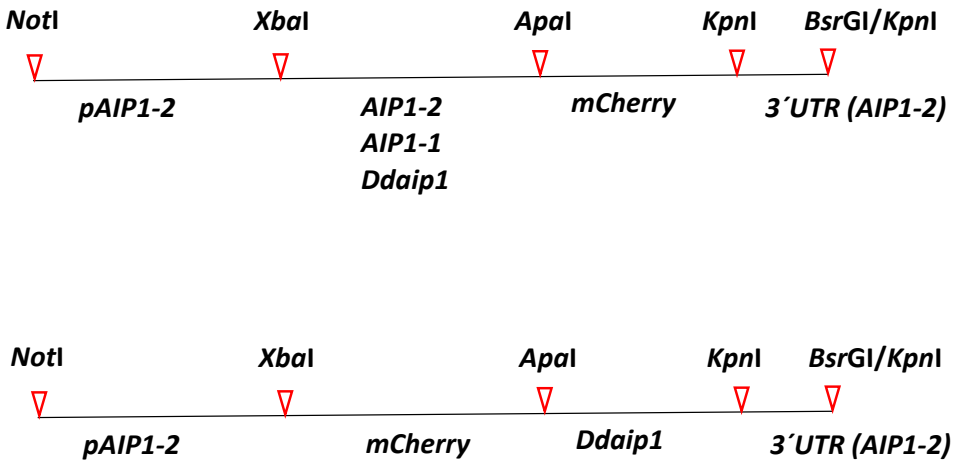

Fig. 2.4: Restriction enzyme cutting sites used for cloning into T-DNA of pGreenII0229 (see also Hellens et al., 2000, Kiefer et al., 2015).

Tab. 2.13: **Plant lines of the *D. discoideum* Aip1 as well as the *Arabidopsis thaliana* AIP1-1 and AIP1-2 coding sequences tagged with mCherry** in *aip1.2-1* and *aip1.2-1 act7-6 A. thaliana* mutant backgrounds.

Genetic background	T-DNA	Comment
Col-0	none	wildtype
aip1.2-1	T-DNA insertion in exon 5 of the *AIP1-2* gene (AT3G18060)	polymorphism: GK063F04
act7-6	T-DNA insertion in exon 1 of the of the *ACT7* gene (AT5G09810)	polymorphism: SALK_131610
aip1.2-1 act7-6	crossing of *aip1.2-1* and *act7-6*	polymorphism: GK063F04 and SALK_131610 (Kiefer et al., 2015)
aip1.2-1 gAIP1-2-mCherry	*pAIP1-2 : gAIP1-2-mCherry : 3'UTR(AIP1-2)*	Kiefer et al., 2015
aip1.2-1 AIP1-1-mCherry	*pAIP1-2 : gAIP1-1-mCherry : 3'UTR(AIP1-2)*	see 2.4.2
aip1.2-1 Ddaip1-mCherry	*pAIP1-2 : coDdaip1(cds)-mCherry : 3'UTR(AIP1-2)*	see 2.4.2
aip1.2-1 mCherry-Ddaip1	*pAIP1-2 : mCherry-coDdaip1(cds) : 3'UTR(AIP1-2)*	see 2.4.2
aip1.2-1 act7-6 gAIP1-2-mCherry	*pAIP1-2 : gAIP1-2-mCherry : 3'UTR(AIP1-2)*	*aip1.2-1 act7-6* X *aip1.2-1 gAIP1-2-mCherry* (Kiefer et al., 2015)
aip1.2-1 act7-6 AIP1-1-mCherry	*pAIP1-2 : gAIP1-1-mCherry : 3'UTR(AIP1-2)*	see 2.4.2
aip1.2-1 act7-6 Ddaip1-mCherry	*pAIP1-2 : coDdaip1(cds)-mCherry : 3'UTR(AIP1-2)*	see 2.4.2
aip1.2-1 act7-6 mCherry-Ddaip1	*pAIP1-2 : mCherry-coDdaip1(cds) : 3'UTR(AIP1-2)*	see 2.4.2

2.4.3 Transformation of *Agrobacteria tumefaciens*

Agrobacterium tumefaciens strain GV3101 was cultured in liquid YEB media (Beef extract 5 g/l, Yeast extract 1 g/l, Peptone 5 g/l, Sucrose 5 g/l, $MgSO_4$ 0.5 g/l) with rifampicine, gentamycine and tetracycline. Electro-transformation was performed using preset program 2 on a MicroPulser Electroporator (BioRad, USA). Transformed cells were transferred into 2 ml liquid YEB media without antibiotics and shaken at 300 rpm for 2 h. After that, cells were pelleted and spread on YEB agar containing all necessary antibiotics for selection. Colonies were grown over 48 h at 28°C.

2.4.4 Transformation of Plants by Floral Dipping

Transformation of plant lines was performed following the floral dipping method established by Clough and Bent (Clough et al., 1998). Plants for transformation were grown in four seedlings in one pot. The main shoot was cut away after reaching a height of 2 cm to initiate the formation of an increased number of side branches leading to an increased number of floral buds being produced. After reaching a larger number of still closed flower buds, plants were dipped into the agrobacteria solution substituted with 100 μM acetosyringone 4 h before usage and additional 0.05% (v/v) Coatasil-77 detergent as well as 4% (w/v) sucrose directly before dipping. Dipping was performed for 15 sec with mild rotation and repeated after 5 min of drying. Plants were kept at 4°C overnight and then put back into the growth chamber. Later, seeds were collected and seedlings were treated with BASTA herbicide for the first selection of transformants. In the next generation, seedlings were additionally tested for homozygosity by fluorescence microscopy.

2.4.5 Crossing of Plants

Parental plant lines were grown on soil. Seedlings were transferred to fresh pots by planting two plants per pot. When reaching a state of numerous closed flower buds, the maternal plant inflorescences were emasculated by removing the stamen with fine forceps (Dumont No. 5) employing a binocular stereo microscope. On the next day, the pollen of the parental plants was applied to the stigma. After the production of the fertilized siliques, the plant was bagged and the seeds were collected.

2.4.6 Extraction of Genomic Plant DNA for PCR

The extraction process of genomic plant DNA was based on Edwards et al., 1991. 1-2 small leaves were harvested and added to a reaction tube already containing five

2 mm glass beads. An extraction buffer was added and the sample was disrupted with a mini mixer mill. Samples were centrifuged at 1500g for 2 min. Centrifugation for 4 min at 1500g and RT followed after the addition of 0.5% (w/v) SDS and vigorously mixing the sample. The supernatant was transferred to a fresh reaction tube filled with an equivalent volume of isopropanol and was carefully mixed. After another centrifugation step for 15 min at 1500g and RT, the liquid was discarded and the pellet washed with 70% (v/v) EtOH, then incubated at RT for 10 min and finally centrifuged 5 min at 1500g. The Ethanol was removed and the pellet was dried. Samples were resuspended in TE buffer and frozen at -20°C.

2.4.7 Protein extracts from *A. thaliana* and SDS-PAGE

Thirty-five 5-day-old seedlings grown on MS media agar plates were harvested and flash-frozen in reaction tubes including 2 mm glass beads using liquid nitrogen. After grinding the samples by using a mini mixer mill, the same volume of ice-cold extraction buffer was added and mixed until the plant powder had dissolved. Samples were centrifuged at 4°C at approximately 20,000g for 10 min and the supernatant was transferred to a fresh tube. Samples could be stored at -80°C. Prior to electrophoresis the samples were mixed 1:3 with SDS sample buffer and incubated at 70°C for 30 min. Discontinuous SDS-PAGE was performed using a Biorad mini-gel system chamber. 12.5% polyacrylamide separation gel with a depth of 1.5 mm was run for 1.5 h at 120 V. A molecular weight standard (Thermo Scientific; PageRuler Prestained Protein Ladder; #26616) was run together with 50 μl of each the samples. Subsequently, the gel was subjected to immunoblotting and protein detection (described in 2.2.2).

2.4.8 Germination Rate

Seeds were sterilized and stratified as mentioned above. 5 days after plating on MS agar plates and initiating growth in the chamber, the ratio of germinated seedlings to all spread seeds was calculated.

2.4.9 Measurement of Main Stem Length

Seeds of all plant lines of interest were sown on the soil. Four seedlings per line were pricked after approximately 8 days and transferred to their own pots. Five weeks after seeding the main stalk length was measured by hand.

2.4.10 Analysis of Curled Stems

Photos from plants used for measurement of main stem length were taken using a Nikon D750 camera with an additional Nikkor AF-S 50mm objective. The ratio of curled stems to the number of total stems per genotype was then calculated from the counts by hand.

2.4.11 Root Hair Positioning in Single Mutant and Rescue Lines

The root hair positions of different plant lines were determined by a quantitative method reported previously (Fischer et al., 2006). In brief, the ratio of the distance from the root hair emerging site to the basal end of the cell divided by the full cell length is calculated. Five-day-old seedlings were transferred from the upright incubated agar plate to a 6-well plate and cleared with a mixture of 70% (v/v) ethanol and 30% (v/v) clearing solution (chloralhydrate, glycerol, and H_2O (8:3:1 in w:v:v)). Seedlings were mounted on a glass slide in only clearing solution, covered with a cover glass, and sealed to prevent the slide from drying out. Slides were kept in the fridge for further analysis. Measurements were done in a single-blind experiment. Images have been taken using a Zeiss Axio Imager M.2 microscope with ZEN software equipped with a PlanApochromat 20x/0.8M27 objective, AxioCamMRR3 camera, and using the DIC method. Six independent experiments each including 50 root hair cells distributed on a minimum of 10 roots were performed, pooled, and analyzed. Two-sample Kolmogorov-Smirnov statistical significance test with a significance level of 0.05 was applied to the data for comparison of the different genotypes (c.f. Pietra et al., 2013).

2.4.12 Root Hair Growth in Single Mutant and Rescue Lines

To analyze root hair growth, plant lines were grown in glass bottom chambers in a 70° almost upright position on MS media in long-day conditions (see 2.4.1 for media and Nakamura et al., 2018b for method). 5 days after germination, the root hairs were imaged using the ZEN software on a ZEISS confocal LSM 880 with Airyscan in Fast mode and LD LCI Plan-Apochromat 40x/1.2 Imm Korr DIC M27 Objective. 488 nm laser with 5.5% intensity for GFP excitation and 561 nm laser with 4% intensity for mCherry excitation were applied to visualize GFP-ABD2-GFP as actin cytoskeleton marker (Wang et al., 2008) and mCherry-tagged Aips. Images were taken every 30 sec over a time interval of 10 min. Image sequences were opened with the open-source image processing tool Fiji (based on ImageJ software). The

tip of the growing root hair was followed by the Manual Tracking plugin and the growth rate was calculated in MS Excel.

2.4.13 Confocal LSM Image Acquisition with Airyscan

To verify the expression of the desired rescue constructs of Aip1, AIP1-1 and AIP1-2 in mutant *A. thaliana* plant lines, fluorescent images of root hairs on seedlings of transformed plant lines were taken using the ZEN software on a ZEISS confocal LSM 880 with Airyscan mode and Plan-Apochromat 63x/1.4 Oil DIC M27 objective. The 561 nm laser with 0.2% laser power was used for mCherry excitation to visualize mCherry-tagged Aips in all rescue lines.

Part I

Coronin-A Mutants

3 Results

Coronin is an active player in actin treadmilling and is therefore important for the amoeboid movement of *D. discoideum*. It interacts with the Arp2/3 complex, which is responsible for actin branching, and with cofilin, which cuts ADP-bound actin into small fragments. Another important function is the dimerization of Coronin-A to cross-link actin filaments. The possibility of gaining more insight into the creation of stable knockouts as well as the creation of sudden loss-of-function mutants by using CID is described in the following part. If a knockout or loss of function mutant of a particular gene is unstable and tends to revert, a solution to overcome this problem should be found. In this thesis, different ways of generating mutants at different levels of protein biosynthesis are investigated. The commonly used classical but reverting CorA loss-of-function mutant will be characterized and compared to a stable knockout generated by the SLI method. Since both methods are based on mutations in the genome, another method focuses on the degradation of Coronin-A mRNA using the RNAi technique to generate a knockdown mutant. Finally, the CID of the tagged protein of interest is induced to generate a loss-of-function mutant that can be switched on and off (knock sideway, KS, see Section 1.7).

All cell lines were evaluated for proliferation rate, ability to produce fruiting bodies and viable spores, cell morphology, cell size, and motility. PCR was performed on extracted gDNA to ensure the correct insertion of the plasmid into the genome. Qualitative evidence for the presence of CorA protein, as well as semi-quantitative analysis of CorA in RNAi mutants, was obtained by protein detection (Western blotting). The characterization of each strain was completed by a motility assay. To obtain doubling rates of the strains, the cell lines were grown in a shaking culture with a defined initial concentration. Every 8 hours the cell concentration was counted and a growth curve was plotted. To observe fruiting body formation, cells were washed to remove residual media and plated on Sørensen buffer agar plates. Photographs were taken at different magnifications immediately after initiation and repeatedly every 24 hours for up to three days. PCR and immunoblot were performed to detect mutations at the gene and protein levels. One of the main focuses was on the movement of *Dictyostelium* cells. To test their motility, cells were seeded at low density in 24-well glass bottom plates and observed by taking images every 30 seconds for 2 hours using a laser scanning microscope and a program-controlled moving stage. After the images were exported, a MATLAB® (2019b, MathWorks,

Natick, MA, USA) routine segmented the cells in the images, calculated their centroid, and tracked the particles (based on Crocker et al., 1996). The resulting tracks were then plotted on the brightfield images (e.g. in Figure 3.1) to allow easy manual selection of misallocated tracks.

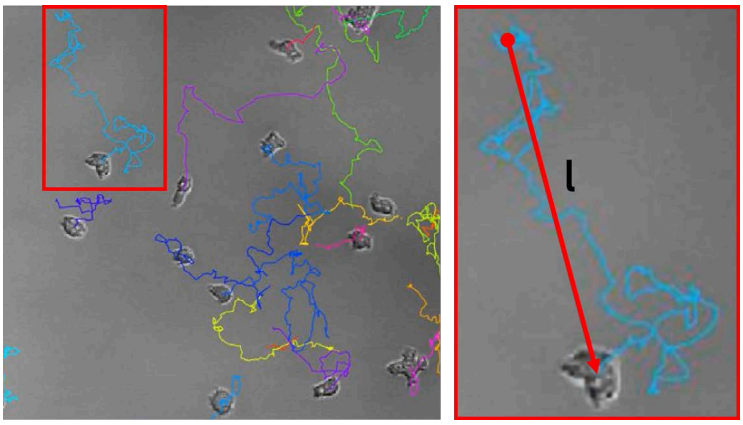

Fig. 3.1: Example of the tracking of cells in motility assay; cells were imaged over 2 hours taking 2 frames per minute; images were segmented and centroids of the cells were tracked using an algorithm based on Crocker et al., 1996; tracks were then overlaid on brightfield images for further manual sorting (left); l: displacement in 10 min (right).

Motility in this work is represented by the mean displacement of cells in a given interval. The full two hours of measurements for a strain can be plotted as a mean squared displacement (MSD) analysis, which has already been described in the methods section of this thesis (see 2.3.11). MSD is a well-established method often used by biophysicists and in colloidal studies to find the displacement mode of a given particle followed over time. MSD can also be used to estimate the parameters of the motion, such as the diffusion coefficient and the persistence time. As shown in Figure 3.2, the MSDs of different amoeba strains can be compared in a single plot. The three different strains shown here as an example move differently depending on whether a shorter (1 minute) or a longer (10 minutes) time interval is observed (see Figure 3.2 MSD of the CorA-null strain compared to the stable AX2 and the knockout *corA*-SLI).

The MSD of *D. discoideum* cells is known to have an anomalous diffusive behavior, typically ranging from superdiffusive to small subdiffusive exponents with increasing observation time (Cherstvy et al., 2018). However, as shown in Figure 3.2, mutations in the actin treadmilling machinery can also affect this property and lead to an even more variable course of the displacement curve. It is important to choose a time interval for comparison that is in a more robust regime of the MSD curve when displacement, rather than velocity, is desired as an observable. In non-polarized cells, the movement of the centroid of the cells in smaller time intervals of up to 1 minute is mostly due to the formation of pseudopods and does not depend on the

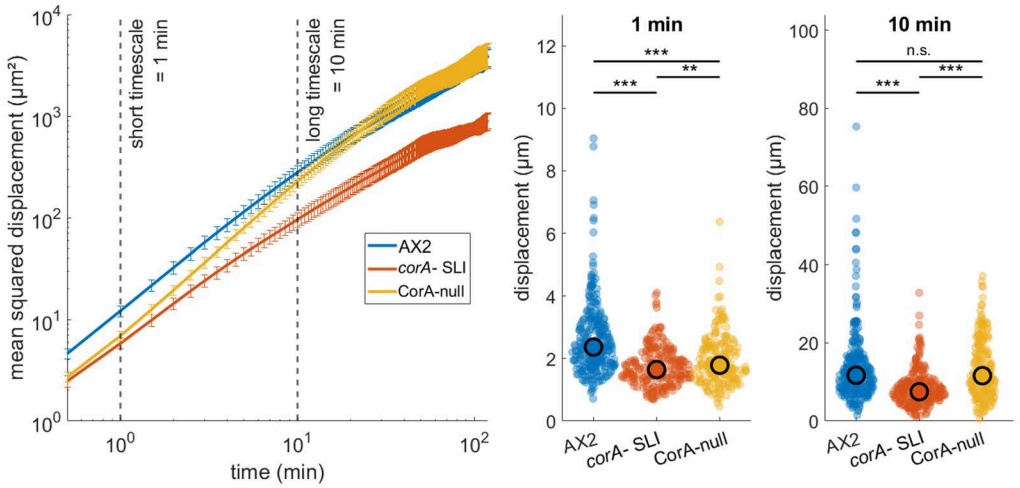

Fig. 3.2: Exemplary motility analysis of *D. discoideum* wildtype, *corA*-SLI and CorA-null mutant cells based on displacement statistics, illustrating that the result of a comparison of strains depends on the considered time interval. Left: log-log plots of mean-square displacement (μm2) plotted versus time. Mean values of at least six independent experiments with corresponding standard error (SE) are displayed to indicate reproducibility of results. Timescales of 1 and 10 minutes are indicated. Right: means of the displacement (μm2) after one and ten minutes for n $\approx 10^2$ cells (for the exact number of analyzed cells see SI 10.3) pooled from at least six independent experiments are displayed in violin plots for the genotypes outlined above. Black circles indicated median values. p-values obtained from Kolmogorov-Smirnov statistical test for differences between distributions are displaced by asterisks: n.s.: not significant at a significance level of 0.05; *: p-value$\leq$ 0.05, **: p-value$\leq$ 0.01, ***: p-value$\leq$ 0.001.

directed movement of the cell. Therefore, a time interval larger than the known persistence time of *D. discoideum* cells of about 8.8 min (Li et al., 2008) was chosen for further investigations (see Figure 3.2, right side, 10 min, violin plot). About one hundred trajectories per strain were pooled and plotted in the MSD curve as explained in Chapter 2.3.11 (for distribution of track lengths and exact numbers see Supplementary Figure 10.7 and Table 10.3). The distribution of displacements at the 10-minute time point was plotted in a violin plot, which can be read like an upright histogram. The broader the distribution, the more data points are at the same displacement value. All the smaller points represent the results of one averaged cell track each, and the one larger point shows the median of the entire distribution, which was chosen as a more robust measure with respect to outliers than the mean (for more details see Chapter 2.3.11).

3.1 Validation of Genetic Modifications and Immunoblot for Coronin-A Protein Detection

Before starting any experiments, all cell lines were checked for their genetic background and production of the protein of interest. This will serve as a control to show the success of the SLI method in *D. discoideum*. Pre-designed primer pairs were used in a polymerase chain reaction (PCR) to verify the correct insertion site of the SLI plasmid into the genome (for primer sequences and design, see Supplementary 10.2). The AX2 cell extract was run with all primer combinations (see Figure 3.3, table) as a wildtype positive control and to ensure non-specific binding of the primer pairs to *D. discoideum* gDNA (see Figure 3.3, lower part, middle right). The negative control was a template-free mixture containing all other components. The correct concentrations in the reaction mix were maintained by replacing the sample with deionized water (see Figure 3.3, bottom, right). Effective gDNA extraction was demonstrated by PCR using Arp2 as a housekeeping gene. By obtaining the correct size band around 1000 bp using Arp2 forward and backward primers (see Figure 3.3, lane 7 and table below), it was shown that all samples contained sufficient gDNA for PCR. The negative controls did not show any bands as predicted. In AX2 wildtype cell extract, the size of the bands for *aip1* (lane 1) and *corA* (lane 2) are consistent with the designed primer binding sites on the endogenous genes. Primers binding to any integration-specific site did not give a signal (lanes 3-6), thus ensuring the specificity of the primer pairs for these reactions. Aip1-null#9.1 cell extract was only tested for the *aip1* insertion mutation (lane 1) and sufficient gDNA extraction (lane 7). In the *corA* SLI cell extract PCR reaction on *aip1*, the wildtype gene could be amplified. The primer pair CorA a and CorA b did not produce a fragment, which would only be the case if the integration of the plasmid at this position was not successful. Both primer pairs confirming the 5' and 3' integration site of the plasmid (5' means upstream and 3' means downstream region of the gene of interest on the chromosome) produced DNA fragments of the correct size (lanes 3+5). The same results were shown for the double knockout (lanes 3+5) in addition to the *aip1* gene disruption (lane 1). Thus, the PCR results demonstrated the integration of the SLI plasmid into the Aip1-null#9.1 mutant background. The CorA-null HG1569#1 loss-of-function mutant also showed no band at the wildtype *corA* level (lane 2), which was identical in the Aip1-/CorA double-null mutant. According to their genetic background, the *aip1* gene was not disrupted in CorA-null cells, but mutated in the double-null strain. To validate the knock sideway (KS) mutation, gDNA from CorA-KS and double-KS cell lines were used as templates in a PCR with specific primer pairs for the 5' and 3' region of the integration site (see Figure 3.3, lower left, lanes 4+6) and produced the expected size fragment. The wildtype Coronin-A coding gene primers were also run on the samples. As shown in lane 2, the

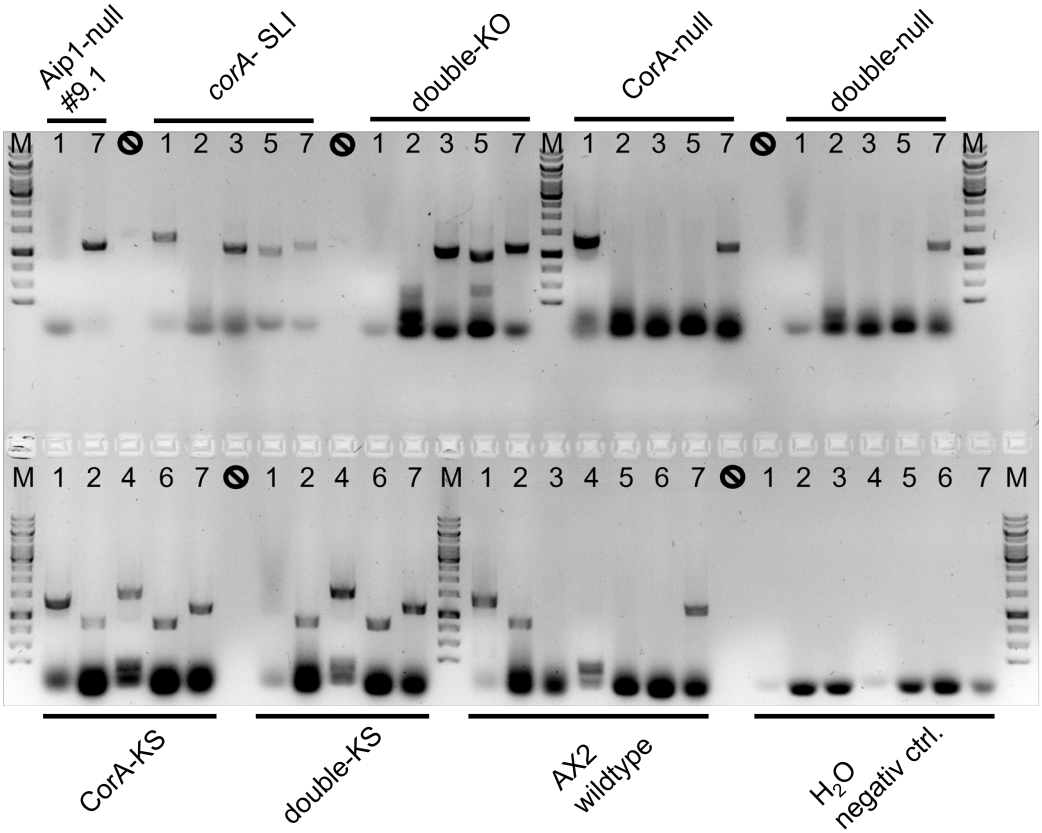

Gene:	Primer combination: No.	P1	P2	Function:
Aip1	1	Aip1 a (fwd)	Aip1 b (rev)	knockout check
Cor A	2	CorA a (fwd)	CorA b (rev)	knockout check
	3	CorA a (fwd)	G418 (rev)	5‘ integration check for SLI knockout
	4	CorA a (fwd)	GFP (rev)	5‘ integration check for SLI knocksideway
	5	bla (fwd)	CorA b (rev)	3‘ integration check for SLI knockout
	6	B4BamHI (fwd)	3‘UTR (rev)	3‘ integration check for SLI knocksideway
Arp 2	7	Arp2 (fwd)	Arp2 (rev)	housekeeping gene for gDNA check

Fig. 3.3: PCR to confirm the *aip1* and *corA* knockouts, as well as the validation of knock sideway constructs on cell extracts of wildtype AX2 cells and *corA* single and Aip1-null/*corA*- SLI double mutants knockouts and knock sideways as well as loss-of-function cell lines; M: Marker, wildtype AX2; Aip1-null#9.1 mutant (see Konzok et al., 1999); *corA*- SLI: *corA* knockout done with SLI method (see 1.7); double-KO: *corA* knockout done with SLI method (see 1.7) in Aip1-null mutant; CorA-null: classical gene disruption mutant of *corA* CorA-null HG1569#1 (see Hostos et al., 1993); CorA-KS: Coronin-A knock sideway done with SLI method; double-KS: Coronin A knock sideway done with SLI method in Aip1-null mutant.

reactions produced a fragment on both strains, as the *corA* gene should still be functional, although tagged with GFP and the 2x FKBP domain. Overall, the results of the polymerase chain reactions confirmed the expected outcome of the analysis

and proved the correct genetic background of all strains. The presence of the RNAi plasmids, as well as the overexpression plasmid for tagged Coronin-A and the mitochondrial anchor in the wildtype and Aip1-null background, could only be proven by resistance to the corresponding selection antibiotics and the resulting expression of fluorescence-labeled proteins observed under LSM and detected by immunoblot (see below).

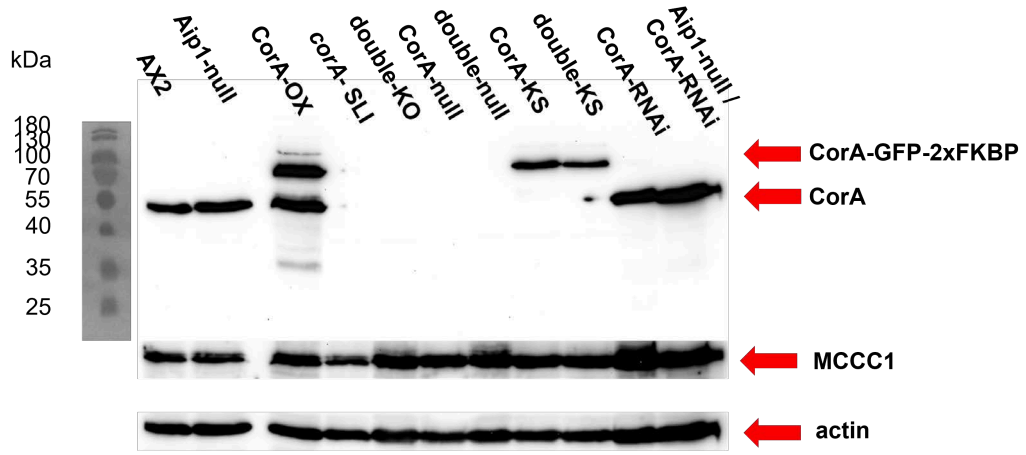

Fig. 3.4: Western blot (immunoblot) for detection of Coronin-A on cell extracts of wildtype AX2 cells, *corA* single and Aip1-null/*corA*- SLI double knockouts and knock sideways as well as loss-of-function cell lines, CorA overexpressor and RNAi in AX2 and Aip1-null background; wildtype AX2, Aip1-null#9.1 mutant (see Konzok et al., 1999); CorA-OX: knock sideway overexpressor; *corA*- SLI: *corA* knockout done with SLI method (see 1.7); double-KO: *corA* knockout done with SLI method (see 1.7) in Aip1-null mutant; CorA-null: classical gene disruption mutant of *corA* CorA-null HG1569#1 (see Hostos et al., 1993); double-null: Aip1-/CorA- strain (Ishikawa-Ankerhold et al., 2010; CorA-KS: Coronin-A knock sideway done with SLI method; double-KS: Coronin A knock sideway done with SLI method in Aip1 mutant; CorA-RNAi: knockdown; Aip1-null/CorA-RNAi: knockdown of CorA in Aip1-null background; MCCC1 and Actin as loading controls (see 2.1.2 for antibodies); one representative example of three independent experiments.

To verify the expression of Coronin-A at the protein level, protein extracts of all strains of interest were subjected to immunoblotting and Coronin-A was detected with specific antibodies (see 2.2.2 and 2.1.2 for methods and materials) as shown in Figure 3.4. The expected molecular weight of native Coronin-A is 49 kDa. The tagged knock sideway version consisting of Coronin-A, GFP, and 2x FKBP domains weighs about 90 kDa. By using a protein weight standard, the two expected bands could be assigned. In AX2 cells only native Coronin-A is present. The CorA overexpressor (OX) strain contains both native Coronin-A and the knock sideway construct with a weight 40 kDa higher. The amount of the knock sideway construct is similar to that of Coronin-A expressed under its endogenous promoter, as indicated by the same strength of the two bands. A small amount of a cleavage product of about

35 kDa is also present. In Aip1-null#9.1 mutant cells, the Coronin-A band shows a strong signal. Consistent with the PCR results, the knockout and loss-of-function mutants show no signal at all in the Coronin-A detection. The integration of the SLI knockout construct and its expression could be verified, as no native Coronin-A was detectable in these samples. Surprisingly, neither in the AX2 background nor in the Aip1-null#9.1 mutant background did RNAi knockdown lead to a significant reduction of Coronin-A protein levels. The overall results show that the SLI mutation method for creating a knock sideway in addition to a novel knockout method can be successfully applied to *D. discoideum corA* gene in both wildtype and Aip1-null#9.1 backgrounds, while overexpression of tagged Coronin-A resulted in a degradation product.

3.2 Classical Gene Disruption vs. SLI Knockout Method

3.2.1 Generation Time + Fruiting Body Formation

The growth of each strain was determined by counting the cell density every 8 hours in the exponential growth phase in a liquid HL-5 shaking culture. The generation time was then calculated (see 2.3.6) and the exponential growth was plotted in a linear-log plot (see Figure 3.5). AX2 wildtype cells had a doubling time of approximately 11 hours. Aip1-null and *corA*-SLI knockout cells showed a much slower growth rate of almost 20 hours, which is almost double the time of the wildtype strain. The slowest growth rates were observed for the CorA-null loss-of-function mutant and the double knockout created by SLI, similar to the double-null mutant.

The formation of fruiting bodies to maintain colony survival was another factor that characterized the *corA* mutants and double mutants in contrast to the wildtype and the Aip1-null#9.1 single mutant. AX2 cells for reference were able to produce spores in a short time of about 24 hours (see Figure 1.1). The following images were taken during differentiation after 48 hours of starvation on agar plates (see Figure 3.6). AX2 cells were able to form huge fruiting bodies about 100μm in diameter containing a large number of spores. Aip1-null cells formed smaller fruiting bodies but were still able to fully differentiate. Both *corA* single mutant cell lines (*corA*- SLI and CorA-null) showed aberrant and delayed fruiting body formation after 48 hours of starvation. While most of the *corA* knockout cells were still in the aggregation phase, the CorA-null strain already formed fruiting bodies from the Mexican hat phase. The double knockout was not able to form any aggregates at all and was still

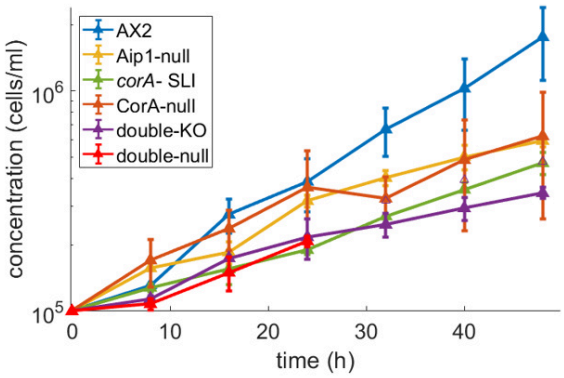

strain	generation time (hours)
AX2	11.3
Aip1-null	19.7
corA-SLI	20.9
CorA-null	26.4
double-KO	27.0
double-null	17.2

Fig. 3.5: **Growth curves in semi-log plot and generation times of different cell strains of *D. discoideum***; wildtype AX2, *corA* knockout done with SLI method (see 1.7), classical gene disruption mutant of *corA* CorA-null HG1569#1 (see Hostos et al., 1993), Aip1-null#9.1 single mutant (see Konzok et al., 1999); *corA* knockout done with SLI method (see 1.7) in Aip1-null mutant and classical gene disruption mutant of *corA* in Aip1-null mutant (see Ishikawa-Ankerhold et al., 2010). Left: Mean cell concentration in shaking culture in HL-5 media (see 2.3) measured in a period of 48 hours, counted as duplicates in 8 hours intervals in two independent experiments, calculated by averaging the mean cell concentration determined for each experiment; error bars show the absolute difference between them. Right: Generation times were determined by an exponential fit.

unable to produce fruiting bodies after 72 hours. The double-null mutant also failed to aggregate. However, parts of the colony seemed to form a miniature version of the finger phase (see Figure 3.6, lower right).

Spores from AX2 wildtype cells were approximately 3 x 8 μm in size and had a homogeneous appearance (see Figure 3.7, top left). The spores of the Aip1-null#9.1 mutant strain were indistinguishable from the wildtype spores. Both types of spores had high viability when resupplied with nutrients. In contrast, the *corA* knockout showed opposing results. The viability of the spores was very low and long-term storage could only be achieved by freezing the cells or using a very high concentration of spores to maximize the chance of survival. As shown in the upper right image in Figure 3.7, the shape of the spores was much more rounded and the spores themselves were shorter and less uniform in size. Interestingly, the CorA-null cells were able to form naturally shaped and sized spores that had medium viability compared to the *corA* knockout and AX2 cells. The double-null mutant did not produce an adequate number of spores because it was still impaired in the formation of fruiting bodies. The few spores produced had strongly reduced viability, even less than the single *corA* knockout. The double knockout did not produce any spores at all because differentiation had already stopped by not reaching the aggregation phase.

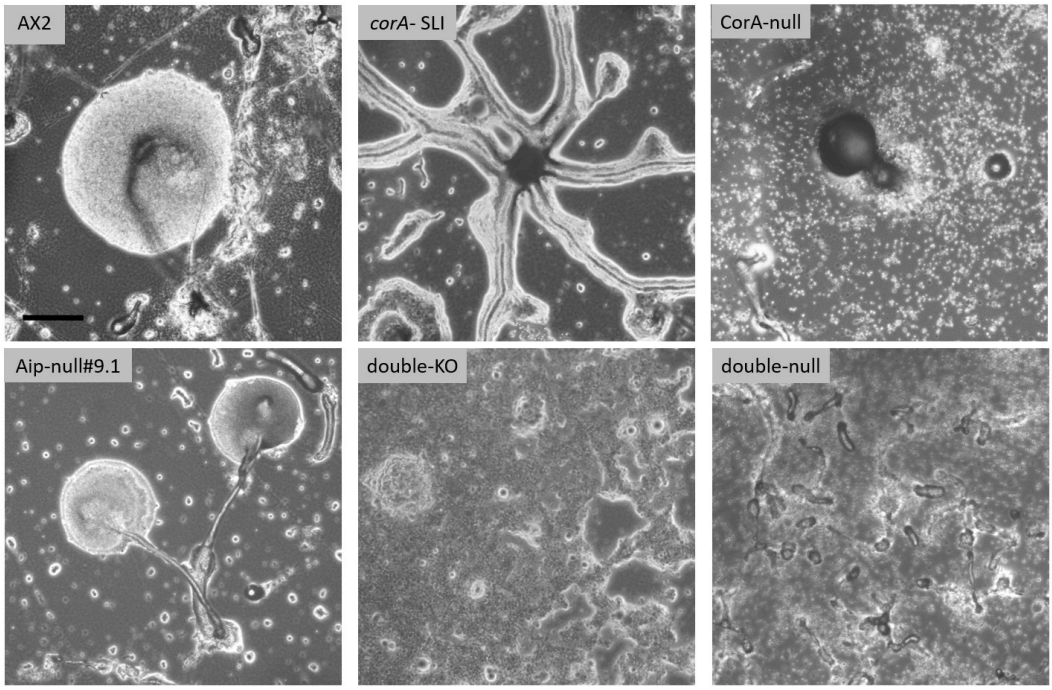

Fig. 3.6: Differentiation in starvation process after 48h of wildtype AX2 cells and *corA* single and Aip1-null/*corA*- double mutants created by different methods; upper left: wildtype AX2, upper middle: *corA* knockout done with SLI method (see 1.7), upper right: classical gene disruption mutant of *corA* CorA-null HG1569#1 (see Hostos et al., 1993), lower left: Aip1-null#9.1 mutant (see Konzok et al., 1999); lower middle: *corA* knockout done with SLI method (see 1.7) in Aip1-null mutant, lower right: classical gene disruption mutant of *corA* in Aip1-null mutant (see Ishikawa-Ankerhold et al., 2010); scale bar: 50μm.

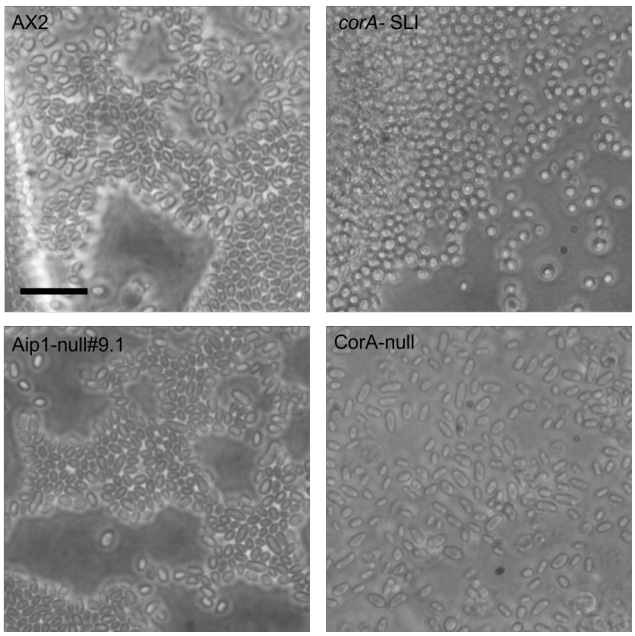

Fig. 3.7: Spores after 48h of wildtype AX2 cells and *corA* mutants created by different methods; upper left: wildtype AX2, upper right: *corA* knockout done with SLI method (see 1.7), lower left: Aip1-null#9.1 mutant (see Konzok et al., 1999); lower right: classical gene disruption mutant of *corA* CorA-null HG1569#1 (see Hostos et al., 1993); both Aip1-null/*corA*- double mutants did not form spores within 48 hours or 72 hours, scale bar: 20μm.

3.2.2 Cell Size and Morphology

Not only the growth rate and the ability to form fruiting bodies were different when comparing the two *corA* mutant strains. Figure 3.8 shows that the variation in cell size and morphology in wildtype AX2 cells was less than in both knockout cell lines, although the loss-of-function mutant had even larger cells. Analysis of the cell area of the wildtype AX2 cells using brightfield images revealed a much narrower distribution compared to both knockout strains. This demonstrated the homogeneity of size in the wildtype cells. The *CorA* mutants varied much more in cell area and also showed enormously large cells up to 700μm^2, which was more than twice the size of the largest detected wildtype cell with a cell area of about 300μm^2 (see Figure 3.9). The distribution of cell areas in the loss-of-function mutant was the widest and showed a clear shoulder at higher areas, demonstrating the diversity of cell areas and the higher incidence of larger cells in this strain. A size of about 1.5 to 2 times larger than in AX2 cells was most common. Therefore, the significant difference in all strains in the cell size distributions was not surprising.

Circularity was determined as a parameter for the influence of the mutations on the morphology of the cells (for details see Chapter 2.3.9). While wildtype AX2 cells showed similar results to the loss-of-function mutant, the SLI knockout cells showed more circular cells, although all three strains differed significantly from each other (see Figure 3.9, right).

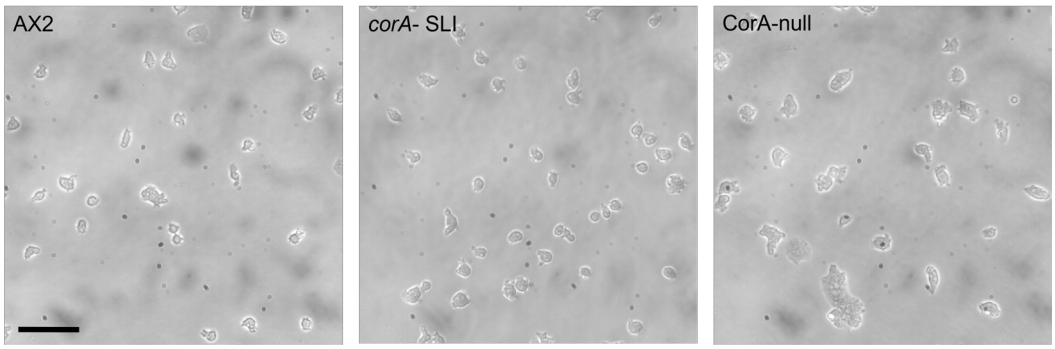

Fig. 3.8: Example of brightfield images for morphological analysis and determination of the cell size in wildtype AX2 cells and *corA* mutants created by different methods; left: wildtype AX2, middle: *corA* knockout done with SLI method (see 1.7), right: classical gene disruption mutant of *corA* CorA-null HG1569#1 (see Hostos et al., 1993); scale bar: 50μm.

Taken together, the results showed that the two mutation methods manifest themselves in opposite ways with respect to cell size and morphology of single mutant cells. This was in contrast to the results obtained in Aip1-null/*corA* double mutants. In both double mutants, cell size was more heterogeneous and, on average, in-

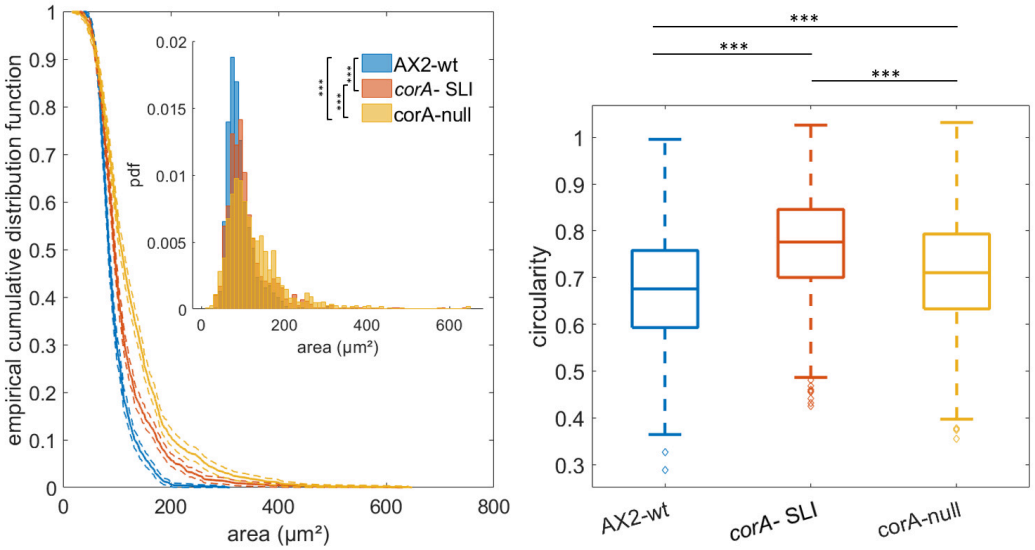

Fig. 3.9: Cell size and cell circularity distributions of *D. discoideum* wildtype AX2 cells and *corA* mutants created by different methods; SLI: *corA* knockout done with SLI method (see 1.7), null: classical gene disruption mutant of *corA* CorA-null HG1569#1 (see Hostos et al., 1993). Left: empirical cumulative distribution function of the cell area, calculated from n $> 10^3$ independent cells, along with 95% confidence interval; inlet: normalized histogram of the same cell areas, giving a sense of the underlying probability density function (pdf). Right: circularity as the parameter for morphological differences, calculated from the same 10^3 cells, graphically represented in box-plots showing the median (line), the lower and upper edge of the box indicate the 25% and 75% percentiles, and whiskers representing ± 2.7 SD; values outside of whiskers are explicitly plotted by points (outliers). p-values obtained from Kolmogorov-Smirnov statistical test for differences between distributions (see SI Table 10.3) are displayed by asterisks: n.s.: not significant at a significance level of 0.05; *: p-value$\leq$ 0.05, **: p-value$\leq$ 0.01, ***: p-value$\leq$ 0.001.

creased. Multinucleated cells of different sizes were more frequent (see Figure 3.11) and the cell size distribution was comparable to that of the CorA-null single mutant (see Figure 3.9). The cells of the double mutants were intermittently clustered (see Figure 3.10), which did not appear to be the case in wildtype or single mutants. All cell size distributions were significantly different from each other. The loss of Aip1 function in the Aip1-null#9.1 mutant did not seem to affect morphology, while the median circularity of the cells was increased in both double mutant strains (see Figure 3.10), although all four strains still differed significantly from each other (see Figure 3.11, right).

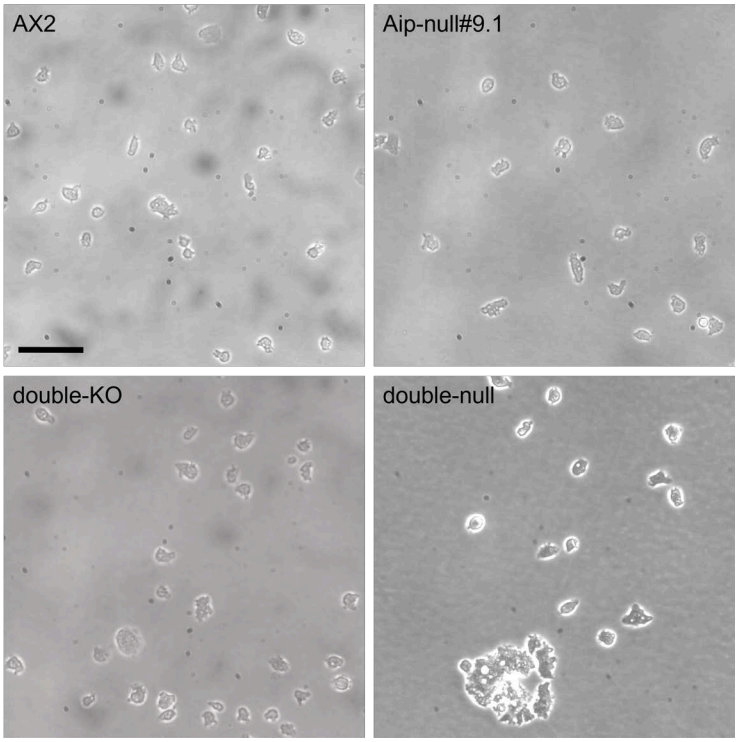

Fig. 3.10: Example of brightfield images for morphological analysis and determination of the cell size in wildtype AX2 cells and Aip1-null/*corA*- double mutants created by different methods; upper left: wildtype AX2, upper right: Aip1-null#9.1 mutant (see Konzok et al., 1999); lower left: *corA* knockout done with SLI method (see 1.7) in Aip1-null mutant, lower right: classical gene disruption mutant of *corA* in Aip1-null mutant (double-null mutant; see Ishikawa-Ankerhold et al., 2010); scale bar: 50μm.

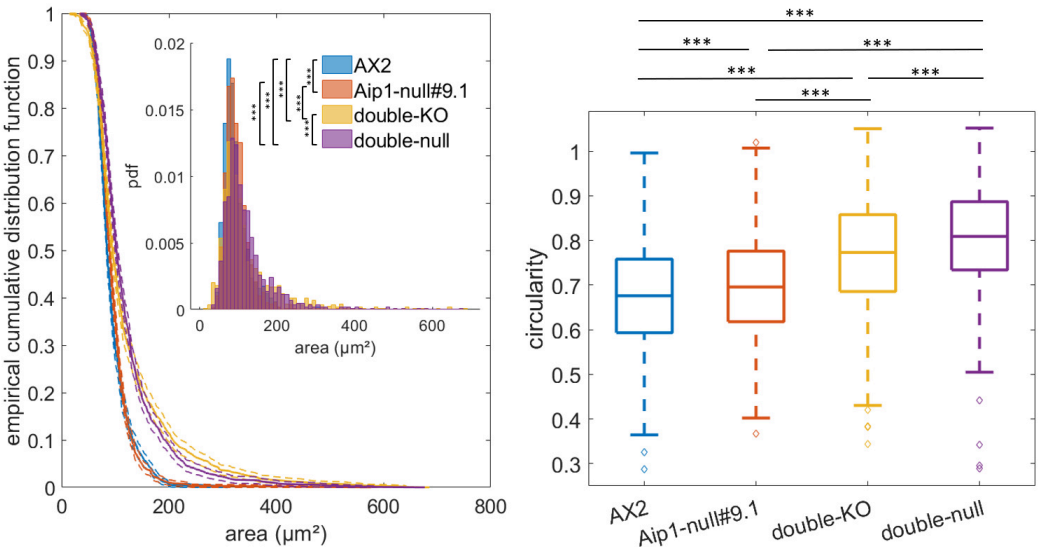

Fig. 3.11: Cell size and cell circularity distributions of *D. discoideum* wildtype AX2 cells and Aip1-null/*corA*- double mutants created by different methods; Aip1-null#9.1 single mutant (see Konzok et al., 1999); double-KO: *corA* knockout done with SLI method (see 1.7) in Aip1-null mutant, double-null: classical gene disruption mutant of *corA* in Aip1-null mutant (see Ishikawa-Ankerhold et al., 2010); Left: empirical cumulative distribution function of the cell area, calculated from $n > 10^3$ independent cells, along with 95% confidence interval; inlet: normalized histogram of the same cell areas, giving a sense of the underlying probability density function (pdf). Right: circularity as the parameter for morphological differences, calculated from the same 10^3 cells, graphically represented in box-plots showing the median (line), the lower and upper edge of the box indicate the 25% and 75% percentiles, and whiskers representing ± 2.7 SD; values outside of whiskers are explicitly plotted by points (outliers). p-values obtained from Kolmogorov-Smirnov statistical test for differences between distributions (see SI Table 10.3) are displayed by asterisks: n.s.: not significant at a significance level of 0.05; *: p-value$\leq$ 0.05, **: p-value$\leq$ 0.01, ***: p-value$\leq$ 0.001.

3.2.3 Motility

The motility of wildtype and *corA* mutant cells was quantified by the averaged tracked displacement of individual cells in a given time. As shown in Figure 3.12, the mean squared displacement (MSD) of AX2 wildtype cells is significantly higher than that of *corA* SLI mutant cells. Although the shape of the two curves is nearly identical, the mutant curve appears to be shifted to lower values, i.e. the MSD is generally smaller.

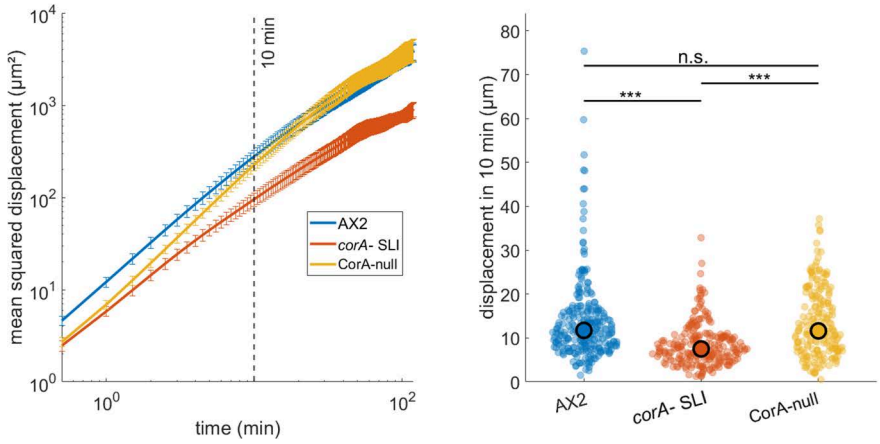

Fig. 3.12: Motility analysis of *D. discoideum* wildtype, *corA*-SLI and CorA-null mutant cells. Left: log-log plots of mean-square displacement (μm2) plotted versus time. Mean values of at least six independent experiments with corresponding standard error (SE) are displayed to indicate reproducibility of results. Right: means of the displacement (μm2) after ten minutes for n $\approx 10^2$ cells (for the exact number of analyzed cells see SI 10.3) pooled from at least six independent experiments are displayed in violin plots for the genotypes outlined above. Black circles indicated median values. p-values obtained from Kolmogorov-Smirnov statistical test for differences between distributions are displaced by asterisks: n.s.: not significant at a significance level of 0.05; *: p-value$\leq$ 0.05, **: p-value$\leq$ 0.01, ***: p-value$\leq$ 0.001.

The CorA-null mutant showed a variation in displacement. For minute time scales, it followed the behavior of the SLI mutant, but for times between 2 and 10 minutes, it approximated the wildtype displacement until it completely reached the wildtype level. In a direct comparison of the displacement distributions of both mutants and wildtype AX2 at 10 minutes, the CorA-null mutant was not significantly different from the wildtype, whereas it was different at an interval of less than 2 minutes (see Figure 3.12).

In contrast to the two *corA* mutants, the Aip1-null#9.1 mutant had a lower displacement over the entire period examined (see Figure 3.13). Compared to the *corA* knockout, the MSD was not as much reduced, but still lower than the wildtype

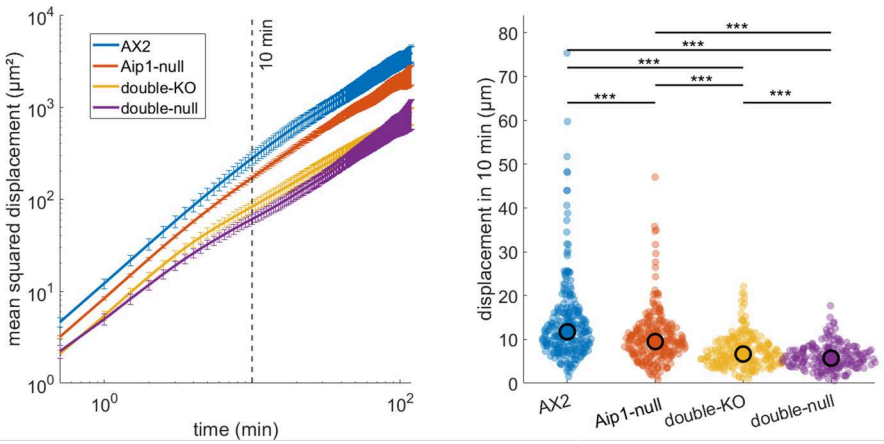

Fig. 3.13: Motility analysis of *D. discoideum* wildtype, Aip1-null single mutant and Aip1-null/*corA*- double mutants created by different methods; double-KO: *corA* knockout done with SLI method (see 1.7) in Aip1-null mutant; Aip1-null#9.1 single mutant (see Konzok et al., 1999); double-null: classical gene disruption mutant of *corA* in Aip1-null mutant (see Ishikawa-Ankerhold et al., 2010). Left: log-log plots of mean-square displacement (μm2) plotted versus time. Mean values of at least six independent experiments with corresponding standard error (SE) are displayed to indicate reproducibility of results. Right: means of the displacement (μm2) after ten minutes for n $\approx 10^2$ cells (for the exact number of analyzed cells see SI 10.3) pooled from at least six independent experiments are displayed in violin plots for the genotypes outlined above. Black circles indicated median values. p-values obtained from Kolmogorov-Smirnov statistical test for differences between distributions are displaced by asterisks: n.s.: not significant at a significance level of 0.05; *: p-value$\leq$ 0.05, **: p-value$\leq$ 0.01, ***: p-value$\leq$ 0.001.

MSD. The shape of the curve was still comparable to that of the wildtype, which was also true for the double knockout (SLI). Cells from the double-null strain also showed a variation in MSD. All four strains differed significantly from each other (p-value$\leq$0.001), although the shift of both double mutants seemed to be similar.

3.3 RNA Interference (RNAi) - Knockdown of Coronin-A

The knockdown of proteins can be achieved by RNA interference (RNAi). In this case, short hairpin RNAs (shRNA) are produced in the cell from an introduced plasmid. These hairpin structures are then digested by endogenous enzymes and cut into small fragments. These fragments are bound to RNA-induced silencing complexes (RISC), which recognize mRNA strands with the appropriate sequence and destroy the mRNA by cleavage. Depending on the amount of mRNA and the efficiency of a single protein of interest, RNAi can result in a knockdown or even a near-knockout

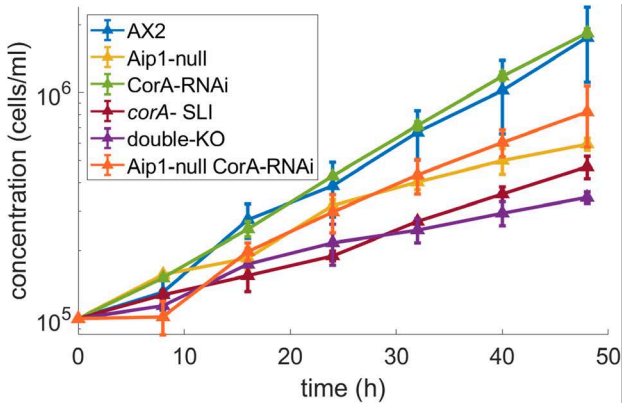

strain	generation time (hours)
AX2	11.3
Aip1-null	19.7
CorA-RNAi	11.0
corA- SLI	20.9
double-KO	27.0
Aip-null + CorA-RNAi	15.9

Fig. 3.14: **Growth curves in semi-log plot and generation times of different cell strains of *D. discoideum***; wildtype AX2, *corA* knockout done with SLI method (see 1.7), Aip1-null#9.1 single mutant (see Konzok et al., 1999); CorA-RNAi knockdown mutant; CorA-RNAi knockdown in Aip1-null mutant; *corA* knockout done with SLI method (see 1.7) in Aip1-null mutant background; Left: Mean cell concentration in shaking culture in HL-5 media (see 2.3) measured in a period of 48 hours, counted as duplicates in 8 hours intervals in two independent experiments, calculated by averaging the mean cell concentration determined for each experiment; error bars show the absolute difference between them. Right: Generation times were determined by an exponential fit.

phenotype. In this chapter, the CorA-null mutant is no longer considered, as there were several strong differences between the knockout and loss-of-function mutant strains. Since a knockdown of Coronin-A expression was assumed, the resulting plasmid-transformed strains were compared to the wildtype AX2 as well as to the *corA*- SLI knockout, which served as upper and lower limits of the possible results.

3.3.1 Generation Time + Fruiting Body Formation

The growth rate of CorA-RNAi-treated AX2 cells showed that there was almost no difference in generation time between wildtype and CorA-RNAi cells. Both had a doubling time of 11 hours. Cells with RNAi knockdown in the Aip1-null mutant background grew as fast as the single mutant Aip1-null cells alone, while for the single and double *corA* knockout extended growth rates of 20 hours and more were calculated (see Figure 3.14).

While *corA*-SLI mutant cells were severely impaired in fruiting body formation and double knockout cells were unable to produce spores at all (see 3.2.1 for details), the RNAi knockdown mutants showed a reduced differentiation capacity. Nevertheless, they were able to produce Mexican hat-like structures within 48 h after the onset of starvation (see Figure 3.15 top center). In the Aip1-null#9.1 mutant background, RNAi did not have a strong effect on cell differentiation. After 48 hours, the phase of fruiting body formation was nearly complete and the appearance of the fruiting

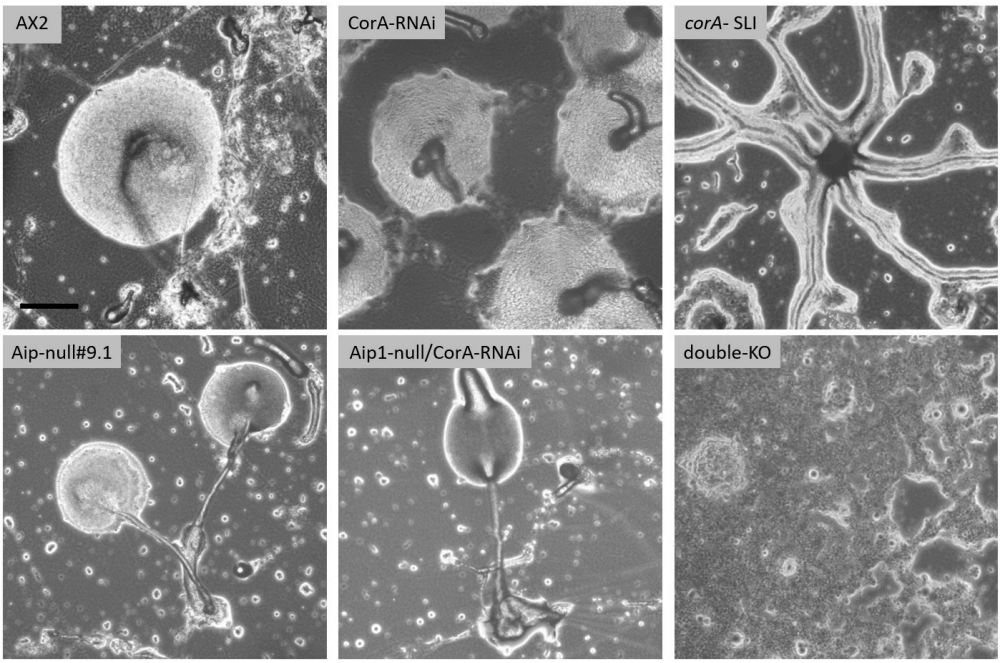

Fig. 3.15: Differentiation in starvation process after 48h of wildtype AX2 cells, *corA* knockout and knockdown by RNAi as well as in Aip1-null mutant (see Aip1-null#9.1 mutant, Konzok et al., 1999) background; upper left: wildtype cells; upper middle: Coronin-A RNAi knockdown mutant; upper right: *corA* knockout done with SLI method; lower left: Aip1-null#9.1 single mutant; lower middle: corA RNAi knockdown in Aip1-null mutant; lower right: *corA* knockout done with SLI method (see 1.7) in Aip1-null mutant background; scale bar: 50μm.

bodies was similar to that of the Aip1-null#9.1 single mutant with respect to size and diameter (see Figure 3.15). This is in complete contrast to the double knockout, which was not even able to form aggregates.

The observed results of the ability to form fruiting bodies were consistent with the production of spores and their viability in RNAi mutants. The CorA RNAi strain produced spores with both AX2 and *corA*-SLI characteristics. The spores were slightly rounder and more heterogeneous in size than their wildtype counterparts, but viability was high compared to the *corA* knockout (see Figure 3.16). Spores produced by cells expressing the RNAi construct in the Aip1-null#9.1 mutant background closely resembled the Aip1-null#9.1 single mutant spores. Both were of normal size and homogeneous appearance, and viability was similarly high (see Figure 3.16).

3.3.2 Cell Size and Morphology

When comparing the cell size and morphology of Coronin-A knockdown cells with wildtype and *corA* knockout cells, the differences were not as obvious as in the knockout or loss-of-function mutant (compare figures 3.17 and 3.8). Knockdown

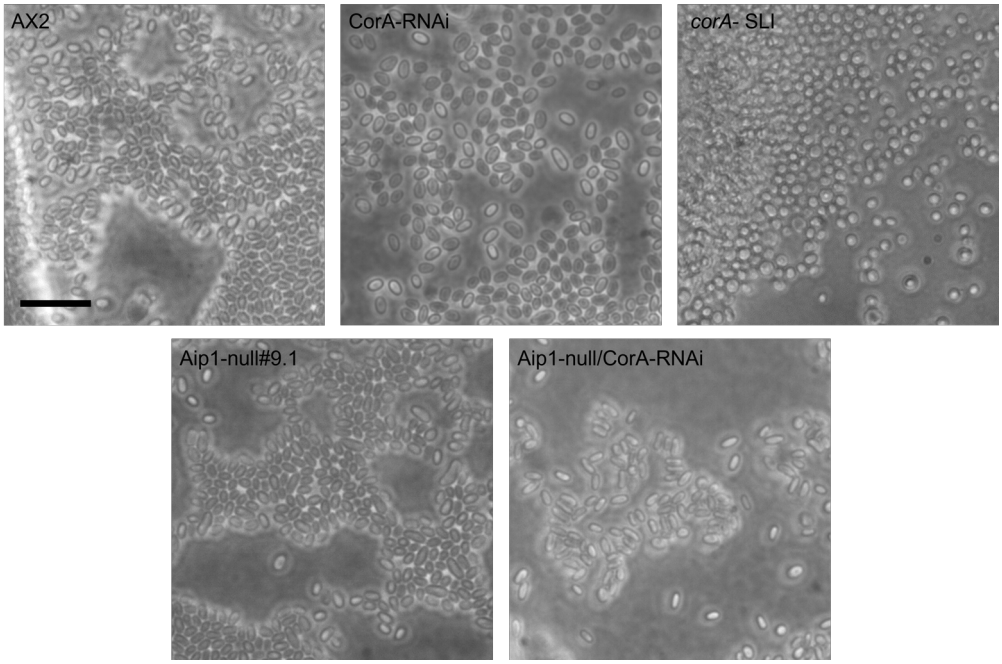

Fig. 3.16: Spores after 48h of wildtype AX2 cells and CorA-RNAi knockdown and *corA*knockout (KO) (see 1.7) as well as RNAi in Aip1-null#9.1 mutant background (see Konzok et al., 1999); upper left: wildtype cells; upper middle: CorA-RNAi knockdown mutant; upper right: *corA* knockout done with SLI method; lower left: Aip1-null#9.1 single mutant; lower right: CorA-RNAi knockdown in Aip1-null mutant; Aip1-null/*corA*- double mutant did not form spores within 48 hours or 72 hours, scale bar: 20μm.

and knockout mutants did not show many multinucleated cells and all three strains could not be easily distinguished by their heterogeneity in cell size.

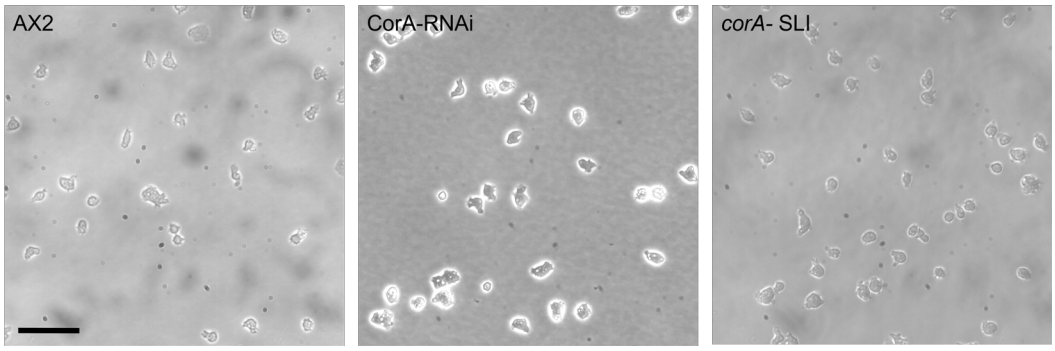

Fig. 3.17: Example of brightfield images for morphological analysis and determination of the cell size in wildtype AX2 cells, SLI *corA* knockout and knockdown of CorA by RNAi; left: wildtype AX2, middle: Coronin-A knockdown by RNAi (see Samereier et al., 2011), right: *corA* knockout done with SLI method (see 1.7); scale bar: 50μm.

However, when analyzed quantitatively, the similarity of the knockdown to the knockout was revealed (see Figure 3.18, left), because the distribution of cell sizes in

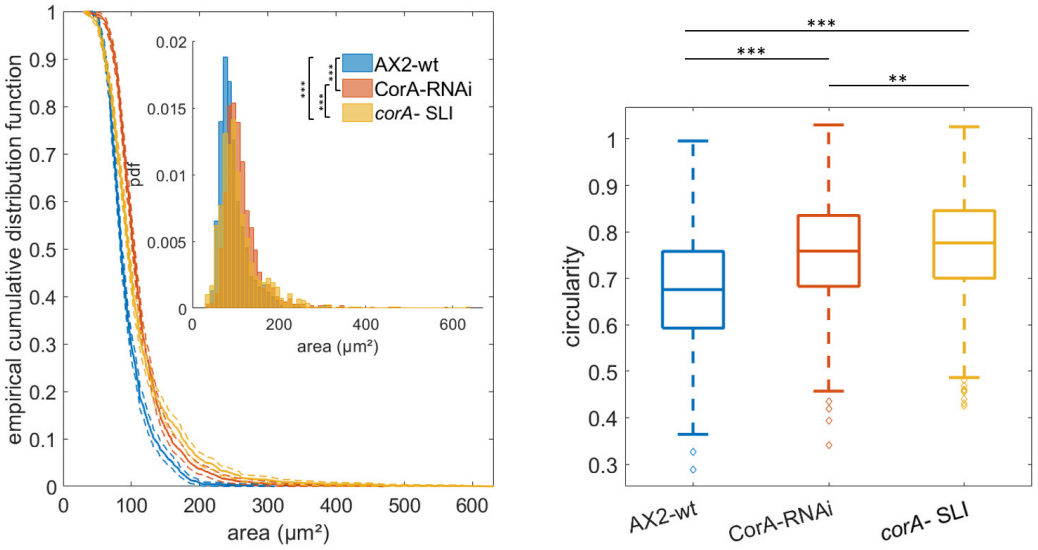

Fig. 3.18: Cell size and cell circularity distributions of *D. discoideum* wildtype AX2 cells, SLI *corA* knockout cells (see 1.7) and knockdown of CorA by RNAi in wildtype cells (see Samereier et al., 2011); Left: empirical cumulative distribution function of the cell area, calculated from n $> 10^3$ independent cells, along with 95% confidence interval; inlet: normalized histogram of the same cell areas, giving a sense of the underlying probability density function (pdf). Right: circularity as the parameter for morphological differences, calculated from the same 10^3 cells, graphically represented in box-plots showing the median (line), the lower and upper edge of the box indicate the 25% and 75% percentiles, and whiskers representing ± 2.7 SD; values outside of whiskers are explicitly plotted by points (outliers). p-values obtained from Kolmogorov-Smirnov statistical test for differences between distributions (see SI Table 10.3) are displayed by asterisks: n.s.: not significant at a significance level of 0.05; *: p-value$\leq$ 0.05, **: p-value$\leq$ 0.01, ***: p-value$\leq$ 0.001.

the knockdown followed that of the knockout mutant cells. All cell size distributions were still significantly different from each other. The knockdown did not seem to alter cell size much within the culture, although much larger cells up to 400μm^2 occasionally occurred, which were not present at all in the wildtype. The morphology of the mutant strains was also similar to each other, but different from the wildtype (see Figure 3.18, right). In knockdown and knockout, the median circularity of the cells was higher, although all three strains differed significantly from each other.

It was shown in the last chapter that Aip1-null#9.1 cells did not differ from wildtype in size but in morphology (see Figure 3.11), which was the case for the knockdown in the Aip1-null#9.1 mutant background as well (see Figure 3.19). After analyzing the cell sizes of the CorA RNAi knockdown in the Aip1-null#9.1 mutant background, it was confirmed that the knockdown construct did affect the cell size distribution, where all compared strains differed significantly from each other (see Figure 3.20).

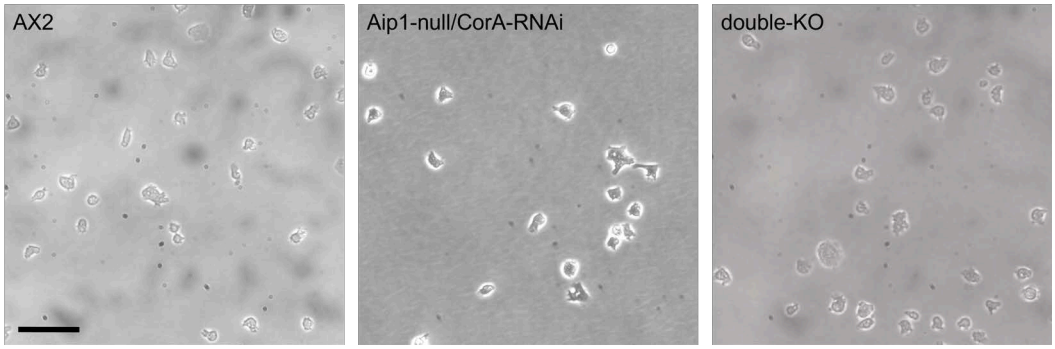

Fig. 3.19: Example of brightfield images for morphological analysis and determination of the cell size in wildtype AX2 cells, Aip1-null/*corA*- SLI double knockout and knockdown of CorA by RNAi in Aip1-null mutant (see Aip1-null#9.1 mutant,Konzok et al., 1999) cells; left: wildtype AX2, middle: Coronin-A knockdown by RNAi (see Samereier et al., 2011) in Aip1-null mutant background, right: *corA* knockout done with SLI method (see 1.7) in Aip1-null mutant background; scale bar: 50μm.

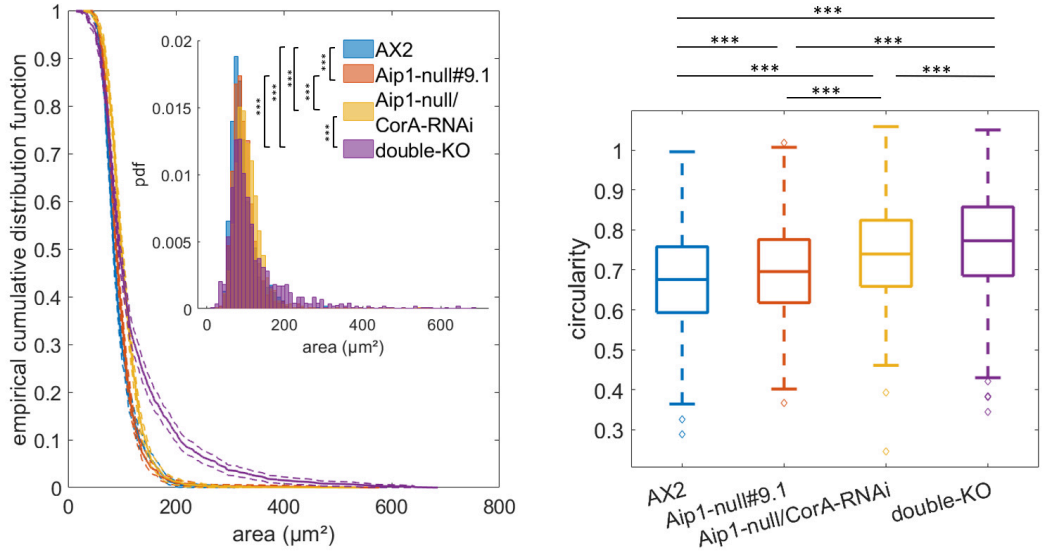

Fig. 3.20: Cell size and cell circularity distributions of *D. discoideum* wildtype AX2 cells and Aip1-null/*corA* double mutants created by different methods; Aip1-null#9.1 single mutant (see Konzok et al., 1999); Aip1-null/CorA-RNAi: RNAi knockdown (see Samereier et al., 2011) used in Aip1-null mutant; double-KO: *corA* knockout done with SLI method (see 1.7) in Aip1-null mutant; Left: empirical cumulative distribution function of the cell area, calculated from n $> 10^3$ independent cells, along with 95% confidence interval; inlet: normalized histogram of the same cell areas, giving a sense of the underlying probability density function (pdf). Right: circularity as the parameter for morphological differences, calculated from the same 10^3 cells, graphically represented in box-plots showing the median (line), the lower and upper edge of the box indicate the 25% and 75% percentiles, and whiskers representing ± 2.7 SD; values outside of whiskers are explicitly plotted by points (outliers). p-values obtained from Kolmogorov-Smirnov statistical test for differences between distributions (see SI Table 10.3) are displayed by asterisks: n.s.: not significant at a significance level of 0.05; *: p-value$\leq$ 0.05, **: p-value$\leq$ 0.01, ***: p-value$\leq$ 0.001.

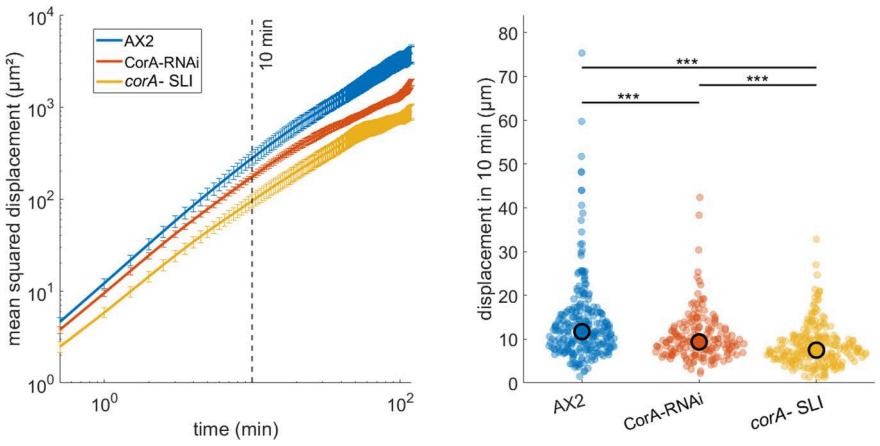

Fig. 3.21: Motility analysis of *D. discoideum* wildtype cells, Coronin A knockdown CorA-RNAi (see Samereier et al., 2011) and *corA* knockout done with SLI method (see Section 1.7). Left: log-log plots of mean-square displacement (μm2) plotted versus time. Mean values of at least six independent experiments with corresponding standard error (SE) are displayed to indicate reproducibility of results. Right: means of the displacement (μm2) after ten minutes for n $\approx 10^2$ cells (for the exact number of analyzed cells see SI 10.3) pooled from at least six independent experiments are displayed in violin plots for the genotypes outlined above. Black circles indicated median values. p-values obtained from Kolmogorov-Smirnov statistical test for differences between distributions are displaced by asterisks: n.s.: not significant at a significance level of 0.05; *: p-value$\leq$ 0.05, **: p-value$\leq$ 0.01, ***: p-value$\leq$ 0.001.

However, the circularity of the cells was significantly different in AX2 cells, Aip1-null#9.1 single mutant, Aip1-null/CorA knockdown, and Aip1-null/*corA* double knockout. As expected, the circularity of most of the knockdown cells was between the median circularity of the Aip1-null#9.1 single mutant and the double knockout (see Figure 3.20, right).

3.3.3 Motility

The MSD of the AX2 wildtype strain was compared with the motility of the *corA* SLI knockout and the RNAi knockdown. The displacement of the knockdown was clearly between the wildtype and the knockout and showed the same course over the whole observation period. Considering an interval of 10 minutes, all three distributions were highly significantly different from each other (see Figure 3.21).

When comparing the motility results for double mutants, the knockout had a strongly decreased MSD compared to the single Aip1-null#9.1 mutant and the wildtype. Furthermore, the difference in MSD between the double-KO and the others seemed to increase with time. A striking observation was made when the motility of the RNAi construct expressing the Aip1-null#9.1 double mutant strain was analyzed.

The motility of this mutant matched that of the wildtype, which was unexpected (see Figure 3.22). Although all other strains compared were significantly different from each other, there was no significant difference in the MSD of these two candidates.

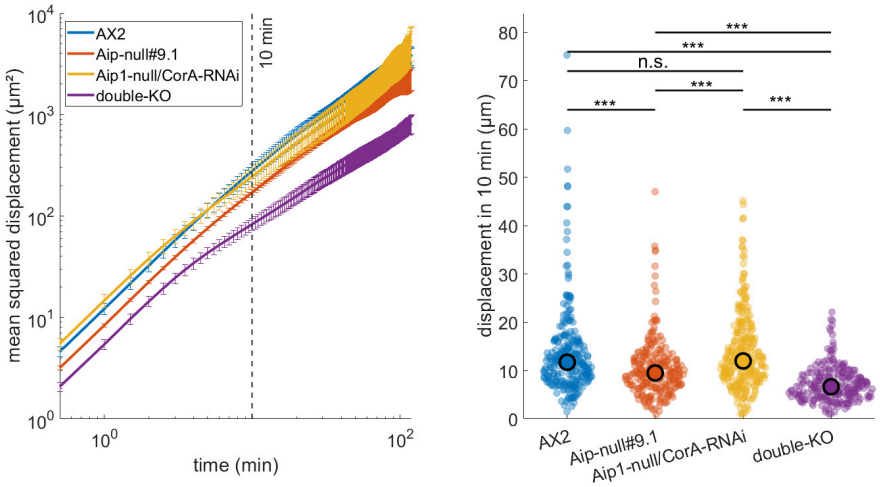

Fig. 3.22: Motility analysis of *D. discoideum* wildtype cells, Aip1-null#9.1 single mutant (see Konzok et al., 1999), Aip1-null/CorA-RNAi knockdown and double-KO. RNAi knockdown (see Samereier et al., 2011) used in Aip1-null mutant; double-KO: *corA* knockout done with SLI method (see 1.7) in Aip1-null mutant. Left: log-log plots of mean-square displacement (μm2) plotted versus time. Mean values of at least six independent experiments with corresponding standard error (SE) are displayed to indicate reproducibility of results. Right: means of the displacement (μm2) after ten minutes for n $\approx 10^2$ cells (for the exact number of analyzed cells see SI 10.3) pooled from at least six independent experiments are displayed in violin plots for the genotypes outlined above. Black circles indicated median values. p-values obtained from Kolmogorov-Smirnov statistical test for differences between distributions are displaced by asterisks: n.s.: not significant at a significance level of 0.05; *: p-value$\leq$ 0.05, **: p-value$\leq$ 0.01, ***: p-value$\leq$ 0.001.

3.4 Knock sideway - Acute Loss of Function

The knock sideway method was based on chemically induced dislocation. This meant that the protein of interest could be dislocated from its site of action by binding to another structure of the cell, such as the mitochondria or the plasma membrane. This is expected to lead to a sudden loss of function of the protein in the cell, which usually cannot be quickly compensated. This work is based on the CID method using rapamycin as the linking chemical (see 1.7 for more details). To test the influence of the binding of Coronin to the mitochondria itself, wildtype AX2 cells were transformed with two different plasmids to create a Coronin overexpressor (CorA-OX). The first one was for the expression of additional GFP and 2xFKBP tagged Coronin-A under a strong *actin 15* promoter. And the second was for the expression

of the mitochondrial anchor with the FRB domain, which was also used in the knock sideways mutants.

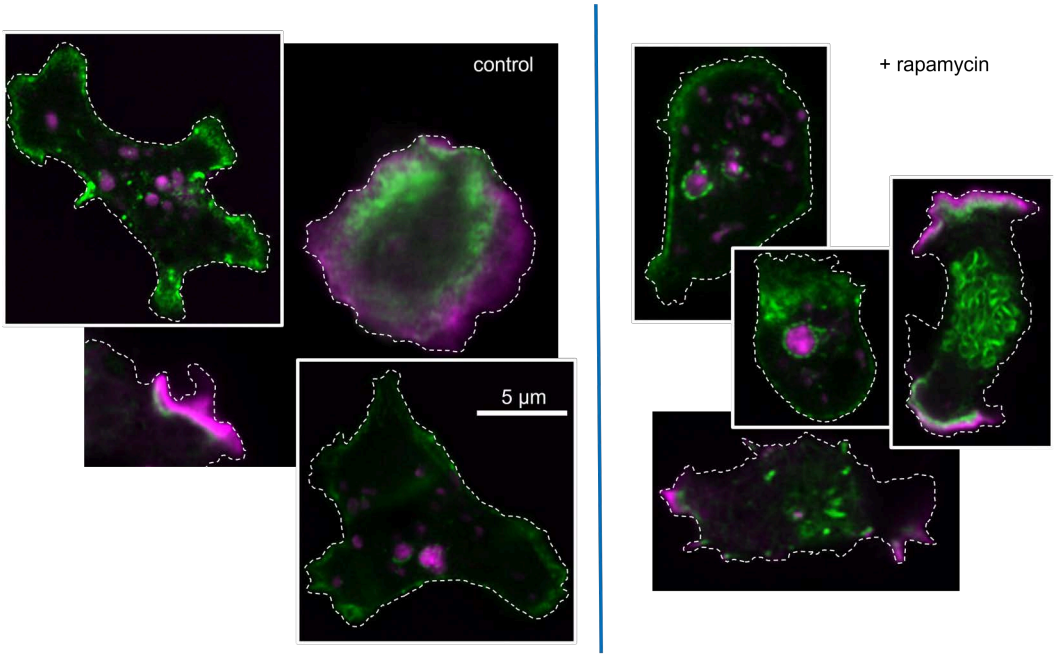

Fig. 3.23: Fluorescence LSM images of Coronin A knock sideway cells created with SLI method (see 1.7) without (left) and with (right) rapamycin treatment for chemical-induced dimerization; Coronin-A-GFP-2xFKBP in green, mRFPmars-LimE in purple; rapamycin dislocalizes Coronin-A-GFP-2xFKBP to the mitochondria.

Microscopic evidence for the translocation of GFP-2xFKBP-tagged Coronin-A is shown in Figure 3.23. While in control cells (left) Coronin (green) was mainly localized in the pseudopods of moving *D. discoideum* cells and co-localized with the actin polymerization marker limE (purple), the recruitment of Coronin-A to the mitochondria can be seen after 20 min of rapamycin treatment (right). Interestingly, limE also appeared to localize to inclusion bodies. In control cells, these structures did not show any Coronin-GFP signal. When rapamycin was added, Coronin translocated to the vesicles and formed a corona-like structure.

3.4.1 Generation Time + Fruiting Body Formation

First, the influence of knock sideway constructs and the influence of rapamycin on the generation time were tested separately. 10 μM rapamycin tripled the doubling time in AX2 wildtype cells. As shown in Figure 3.24, the generation time changed from 11 hours without treatment to 33 hours with rapamycin. When, in addition to Coronin-A, the knock sideway tagged Coronin-A and the mitochondrial anchor from

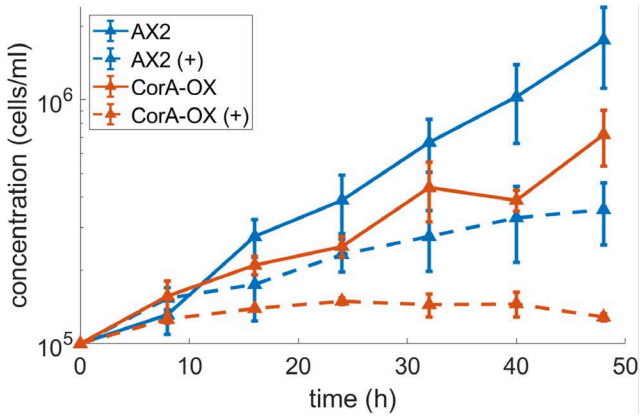

strain	generation time (hours)
AX2	11.3
AX2 (+)	33.7
CorA-OX	19.7
CorA-OX (+)	no growth

Fig. 3.24: **Growth curves in semi-log plot and generation times of different cell strains of *D. discoideum***; wildtype AX2 and overexpressor CorA-OX treated with (+) and without 10 μM rapamycin; Left: Mean cell concentration in shaking culture in HL-5 media (see 2.3) measured in a period of 48 hours, counted as duplicates in 8 hours intervals in two independent experiments, calculated by averaging the mean cell concentration determined for each experiment; error bars show the absolute difference between them. Right: Generation times were determined by an exponential fit.

extrachromosomal plasmids were overexpressed in wildtype cells, the growth rate was already reduced to 19.7 hours. When these cells were treated with rapamycin, almost no growth was detectable over 48 hours.

To compare the effect of rapamycin with the effect of the Coronin-A knock sideway (CorA-KS) method, wildtype, and *corA* knockout were also considered. As discussed in the previous paragraph, AX2 cells grew much slower in the presence of rapamycin. For the knockout, a 4.5-fold increase in generation time was measured when the cells were treated with rapamycin. The Coronin-A knock sideway strain was also inhibited in growth with rapamycin. The growth rate was increased by a factor of 5, resulting in a doubling time of 150 hours (see Figure 3.25).

When comparing the Aip1-null cells with the *corA* knockout or knock sideway in the Aip1-null background, untreated double mutant knock sideway (double-KS) cells doubled nearly as fast as the Aip1-null single mutant. The double knockout (double-KO) cell line had a generation time of 27 hours. Treatment with 10μM rapamycin increased this by 2.5-fold. Aip1-null cells prolonged their doubling time from 19 hours to 29 hours when cultured with rapamycin. The greatest change in growth rate was seen in double-KS cells under treatment. Rapamycin-treated cells doubled more than 10 times slower than control cells (see Figure 3.26).

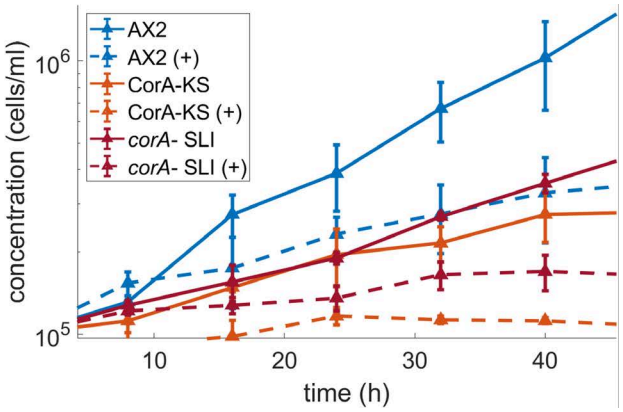

strain	generation time (hours)
AX2	11.3
AX2 (+)	33.7
corA-KS	30.3
corA-KS (+)	150.1
corA- SLI	20.9
corA- SLI (+)	91.0

Fig. 3.25: **Growth curves in semi-log plot and generation times of different cell strains of *D. discoideum***; wildtype AX2, knock sideway done with SLI method (see 1.7) and *corA*- SLI knockout treated with (+) and without 10 μM rapamycin; Left: Mean cell concentration in shaking culture in HL-5 media (see 2.3) measured in a period of 48 hours, counted as duplicates in 8 hours intervals in two independent experiments, calculated by averaging the mean cell concentration determined for each experiment; error bars show the absolute difference between them. Right: Generation times were determined by an exponential fit.

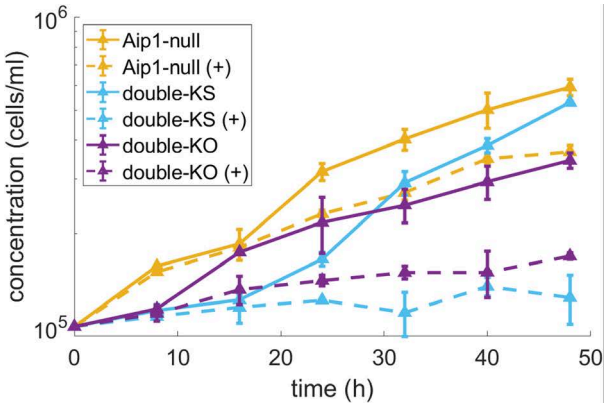

strain	generation time (hours)
Aip1-null	19.7
Aip1-null (+)	29.4
double-KS	16.5
double-KS (+)	195.4
double-KO	27.0
double-KO (+)	75.6

Fig. 3.26: **Growth curves in semi-log plot and generation times of different cell strains of *D. discoideum***; Aip1-null#9.1 single mutant (see Konzok et al., 1999), double knock sideway done with SLI method (see 1.7) in Aip1-null mutant and *corA* knockout done with SLI method in Aip1-null mutant treated with (+) and without 10 μM rapamycin; Left: Mean cell concentration in shaking culture in HL-5 media (see 2.3) measured in a period of 48 hours, counted as duplicates in 8 hours intervals in two independent experiments, calculated by averaging the mean cell concentration determined for each experiment; error bars show the absolute difference between them. Right: Generation times were determined by an exponential fit.

The formation of fruiting bodies and the ability to produce spores were also examined in the strains used in the knock sideway experiments of this work. Comparing the wildtype AX2 strain with the mutants and corresponding knockouts, both generated by the SLI method, a clear difference in differentiation during the starvation process

could be observed between the functional but tagged Coronin-A in knock sideway and the missing Coronin-A in knockouts. CorA-KS mutants were not impaired in streaming and fruiting body formation, although they did not form spore-containing heads as large as in the wildtype. The size of the fruiting bodies was more comparable to that of the Aip1-null#9.1 mutant (see Figure 3.27). In the Aip1-null background, CorA-KS led to the development of even smaller spore heads (see Figure 3.27, lower middle). However, the difference to the non-streaming double mutant was large, in contrast to the small differentiation limitations similar to the Aip1-null single mutant.

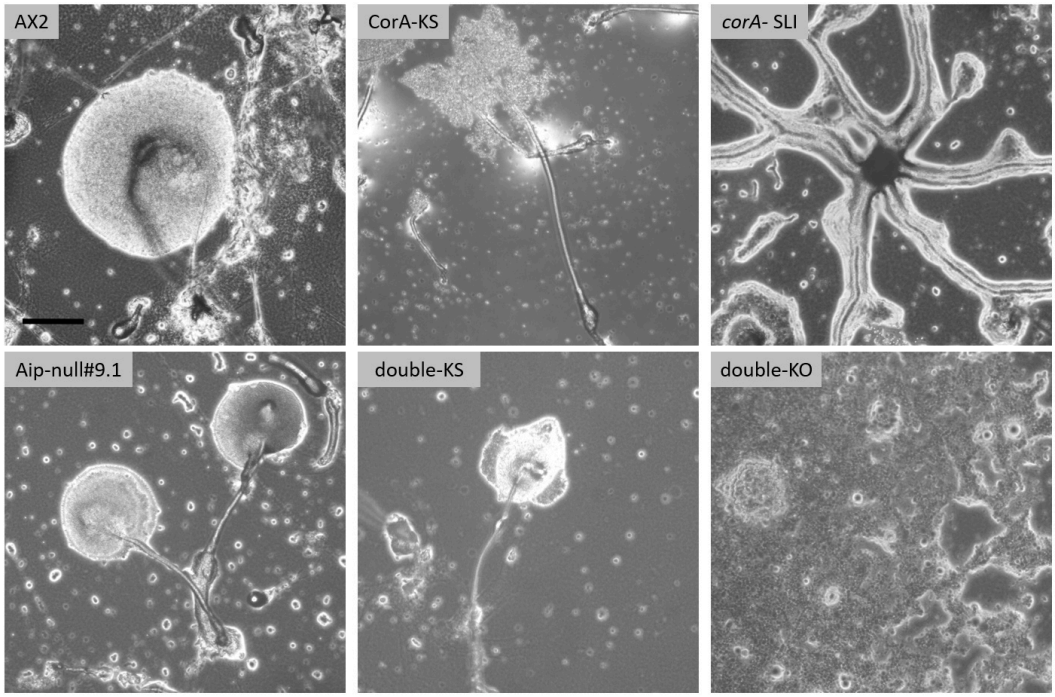

Fig. 3.27: Differentiation in starvation process after 48h of wildtype AX2 cells and Coronin A single and Aip1-null/CorA double knock sideway mutants created by SLI (see 1.7); upper left: wildtype AX2, upper middle: Coronin-A knock sideway; upper right: *corA* knockout, lower left: Aip1-null#9.1 mutant (see Konzok et al., 1999); lower middle: double-KS done with SLI method (see 1.7) in Aip1-null mutant, lower right: double-KO by SLI in Aip1-null mutant; scale bar: 50μm.

As mentioned above (see Section 3.2.1), the *corA*- SLI knockout spores differed in shape from the wildtype spores, and the double mutant did not produce any spores at all. The shape and viability of the spores of the CorA-KS mutant were almost identical to those of the CorA-RNAi mutant (see also Figure 3.16). They also showed a more heterogeneous phenotype but were not as rounded as the knockout mutant spores (see Figure 3.28, top row).

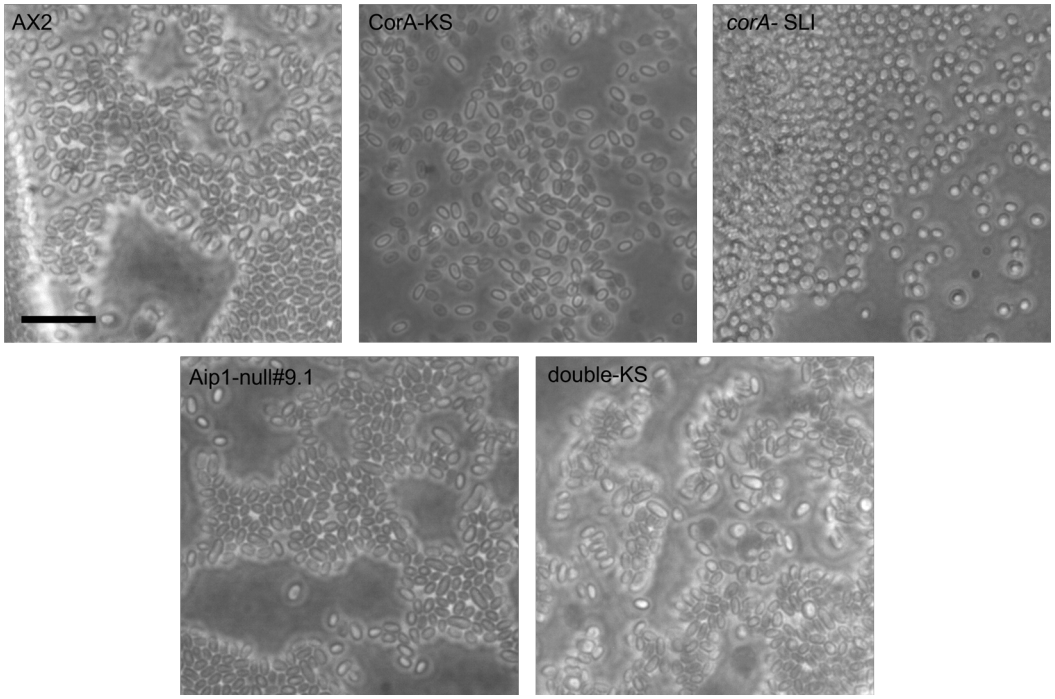

Fig. 3.28: **Spores after 48h** of wildtype AX2 cells and SLI *corA* knock sideway (KS) and knockout (KO) (see 1.7) as well as KS and KO in Aip1-null#9.1 mutant background (see Konzok et al., 1999); upper left: wildtype cells; upper middle: Coronin-A knock sideway mutant; upper right: *corA* knockout done with SLI method; lower left: Aip1-null#9.1 single mutant; lower right: double-knock sideway mutant; control experiment without rapamycin; Aip1-null/*corA*- double mutant did not form spores within 48 hours or 72 hours, scale bar: 20μm.

In the CorA-KS mutant in the Aip1-null background, spore production was also unaffected. Although the heterogeneity was even more pronounced (see Figure 3.28, bottom), the viability was comparable to the knockdown and the Aip1-null single mutant and almost at the wildtype level.

3.4.2 Cell Size and Morphology

The cell size of at least one thousand CorA knock sideway cells was determined in comparison to the size of AX2 wildtype and CorA knock sideway overexpressor cells (see Figure 3.30). Both CorA mutant cells are visibly larger in cell area than their wildtype counterparts. It was hypothesized that AX2 wildtype, CorA knock sideway (KS), and the overexpressor (OX) should have similar properties since they all have a functional *corA* gene (see also Figure 3.29). The knock sideway overexpressor additionally produced Coronin-A tagged with GFP and the 2xFKBP domain from a cytosolic plasmid. The results showed that the AX2 and CorA-OX had a larger proportion of smaller cells compared to the CorA-KS. However, some larger cells could also be found in the OX, while large cells were very rare in the wildtype

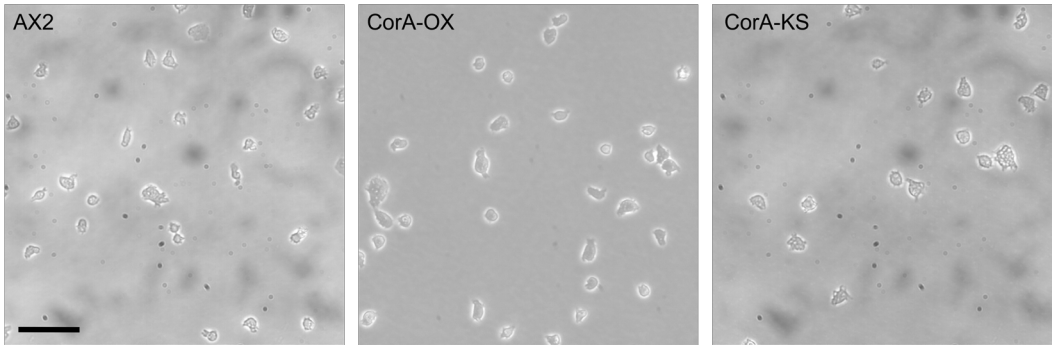

Fig. 3.29: Example of brightfield images for morphological analysis and determination of the cell size in wildtype AX2 cells, SLI *corA* knock sideway (KS) and knock sideway constructs overexpressor (OX) of tagged CorA; left: wildtype AX2, middle: Coronin-A knock sideway proteins overexpressor, right: *corA* SLI knock sideway method (see 1.7); control experiment without rapamycin; scale bar: 50μm.

background (see Figure 3.30, left). Overall, the area in μm^2 was highly significantly different from one strain to the other.

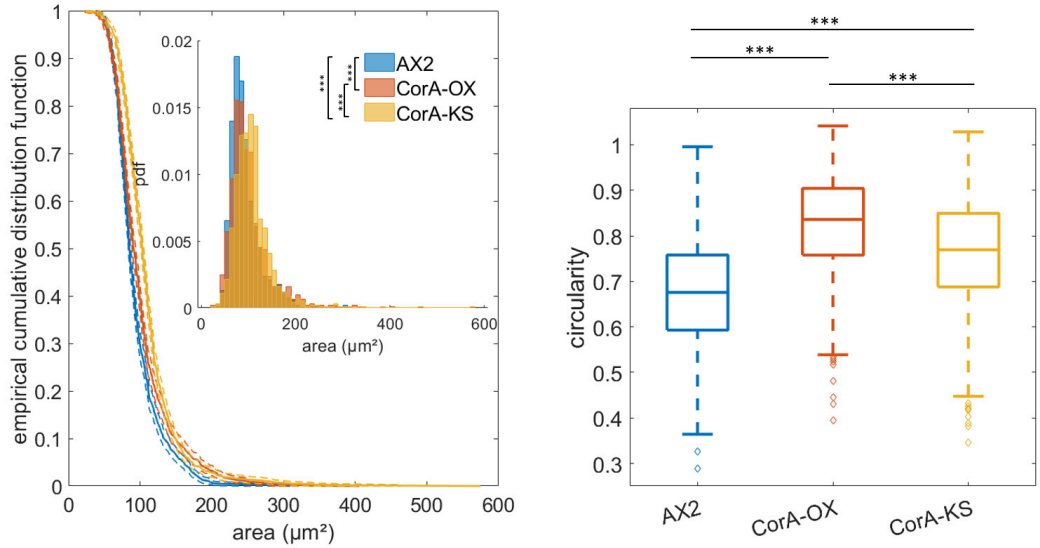

Fig. 3.30: Cell size and cell circularity distributions of *D. discoideum* wildtype AX2 cells, SLI *corA* knock sideway (KS) (see 1.7) and knock sideway constructs overexpressor (OX) of tagged CorA; control experiment without rapamycin; Left: empirical cumulative distribution function of the cell area, calculated from $n > 10^3$ independent cells, along with 95% confidence interval; inlet: normalized histogram of the same cell areas, giving a sense of the underlying probability density function (pdf). Right: circularity as the parameter for morphological differences, calculated from the same 10^3 cells, graphically represented in box-plots showing the median (line), the lower and upper edge of the box indicate the 25% and 75% percentiles, and whiskers representing ± 2.7 SD; values outside of whiskers are explicitly plotted by points (outliers). p-values obtained from Kolmogorov-Smirnov statistical test for differences between distributions (see SI Table 10.3) are displayed by asterisks: n.s.: not significant at a significance level of 0.05; *: p-value$\leq$ 0.05, **: p-value$\leq$ 0.01, ***: p-value$\leq$ 0.001.

Interestingly, and contrary to previous expectations, overexpression of Coronin-A resulted in a higher median circularity of the cell shape compared to the wildtype and CorA-KS cells. In CorA-KS cells, the median cellular circularity was already significantly increased compared to the wildtype, but also significantly differed from the even more rounded overexpressor cells (see Figure 3.30, right).

To compare the size and influence of the knock sideway constructs on the morphology of the double mutants as well as the single mutants, images of the cells of the wildtype, Aip1-null#9.1, double-KS and double-KO strains were taken. By eye, it was not possible to differentiate between the four strains examined (see Figure 3.31), but significant differences in the size and shape of the knockout could be observed during quantitative analysis.

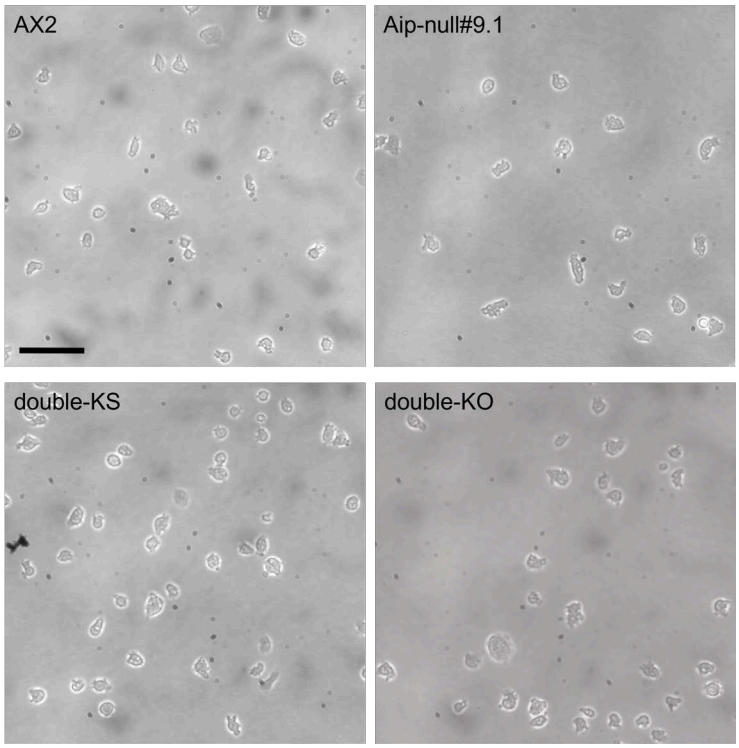

Fig. 3.31: Example of brightfield images for morphological analysis and determination of the cell size in wildtype AX2 cells and SLI *corA* knock sideway (KS) and knockout (KO) (see 1.7) in Aip1-null#9.1 mutant background (see Konzok et al., 1999); upper left: wildtype cells; upper right: Aip1-null#9.1 single mutant; lower left: double-knock sideway mutant; lower right: *corA* knockout done with SLI method in Aip1-null mutant background; control experiment without rapamycin; scale bar: 50μm.

The size of the cells was distributed differently in the double-KO, while the wildtype, the Aip1-null single mutant and the CorA-KS expressing double mutant in the Aip1-null background showed indistinguishable results. Only the double knockout showed

larger cells, up to 1.5 to 2 times larger than the others (see Figure 3.32). All cell size distributions differed significantly from each other.

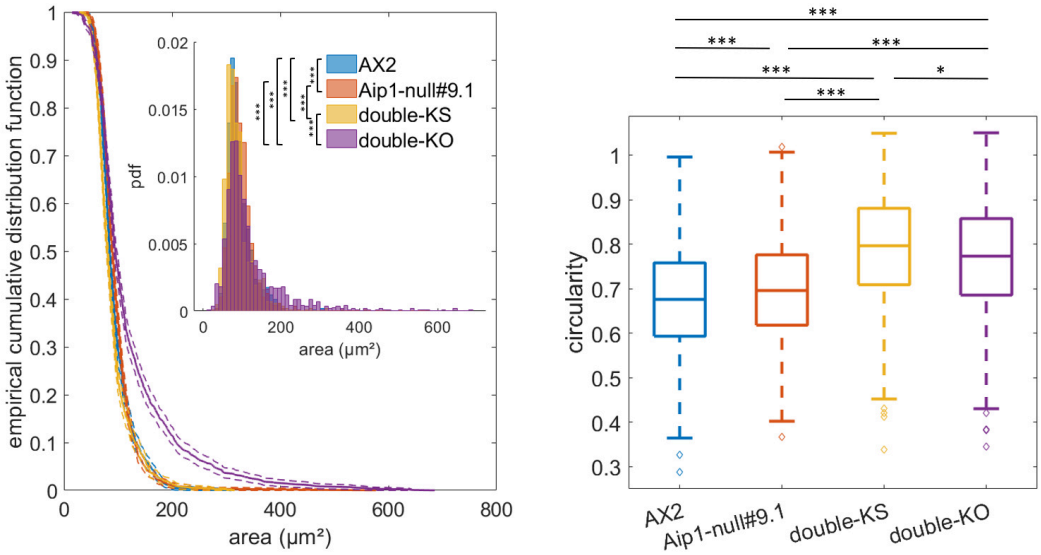

Fig. 3.32: Cell size and cell circularity distributions of *D. discoideum* wildtype AX2 cells, Aip1-null#9.1 single mutant (see Konzok et al., 1999), SLI *corA* knock sideway (KS) and knockout (KO) (see 1.7) in Aip1-null#9.1 mutant background; Left: empirical cumulative distribution function of the cell area, calculated from $n > 10^3$ independent cells, along with 95% confidence interval; inlet: normalized histogram of the same cell areas, giving a sense of the underlying probability density function (pdf). Right: circularity as the parameter for morphological differences, calculated from the same 10^3 cells, graphically represented in box-plots showing the median (line), the lower and upper edge of the box indicate the 25% and 75% percentiles, and whiskers representing ± 2.7 SD; values outside of whiskers are explicitly plotted by points (outliers). p-values obtained from Kolmogorov-Smirnov statistical test for differences between distributions (see SI Table 10.3) are displayed by asterisks: n.s.: not significant at a significance level of 0.05; *: p-value$\leq$ 0.05, **: p-value$\leq$ 0.01, ***: p-value$\leq$ 0.001.

The analysis of cell morphology did not mirror the cell size results. Although the single Aip1-null mutant and the wildtype showed similar results for their median circularity, the CorA-KS double mutant had the highest number of nearly round cells, which was not even the case in the double-KO. Both double mutants showed more comparable results for their median cell circularity (see Figure 3.32).

3.4.3 Motility

Motility was determined by the displacement of single cells in a 10 minutes time interval. First, the influence of the translocation of tagged Coronin-A to the mitochondria on motility was analyzed. As shown in Figure 3.33, the motility of AX2

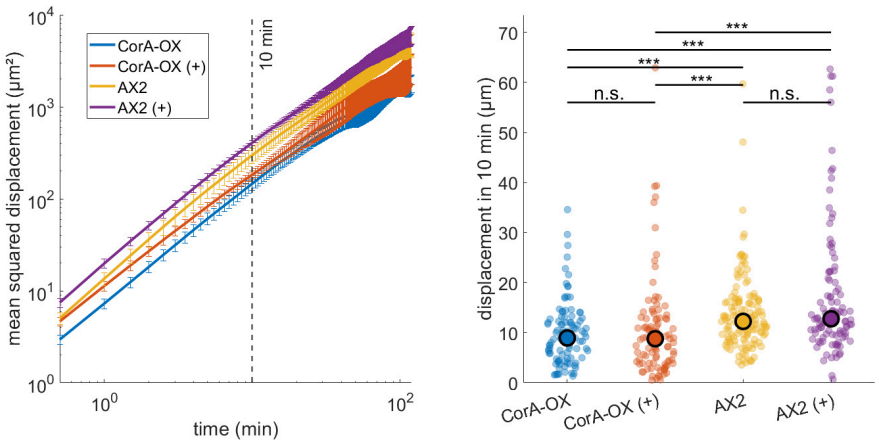

Fig. 3.33: Motility analysis of *D. discoideum* Coronin-A knock sideway overexpressor (CorA-OX) cells and wildtype (AX2) cells with only endogenous Coronin-A. (+): cells treated with 10 μM rapamycin (the chemical which induces the binding of tagged Coronin-A by to the mitochondria) in DMSO. Left: log-log plots of mean-square displacement (μm2) plotted versus time. Mean values of at least six independent experiments with corresponding standard error (SE) are displayed to indicate reproducibility of results. Right: means of the displacement (μm2) after ten minutes for n $\approx 10^2$ cells (for the exact number of analyzed cells see SI 10.3) pooled from at least six independent experiments are displayed in violin plots for the genotypes outlined above. Black circles indicated median values. p-values obtained from Kolmogorov-Smirnov statistical test for differences between distributions are displaced by asterisks: n.s.: not significant at a significance level of 0.05; *: p-value$\leq$ 0.05, **: p-value$\leq$ 0.01, ***: p-value$\leq$ 0.001.

cells with additional KS constructs is not affected by the addition of rapamycin and the associated binding of Coronin-A to the mitochondria. Endogenous Coronin-A does not seem to be affected.

AX2 wildtype and Coronin-A SLI knockout cells were treated with rapamycin and with DMSO as a sham-treated control. Rapamycin treatment was necessary to compare the influence of rapamycin on the results with those of the knock sideway strain. The Kolmogorov-Smirnov significance test was performed. The result showed no significant changes in motility when AX2 and SLI knockout cells were treated with or without rapamycin. There was already a small but significant difference between AX2 and untreated knock sideway cells (see Figure 3.34). The difference between the untreated knock sideway cells and the rapamycin-treated cells was large in comparison. A difference in motility could be seen when rapamycin suddenly bound Coronin-A to the mitochondria. This difference was so large that there was no longer a significant difference between the treated knock sideway mutant and the SLI *corA* knockout, which was previously highly significant (*** p-value$\leq$ 0.01).

In contrast to the well-functioning knock sideway construct in the single mutant, the knock sideway mutation in the Aip1-null background led to a phenotypic change

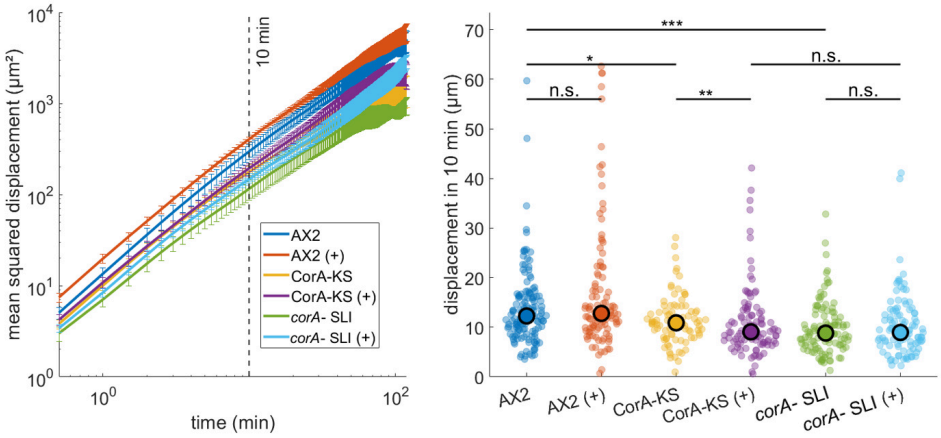

Fig. 3.34: Motility analysis of *D. discoideum* wildtype (AX2), Coronin-A-knock sideway (CorA-KS) cells and *corA*-knockout (*corA*- SLI) cells. (+): cells treated with 10 μM rapamycin (the chemical which induces the binding of tagged Coronin-A by to the mitochondria) in DMSO. Left: log-log plots of mean-square displacement (μm2) plotted versus time. Mean values of at least six independent experiments with corresponding standard error (SE) are displayed to indicate reproducibility of results. Right: means of the displacement (μm2) after ten minutes for n $\approx 10^2$ cells (for the exact number of analyzed cells see SI 10.3) pooled from at least six independent experiments are displayed in violin plots for the genotypes outlined above. Black circles indicated median values. p-values obtained from Kolmogorov-Smirnov statistical test for differences between distributions are displaced by asterisks: n.s.: not significant at a significance level of 0.05; *: p-value$\leq$ 0.05, **: p-value$\leq$ 0.01, ***: p-value$\leq$ 0.001.

similar to the knockout, even when not treated with rapamycin (see Figure 3.35). The influence of the tagged Coronin-A protein and the missing Aip1 was too strong to test the rapamycin CID on these cells.

3.5 Removal of the N-terminal protein part of Coronin-A in the loss-of-function background

To get an idea of the possible effects of the truncated Coronin-A protein, the RNAi plasmid responsible for the degradation of the 5'-mRNA part of the *corA* gene transcript was introduced into CorA-null and into the *corA*- SLI cells by transformation (for more details see Chapter 3.3 and for the structure of the plasmid see Chapter 2.3.2). Unfortunately, the expression or translational silencing of this part of the protein could not be verified by immunoblot because the antibody used was directed against the C-terminal part of the protein, which was not expressed in the *corA* mutants anyway.

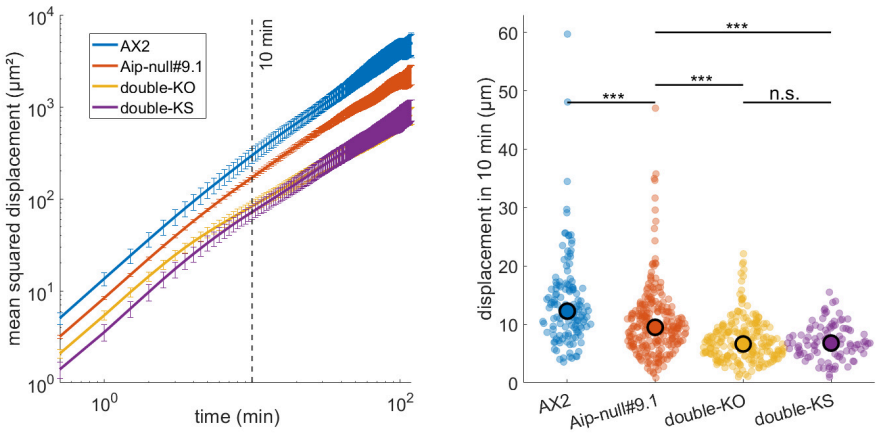

Fig. 3.35: Motility analysis of *D. discoideum* wildtype cells, Aip1-null single mutant, Coronin-A knock sideway and *corA*-knockout in Aip1-null background (double-KS and double-KO, respectively). Left: log-log plots of mean-square displacement (μm2) plotted versus time. Mean values of at least six independent experiments with corresponding standard error (SE) are displayed to indicate reproducibility of results. Right: means of the displacement (μm2) after ten minutes for n $\approx 10^2$ cells (for the exact number of analyzed cells see SI 10.3) pooled from at least six independent experiments are displayed in violin plots for the genotypes outlined above. Black circles indicated median values. p-values obtained from Kolmogorov-Smirnov statistical test for differences between distributions are displaced by asterisks: n.s.: not significant at a significance level of 0.05; *: p-value$\leq$ 0.05, **: p-value$\leq$ 0.01, ***: p-value$\leq$ 0.001.

3.5.1 Generation Time + Fruiting Body Formation

First, growth and generation time were measured for the CorA-null mutant in comparison to the *corA* SLI mutant. The CorA-null mutant showed slower growth and the generation time was two times higher than in wildtype AX2 cells and much slower than in the SLI mutant. After transformation with the RNAi plasmid, the growth rate was increased and the generation time decreased to about 16 hours (see Figure 3.36). This was even faster than the *corA*-SLI mutant.

After 48 hours of starvation, fruiting body formation in the RNAi-modified CorA-null mutant was as inhibited as in the SLI mutant (see Figure 3.37). Based on the previous RNAi results, it was shown that the RNAi method did not completely silence translation. Therefore, the differentiation phase was different from SLI mutant cells. Consistent with previous findings, the appearance of the spores changed to the more rounded and heterogeneously shaped spores of the knockout (see Figure 3.38), but did not change completely.

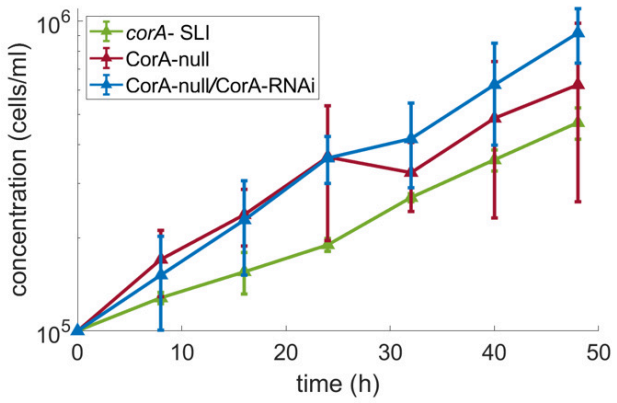

strain	generation time (hours)
corA- SLI	20,9
CorA-null	26,4
CorA-null / CorA-RNAi	15.9

Fig. 3.36: **Growth curves in semi-log plot and generation times of different cell strains of *D. discoideum***; *corA*- SLI knockout (see 1.7), CorA-null HG1569#1 (see Hostos et al., 1993 mutant and CorA-null mutant additionally expression a CorA-RNAi plasmid; Left: Mean cell concentration in shaking culture in HL-5 media (see 2.3) measured in a period of 48 hours, counted as duplicates in 8 hours intervals in two independent experiments, calculated by averaging the mean cell concentration determined for each experiment; error bars show the absolute difference between them. Right: Generation times were determined by an exponential fit.

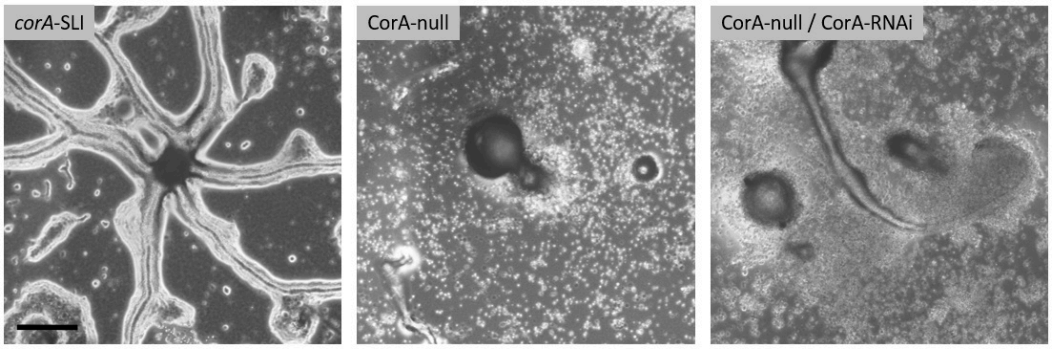

Fig. 3.37: **Differentiation in starvation process after 48h** of SLI *corA* knockout (KO, left, see 1.7) as well as CorA-null HG1569#1 (see Hostos et al., 1993, middle) cells and CorA-null mutant cells expressing the RNAi plasmid (see Samereier et al., 2011 and 2.3.2, right); scale bar: 50μm.

3.5.2 Cell Size and Morphology

Although differentiation in the modified loss-of-function mutant shifted more in the direction of the knockout, unexpected results were obtained when looking at the cell size distribution in culture and the morphological circularity of the cells. By introducing the RNAi plasmid into the *corA*-SLI mutant, the cell sizes increased to the level of the CorA-null mutant (see Figure 3.39, left). The resulting cell size distribution of the RNAi-expressing CorA-null mutant had not been predictable,

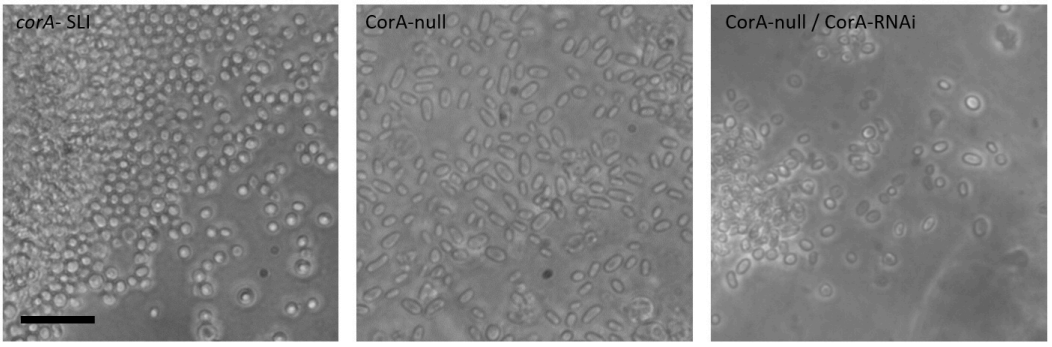

Fig. 3.38: **Spores after 48h** of SLI *corA* knockout (KO) (see 1.7) as well as CorA-null HG1569#1 (see Hostos et al., 1993) cells and CorA-null mutant cells expressing the RNAi plasmid (see Samereier et al., 2011 and 2.3.2); scale bar: 20μm.

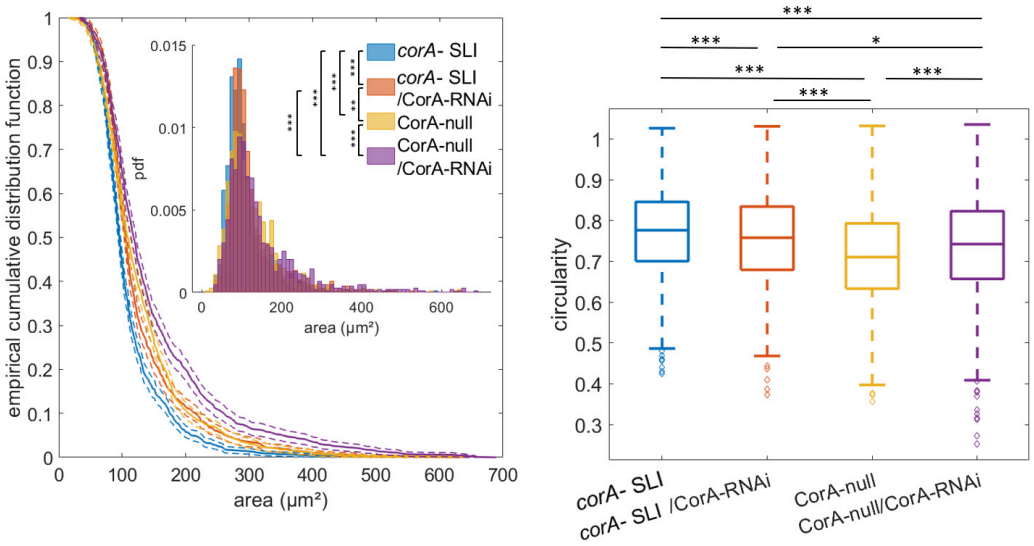

Fig. 3.39: **Cell size and cell circularity distributions of *D. discoideum* SLI *corA* knockout (KO) (see 1.7) as well as CorA-null HG1569#1 (see Hostos et al., 1993) cells and CorA-null mutant cells and knockouts expressing the RNAi plasmid (see Samereier et al., 2011 and 2.3.2)**; Left: empirical cumulative distribution function of the cell area, calculated from n $> 10^3$ independent cells, along with 95% confidence interval; inlet: normalized histogram of the same cell areas, giving a sense of the underlying probability density function (pdf). Right: circularity as the parameter for morphological differences, calculated from the same 10^3 cells, graphically represented in box-plots showing the median (line), the lower and upper edge of the box indicate the 25% and 75% percentiles, and whiskers representing ± 2.7 SD; values outside of whiskers are explicitly plotted by points (outliers). p-values obtained from Kolmogorov-Smirnov statistical test for differences between distributions (see SI Table 10.3) are displayed by asterisks: n.s.: not significant at a significance level of 0.05; *: p-value$\leq$ 0.05, **: p-value$\leq$ 0.01, ***: p-value$\leq$ 0.001.

but showed the same shift to even larger cells like in the *corA*-SLI mutant. All cell size distributions were still highly significantly different from each other. The analysis

of circularity as a parameter of morphological characteristics led to significant differences for all four knockout lines. The introduction of the RNAi plasmid into the SLI knockout did not affect the median circularity, while the median circularity of the CorA-null mutant was lower and returned to the knockout level under RNAi treatment (see Figure 3.39, right).

3.5.3 Motility

When the motility of the RNAi loss-of-function mutant was analyzed, the results were striking. The MSD of the CorA-null RNAi mutant did not show the same behavior as the CorA-null cells alone (see Figure 3.12 for comparison), but was not different anymore from the SLI mutant. In the *corA*-SLI mutant cells with and without the RNAi plasmid (see Figure 3.40), the displacement was not significantly different after 10 minutes. The CorA-null mutant was significantly different from both SLI knockouts and the CorA-null/CorA-RNAi strain.

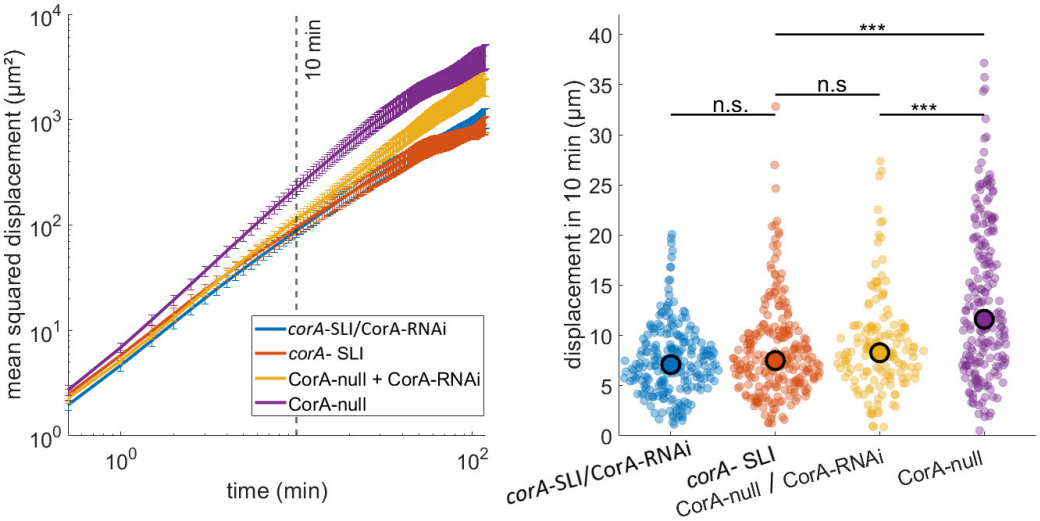

Fig. 3.40: Motility analysis of *D. discoideum corA*-SLI knockout cells (see 1.7) as well as CorA-null mutant cells with or without RNAi construct. *corA*- SLI-RNAi: *corA* knockout cells expressing the RNAi plasmid (see Samereier et al., 2011 and 2.3.2), CorA-null HG1569#1 (see Hostos et al., 1993) cells and CorA-null mutant cells expressing the RNAi plasmid. Left: log-log plots of mean-square displacement (μm2) plotted versus time. Mean values of at least six independent experiments with corresponding standard error (SE) are displayed to indicate reproducibility of results. Right: means of the displacement (μm2) after ten minutes for n $\approx 10^2$ cells (for the exact number of analyzed cells see SI 10.3) pooled from at least six independent experiments are displayed in violin plots for the genotypes outlined above. Black circles indicated median values. p-values obtained from Kolmogorov-Smirnov statistical test for differences between distributions are displaced by asterisks: n.s.: not significant at a significance level of 0.05; *: p-value$\leq$ 0.05, **: p-value$\leq$ 0.01, ***: p-value$\leq$ 0.001.

4 Discussion

This part of the work aimed to find differences and similarities in different types of mutation methods that could influence the expression and functionality of Coronin-A as a known actor in actin treadmilling and differentiation processes. Taken together, not only a new knockout method in *D. discoideum* could be established, but also the ability to influence the expression and function of a protein at different levels of protein biosynthesis could be achieved.

4.1 Comparison of the Loss-of-Function and the SLI Mutant

Comparing the characteristics of the cells produced by the loss-of-function mutation and SLI mutation methods of the *corA* gene, a huge improvement was seen when using the SLI method. The advantage of a gene knockout method that cannot be reversed is great, although in the past many stable loss-of-function mutants could be generated, such as the Aip1-null mutant line also used in this work. CorA-null knockouts still express a truncated Coronin-A mRNA of about 600 bp in length, resulting in a truncated protein of 200 amino acids. This is almost half of the full-length Coronin-A protein. Most strikingly, this does not appear to be the case in *corA*-SLI mutants, where the mRNA of the 700 bp homologous region is linked to the mRNA of the resistance gene by the 2A skip peptide coding sequence (see also Chapter 1.7). Strong differences in phenotype and motility between the two knockout types have already suggested that their proteome composition is not identical and that this must be based on the mutation method. Although this has not been proven by proteomic analysis or similar methods, it is the most plausible explanation for all the results obtained.

Compared to SLI knockouts, CorA-null mutants were still able to produce fruiting bodies and spores. Double-null mutants retained their ability to migrate, while SLI double knockouts could not even migrate together but stayed in place (return to Figure 3.6). The wildtype appearance of the spores led to the conclusion that partially expressed Coronin-A is at least involved in the differentiation process and the formation of fruiting bodies and spores. In addition, cells with reverted *corA* could compensate for mutant cells and build the stalk and fruiting body. The

differences in cell size and morphology were also not negligible. CorA-null cells showed a wider range of cell sizes compared to the SLI mutant and their morphology was more similar to the wildtype. In double mutants, this effect was less pronounced, but the already disturbed actin treadmill homeostasis due to missing Aip1 was probably not much disturbed whether Coronin-A was missing or only semi-functional. Nevertheless, the double-null cells seemed to be larger and more clumped together than the double-KO cells.

A strong difference in motility was observed when the motility of *corA* SLI mutants was compared to the motility of CorA-null cells (return to Figure 3.12). The loss-of-function mutant had a displacement similar to that of the AX2 wildtype and different from that of its SLI mutant relative in a 10-minute interval. The knockout was severely impaired in its movement but retained the persistence of the wildtype. This conclusion could be drawn from the downshifted MSD curve, which was not altered in shape. In contrast, the CorA-null mutant showed a split behavior. Considering smaller time steps around one minute, the movement of the loss-of-function mutant was comparable to that of the SLI mutant. This is consistent with previous findings and characterizations of the CorA-null mutant that calculated the average velocity of the cell line by the average ratio of the cell's position change in 30 seconds (Hostos et al., 1993, Ishikawa-Ankerhold et al., 2010).

A closer look at the actual movement of the CorA-null mutant over a 10-minute time interval showed that the results were not significantly different from the AX2 wildtype. A transition in the movement and the corresponding displacement occurred between an observation period of 2 to 10 minutes when the displacement curve becomes even more superdiffusive than at the beginning. A possible explanation could be that the amoeboid movement was inhibited as in the *corA* knockout. This includes the formation of pseudopodia and protrusions in general, which allow the direct shape change and shifting of the cell's center of mass. After polarization of the cell and localization of the truncated Coronin-A protein, it appeared that the persistence was close to the wildtype. Since this change in translocation behavior is not observed in *corA*-SLI mutants, a possible explanation could be that the truncated protein lacks the C-terminal coiled-coil (CC) domain and therefore does not have the full ability to inhibit cofilin as the full-length protein would (Lin et al., 2010). In addition, translocation to other parts of the moving cell may not be as easy as intended. This would prolong the movement of a cell in a particular direction and maintain wildtype-like persistence. Since the CC domain is also important for multimerization (Srivastava et al., 2015, Salamun et al., 2014, Gatfield et al., 2005, Kammerer et al., 2005, Asano et al., 2001), a 2/3 of the propeller structure may have a negative effect, as it may bind to actin but block binding sites of other proteins and is not able to interact with other proteins or dimerize due to the missing C-terminus.

Why the RNAi construct led to such accelerated growth in the CorA-null mutant despite the absence of Coronin-A is an open question. Hypothetically, the mutation in the CorA-null mutant could have led to an adaptation and possible up-regulation of genes that might express other cooperating proteins, which was still manifested even after the trigger was removed. It could have been suggested that the cell size distribution should remain in the same range as the SLI mutant with or without RNAi influence, but the analysis showed that it was even wider than in the unprocessed strain. Therefore, the cell size distribution could not be used as the parameter of choice, to distinguish between the two mutation methods. Removal of partially expressed RNA of the *corA* gene in null mutants by RNAi resulted in a similar motility pattern as in SLI knockout cells, whereas the RNAi construct expressing *corA*-SLI cells were not influenced at all in their motility.

The formation of fruiting bodies as well as the differentiation phases were strongly affected and differed substantially between the two knockouts and the also RNAi expressing null mutant.

Although the expression of the N-terminal part of the CorA protein in one or the other mutant could not be proven or rejected by immunoblot, these results clearly demonstrate the total absence of CorA protein parts in the *corA*-SLI mutant. The cause of this missing N-terminal part of the protein could not be identified. Numerous publications can be found that show that the degradation and miss-spicing of mRNA (reviewed in Popp et al., 2013), as well as the miss-folding (reviewed in Karamyshev et al., 2018) and truncation of proteins generating a new C-terminus (reviewed in Fortelny et al., 2015), can lead to rapid degradation of premature proteins and ultimately to ineffective expression of a protein (reviewed in Timms et al., 2020, Yeh et al., 2021 and Eisenack et al., 2023).

Since all observed properties are different from the SLI mutant, the CorA-null mutant should not be called a loss-of-function mutant as expected, but a loss-of-function mutant with a dominant negative effect.

4.2 Comparison of the different Methods of Influencing Gene Expression and Function of Coronin-A

The results obtained from the different mutation methods showed the effects of Coronin-A on the selected parameters. Not only the formation of fruiting bodies and the ability to maintain the colony's survival were affected by the amount and function

of the protein. Changes in cell shape and motility were also observed. The results revealed the advantages and disadvantages of a classical loss-of-function mutation compared to the newly implemented selection-linked integration (SLI) knockout method. The possibility of generating a knockdown with the RNAi technique or a sudden loss of function with knock sideway constructs was also investigated and showed the applicability of the different methods for different questions.

First, the gene expression and the comparison of the gene mutation methods raised the question of why and how a small N-terminal piece of the Coronin-A protein could have an influence or even a negative effect on the observed and measured parameters. After the comparison of wildtype, knockout, and loss-of-function mutants, obvious disadvantages of the null mutation could be shown, as already discussed above.

The growth of each strain was determined by counting cell density every 8 hours in the log phase in a liquid HL-5 shaking culture. Non-axenic strains grown on bacteria have shown a doubling time of 4-6 hours (Fey et al., 2007). AX2 wildtype cells in this work had a doubling time of about 11 hours, which is longer than the published values of 8 hours (Zada-Hames et al., 1978). This can only be achieved if the optimum growth temperature of 22°C is maintained. In the experiments described here, a culture temperature of 20°C was used. This reflects the known increase in generation time between 8 hours at 22°C and 12 hours at 19°C (Zada-Hames et al., 1978, Fey et al., 2007), which is also sensitive to the exact composition of the media and the presence of selective drugs (Fey et al., 2007). Both Aip1-null and *corA*-SLI single knockout cells have a much slower doubling time of nearly 20 hours, which is almost double the time of the wildtype strain, but still seven hours faster than the double mutant. When the RNAi was transcribed from the plasmid in the wildtype or mutant background, there was almost no difference in growth rate compared to the background cell line. Thus, it seems that the knockdown level of Coronin-A is not sufficient to affect its functionality in cell growth and division. The different shapes of spores and the large differences in viability, dormancy, and germination of spores are influenced by actin rods (Sameshima et al., 2001). Lack of Aip1 leads to arrest of rod formation in the nucleus (Ishikawa-Ankerhold et al., 2017). Considering that Coronin-A is involved in actin branching, the hexagonal arrangement of actin tubules (Sameshima et al., 2001) may also be inhibited. This may explain the low viability of spores produced by the double mutant.

Since the knock sideway method includes treatment with rapamycin, this was also tested on the different strains. Rapamycin is known to induce differentiation and cause upregulation of many genes associated with this process (Jaiswal et al., 2019). Previous results show that *D. discoideum* cells were already inhibited in growth after 12 hours and at a rapamycin concentration of 50 nM (Swer et al., 2014), which is 200 times lower than the rapamycin treatment in this work (10 μM).

Lower concentrations are typically used in studies of signal transduction and TOR complexes. The much higher concentration in this work is due to previous findings of rapamycin concentrations for CID in *D. discoideum*, which are also in the low micromolar range (e.g. Hoeller et al., 2016, Miao et al., 2017). Since CID is usually not studied over many hours to days, the influence of such high concentrations of rapamycin on cell growth has never been of much research interest. In addition to this growth inhibition, even low concentrations of rapamycin led to a decrease in viability after 36 hours of treatment, which was shown to drop dramatically to 60% after 48 hours (Swer et al., 2014). All cell lines examined responded strongly to rapamycin treatment and growth was severely impaired. The Coronin knock sideway cell line grew much slower than expected. The generation time was extended to 30 hours, which is even slower than the double mutant. Interestingly, the *corA* knockout cells with and without rapamycin responded very similarly in comparison to the CorA-KS cell. Both cell lines increased their doubling time by a factor of 5, resulting in almost undetectable growth of the treated CorA-KS cells.

Tagged Coronin-A had a negative effect on growth, but did not change the size of the cells, either in the AX2 background or in the Aip1-null mutant background. When overexpressed in the AX2 background, it led to an increased circularity of the cells, which was even higher than in the knockout. This showed that the mixture of endogenous Coronin-A and extrachromosomally expressed Coronin-A with the knock sideway tag leads to a competition of both Coronin proteins and to a clear negative effect. The cells may then take the opportunity to degrade the excess Coronin-A, resulting in the smaller fragment (35 kDa) seen in the immunoblot. Thus, the Coronin-A protein in knock sideway mutants, although expressed under its endogenous promoter, probably needs a free C-terminus to be fully functional, while binding to actin still works at the N-terminus. Perhaps the multimerization of Coronin-A is much more important for growth and cell size and morphology than previously thought. In *Xenopus* it has been shown that dimerization of Coronin is important for its function and also for its localization (Asano et al., 2001). This would explain why the N-terminal 200 aa expressed in the CorA-null mutant are non-functional. However, this has a strong effect on cell size and morphology, as the cell morphology in CorA-null cells was not physiological. The formation of fruiting bodies and spores was less impaired in the CorA-null mutant than in the knockout. When RNAi knockdown was introduced into wildtype cells, a similar effect on differentiation was observed. Coronin-A dimerization appeared to be critical for the ability to stream and survive (Drexler et al., 2016; Fiedler et al., 2020).

The strong influence of the truncated version of the protein in CorA-null cells was not expected but showed that the binding of Coronin-A to actin is probably more important in this process than the formation of multimers or the binding of the CC domain to link actin. Another result supporting this hypothesis was that the knock

sideway Coronin-A was tagged at the C-terminus with a fluorescent protein and the double FKBP domains, but still functioned close to normal. Steric hindrance and reduced binding efficiency were not shown to affect differentiation processes. The fact that RNAi-treated wildtype cells were able to form fruiting bodies as well as untreated controls confirmed that a lower amount of Coronin-A protein is sufficient to maintain its function. These results are also supported by the motility analysis. The displacement of the RNAi knockdown is less pronounced than in the AX2 wildtype, but still better than in the knockout. In the Aip1-null mutant background, RNAi had the unexpected effect of enhancing the displacement, which was never expected, but the positive effect on the motility of removing Coronin-A from Aip1-deficient cells has been shown previously in zebrafish neutrophils (Bowes et al., 2019). In the double knockout, motility was not higher compared to the Aip1-null#9.1 mutant. The knock sideway system was fully functional when examining the motility of the cells. In the absence of rapamycin, the cells moved almost as well as the wildtype, and when rapamycin was added, the displacement was as impaired as in the knockout.

Part II

Complementing *Dictyostelium discoideum* Aip1-null Mutant Phenotype

5 Results

The weak differences between the Aip1-null#9.1 mutant cell line and the AX2 wildtype are not surprising considering the life cycle, growth, and cell morphology (see Figures 3.5, 3.6, 3.7 and 3.11). In contrast, motility, as measured over 10-minute time intervals, provided a significantly different feature that was used in this part of the work to perform complementation assays (see Figure 3.13). To complement a mutant background, the gene of interest is reintegrated into the genome or expressed from a cytosolic plasmid under the native or a strong promoter. For *D. discoideum* cells, this is usually done with cytosolic plasmids. A derivative of the pDM358 plasmid (Veltman et al., 2009) expressing the gene of interest under a *actin*-15 promoter and terminated by an *actin*-8 terminator sequence has been used in this work as an expression vector for the various Aip1 encoding genes from both *A. thaliana* and *D. discoideum*. The backbone carried a hygromycin resistance cassette for selection by antibiotics. Hygromycin was used because the blasticidin resistance cassette was already present in the Aip1-null mutant and the additional geneticin resistance in the just created and established double knockout mutant (Aip1-null#9.1/*corA*-SLI, see above).

As has been known for twenty years, DdAip1 is not functional when tagged at the C-terminus. For the N-terminally tagged protein, an 80% rescue was found concerning the phagocytosis rate phenotype. Despite being functional or not, both proteins were able to localize to the site of action and both could be detected in the pseudopods of moving *D. discoideum* cells. (Konzok et al., 1999)

Interestingly, in *A. thaliana*, both AIP1 proteins are functional and show a rescue when C-terminally tagged, although the pollen-specific AIP1-1 seems to be slightly affected in its localization (Kiefer et al., 2015, Diao et al., 2020). Therefore, to complement the mutant phenotype in *D. discoideum*, AtAIP1-1 and AtAIP1-2 were tested with mCherry tags fused on either the N- or the C-terminus to reveal host- or donor-specific functionality. To improve the translation, all Aip1 coding DNA sequences were codon-optimized for host codon usage and only the CDS was expressed to avoid mis-splicing. For completeness and for different genetic backgrounds and stronger phenotypes, all Aip1 constructs were expressed in the Aip1-null single mutant as well as in the double-KO derived from the *corA*- SLI knockout method in Aip1-null#9.1 cells.

5.1 Validation of Aip1 Expression by Immunoblot and Fluorescence Microscopy

To demonstrate the full-length expression of all Aip1s in *D. discoideum* cells, protein extracts of all strains were prepared and subjected to SDS-PAGE and immunoblotting (see Section 2.2.2). A mCherry antibody was used to detect both the *A. thaliana* AIPs as well as DdAip1 and free mCherry. The plant and amoeba proteins differ by only 3 kDa in molecular weight (63 kDa and 66 kDa) and were therefore not distinguishable by size on the immunoblot. Since all proteins were tagged with mCherry (27 kDa), the total molar weight was 90-93 kDa.

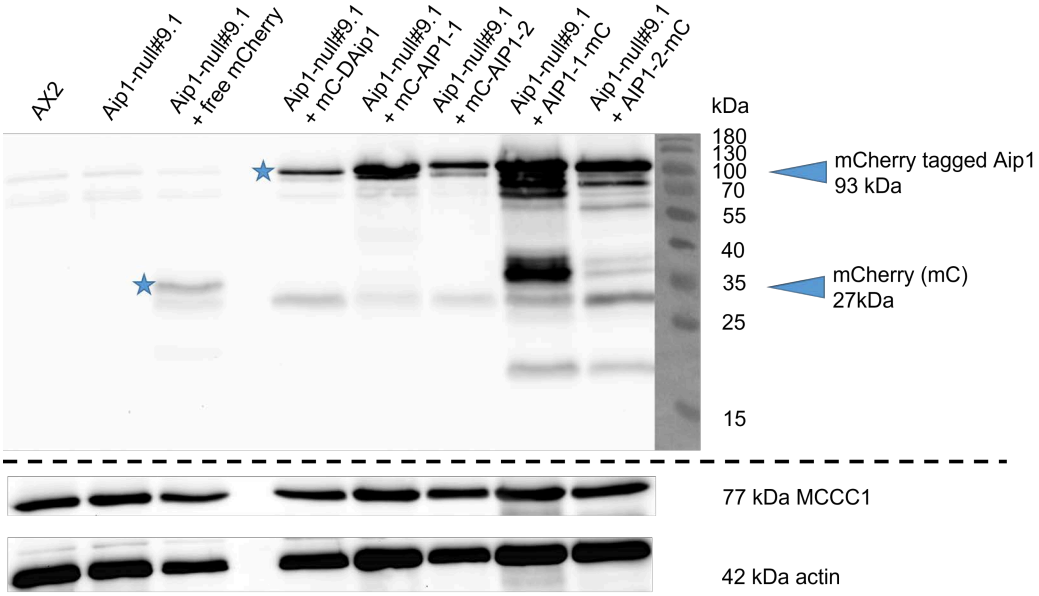

Fig. 5.1: Western blot (immunoblot) on protein extracts of wildtype (AX2) cells, Aip1-null#9.1 mutant (see Konzok et al., 1999) and complementation assay candidates: endogenous DdAip1 tagged N-terminal with mCherry; AtAIP1-1 and AtAIP1-2 each tagged on either side with mCherry, expression of free mCherry for comparison; all proteins were expressed under the control of the act15-promoter sequence; MCCC1 and Actin as loading controls (see 2.1.2); one representative example of three independent experiments.

The AX2 and Aip1-null#9.1 mutant strain, which did not express mCherry, showed a low background signal due to sparse unspecific binding of the mCherry antibody to proteins of approximately 70 kDa and 100 kDa molecular weight (see Figure 5.1, lane 1+2). Expression levels of Aip1 proteins were similar in all complementing strains (see Figure 5.1, lane 4-8) when comparing the signal strength with actin protein detection and MCCC1 expression as loading controls. The number of plasmids per

cell varied, but the extract of many cells should still give an average amount of protein for all strains. Aip1-null mutant cells expressing free mCherry showed two specific bands at 27 kDa and 29 kDa in addition to the unspecific bands (see Figure 5.1, lane 3). Interestingly, the free mCherry itself was partially cleaved from its linker, allowing the detection of the second product of nearly identical size, which was also present in all other mCherry-expressing lines. Full-length expression of all tagged Aip could be demonstrated, despite the presence of potential cleavage products. In N-terminally tagged versions of the protein (see Figure 5.1, lane 4-6), only one cleavage appeared to occur, resulting in two smaller fragments of the full-length protein. C-terminal mCherry-tagged AIP1 from *A. thaliana* showed many different cleavage sites, yielding 8 fragments ranging from 20 kDa to 80 kDa in addition to the full-length protein (see Figure 5.1, lane 7+8). AIP1-1-mCherry was more strongly expressed than all other detected proteins and a degradation product of about 37 kDa was very prominent compared to the AIP1-2-mCherry line. In summary, expression of full-length tagged Aip1 proteins was demonstrated for all strains, although additional cleavage products were also detected.

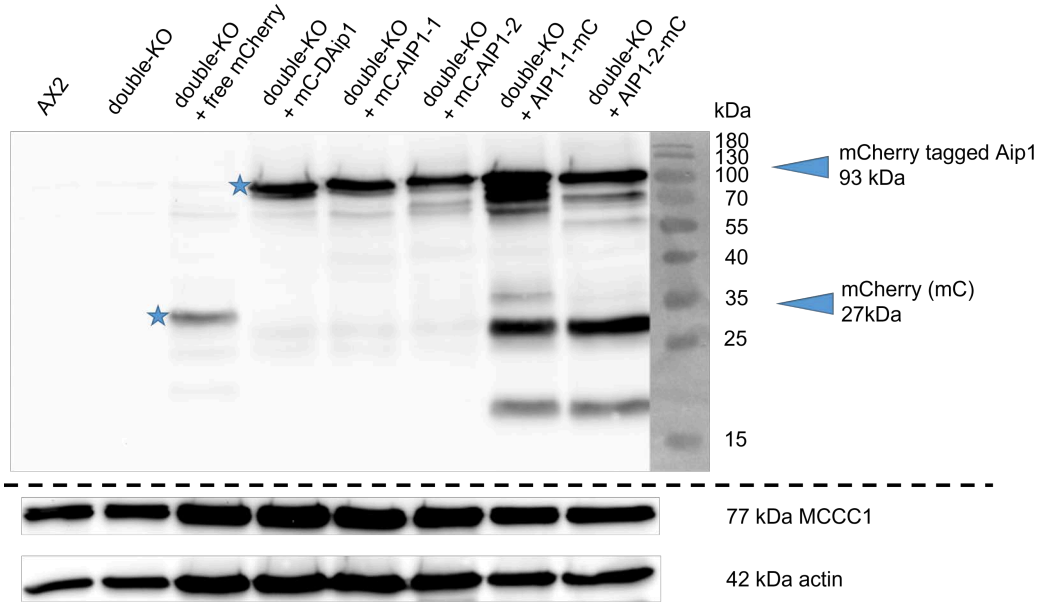

Fig. 5.2: Western blot (immunoblot) on protein extracts of wildtype (AX2) cells, Aip1-null#9.1 mutant (see Konzok et al., 1999) and complementation assay candidates in Aip1-null/*corA*- double-KO mutant background: endogenous DdAip1 tagged N-terminal with mCherry; AtAIP1-1 and AtAIP1-2 each tagged on either side with mCherry, expression of free mCherry for comparison; all proteins were expressed under the control of the act15-promoter sequence; MCCC1 and Actin as loading controls (see 2.1.2); one representative example of three independent experiments

The immunoblot of the complementation cell lines in the double-KO background showed the same results as the blot of the single mutant background (see Figures 5.1 and 5.2). Strikingly, in the double mutant background, AIP1-1-mCherry did not show the prominent cleavage product at 37 kDa like its homolog, but the amount of the fragment of mCherry at 27 kDa was much higher in both (see Figure 5.2, lane 7+8).

As shown in Figure 5.3, all versions of the Aip1 protein were localized to the forming pseudopods and were not as homogeneously distributed as the free mCherry in the Aip1-null knockout background. The endogenous tagged DdAip1 appeared more dotted than its more uniformly distributed foreign homologs AIP1-1 and AIP1-2.

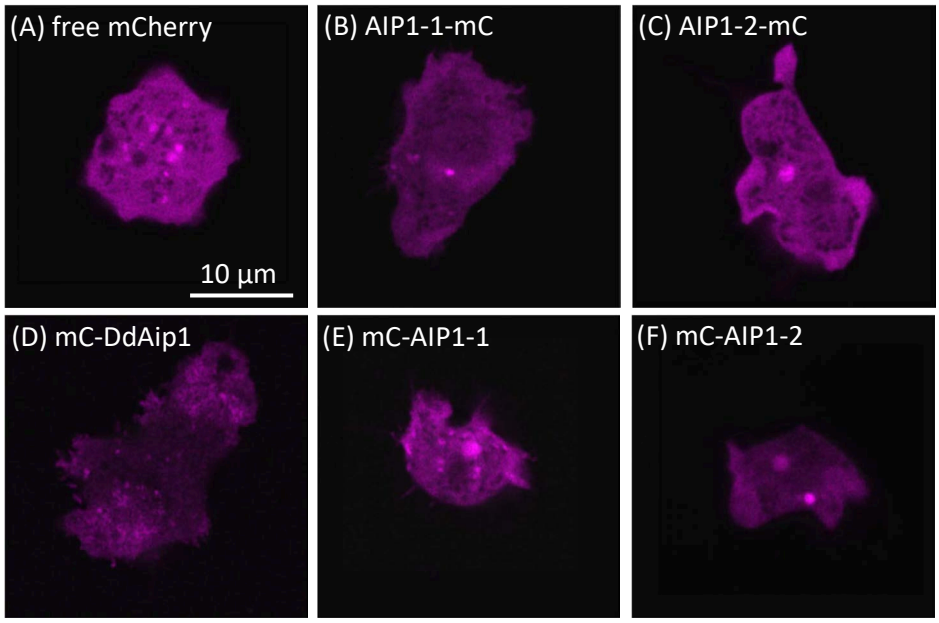

Fig. 5.3: Fluorescence LSM images of mCherry(mC)-tagged Aip1 expression in Aip1-null#9.1 mutant background (see Konzok et al., 1999); (A) free mCherry and (B) AIP1-1 and (C) AIP1-2 both C-terminally tagged with mCherry; (D) DdAip1, (E) AIP1-1, (F) AIP1-2 all N-terminally tagged with mCherry; all proteins were expressed under the control of the act15-promoter sequence.

In the Aip1-null/*corA*- SLI double mutant background, the expression of the different versions of the Aip1 protein could also be successfully verified by fluorescence microscopy (see Figure 5.4). All proteins, whether tagged at the N- or C-terminus, localized to actin polymerization sites in the forming pseudopods as expected. In the control cell line expressing free mCherry, mCherry was uniformly distributed throughout the cell (see Figure 5.4, lower left).

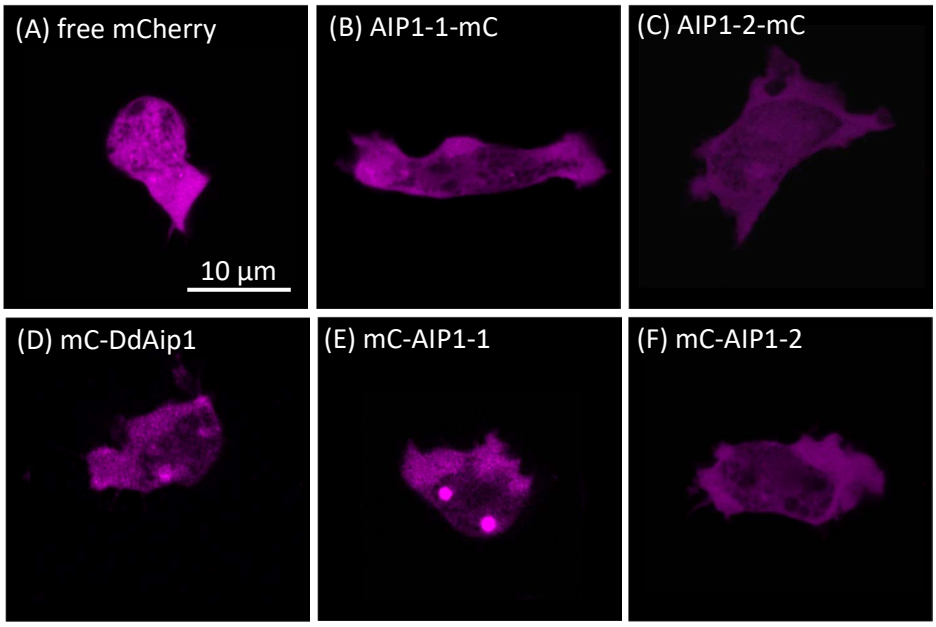

Fig. 5.4: Fluorescence LSM images of mCherry(mC)-tagged Aip1 expression in Aip1-null/*corA*- SLI double-KO mutant background; (A) free mCherry and (B) AIP1-1 and (C) AIP1-2 both C-terminally tagged with mCherry; (D) DdAip1, (E) AIP1-1, (F) AIP1-2 all N-terminally tagged with mCherry; all proteins were expressed under the control of the act15-promoter sequence.

5.2 Complementation of Aip1-lacking Mutants with endogenous DdAip1

5.2.1 Complementation of Aip1-null#9.1 single mutant

Motility as a parameter for complementation of the Aip1-null#9.1 single mutant phenotype was demonstrated in Aip1 loss-of-function mutants expressing N-terminal mCherry-tagged DdAip1, which is known to partially rescue the phagocytosis phenotype (Konzok et al., 1999). Interesting results were obtained when comparing the MSD curves of the Aip1-null knockout, the wildtype AX2, and the complementation cell line of DdAip1-expressing mutants (see Figure 5.5, A). Knockout and wildtype showed a very similar course of the MSD curve, although the knockout displaced more slowly. In the rescue line, there was a transition from a wildtype-like to a slower movement over time. On short timescales of around one minute, a clear complementation of the knockout phenotype could be shown (see Figure 5.5, B), while on longer timescales the movement mode approximated a non-rescue behavior. On a time scale of ten minutes, the movement of the rescue cells was still close to that of the wildtype cells (p-value of * =0.02,), but not significantly different from

the knockout (see Figure 5.5, B). Since it is known that a GFP-tagged protein variant did not fully rescue the phenotype (Konzok et al., 1999), such a partial rescue was to be expected.

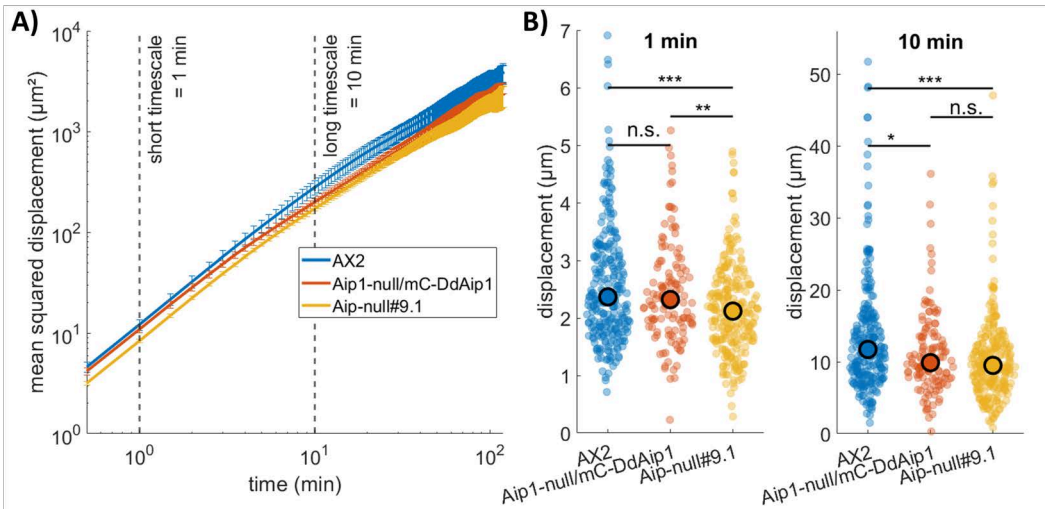

Fig. 5.5: Motility of the tested strains based on MSD and displacement in different time intervals; A) MSD of wildtype (AX2) cells, Aip1-null#9.1 mutant (see Konzok et al., 1999) and complementation with endogenous DdAip1 tagged N-terminal with mCherry; B) Displacement of the same cells as in A) in a short (1 min) and longer (10 min) time interval; Kolmogorov–Smirnov-Test; n.s.: not significant; *: p-value$\leq$ 0.05, **: p-value$\leq$ 0.01, ***: p-value$\leq$ 0.001; data are pooled from at least six independent experiments, employing around 100 cells per genotype (for the total number of analyzed cells see SI 10.4).

5.2.2 Complementation of Aip1-null/*corA*- SLI double mutant

In the complementation assay of the double mutant rescue with N-terminally tagged DdAip1, no significant difference could be detected in the *corA*- single mutant, the Aip1-null/*corA*- double mutant, and the rescue line. Although the curves appeared to be different (see Figure 5.6, A), the statistical KS test showed no significance at all, whether tested after 1-minute or 10-minute intervals (see Figure 5.6, B).

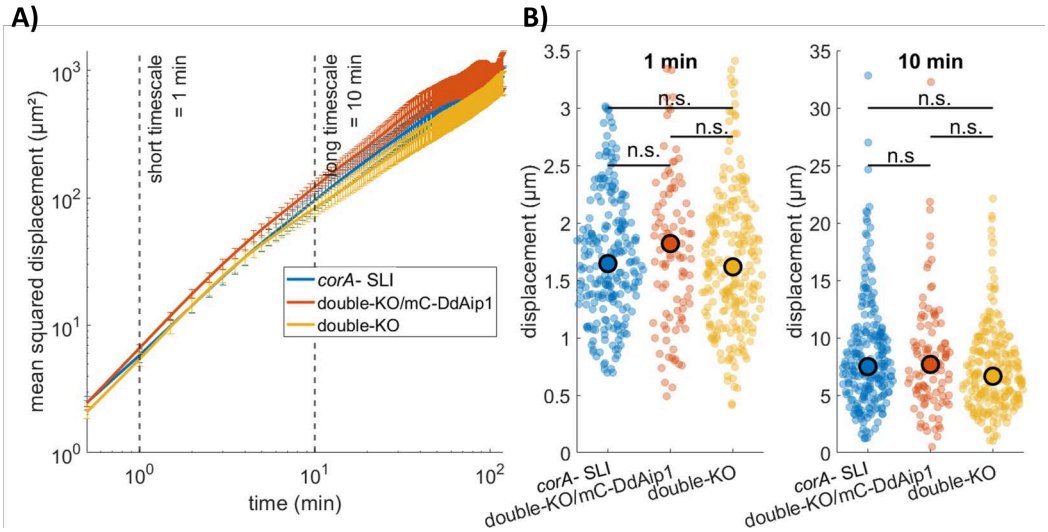

Fig. 5.6: Motility of the tested strains based on MSD and displacement in different time intervals; A) MSD of *corA*- SLI single mutant, Aip1-null/*corA*- SLI double-KO mutant and complementation with endogenous DdAip1 tagged N-terminal with mCherry; B) Displacement of the same cells as in A) in a short (1 min) and longer (10 min) time interval; Kolmogorov–Smirnov-Test; n.s.: not significant; *: p-value$\leq$ 0.05, **: p-value$\leq$ 0.01, ***: p-value$\leq$ 0.001; data are pooled from at least six independent experiments, employing around 100 cells per genotype (for the total number of analyzed cells see SI 10.4).

5.3 Interspecies complementation of Aip1-lacking *Dictyostelium discoideum* mutants with *Arabidopsis thaliana* AIP1-1 and AIP1-2

As already described in the theoretical background part of this work, actin is highly conserved across many species. Over 90% sequence identity is given between the major actin in *D. discoideum* and *A. thaliana*. Aip1 is known to interact with actin in both species. Therefore, an interspecies exchange of Aip1 was performed to investigate the potential of functional replacement or partial functionality od a homolog from another species in the heterologous host. It is known that *A. thaliana* AIP1 is functional when tagged at the C-terminus (Kiefer et al., 2015), in contrast to DdAip1 (Konzok et al., 1999). Therefore, both plant homologs were tagged on both sides to see if a possible dysfunction of the protein is caused by a steric hindrance of the interaction of the protein with actin or by poor cooperation with other proteins.

5.3.1 Interspecies complementation of Aip1-null#9.1 single mutant

First, the C-terminally tagged versions of AIP1-1 and AIP1-2 were expressed in Aip1-null#9.1 single mutants using the codon-optimized coding sequence linked to mCherry. Although the sequence similarities for Aip1 are more similar when comparing DdAip1 and AIP1-2, in this case, AIP1-1 C-terminally tagged with mCherry rescued the mutant phenotype, while the C-terminally tagged AIP1-2 behaved still identical to the knockout (see Figure 5.7, A) also when considering short time interval (see Figure 5.7, B). After 10 minutes, the rescue of AIP1-1 was still working as before, but the AIP1-2 became more different from the mutant, although it was still not rescuing (see Figure 5.7, B).

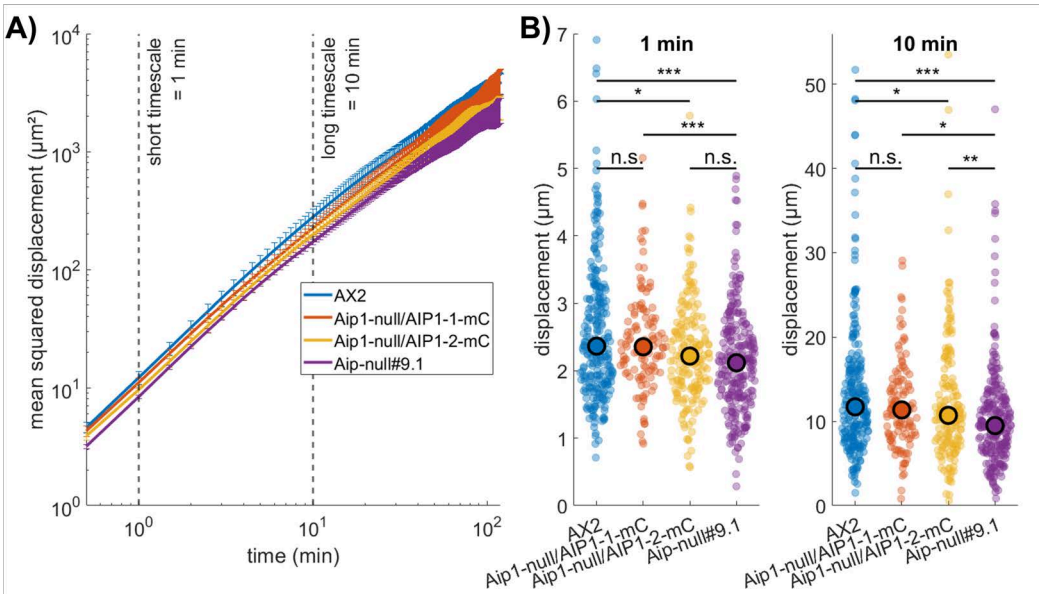

Fig. 5.7: Motility of the tested strains based on MSD and displacement in different time intervals; A) MSD of wildtype (AX2) cells, Aip1-null#9.1 mutant (see Konzok et al., 1999) and complementation with *A. thaliana* AIP1-1 and AIP1-2 both C-terminally tagged with mCherry; B) Displacement of the same cells as in A) in a short (1 min) and longer (10 min) time interval; Kolmogorov–Smirnov-Test; n.s.: not significant; *: p-value$\leq$ 0.05, **: p-value$\leq$ 0.01, ***: p-value$\leq$ 0.001; data are pooled from at least six independent experiments, employing around 100 cells per genotype (for the total number of analyzed cells see SI 10.4).

Furthermore, the N-terminally tagged versions of AIP1 were tested. In contrast to DdAip1, which is functional only in its N-terminally tagged version, N-terminally tagged AIP1-2 even had a negative influence on the motility of *D. discoideum* cells (see Figure 5.8, shown in yellow). This did not change when the observation interval was changed (see Figure 5.8, B). The very uniform course of the MSD plot could also be observed for C-terminally tagged AIP1 (see Figure 5.8 and 5.7, A). Thus, the

non-rescued cell lines and the mutant cell line were simply slower than wildtype AX2.

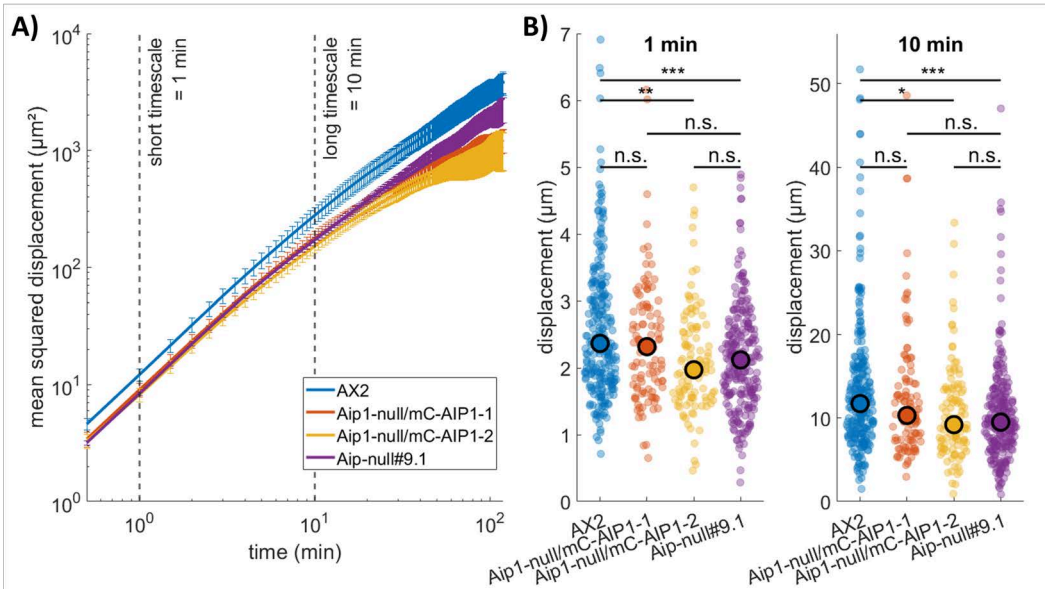

Fig. 5.8: Motility of the tested strains based on MSD and displacement in different time intervals; A) MSD of wildtype (AX2) cells, Aip1-null#9.1 mutant (see Konzok et al., 1999) and complementation with *A. thaliana* AIP1-1 and AIP1-2 both N-terminally tagged with mCherry; B) Displacement of the same cells as in A) in a short (1 min) and longer (10 min) time interval; Kolmogorov–Smirnov-Test; n.s.: not significant; *: p-value$\leq$ 0.05, **: p-value$\leq$ 0.01, ***: p-value$\leq$ 0.001; data are pooled from at least six independent experiments, employing around 100 cells per genotype (for the total number of analyzed cells see SI 10.4).

5.3.2 Interspecies complementation of Aip1-null/*corA*- SLI double mutant

Since the results obtained by complementing the single mutant with AIP1 were unexpected, a motility change was also assumed for the rescue of the double mutant. As shown in Figure 5.9 B, on short time scales (1 min), the motility of cells expressing C-terminally tagged AIP1 in the double mutant background greatly exceeded that of the single mutant. AIP1-1 and its homolog AIP1-2 showed no significant difference from each other. In an interval of 10 minutes (see Figure 5.9, B), the AIP1-1 expressing cells showed the same higher motility as for short periods, while the motility of the AIP1-2 expressing cells was comparable to the motility of the single mutant and was not significantly different to it. Regarding the MSD (see Figure 5.9 A), both rescue strains showed the same behavior and were displacing to a greater extent and faster than the single mutant and double mutant.

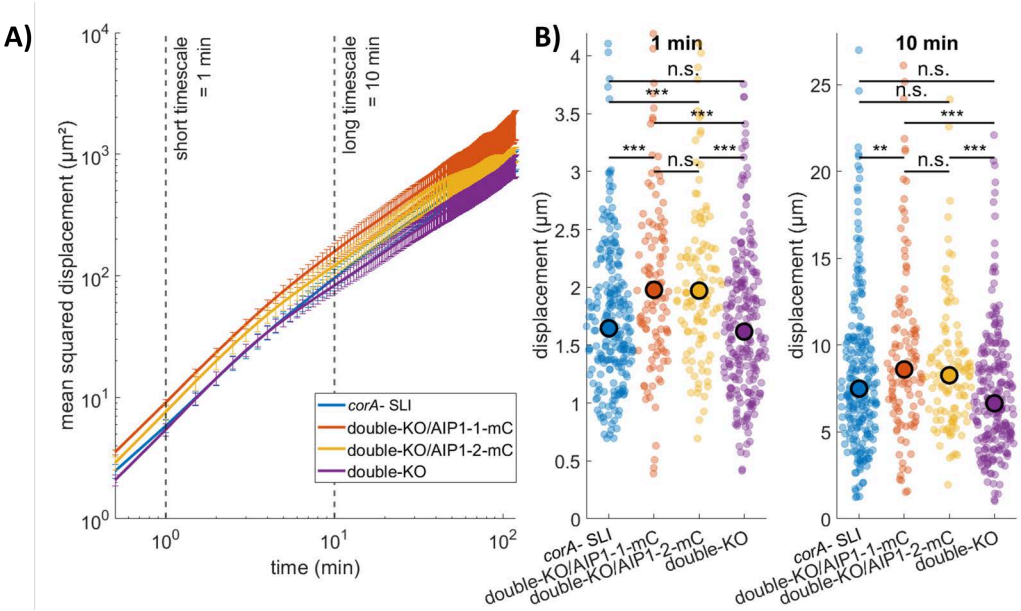

Fig. 5.9: Motility of the tested strains based on MSD and displacement in different time intervals; A) MSD of *corA*- SLI single mutant, Aip1-null/*corA*- SLI double-KO and complementation with *A. thaliana* AIP1-1 and AIP1-2 both C-terminally tagged with mCherry; B) Displacement of the same cells as in A) in a short (1 min) and longer (10 min) time interval; Kolmogorov–Smirnov-Test; n.s.: not significant; *: p-value$\leq$ 0.05, **: p-value$\leq$ 0.01, ***: p-value$\leq$ 0.001; data are pooled from at least six independent experiments, employing around 100 cells per genotype (for the total number of analyzed cells see SI 10.4).

When comparing the motility of the N-terminally tagged versions of AIP1 expressed in the double mutant background, an even more striking result was obtained for tagged AIP1-2 (see Figure 5.10). The entire distribution of measured motilities showed a strong increase in median motility, up to 1.5 times compared to other strains, for both shorter and longer time intervals (see Figure 5.10, B) in comparison to the single and the double mutant and to the rescue line with the tagged AIP1-1. Although the displacement was much faster than the others, for shorter times in the MSD (see Figure 5.10, A), the curve got closer to the others at larger time scales. A small shift in motility distribution could also be seen for N-terminally tagged AIP1-1, but after 10 min it was no longer significantly different from the others (see Figure 5.10, B).

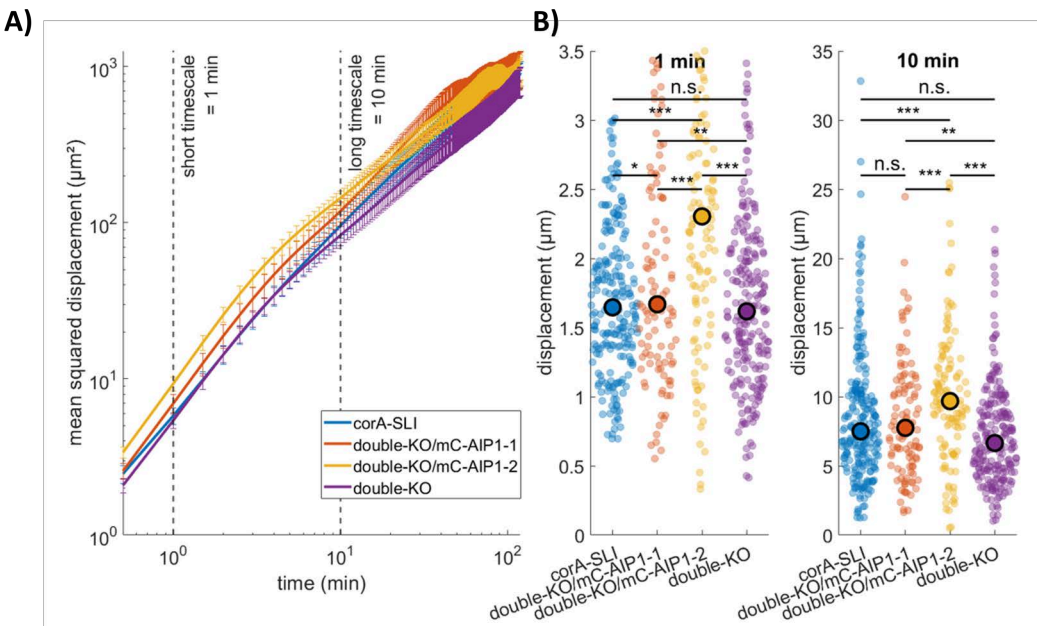

Fig. 5.10: Motility of the tested strains based on MSD and displacement in different time intervals; A) MSD of *corA*- SLI single mutant, Aip1-null/*corA*- SLI double-KO and complementation with *A. thaliana* AIP1-1 and AIP1-2 both N-terminally tagged with mCherry; B) Displacement of the same cells as in A) in a short (1 min) and longer (10 min) time interval; Kolmogorov–Smirnov-Test; n.s.: not significant; *: p-value$\leq$ 0.05, **: p-value$\leq$ 0.01, ***: p-value$\leq$ 0.001; data are pooled from at least six independent experiments, employing around 100 cells per genotype (for the total number of analyzed cells see SI 10.4).

6 Discussion

The complementation of a knockout mutant is an important way to test for whether the mutation is the actual cause of the phenotype. It can be further used to assess the functionality of the (tagged) protein. It can reveal if the phenotype is due to the missing or mutated gene, or if it is caused by an off-target effect introduced by the mutation method such as additional mutations and/or insertions in the genome or targeting of a similar gene in case of e.g. miRNA, antisense and/or CRISPR/Cas9 approaches. For *D. discoideum* a cytosolic expression vector with a strong *actin15* promoter was used. Ideally, more adequate results would have been obtained by using the endogenous promoter and reintegrating the construct into the genome, which could not be accomplished in this work.

In the immunoblot, full-length expression of all proteins was detected (see Figures 5.1 and 5.2). The expression of free mCherry resulted in a weak double band at 29 kDa and 27 kDa. The difference of 2 kDa is exactly the size of the linker added to free mCherry. This linker appeared to be completely cleaved from mCherry. A band of the exact size of free mCherry was seen in every sample, whether expressed in the single or double mutant background (see Figure 5.1 and Figure 5.2). All N-terminally tagged proteins showed bands of the expected protein size at around 90 kDa and a slightly smaller band that appears to be an unidentified cleavage product that still carries a small portion of mCherry. mCherry-AIP1-1 was most highly expressed in the single mutant but did not show the same ratio of cleaved free mCherry as Aip1 and its direct homolog AIP1-2 (see Figure 5.1, lanes 5+6). This behavior could not be shown for its expression in double-KO (see Figure 5.2, lanes 5+6). C-terminally tagged AIP1-1 and AIP1-2 showed many degradation products. Presumably, the degradation of C-terminally tagged Aip1 may have accounted for the lacking rescue ability in the experiments in this study as well as for the C-terminally-tagged DdAIP1-GFP in *D. discoideum* in the past (Konzok et al., 1999). The strong band at about 17 kDa indicated that mCherry itself is also cleaved in these samples (see Figure 5.1 and Figure 5.2, lanes 7+8). In the double-KO, mCherry was cleaved from the C-terminus of the protein at a high rate, resulting in a strong band at 27 kDa.

In addition, LSM images of all complementation cell lines showed the strongest intensity of emitted light in the mCherry-specific region of the spectrum. As expected, free mCherry resulted in a homogeneous signal throughout the cell, while

all mCherry-tagged AIP1 and Aip1 proteins localized to the pseudopods as expected (see Figures 5.3 and 5.4). This had previously been observed for N-terminally or C-terminally GFP-tagged Aip1 (Konzok et al., 1999). In the images of knockouts expressing C-terminally tagged AIP1-1 and AIP1-2 (see Figures 5.3 and 5.4, top row, middle and right), a strong cytosolic signal could be detected compared to the signal of the localized protein. This is consistent with the large amount of cleaved free mCherry and other fragments detected in the immunoblot.

6.1 Complementation of Aip1 single and Aip1-null/*corA*- SLI double mutant with endogenous Aip1

Since it has already been shown that C-terminally GFP-tagged DdAip1 localizes to the correct side in the cell but is not functional (Konzok et al., 1999), only N-terminally mCherry-tagged DdAip1 was used in this study. Strong significant differences in motility were observed between the AX2 wildtype cell line and the Aip1-null#9.1 mutant. The complementation cell line Aip1-null#9.1+mC-DdAip1 showed a complete rescue at short time scales, where it displayed significant differences to the knockout (see Figure 5.5, B). However, after the crossover point at 4 min, the MSD of the rescue line changed from faster than normal diffusion (superdiffusive regime) to slower diffusion (subdiffusive regime) (see Cherstvy et al., 2018 for more details), while the wildtype still showed a faster diffusion until the crossover point was reached at a time interval of 10 min (see Figure 5.5, A).

This led to an alignment of the MSD curves of the mutant and the complementation line so that the difference between these two lines was not significant at the later time points (see Figure 5.5, B). As only a partial rescue of the phagocytosis phenotype up to 80% had been observed for GFP-tagged DdAip1 in the past (Konzok et al., 1999), the observed partial rescue of the displacement phenotype at 10 min further supports a partial functionality even of the N-terminally mCherry-tagged DdAip1 protein. Whether this was due to overexpression of Aip1 under a strong promoter or to the influence of the fluorescent tag cannot be assessed. A possible explanation could be that only untagged Aip1 is functional, and therefore only the small amount of correctly cleaved Aip1 from mCherry could do its job. Then the combination of overexpression and a partial amount of cleaved protein could be the reason for the 80% rescue phenotype. The motility of the mutant was shown to be half that of the wildtype and a full rescue was obtained (Ishikawa-Ankerhold et al., 2010, Konzok et al., 1999). Since this motility was calculated from 30-second time-lapse intervals,

it supports the results of the present study at 1-minute time intervals, where the fusion protein was still able to fully correct the mutant phenotype.

Interestingly, the results of mCherry-DdAip1 expression in the Aip1-null/*corA*- SLI double mutant did not show any significant rescue regarding cell motility at neither 1 min nor 10 min intervals (see Figure 5.6). However, overexpression of endogenous Aip1 resulted in a slight but not significant increase in displacement, which became more pronounced with increasing time intervals. Comparison of displacements at even longer time intervals than 10 min would likely have resulted in a significant difference between single knockout, double knockout, and rescue cell lines. Although *corA* single mutants are reported to be twice as fast as the double mutant cells (Ishikawa-Ankerhold et al., 2010), this could not be demonstrated in this study (see Figure 5.6, B). The phenotype of the complete *corA*- SLI knockout was already very strong. Therefore, the complementation of the double knockout with a non-fully rescuing tagged protein was poor as expected.

6.2 Complementation of Aip1-null single and Aip1-null/*corA*- SLI double mutant with and interspecies interchanged Aip1

Studying the interchangeability of proteins between different species is a good way to test whether the protein can restore the wildtype phenotype in phylogenetically distant species despite differences in structure and sequence. Chimeric proteins have also been tested in the past. For example, the chimeric rabbit and human epidermal growth factor I has successfully interacted with foreign proteins *in vitro* (Williamson et al., 2005). Interestingly, it has been shown that interspecies exchange of homologous genes can be a natural process in prokaryotic cells such as bacteria (Château et al., 1994) as well as in eukaryotic polyploid plants such as wheat and *Arabidopsis* (Zhang et al., 2020; Oruganti et al., 2023).

In this study, the Aip1 of *D. discoideum* and the two homologs of the flowering plant *A. thaliana*, were studied and exchanged. The reproductive version of Aip1 in *A. thaliana* AIP1-1 and the vegetatively expressed AIP1-2 are still closely related to each other (sequence identity of AIP1-1 and AIP1-2 is 68% with 81% positives), sharing only about 40% amino acid sequence identity with the *D. discoideum* Aip1 (DdAip1) (see SI 10.1, Figure 10.1). As discussed above, the C-terminally tagged version of DdAip1 is not functional in *D. discoideum* cells (Konzok et al., 1999). For AIP1-1 and AIP1-2, it has been shown that both proteins are functional when C-terminally tagged, reintegrated into their host, and expressed under their own

promoter (Kiefer et al., 2015; Diao et al., 2020). To complement the amoeba cells, the DdAip1 and the *A. thaliana* AIP1s were expressed using the same plasmid harboring the strong *act15* promoter. To ensure the correct translation of the plant proteins a codon-optimized version was used and both proteins were tagged on both sides (see Section 5). In both the single and double mutants, expression of the Aip1 versions was confirmed by immunoblot (see Figures 5.1 and 5.2). N-terminally tagged proteins showed fewer degradation products and full-length expression, although the mCherry tag was cleaved from a small fraction of the total expressed protein (see Figures 5.1 and 5.2, lanes 4-6). This was different for both C-terminally tagged AIP1, where many cleavage products were found (see Figures 5.1 and 5.2, lanes 7+8). These results are consistent with those for DdAip1 (see above).

When observing and analyzing the motility of AX2 wildtype cells compared to the single knockout and the different versions of complementation cell lines expressing foreign AIP1, a clear advantage of AIP1-1 over AIP1-2 was discovered (see Figures 5.7 and 5.8). This effect was found for both N- and C-terminally tagged AIP1-1 and AIP1-2. AIP1-1 showed a complete rescue for displacements during time intervals of 1 min and 10 min observed for both tags. However, since many cleavage products were seen in the immunoblot, it is possible that the C-terminal mCherry and another unessential part of AIP1-1 are cleaved, resulting in a functional AIP1-1 and a fragment of 37 kDa size. This could also explain the partial rescue of the motility phenotype in single mutants by AIP1-2-mCherry (see Figure 5.7) as tethering a fluorescent protein to Aip reduces its functionality by at least 20% in *D. discoideum* cells (Konzok et al., 1999). Thus, tag removal may be a coping strategy of the amoeba to gain as much functional protein as possible. N-terminally tagged AIP1-2 had an even stronger and negative effect (see Figure 5.8) and did not show strong cleavage fragments of the expressed proteins. It may therefore exert a dominant-negative mutant behavior.

In the Aip1-null/*corA*- SLI double mutant expressing the rescue constructs, a behavior similar to the mCherry-DdAip1 could be shown (see 5.9 and 5.10). Tagged versions of AIP1 also resulted in a strong increase in motility compared to the single and double mutant results. Interestingly, these effects were more pronounced and equally strong in C-terminally tagged versions of AIP1-1 and AIP1-2 (see Figure 5.9), but absent in N-terminally tagged AIP1-2 (see Figure 5.10) for smaller time intervals. The overcompensation may have been initiated by cleavage of the protein and the fluorescent tag, which is much more pronounced in the double mutant (see Figure 5.2) than in the single mutant. Therefore, a large amount of overexpressed free AIP1 protein is available and the large excess would likely lead to increased motility. In the case of EGF1, a foreign protein also showed much higher activity than the endogenous one (Williamson et al., 2005). mCherry-AIP1-1 showed no or only minor differences to the single mutant and thus a partial rescue of the double mutant

phenotype. Perhaps the C-terminally tagged DdAip1 was not cleaved and therefore did not show any functionality.

Although AIP1-1 and AIP1-2 differ by only 3% in sequence identity in direct comparison with *D. discoideum* Aip1, the ability to rescue the mutant phenotype varied clearly. The more similar AIP1-2 showed stronger negative effects than its evolutionarily younger homolog AIP1-1. These effects support the hypothesis that amino acid composition may not be as important as structure when comparing homologs of proteins from different species. By expressing different versions of Aip1 in *D. discoideum*, it was found that its function is strongly influenced by fluorescent tags. A possible approach to reduce this effect could be the use of smaller tags such as the commonly used Myc-tag or polyhistidine-tag.

Part III

Complementing *Arabidopsis thaliana* *aip1-2.1* and *aip1.2-1 act7-6* Double Mutant Phenotypes

7 Results

A mild epidermal planar polarity phenotype was detected in two *A. thaliana aip1-2* mutants compared to the wildtype Col-O accession (Kiefer et al., 2015). However, in about five years since then, a significant difference and the corresponding rescue could be obtained after complementation with endogenous *AIP1-2*. *aip1.2-1* mutants showed a basal shift of the root hair initiation site along the root hair cell compared to the slightly more apical site in Col-0 wildtype (see Kiefer et al., 2015 for details). These phenotypes could be reproduced several times in different experiments since then and were also part of the experiments in this work as the initial idea was to test the potential rescue of this phenotype by *Ddaip1*. To minimize the translational influence on the expression of the protein, the *Ddaip1* coding sequence (cds) was codon-optimized for expression in *A. thaliana*.

7.1 Complementation of *aip1.2-1* Single Mutant

7.1.1 Validation of Aip1 Expression in *aip1.2-1* by Immunoblot and Fluorescence Microscopy

The expression of mCherry-tagged Aip1 in the *aip1.2-1* mutant background was tested by immunoblot detection of mCherry in plant protein extracts from approximately 30 seedlings per genotype and line. The Col-0 accession and the mutant were run as negative controls together with the positive control expressing AIP1-2-mCherry under control of a larger fragment of its genomic region (created by Kiefer et al., 2015) and a free mCherry expressing *aip1.2-1* mutant line for comparison. Two insertion lines of each rescue construct were tested in the *aip1.2-1* background. BIP, an ER-localized heat shock protein, and actin proteins were detected as a double loading control since an influence of expressed Aip1 on actin levels could be hypothesized (see 2.1.2 for antibodies).

Aip1 tagged with mCherry has a molar mass of 90-93 kDa, depending on whether it is the *D. discoideum* protein or one of the two *A. thaliana* homologs. Differences in these sizes could not be distinguished in the immunoblot, so AIP1-2-mCherry, AIP1-1-mCherry, and both tagged *Dictyostelium* constructs showed the same molar weight

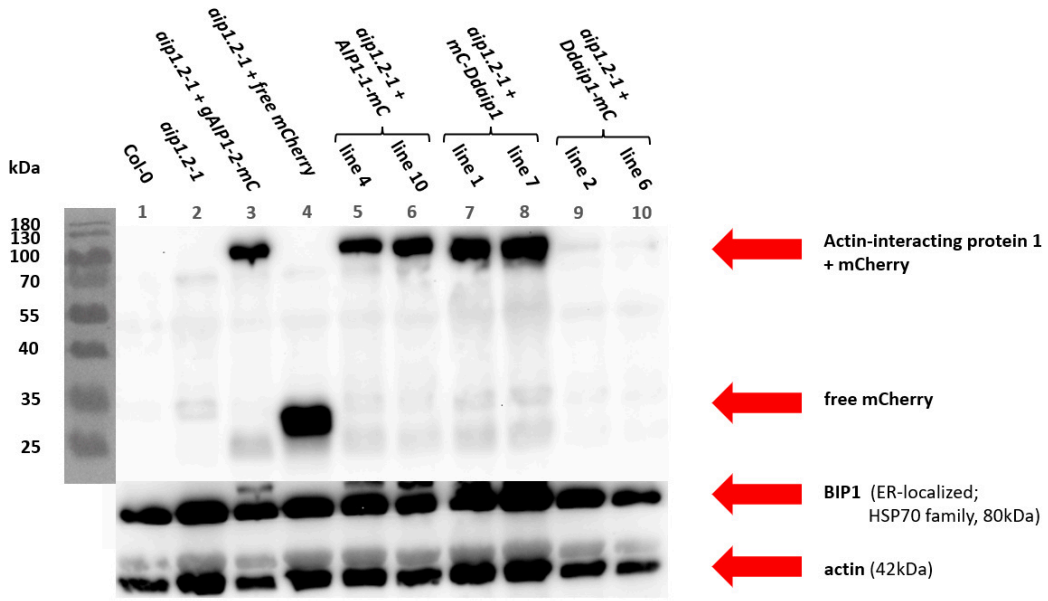

Fig. 7.1: Expression of mCherry-tagged Aip1 homologs in *A. thaliana aip1.2-1* mutants. Western blot (immunoblot) for detection of mCherry and mCherry-tagged (mC) Aip1 homologs in protein extract of plant lines of interest; Col-0 und *aip1.2-1* as negative controls; positive control lines expressing *A. thaliana* AIP1-2-mC in *aip1.2- 1* mutant background (Kiefer et al., 2015) or free mC; two insertion lines of each rescue construct Ddaip1-mC, mCh-Ddaip1 and AtAIP1-1-mC all expressed in *aip1.2-1* background under the control of the pAIP1-2-promoter sequence were tested; anti-BIP1 (BIP) and anti-Actin (actin) antibodies were used to detect BIP1 and different actin isoforms as loading controls (see 2.1.2 for antibodies), left: molar weight standard; top, grey: lane numbers; one representative example of three independent experiments.

in the blot (see Figure 7.1). The amount of expressed free mCherry under *AIP1-2* genomic regulatory sequences was higher compared to the AIP1 homolog mCherry fusion proteins in all plant lines (lane 4). AIP1-1 (lanes 5+6) showed similar levels to its homolog and the N-terminally tagged DdAip1 (lanes 7+8). Unexpectedly, the C-terminally tagged DdAip1 (lanes 9+10) was barely detectable in both selected plant lines (see Figure 7.1). In Col-0 (lane 1) only a very faint band at about 50 kDa could be detected for unspecific binding of the antibody. In the *aip1.2-1* mutant (lane 2), three faint unspecific bands were detected at 70 kDa, 50 kDa, and around 30 kDa, which were also present in all other plant lines with the mutant background. All plant lines except the negative controls showed an additional faint band at 25 kDa, which was also present in the free mCherry expressing line. Both loading controls showed proportional results. The total amount of loaded protein was satisfactory and comparable in all samples. Taken together, all AIP1 homolog-mCherry fusion proteins were expressed at full length displaying little to no degradation products except for C-terminally tagged DdAip1 which was expressed at very low barely detectable levels.

To gain insight into the expression and localization of mCherry-tagged Aip1, all plant lines of interest were additionally tested for their mCherry-specific fluorescence using an LSM 880 with AiryScan detector (Zeiss, Germany) and a laser excitation at 561 nm. Seeds of the different plant lines were sown in glass bottom chambers and root hairs were imaged 5-6 days after germination.

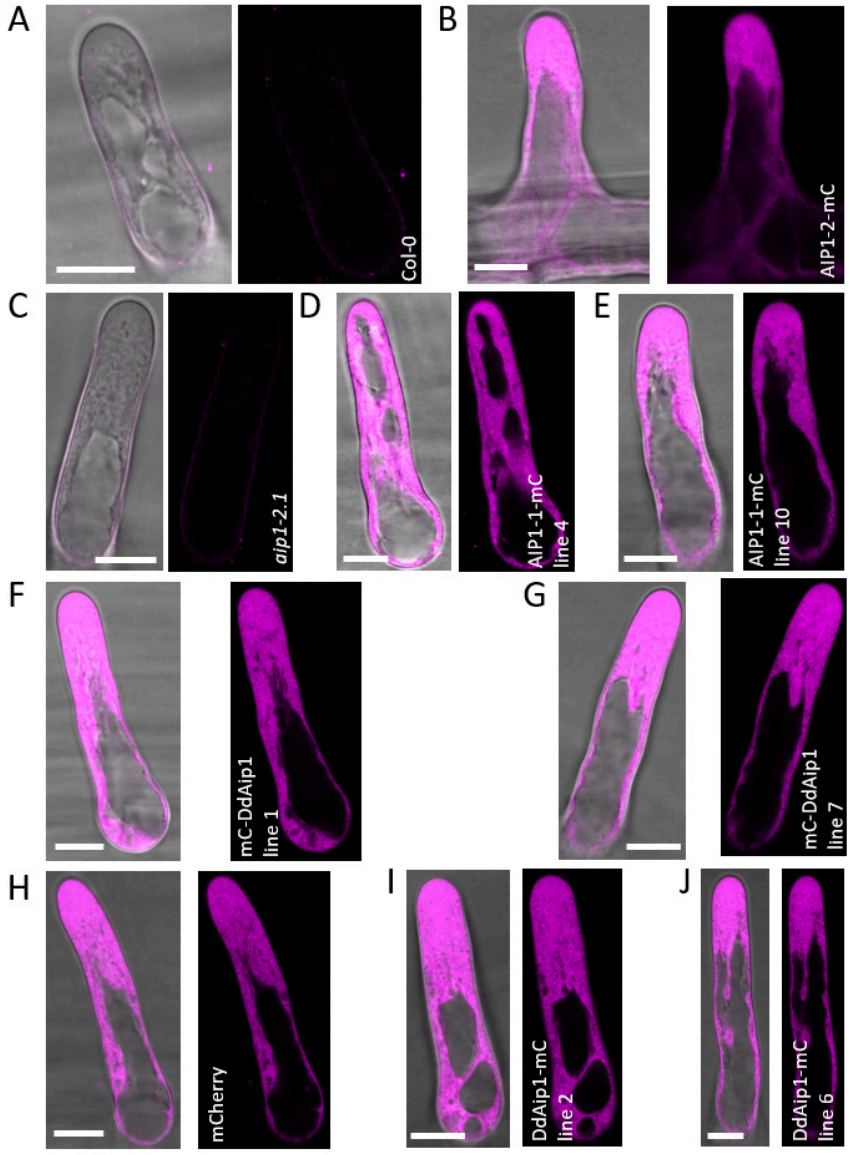

Fig. 7.2: Subcellular localization of mCherry(mC)-tagged Aip1 homologs in root hairs of *A. thaliana aip1.2-1* mutants. Representative Airy Scan LSM images of Col-0 (A) and *aip1.2-1* (C) as negative controls; positive control lines expressing *A. thaliana* AIP1-2-mC in *aip1.2- 1* mutant background (Kiefer et al., 2015) (B) or free mC (H); two insertion lines of each rescue construct Ddaip1-mC, mC-Ddaip1 and AtAIP1-1-mC all expressed in *aip1.2-1* background under the control of the pAIP1-2-promoter sequence were tested (D-G, I-J); merged image of fluorescent and brightfield image (left) and fluorescent image (right) only; scale bar: 10 μm.

Figure 7.2 shows the merged fluorescence and brightfield images of root hairs from different plant lines. In contrast to the low expression levels of the C-terminally tagged DdAip1 shown in the immunoblot (see above), the images did not show a clear difference in signal reduction compared to the other Aip1 expressing lines, when keeping the laser excitation and detector settings constant. As expected, only a very weak background signal was detectable in Col-0 wildtype (A) and *aip1.2-1* mutant (C). The distribution of free mCherry (H) and mCherry-tagged proteins (B,D-G,I-J) seemed to be almost homogeneous in the cytoplasm and was only influenced by the different sizes of the vacuole and the strong actin filaments in the cell.

7.1.2 Root Hair Positioning in *aip1.2-1* Single Mutant

The basal shift in root hair positioning previously shown by the working group (Kiefer et al., 2015 and others) could not be reproduced in this work, although a significant difference between the *aip1.2-1* single mutant and the Col-0 wildtype could be demonstrated in the initial experiments (see Figure 7.3).

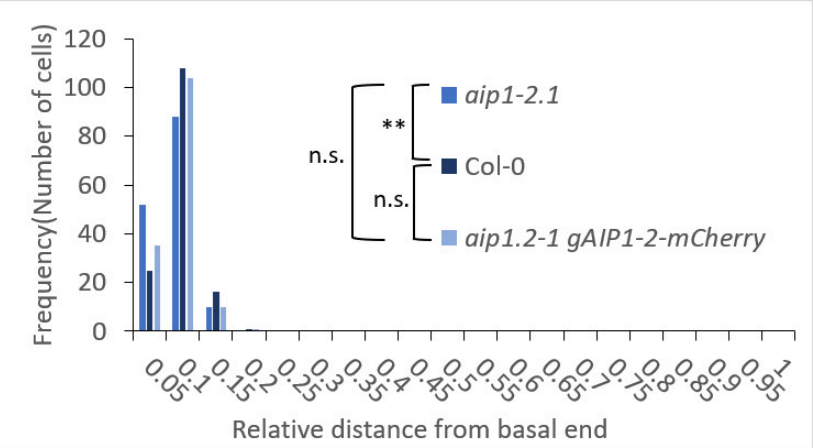

Fig. 7.3: Quantitative analysis of relative root hair positioning in wild type Col-0, *aip1.2-1* single mutant and the rescue line *aip1.2-1 gAIP1-2-mCherry* under the control of the pAIP1-2-promoter sequence). Number of root hair cells (frequency) with relative hair positioning classed from 0 (basal-most) to 1 (apical-most); pooled data from three experiments, on a total of n=150 cells per genotype; p-values obtained from Kolmogorov-Smirnov statistical test for differences between distributions are displaced by asterisks: n.s.: not significant at a significance level of 0.05; *: p-value$\leq$ 0.05, **: p-value$\leq$ 0.01, ***: p-value$\leq$ 0.001. Col-0 vs. *aip1.2-1*: p=0.882, Col-0 vs. *aip1.2-1 gAIP1-2-mCherry*: p=0.216, *aip1.2-1* vs. *aip1.2-1 gAIP1-2-mCherry*: p=0.167.

However, as shown in Figure 7.4, the relative distance from the basal end of the root hair cell was not significantly different between the mutant and the Col-0 line in later experiments (data tested for significance by Kolmogorov-Smirnov test).

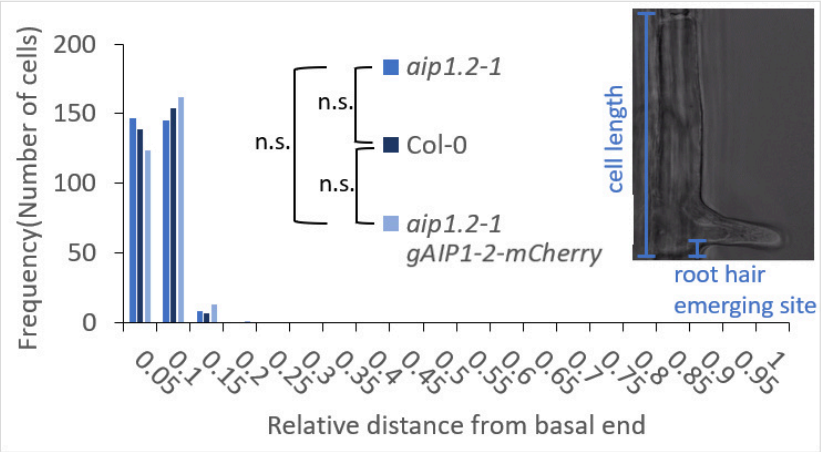

Fig. 7.4: Quantitative analysis of relative root hair positioning in wild type Col-0, *aip1.2-1* single mutant and the rescue line *aip1.2-1 gAIP1-2-mCherry* under the control of the pAIP1-2-promoter sequence). Number of root hair cells (frequency) with relative hair positioning classed from 0 (basal-most) to 1 (apical-most); pooled data from six experiments, on a total of n=300 cells per genotype; p-values obtained from Kolmogorov-Smirnov statistical test for differences between distributions are displaced by asterisks: n.s.: not significant at a significance level of 0.05; *: p-value$\leq$ 0.05, **: p-value$\leq$ 0.01, ***: p-value$\leq$ 0.001. Col-0 vs. *aip1.2-1*: p=0.001, Col-0 vs. *aip1.2-1 gAIP1-2-mCherry*: p=0.167, *aip1.2-1* vs. *aip1.2-1 gAIP1-2-mCherry*: p=0.128.

Therefore, root hair positioning in the *aip1-2* mutant background did no longer provide a stable readout for the characterization of rescue lines and was not further considered, when planning the characterization and corresponding complementation assays for the mutant phenotype. To find another phenotype for comparison, other parameters were analyzed in the mutant, wildtype, and rescue line, as described in the following section.

7.1.3 Root Hair Growth and Cell Length in *aip1.2-1* Single Mutant

Since Aip1 is known to affect actin treadmilling and actin depolymerization, the effect of the *aip1-2* mutation on root hair tip growth was analyzed to find a new robust mutant phenotype. The growth of the root hair tip in the different plant lines was followed by time-lapse imaging using the AiryScan LSM technique and the manual tracking analysis tool in the free ImageJ software (see also Methods used for *A. thaliana*). The averaged values of the growth and the SD as error bars were plotted in the graph shown in Figure 7.5.

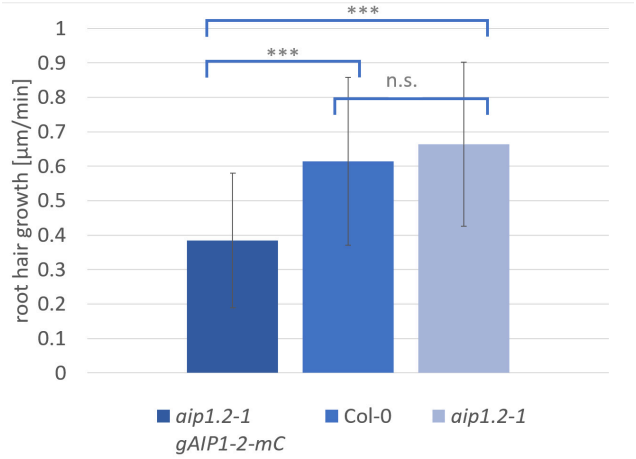

Fig. 7.5: Root hair growth analyses of wild type Col-0, *aip1.2-1* single mutant and the rescue line *aip1.2-1 gAIP1-2-mCherry* under the control of the pAIP1-2-promoter sequence). Quantitative analysis of root hair growth displayed in μm per min. Pooled data from 3 experiments, n=30 root hairs; error bars: SD; the significant difference could be shown for the rescue line to the mutant as well as to the Col-0 wildtype; no significant difference was shown between the wildtype and the mutant line; (data analyzed by t-test; see p-values in SI 10.4).

When a t-test was applied to the data, the rescue line showed a significant difference from both the mutant and the Col-0 wildtype, but no significant difference between the wildtype and the mutant line. Root hair growth was reduced by a third in the rescue line (0.39$\pm$0.2 μm/min) compared to the *aip1.2-1* (0.66$\pm$0.24 μm/min) and Col-0 lines (0.61$\pm$0.24 μm/min). Therefore, root hair tip growth was not suitable for a new phenotype marker of the *aip1.2-1* mutant.

Another possible approach was to compare root hair cell lengths. Since these were already measured in the root hair displacement analyses, the values obtained for each plant line were pooled and the mean and standard deviation were calculated. The resulting plot is shown in Figure 7.6. The rescue line *aip1.2-1 gAIP1-2-mCherry* had the longest root hair cells with a mean value of 181$\pm$7 μm. Col-0 showed a cell length of 174$\pm$7 μm and the shortest root hair cells were found in the *aip1.2-1* mutant with a mean of only 169$\pm$6 μm.

The statistical KS test revealed a highly significant difference in the cell lengths of the rescue line compared to the Col-0 wildtype and the mutant. Col-0 and the mutant again showed similar cell lengths and therefore did not show significant differences. A t-test showed only a barely significant difference between the mutant and the rescue line (p-value$\approx$0.02).

Although the Aip constructs of homologous AIP1-1-mCherry and tagged DdAip1 could be shown to be expressed in the mutant background (see above), a clear

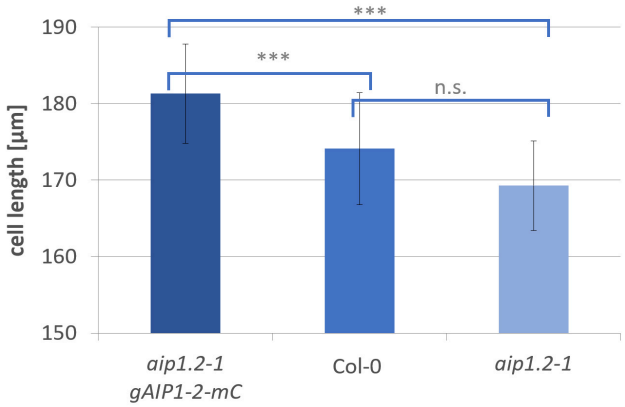

Fig. 7.6: Cell length analyses of wild type Col-0, *aip1.2-1* single mutant and the rescue line *aip1.2-1 gAIP1-2-mCherry* under the control of the pAIP1-2-promoter sequence). Quantitative analysis on pooled data from six experiments, on a total of n=300 cells per genotype; error bars: SD; the significant difference could be shown for the rescue line to the mutant as well as to the Col-0 wildtype; no significant difference was shown between the wildtype and the mutant line; (data tested for significance by Kolmogorov–Smirnov test).

analysis of the complementation assay was not possible because the positioning of the mutant root hairs was too similar to the wildtype. Other approaches, such as analysis of root hair tip growth and average root hair cell length, also showed no significant differences at the hair and cell numbers investigated under standard conditions. Therefore, the stronger phenotype of the *aip1.2-1 act7-6* double mutant was employed for further complementation analyses.

7.2 Complementation of *aip1.2-1 act7-6* Double Mutant

The phenotype of the *aip1.2-1 act7-6* double mutant is much more severe than either single mutant alone (see Kiefer et al., 2015 for full details). Strong defects in planar polarity formation and ROP positioning as well as in embryogenesis, leading to high lethality, were observed in this mutant. Finally, mCherry-tagged AIP1-homologs were also transformed into the *aip1.2-1 act7-6* mutant background.

7.2.1 Validation of AIP-Homolog Expression in *aip1.2-1 act7-6* by Immunoblot and Fluorescence-Microscopy

After testing the expression of the different tagged Aip1 homologs in the *aip1.2-1* single mutant, the expression of the same constructs in the *aip1.2-1 act7-6* double mutant background was also tested by immunoblot. The Col-0 accession and both single mutants (*aip1.2-1* and *act7-6*) as well as the double mutant *aip1. 2-1 act7-6* were run as negative controls along with the positive control expressing AIP1-2-mCherry (created by crossing the double mutant and the existing single mutant rescue line from Kiefer et al., 2015) and a free mCherry expressing double mutant line for comparison. Two insertion lines of each rescue construct were tested in the *aip1.2-1 act7-6* background. BIP was used as a loading control and actin to test for potentially reduced actin levels due to *act7-6* mutation.

As shown in Figure 7.7, all four control lines showed non-specific binding of the mCherry antibody to a protein of 70 kDa and a very weak signal of a protein of about 30 kDa. The 70 kDa protein signal was also found in all other samples, while the 30 kDa band was present but barely visible in the samples. The rescue line expressing endogenous AIP1-2-mCherry (lane 5) showed a strong signal at the expected size of 90-93 kDa. The free mCherry expressing line (lane 6) showed a less strong but specific signal for mCherry at 27 kDa. For the AIP1-1 expressing construct, two lines with very different expression levels could be shown (lanes 7+8). While line 1 showed a similar expression as the AIP1-2-mCherry rescue line, the second AIP1-1 line overexpressed the protein and showed additional cleavage products at 37 kDa as well as cleaved mCherry. The N-terminally tagged DdAip1 expressing lines (lanes 9+10) also differed in their protein expression. Based on the comparison with the BIP loading control, line 1 showed much less signal for the DdAip1 protein than line 2 and much lower levels of the protein compared to the rescue line. Both N-terminally tagged DdAip1 lines also showed the 37 kDa fragment that was already found in both AIP1-1 expressing lines. The signal of C-terminal *Dictyostelium* Aip1 (lanes 11+12) was barely visible in line 1 and overexpressed in line 2. Both also showed cleavage products and the 37 kDa band. The loading of all samples with respect to the BIP antibody signal was very comparable. For the actin loading control, the mutation of the *ACT7* gene resulted in an about two-fold reduction of the total actin signal compared to lines in which *ACT7* was functional (Col-0 and *aip1.2-1*). Line 2 of the C-terminal DdAip1 expressing replicates showed a stronger signal in actin detection. It appeared that there was contamination or unintentional backcrossing to the wildtype *ACT7*. Taken together, all Arabidopsis lines expressing an mCherry-tagged AIP1-homolog fusion protein did predominantly

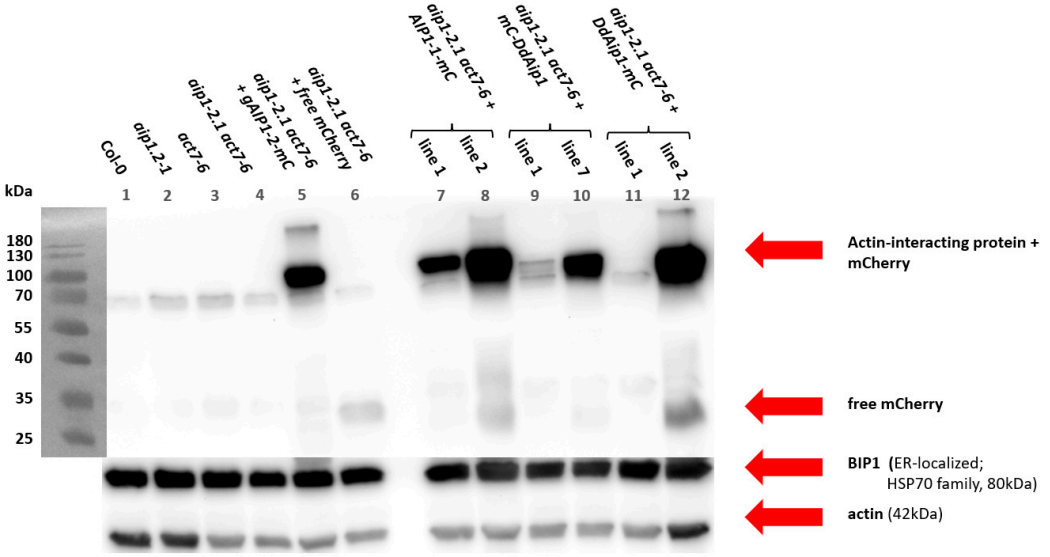

Fig. 7.7: Expression of mCherry-tagged Aip1 homologs in *A. thaliana aip1.2-1 act7-6* mutants. Western blot (immunoblot) for detection of mCherry and mCherry-tagged (mc) Aip1 homologs in protein extract of plant lines of interest; Col-0, *aip1.2-1*, *act7-6* and *aip1.2-1 act7-6* as negative controls; positive control lines expressing *A. thaliana* AIP1-2-mC in *aip1.2-1 act7-6* mutant background or free mC; two insertion lines of each rescue construct Ddaip1-mC, mCh-Ddaip1 and AtAIP1-1-mC all expressed in *aip1.2-1 act7-6* background under the control of the pAIP1-2-promoter sequence were tested; anti-BIP1 (BIP) and anti-Actin (actin) antibodies were used to detect BIP1 and different actin isoforms as loading controls (see 2.1.2 for antibodies), left: molar weight standard; top, grey: lane numbers; one representative example of three independent experiments.

express the full-length proteins with very little detectable proteolytically cleaved mCherry.

To further analyze the expression of the different constructs *in vivo*, AiryScan LSM images were taken using a 561 nm laser to excite mCherry. Seeds of the different plant lines were sown in glass bottom chambers and root hairs were imaged after 5-6 days. Col-0 and the *aip1.2-1 act7-6* double mutant showed a very weak background signal when excited at 561 nm (see Figure 7.8, A+B). The signal of the mCherry-tagged proteins was generally lower than in the single mutant. AIP1-1 expressing lines showed a strong signal (D+E). The free mCherry expressing mutant line (J) and the rescue line *aip1.2-1 act7-6 gAIP1-2-mCherry* (C) showed the strongest signal. The DdAip1 signal was generally weaker, regardless of whether it was labeled at the N- or C-terminus (F-I). The distribution and localization of the proteins did not differ as they all showed a cytosolic distribution. Since the cytosol is rather dense towards the root hair tip in the apical cytoplasm, where little vacuolization occurs, the signal appears enriched in this region but is not specifically associated with the apical membrane at the root hair tip with a similar distribution to free mCherry.

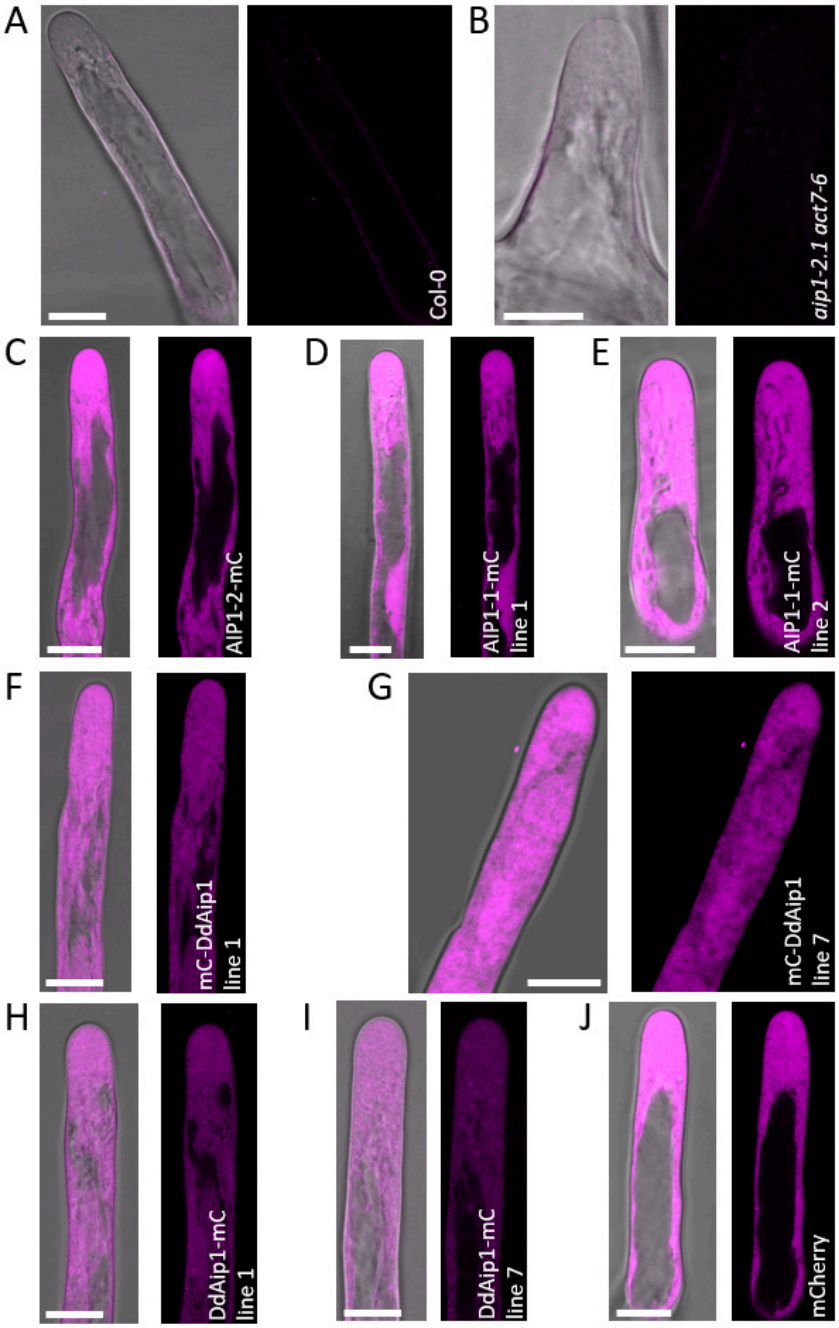

Fig. 7.8: Subcellular localization of mCherry(mC)-tagged Aip1 homologs in root hairs of *A. thaliana aip1.2-1 act7-6* mutants. Representative Airy Scan LSM images of Col-0 (A) and *aip1.2-1 act7-6* (B) as negative controls; positive control lines expressing *A. thaliana* AIP1-2-mC in *aip1.2- 1 act7-6* mutant background (C) or free mC (J); two insertion lines of each rescue construct Ddaip1-mC, mCh-Ddaip1 and AtAIP1-1-mC all expressed in *aip1.2-1 act7-6* background under the control of the pAIP1-2-promoter sequence were tested (D-I); merged image of fluorescent and brightfield image (left) and fluorescent image (right) only; scale bar: 10 μm.

7.2.2 Complementation of *aip1.2-1 act7-6* Double Mutant Germination Rates

The germination of the *aip1.2-1 act7-6* double mutant was severely impaired compared to both single mutants and the Col-0 wildtype (Kiefer et al., 2015). The germination rate of the double mutant was only about 17% with a high variation of about 10% between experiments. Lethality in such a high proportion could not be shown for *aip1.2-1* or *act7-6* mutants. Figure 7.9 shows the main different lines of interest. The compromised germination efficiency and impaired growth of *aip1.2-1 act7-6* seeds five days after plating are visible. The same could be shown for the control line expressing free mCherry (Figure 7.9, bottom).

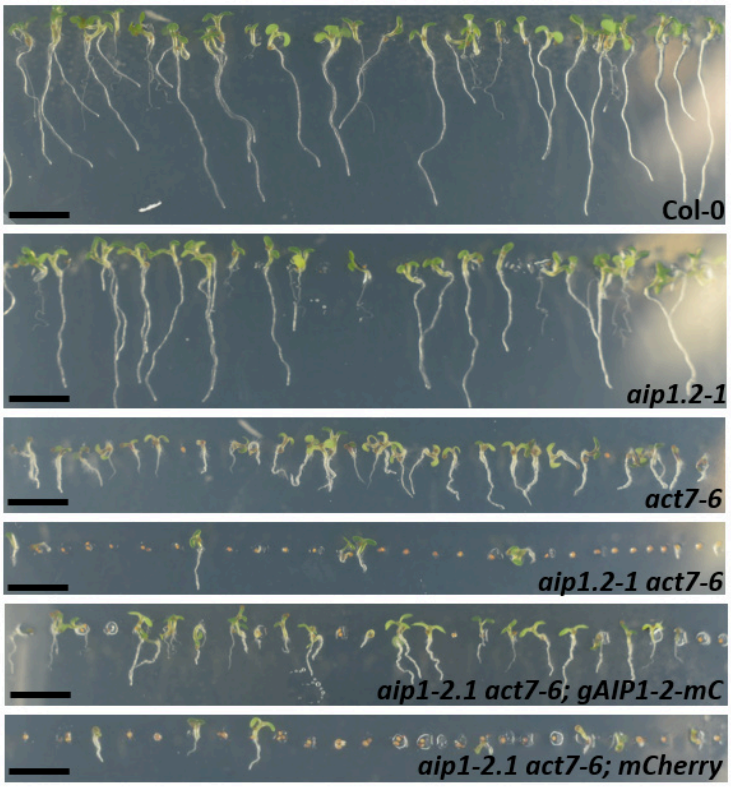

Fig. 7.9: Five-day-old seedlings of the different wildtype, mutant and rescue plant lines; Five-day-old Col-0, *aip1.2-1*, *act7-6*, *act7-6 aip1.2-1* and *act7-6 aip1.2-1 gAIP1-2-mCherry* seedlings as well as also under pAip1-2 promoter sequence expressed free mCherry in *act7-6 aip1.2-1* seedlings. Germination of seeds in both *act7-6 aip1.2-1* control lines is strongly reduced compared with Col-0, *act7-6*, *aip1.2-1* and the *act7-6 aip1.2-1 gAIP1-2-mCherry* rescue line; scale bar 1 cm.

Comparable germination rates and growth were found in the Col-0 and the single *aip1.2-1* mutant lines. Although the germination rate of the *act7-6* mutant was similar to that of the *aip1.2-1* mutant and the wildtype, the appearance of the *act7-6* mutant was very different. The roots of the *act7-6* mutant were twisted, agravitropic,

and much shorter compared to the *aip1.2-1* and wildtype roots (Figure 7.9) as previously observed (Kiefer et al., 2015).

To measure germination rates for all plant lines of interest, between 525 and 1185 seeds per genotype were sown on MS agar plates and germinated seedlings were counted after 5 days. The ratio of seedlings to the total number of seeds sown was calculated and the percentage of germinating seeds is shown in a histogram in Figure 7.10.

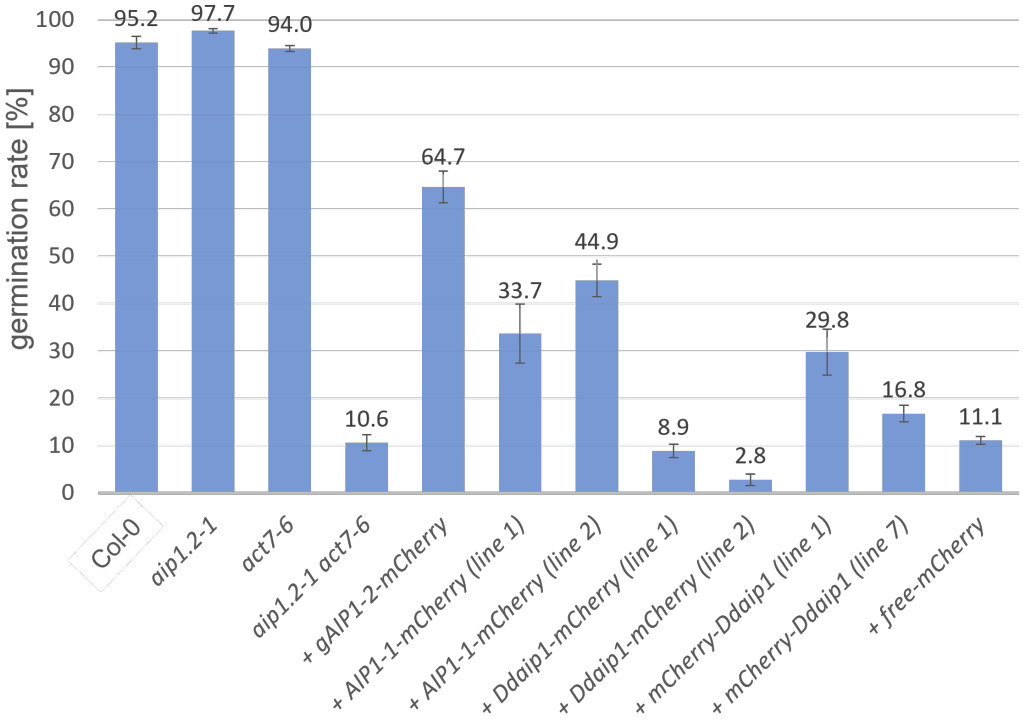

Fig. 7.10: Germination rate of the different wildtype, mutant and rescue plant lines; Percentages of germinated seeds of Col-0, *aip1.2-1*,*act7-6*, *act7-6 aip1.2-1*, *act7-6 aip1.2-1 gAIP1-2-mCherry* and all rescue lines of interest; free mCherry expressing *act7-6 aip1.2-1* line as additional negative control; averages of n=3 independent germination experiments ± SD employing a total of 525≤n≤1185 seeds per genotype; for statistical data see supplementary Figure 10.5.

The germination rates of wildtype Col-0 and the two single mutants *aip1.2-1* and *act7-6* are comparable, ranging from 94% to 98%. Only 10% of the double mutant seeds germinated, which is comparable to previous results (Kiefer et al., 2015) and to the free mCherry expressing double mutant with 11% germination rate. Interestingly, the rescue *aip1.2-1 act7-6 gAIP1-2-mCherry* did not fully restore the germination rate to *act7-6*. Only 64.7% of the seeds germinated on average. Plant lines expressing the second plant homolog AIP1-1 showed germination rates of 33.7% and 44.9% but with more variation between experiments. The C-terminally tagged versions of

DdAip1 were not rescued at all. In line 2, there was even a reduction in germination compared to the *aip1.2-1 act7-6* double mutant. Both N-terminally tagged DdAip1 showed a partial rescue compared to the *AIP1-2* rescue line with 16.8% and 29.8% germination which, however, was significantly and reproducibly higher than in the *aip1.2-1 act7-6* mutant (see Table SI 10.5).

7.2.3 Complementation of *aip1.2-1 act7-6* Double Mutant Main Stem Length

The growth and development of *aip1.2-1 act7-6* double mutant seedlings were severely impaired. When comparing the main stem length after 5 weeks, the differences were striking. A photograph of a *act7-6 aip1.2-1* mutant plant and the wildtype Col-0 accession and examples of both single mutants are shown in the following section (see Figure 7.12). The main stem lengths of all plant lines were measured and plotted in Figure 7.11.

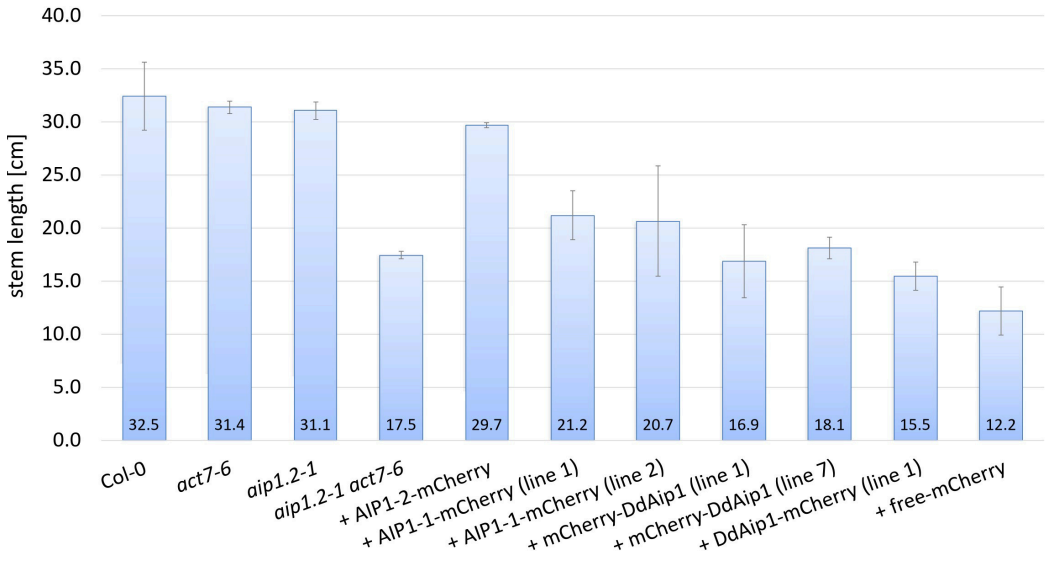

Fig. 7.11: Main stem length of the different wildtype, mutant and rescue plant lines; Main stem length of Col-0, *aip1.2-1*, *act7-6*, *act7-6 aip1.2-1*, *act7-6 aip1.2-1 gAIP1-2-mCherry* and all rescue lines of interest; free mCherry expressing *act7-6 aip1.2-1* line as additional negative control; averages of n=3 experiments ± SD with employing 4 plants per genotype per experiment.

In agreement with the results of the germination rate experiment, the wildtype Col-0 and both single mutants also showed a statistically similar main stem length of about 32 cm. The *act7-6 aip1.2-1* double mutant was more variable in length, but grew on average up to 17.5±0.3 cm, which was only half as high and significantly different from the others. The free expressing mCherry line was even shorter

at 12.2±2.3 cm but also varied widely between experiments. The rescue line expressing AIP1-2-mCherry under the control of the genomic *AIP1-2* regulatory sequences,*aip1.2-1 act7-6 gAIP1-2-mCherry*, completely rescued back to the *act7-6* mutant and wildtype stem length (for all p-values see table in supplementary Figure 10.6). Plant lines expressing AIP1-1 showed a partial rescue with an average stem length of 21 cm, although this could not be verified by the t-test significance level. All DdAip1-containing constructs did not rescue stem length at all and varied between 15.5 cm and 18.1 cm displaying high variance. The t-test results showed that none of the rescue constructs, except for plants expressing AIP1-2-mCherry, closely and statistically significantly conferred rescue back to the *act7-6* main stem length, although the AIP1-1-mCherry expressing lines showed a very similar (21.2±2.3 and 20.7±5.2) stem length that was higher than the length of the *aip1.2-1 act7-6* double mutant but did not prove statistically significant.

7.2.4 Complementation of *aip1.2-1 act7-6* Double Mutant Curled Stem Phenotype

In the past, an influence of the mutation of both genes, *AIP1-2* and *ACT7*, on the main stem of double mutant plants has been shown (Kiefer et al., 2015). The defects in silique arrangement and orientation and shoot twisting were found in all *aip1-2 act7* double mutants examined. In this work, an even more severe phenotype was observed that had previously been observed for dominant *act8* single mutants (Kato et al., 2010). Although the stems were short, most of the lateral stems showed a loop during their growth, usually in the lower part of the stem where no siliques were formed (see Figure 7.12). Siliques on the main stem showed abnormal orientation and appeared much shorter than in either single mutant (see Figure 7.12).

Figure 7.12 (B) shows an example of a typical 5-week-old *aip1.2-1 act7-6* double mutant plant. The stem is about half the height of the single mutants and Col-0 wildtype (Figure 7.12 (A,C,D)). All three lateral stems have loops, which are shown enlarged in the right part of the figure. For visual comparison, 5-week-old Col-0 wildtype (A), *aip1.2-1* (C), and *act7-6* (D) single mutants were also photographed. The shoots are straight in all three genotypes, and the siliques show normal growth.

All plant lines were sown on agar plates and transferred to pots. After five weeks of growth under long-day light conditions, the plants were photographed, looped stems were examined and counted, and the ratio of looped stems to the total number of stems was calculated (see Table 7.1).

Tab. 7.1: Table of Complementation Analysis of Looped Side Stem Phenotype. Photos of 5-weeks-old plants were taken and analyzed and the ratio of curled stems to the number of total side stems per genotype was calculated.

Genotype	Plants with Loops	% of Looped Side Stem
Col-O	0 / 12	0
act7-6	0 / 12	0
aip1.2-1	0 / 12	0
aip1.2-1 act7-6	12 / 12	58.8
aip1.2-1 act7-6 +*gAIP1-2-mCherry*	0 / 12	0
aip1.2-1 act7-6 +*AIP1-1-mCherry* (line 1)	0 / 12	0
aip1.2-1 act7-6 +*AIP1-1-mCherry* (line 2)	0 / 12	0
aip1.2-1 act7-6 +*mCherry-Ddaip1* (line 1)	12 / 12	60.9
aip1.2-1 act7-6 +*mCherry-Ddaip1* (line 7)	12 / 12	62.7
aip1.2-1 act7-6 +*Ddaip1-mCherry* (line 1)	12 / 12	67.4
aip1.2-1 act7-6 +*free mCherry*	12 / 12	63.6

As mentioned above, no loops could be found in any stem of the single mutants *aip1.2-1* and *act7-6*, and the Col-0 wildtype. All plants of the *aip1.2-1 act7-6* double mutant showed looped stems, as did the control line expressing free mCherry. Approximately 60% of all stems in both lines looped during their growth. Looping was never observed in the first main stem. Twisted stems were also found only in the double mutant lines. In the *aip1.2-1 act7-6 gAIP1-2-mCherry* rescue line no loops could be detected at all. The stems looked normal and the siliques grew straight. Thus, the normal stem and growth phenotype could be fully restored by expressing *AIP1-2* in the double mutant background. AIP1-1 expressing lines also rescued the phenotype. No loops were found in the stems, but the pedicels still showed irregular twisting. Interestingly, but in agreement with the stem length phenotype results, no rescue could be found in the *aip1.2-1 act7-6* mutants expressing N- or C-terminally tagged DdAip1. All of these plants also showed loops and twisted pedicels, just like the double mutant itself. The same ratio of looped stems to all stems counted was found to be identical and did not vary much. The double mutant *aip1.2-1 act7-6* itself showed loops in about 60% of all stems. The values of the non-rescuing DdAip1 lines also varied only between 61% and 67%. So it seems that the rescue of the looped phenotype can only be either complete or not at all.

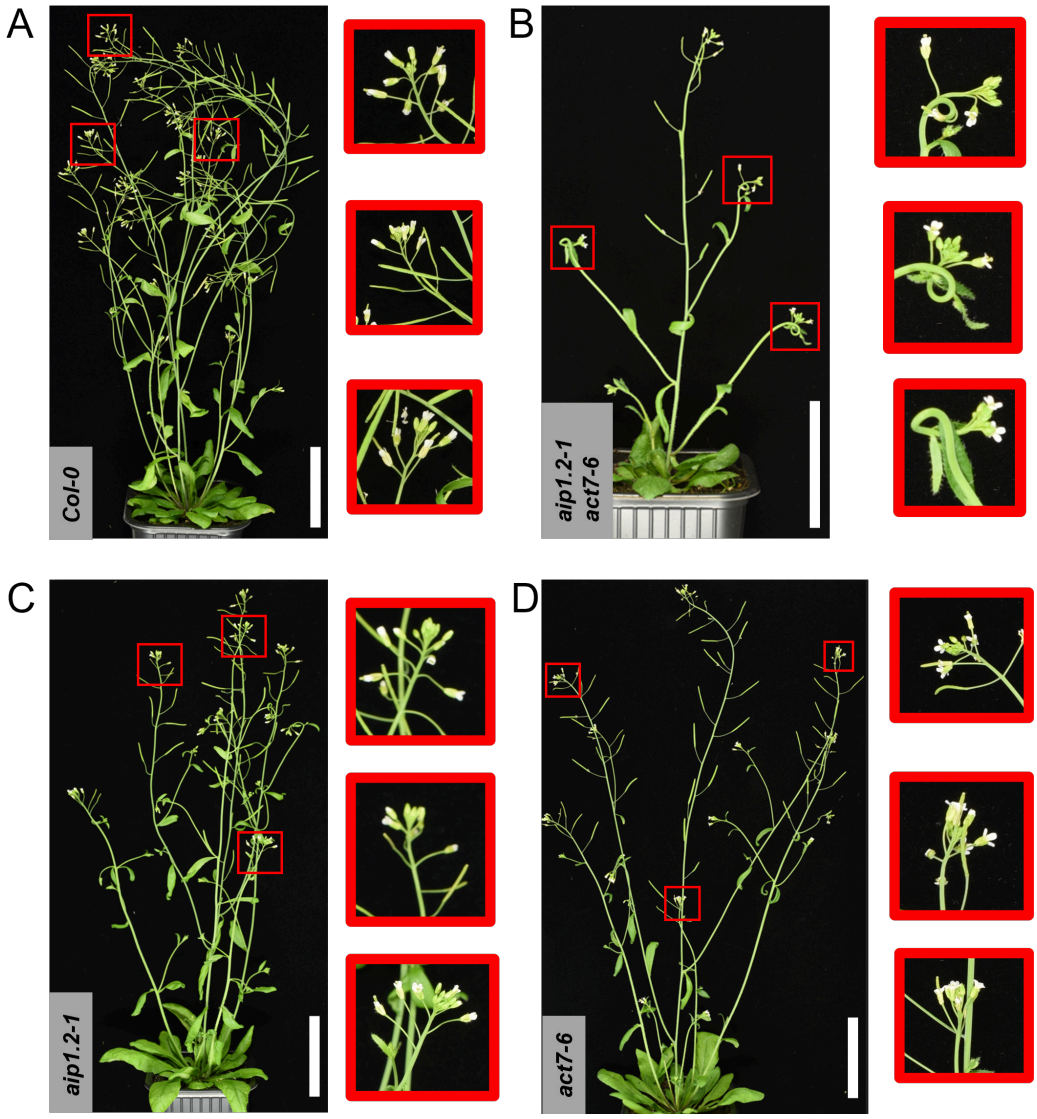

Fig. 7.12: **5-weeks-old plants of the different wildtype and mutant lines**; Photos of typical stem phenotype in 5-weeks-old Col-0 (A), *aip1.2-1* (C), *act7-6* (D) plant lines and typical curled stem phenotype in 5-weeks-old *aip1.2-1 act7-6* double mutant line (B); blow-ups for better visualization; scale bar 5 cm.

8 Discussion

8.1 Summary on *aip1.2-1* Single Mutant Phenotype and Complementation

In conclusion, the previously described phenotype of the single *aip1.2-1* mutant is still slightly present, but the Col-0 wildtype and the mutant have become more similar. In the past, it could be shown that $\frac{2}{3}$ of the examined relative root hair positions of the mutant were between 0 and 0.05, and $\frac{1}{3}$ were in the range of 0.05 and 0.1. The Col-0 wildtype showed exactly the opposite picture. The more basal part of the root hairs was only $\frac{1}{3}$ and the more apical part between 0.05 and 0.1 was $\frac{2}{3}$. The same distribution could be shown for the rescue line *aip1.2-1 gAIP1-2-mCherry* (see Kiefer et al., 2015, Figure 4D for comparison). In this work, half of the mutant cells and half of the wildtype cells showed a similar behavior of basally displaced root hairs (see 7.4). Interestingly, the proportion of more apically emerging root hairs was also larger in this work in all three lines tested, which is consistent with previously published results (see Kiefer et al., 2015, Figure 4E for comparison) and raises the question of whether root hair positioning was ever a good parameter or not, as it also varied widely between experiments. It seems that the mutant phenotype became even milder and the wildtype phenotype changed to more basally emerging root hairs. These results were in strong agreement with the root hair growth and cell length measurements. A strong reduction of root hair growth could not be observed as in the RNAi mutants targeting both AIPs (Ketelaar et al., 2004). Why and how the *aip1.2-1* planar polarity mutant phenotype disappeared after having been reproduced by several researchers between 2010 and 2020 can only be hypothesized. The differences could arise over time through epigenetic mechanisms or simple compensation in response to slight changes in light and growth conditions that may have been barely detectable. It is likely that changes in the composition of the media used from one batch to another resulted in epigenetic differences that were inherited by the next generation. For example, it has been shown in the past that epigenetic differences can occur under selection in as few as five generations. They have been shown to lead to phenotypic changes in growth and development (Schmid et al., 2018). After 30 generations, the differences in gene expression are already very strong, even though no special selection has been applied (Becker et al., 2011). Aside from this, it could be shown that the homolog AIP1-1 and the foreign

N-terminally tagged DdAip1 are expressed in the single mutant *aip1.2-1* at very similar levels. Strikingly, the C-terminally tagged versions were barely detectable by immunoblot but were still visible by confocal microscopy. All expressed Aip1 versions seem to be homogeneously distributed in the cells and are cytosolic, as could also be shown for Aip1 in *Physcomitrella patens* (Augustine et al., 2011). A good approach would be to find a new robust phenotype for further study of *aip1.2-1* single mutants in *A. thaliana*.

8.2 Complementation of *aip1.2-1 act7-6* Double Mutant Phenotype with Endogenous and Foreign Aip1

The complementation of the already characterized double mutant *aip1.2-1 act7-6* was the next step after the root hair positioning phenotype of the single mutant *aip1.2--1* was no longer detectable. As shown in the past, the phenotype of the double mutant was very strong compared to the single mutant and included a low germination rate, slow growth, and short roots as well as twisted stems and non-physiological arrangement and orientation of the siliques (Kiefer et al., 2015). To test the possible complementation of the double mutant phenotype back to the mild *act7-6* phenotype, all constructs already used for the experiments in the single mutant background were also transformed into the double mutant. The second *A. thaliana* homolog *AIP1-1* was only used in a C-terminally tagged version. However, *Ddaip1* was used in both possible tagged versions because it was not clear whether the non-rescuing DdAip1-mCherry in *Dictyostlium discoideum* was functional in another host or not. The drastic change in phenotype when both *AIP1-2* and *ACT7* genes were mutated led to the conclusion that this is caused by a change in AIP1 function and a possible change in the actin homeostasis together. actin-7 mutant proteins are said to be unable to bind to each other or form polymers. A significant reduction in total actin levels has also been found in plant extracts (Kandasamy et al., 2001). *ACT7* expression is increased in root tissue (Kandasamy et al., 2001), which seems to be the reason for the non-existent shoot phenotype of the *act7-6* mutant but the short twisted roots. Taken together, the inability to upregulate *ACT7* in roots and the impaired actin turnover caused by the mutation of the *AIP1* gene are responsible for the strong phenotype. Since ADFs are the major linker between actin and AIP1 in actin treadmilling (Inada, 2017,Nomura et al., 2016,Kanellos et al., 2016), altered ADF binding also seemed to be involved in the performance. Hypothetically, the binding of ADFs to actin or AIP1 could be enhanced or inhibited, leading to a reduced or enhanced turnover of the remaining actin and, consequently, cytoplasmic transport in the cells. This would result in slower plant growth, as the

development of root hairs and roots is critical for adequate nutrient uptake and transport.

8.2.1 Complementation of *aip1.2-1 act7-6* Germination Phenotype

Seeds were sown to study the germination rates of the different plant lines and their germination was counted after 5 days. The resulting germination rates of the Col-0 wildtype, the two single mutants *aip1.2-1* and *act7-6*, and the double mutant *aip1.2-1 act7-6* were in agreement with the results obtained previously (Kiefer et al., 2015). There were only minor quantitative deviations from the published results. The *aip1.2-1* single mutant had the best germination rate, followed by the Col-0 and *act7-6* mutant. The double mutant germinated only in about 10% of the observed cases, which has been shown to be 1.5 times higher in the past (16%, Kiefer et al., 2015). Interestingly, the endogenous AIP1-2-mCherry could not fully restore the germination rate to the *act7-6* level. Since it was also expressed under its endogenous promoter, it was concluded that the fluorescent protein tag provides a steric hindrance or otherwise inhibits the function of AIP1-2 by $\frac{1}{3}$. Although the pollen-specific AIP1-1 was also expressed under the *AIP1-2* promoter and is known to function in actin turnover in pollen tubes (Diao et al., 2020), it could not rescue the germination rate phenotype to the same extent as its homolog AIP1-2. Depending on the complementation line, the germination rate varied between 34% and 45%, which was still at least three times better than in the *aip1.2-1 act7-6* double mutant. The C-terminally tagged DdAip1 did not rescue at all, while the N-terminally tagged DdAip1 at least slightly but significantly increased the germination rate in both lines observed. The results of the AIP1-2-mCherry and the tagged AIP1-1 suggest that the C-terminus contributes to the normal function of AIP1 proteins in growth and development. It is likely that the differences in amino acid sequence lead to a modified binding of ADFs or an altered interaction with other potential binding partners already during embryogenesis and seed production. It can be hypothesized that the absence of functional *ACT7* and *AIP1-2* leads to such a strong influence on actin dynamics that seed production is impaired, resulting in the changes and variation in the appearance of the double mutant seeds (McDowell et al., 1996; Xu et al., 2023).

8.2.2 Complementation of *aip1.2-1 act7-6* Growth and Looping Stem Phenotype

After 5 weeks of growth, the double mutant showed a severe delay in development and growth compared to the single mutants *aip1.2-1*, *act7-6* and the Col-0 wildtype.

It was striking that only AIP1-2-mCherry could rescue the stem-length phenotype. Since all other rescue lines were not significantly different from the double mutant, the importance of fully functional AIP1 for shoot growth in the *act7-6* mutant could be verified. The combination of reduced actin and non-functional AIP1 also led to the second major phenotype of the double mutant. Twisted and zigzagging stems as well as misaligned siliques have been reported in the past (Kiefer et al., 2015). In this work, the looping of the stems was primarily described in this double mutant, while the twisted stems were no longer found, although the looping may just reflect a stronger manifestation of a twisting phenotype. As also shown in Figure 7.12, the stems showed a full loop near the outermost pedicel. The pedicels were still partially misaligned and the siliques were shorter than in the single mutants and Col-0. About 60% of all pedicels in the double mutant had looped pedicels, and there was not a single plant without a looped pedicel. No looping could be detected in the main stems of the double mutant. None of the *D. discoideum* Aip1 variants could rescue this phenotype. AIP1-1-mCherry completely rescued straight stems. Direct comparison of the three AIPs (see SI 10.1) suggests that both structural identity and amino acid composition in the structure are important for the binding and thus the functionality of Aip in plants. Although the C-terminus of Aip1 faces away from the open shell structure, the steric hindrance of the fluorescent tag seems to be the most likely explanation for a partially functional Aip1. Comparing the amino acid sequences and the positions of the changes in the protein model (see Consortium, 2021), it can be seen that in two regions of the protein, the stronger change in the amino acid sequence is in the β-sheet of the leaflets and therefore cannot be predicted to have such a strong influence. Position 400 in the amino acid sequence is close to where the two propellers are connected and may be part of the binding region for ADFs. The potentially affected binding of *A. thaliana* ADFs in this structural region of Aip1 could explain the severe deficiencies of DdAip1 compared to the plant proteins. By comparing AIP1-1 and AIP1-2, the composition of ADFs in pollen might be different from that in non-reproductive cells. Thus, each ADF might not function as well as the other when combined with one of the two AIP1 homologs. There might be fewer functional combinations and the binding efficiency might be affected.

9 Conclusions and Future perspectives

9.1 Conclusions on Coronin-A Mutants and SLI Methods

In the first part of this thesis, different ways of influencing the expression of the *CorA* gene or the function of the Coronin-A protein in *D. discoideum* were described. It has been shown that not all of the investigated properties are affected in the expected way. For example, while the predictable grading of motility could be shown for wildtype, knockdown mutant, and knockout, the amount of Coronin-A did not lead to significantly different results for spore formation and appearance or cell size and morphology. Therefore, it seems crucial to test different phenotypes and traits and different methods of mutation to see related changes in phenotype and behavior. The creation or use of a double mutant with a strong phenotype has been shown to reveal additional advantages of mutation methods. For example, since freezing cells is not as effective and sometimes the unfrozen fraction of viable cells is low, knock sideways or RNAi can be useful when a double mutant is unable to produce spores, such as the Aip1-null/*corA*- SLI mutant. This provides an opportunity to combine the fast-growing and easy-to-handle knock sideway mutants with the sudden loss-of-function CID.

The SLI method may still represent a specific and targeted method of choice to achieve a knockout of a gene, although CRISPR/Cas-9-based methods have recently been established for *D. discoideum* (Iriki et al., 2019,Ogasawara et al., 2022). The importance of a complete knockout compared to a partial loss-of-function mutation cannot be ignored, as shown in this work. Partially expressed proteins may not only be deleterious in specific conditions but may also affect the entire protein-mediated pathways, leading to the appearance of new phenotypes that could be misinterpreted.

The newly established combination of SLI and CID is a perfect way to express a knock sideway protein under its own promoter while at the same time knocking out endogenous gene expression. A new goal may be to express the anchor of choice in an equimolar concentration to the protein of interest to reduce the possible effects of over- or even under-expressed anchor protein. This should provide a clearer and more consistent phenotype for sudden loss-of-function experiments.

9.2 Conclusions on Aip1 Mutants and Rescue in Amoeba and Plants

Although actin is highly conserved across species, the interacting and modulating proteins have changed slightly during evolution. Interestingly, the function and structure were largely conserved, but the sequence of amino acids and even the sequence of bases were greatly altered. Without codon optimization, the proteins might not even have been expressed at physiological levels, since the codon usage varies greatly between *A. thaliana* and *D. discoideum* (Sahoo et al., 2019; Sharp et al., 1989).

It was shown that the use of fluorescent tags and the site of the tagging need to be carefully reconsidered, as steric hindrance may occur or the function of the tagged terminus may be prohibited, as has been shown for the non-rescuing C-terminally tagged DdAip1 in *Dictyostelium* (Konzok et al., 1999) and the only partially rescuing AIP1-2-mCherry, when scored for the germination phenotype in plants. Unexpectedly, the C-terminal tags of the two AIP1s were mostly cleaved from the protein in the amoeba cells, as revealed by the immunoblot. This raises the question of whether the tagged protein is simply being degraded or whether this is a compensatory response by the cells to get rid of the tag. If a reintroduced protein does not fully rescue the phenotype, one should consider tagging the other terminus or using a smaller tag and/or a possible linker. Whether a non-tagged version of the proteins might have improved the rescue in the exchange experiments was not part of this study, but may be of interest in the future.

The ability to use the *aip1.2-1 act7-6* double mutant plant line to rescue its phenotype back to *act7-6* was an advantage in this work, since the *aip1.2-1* single mutant could no longer be used for the parameters previously described.

As shown for *Aip1* in *Dictyostelium*, the use of a stronger phenotype in a double mutant such as Aip1-null/*corA*- SLI may not be a suitable alternative in compensation assays. As shown, the double mutant phenotype could not be rescued, and the results for the double mutant itself were mostly inconsistent with the expected assumptions. This was probably also due to the different levels of Aip1 from one cell to another. The use of extrachromosomal plasmids in unequal numbers and the expression of the protein of interest under a strong promoter instead of the endogenous one should be avoided. This could lead to more consistent and uniform results and better interpretability. However, attempts to integrate the mCherry fusions into the genomic Aip1 of *D. dictyostelium* locus were unsuccessful at the beginning of the thesis, which was the reason why I resorted to using extrachromosomal plasmids. Nonetheless, a partial functionality of the AIP1-1 and AIP1-2 proteins in restoring amoeboid motility as well as of Aip1 in partially restoring some functions essential for seed development or germination could be demonstrated in this thesis. These

results underpin the partial evolutionary conservation of some functions of the AIP1 proteins from two-distantly related species during the evolution of eukaryotes.

Bibliography

Alberts, B., ed. (2008): *Molecular biology of the cell*. 5th ed. New York: Garland Science.

Allwood, E. G., Anthony, R. G., Smertenko, A. P., Reichelt, S., Drobak, B. K., Doonan, J. H., Weeds, A. G. and Hussey, P. J. (2002): "Regulation of the Pollen-Specific Actin-Depolymerizing Factor LlADF1" *The Plant Cell* **14** (11), pp. 2915–2927.

Amberg, D. C., Basart, E. and Botstein, D. (1995): "Defining protein interactions with yeast actin in vivo" *Nature Structural Biology* **2** (1), pp. 28–35.

Arabidopsis Genome Initiative (2000): "Analysis of the genome sequence of the flowering plant Arabidopsis thaliana" *Nature* **408** (6814), pp. 796–815.

Asano, S., Mishima, M. and Nishida, E. (2001): "Coronin forms a stable dimer through its C-terminal coiled coil region: an implicated role in its localization to cell periphery: Coronin dimerization" *Genes to Cells* **6** (3), pp. 225–235.

Ashworth, J. M. and Watts, D. J. (1970): "Metabolism of the cellular slime mould Dictyostelium discoideum grown in axenic culture" *Biochemical Journal* **119** (2), pp. 175–182.

Augustine, R. C., Pattavina, K. A., Tüzel, E., Vidali, L. and Bezanilla, M. (2011): "Actin Interacting Protein1 and Actin Depolymerizing Factor Drive Rapid Actin Dynamics in Physcomitrella patens" *The Plant Cell* **23** (10), pp. 3696–3710.

Becker, C., Hagmann, J., Müller, J., Koenig, D., Stegle, O., Borgwardt, K. and Weigel, D. (2011): "Spontaneous epigenetic variation in the Arabidopsis thaliana methylome" *Nature* **480** (7376), pp. 245–249.

Benitez-Alfonso, Y. (2014): "Symplastic intercellular transport from a developmental perspective" *Journal of Experimental Botany* **65** (7), pp. 1857–1863.

Berardini, T. Z., Reiser, L., Li, D., Mezheritsky, Y., Muller, R., Strait, E. and Huala, E. (2015): "The arabidopsis information resource: Making and mining the "gold standard" annotated reference plant genome: Tair: Making and Mining the "Gold Standard" Plant Genome" *genesis* **53** (8), pp. 474–485.

Birnbaum, J., Flemming, S., Reichard, N., Soares, A. B., Mesén-Ramírez, P., Jonscher, E., Bergmann, B. and Spielmann, T. (2017): "A genetic system to study Plasmodium falciparum protein function" *Nature Methods* **14** (4), pp. 450–456.

Blanchoin, L., Boujemaa-Paterski, R., Sykes, C. and Plastino, J. (2014): "Actin Dynamics, Architecture, and Mechanics in Cell Motility" *Physiological Reviews* **94** (1), pp. 235–263.

Bosgraaf, L. and Van Haastert, P. J. M. (2009): "The Ordered Extension of Pseudopodia by Amoeboid Cells in the Absence of External Cues" *PLoS ONE* **4** (4). Ed. by N. Hotchin, e5253.

Bowes, C., Redd, M., Yousfi, M., Tauzin, M., Murayama, E. and Herbomel, P. (2019): "Coronin 1A depletion restores the nuclear stability and viability of Aip1/Wdr1-deficient neutrophils" *Journal of Cell Biology* **218** (10), pp. 3258–3271.

Bretschneider, T., Diez, S., Anderson, K., Heuser, J., Clarke, M., Müller-Taubenberger, A., Köhler, J. and Gerisch, G. (2004): "Dynamic Actin Patterns and Arp2/3 Assembly at the Substrate-Attached Surface of Motile Cells" *Current Biology* **14** (1), pp. 1–10.

Brown, D. and Strassmann, J. E. (2022): *http://dictybase.org/Multimedia/DdLifeCycles/; 2022-09-05*.

Cai, L., Marshall, T. W., Uetrecht, A. C., Schafer, D. A. and Bear, J. E. (2007): "Coronin 1B Coordinates Arp2/3 Complex and Cofilin Activities at the Leading Edge" *Cell* **128** (5), pp. 915–929.

Carlier, M.-F., Pernier, J., Montaville, P., Shekhar, S., Kühn, S. and Cytoskeleton Dynamics and Motility group (2015): "Control of polarized assembly of actin filaments in cell motility" *Cellular and molecular life sciences: CMLS* **72** (16), pp. 3051–3067.

Château, M. de and Björck, L. (1994): "Protein PAB, a mosaic albumin-binding bacterial protein representing the first contemporary example of module shuffling." *Journal of Biological Chemistry* **269** (16), pp. 12147–12151.

Cherstvy, A. G., Nagel, O., Beta, C. and Metzler, R. (2018): "Non-Gaussianity, population heterogeneity, and transient superdiffusion in the spreading dynamics of amoeboid cells" *Physical Chemistry Chemical Physics* **20** (35), pp. 23034–23054.

Chisholm, R. L. and Firtel, R. A. (2004): "Insights into morphogenesis from a simple developmental system" *Nature Reviews Molecular Cell Biology* **5** (7), pp. 531–541.

Clark, M. G. (2006): "A Genetic Dissection of Aip1p's Interactions Leads to a Model for Aip1p-Cofilin Cooperative Activities" *Molecular Biology of the Cell* **17** (4), pp. 1971–1984.

Clough, S. J. and Bent, A. F. (1998): "Floral dip: a simplified method for Agrobacterium -mediated transformation of Arabidopsis thaliana" *The Plant Journal* **16** (6), pp. 735–743.

Consortium, T. U. (2021): "UniProt: the universal protein knowledgebase in 2021" *Nucleic Acids Research* **49** (D1), pp. D480–D489.

Crocker, J. C. and Grier, D. G. (1996): "Methods of Digital Video Microscopy for Colloidal Studies" *Journal of Colloid and Interface Science* **179** (1), pp. 298–310.

Dasgupta, S. K., Le, A., Da, Q., Cruz, M., Rumbaut, R. E. and Thiagarajan, P. (2016): "Wdr1-Dependent Actin Reorganization in Platelet Activation" *PLOS ONE* **11** (9). Ed. by K. Freson, e0162897.

Daunderer, C. and Gräf, R. (2002): "Molecular analysis of the cytosolic Dictyostelium γ-tubulin complex" *European Journal of Cell Biology* **81** (4), pp. 175–184.

Davidson, A. J., King, J. S. and Insall, R. H. (2013): "The use of streptavidin conjugates as immunoblot loading controls and mitochondrial markers for use with *Dictyostelium discoideum*" *BioTechniques* **55** (1), pp. 39–41.

DeRose, R., Miyamoto, T. and Inoue, T. (2013): "Manipulating signaling at will: chemically-inducible dimerization (CID) techniques resolve problems in cell biology" *Pflugers Archiv: European Journal of Physiology* **465** (3), pp. 409–417.

Diao, M., Li, X. and Huang, S. (2020): "Arabidopsis AIP1-1 regulates the organization of apical actin filaments by promoting their turnover in pollen tubes" *Science China Life Sciences* **63** (2), pp. 239–250.

Drexler, S. K., Brogna, F., Vinet, A. and Pieters, J. (2016): "Investigating the Function of Coronin A in the Early Starvation Response of Dictyostelium discoideum by Aggregation Assays" *Journal of Visualized Experiments* (112).

Duan, Q., Kita, D., Li, C., Cheung, A. Y. and Wu, H.-M. (2010): "FERONIA receptor-like kinase regulates RHO GTPase signaling of root hair development" *Proceedings of the National Academy of Sciences of the United States of America* **107** (41), pp. 17821–17826.

Dünser, K., Gupta, S., Herger, A., Feraru, M. I., Ringli, C. and Kleine-Vehn, J. (2019): "Extracellular matrix sensing by FERONIA and Leucine-Rich Repeat Extensins controls vacuolar expansion during cellular elongation in *Arabidopsis thaliana*" *The EMBO Journal* **38** (7).

Eckert, C., Hammesfahr, B. and Kollmar, M. (2011): "A holistic phylogeny of the coronin gene family reveals an ancient origin of the tandem-coronin, defines a new subfamily, and predicts protein function" *BMC Evolutionary Biology* **11** (1).

Edwards, K., Johnstone, C. and Thompson, C. (1991): "A simple and rapid method for the preparation of plant genomic DNA for PCR analysis" *Nucleic Acids Research* **19** (6), p. 1349.

Eisenack, T. J. and Trentini, D. B. (2023): "Ending a bad start: Triggers and mechanisms of co-translational protein degradation" *Frontiers in Molecular Biosciences* **9**, p. 1089825.

Etzioni, A. and Ochs, H. D. (2020): "Lazy Leukocyte Syndrome—an Enigma Finally Solved?" *Journal of Clinical Immunology* **40** (1), pp. 9–12.

Fabrice, T. N., Fiedler, T., Studer, V., Vinet, A., Brogna, F., Schmidt, A. and Pieters, J. (2020): "Interactome and F-Actin Interaction Analysis of Dictyostelium discoideum Coronin A" *International Journal of Molecular Sciences* **21** (4), p. 1469.

Fey, P., Kowal, A. S., Gaudet, P., Pilcher, K. E. and Chisholm, R. L. (2007): "Protocols for growth and development of Dictyostelium discoideum" *Nature Protocols* **2** (6), pp. 1307–1316.

Fiedler, T., Fabrice, T. N., Studer, V., Vinet, A., Faltova, L., Kammerer, R. A., Steinmetz, M. O., Sharpe, T. and Pieters, J. (2020): "Homodimerization of coronin A through the C-terminal coiled-coil domain is essential for multicellular differentiation of Dictyostelium discoideum" *FEBS Letters* **594** (13), pp. 2116–2127.

Fischer, M., Haase, I., Simmeth, E., Gerisch, G. and Müller-Taubenberger, A. (2004): "A brilliant monomeric red fluorescent protein to visualize cytoskeleton dynamics in Dictyostelium" *FEBS Letters* **577** (1-2), pp. 227–232.

Fischer, U., Ikeda, Y., Ljung, K., Serralbo, O., Singh, M., Heidstra, R., Palme, K., Scheres, B. and Grebe, M. (2006): "Vectorial information for Arabidopsis planar polarity is mediated by combined AUX1, EIN2, and GNOM activity" *Current biology: CB* **16** (21), pp. 2143–2149.

Fletcher, D. A. and Mullins, R. D. (2010): "Cell mechanics and the cytoskeleton" *Nature* **463** (7280), pp. 485–492.

Flores, L. R., Keeling, M. C., Zhang, X., Sliogeryte, K. and Gavara, N. (2019): "Lifeact-TagGFP2 alters F-actin organization, cellular morphology and biophysical behaviour" *Scientific Reports* **9** (1), p. 3241.

Fortelny, N., Pavlidis, P. and Overall, C. M. (2015): "The path of no return—Truncated protein N-termini and current ignorance of their genesis" *PROTEOMICS* **15** (14), pp. 2547–2552.

Gandhi, M., Achard, V., Blanchoin, L. and Goode, B. L. (2009): "Coronin switches roles in actin disassembly depending on the nucleotide state of actin" *Molecular cell* **34** (3), pp. 364–374.

Gandhi, M. and Goode, B. L. (2008): "Coronin: the double-edged sword of actin dynamics" *Sub-Cellular Biochemistry* **48**, pp. 72–87.

Gatfield, J., Albrecht, I., Zanolari, B., Steinmetz, M. O. and Pieters, J. (2005): "Association of the leukocyte plasma membrane with the actin cytoskeleton through coiled coil-mediated trimeric coronin 1 molecules" *Molecular Biology of the Cell* **16** (6), pp. 2786–2798.

Goehring, N. W. and Grill, S. W. (2013): "Cell polarity: mechanochemical patterning" *Trends in Cell Biology* **23** (2), pp. 72–80.

Goldsmith, M. H. (1993): "Cellular signaling: new insights into the action of the plant growth hormone auxin." *Proceedings of the National Academy of Sciences* **90** (24), pp. 11442–11445.

Goode, B. L., Wong, J. J., Butty, A.-C., Peter, M., McCormack, A. L., Yates, J. R., Drubin, D. G. and Barnes, G. (1999): "Coronin Promotes the Rapid Assembly and Cross-linking of Actin Filaments and May Link the Actin and Microtubule Cytoskeletons in Yeast" *The Journal of Cell Biology* **144** (1), pp. 83–98.

Graef, I. A., Holsinger, L. J., Diver, S., Schreiber, S. L. and Crabtree, G. R. (1997): "Proximity and orientation underlie signaling by the non-receptor tyrosine kinase ZAP70" *The EMBO journal* **16** (18), pp. 5618–5628.

Grierson, C., Nielsen, E., Ketelaarc, T. and Schiefelbein, J. (2014): "Root Hairs" *The Arabidopsis Book* **2014** (12).

Griffing, L. R. (1991): "Comparisons of golgi structure and dynamics in plant and animal cells" *Journal of Electron Microscopy Technique* **17** (2), pp. 179–199.

Gu, Y., Li, S., Lord, E. M. and Yang, Z. (2006): "Members of a Novel Class of *Arabidopsis* Rho Guanine Nucleotide Exchange Factors Control Rho GTPase-Dependent Polar Growth" *The Plant Cell* **18** (2), pp. 366–381.

Hellens, R. P., Edwards, E. A., Leyland, N. R., Bean, S. and Mullineaux, P. M. (2000): "pGreen: a versatile and flexible binary Ti vector for Agrobacterium-mediated plant transformation" *Plant molecular biology* **42** (6), pp. 819–832.

Hoeller, O., Toettcher, J. E., Cai, H., Sun, Y., Huang, C.-H., Freyre, M., Zhao, M., Devreotes, P. N. and Weiner, O. D. (2016): "Gβ Regulates Coupling between Actin Oscillators for Cell Polarity and Directional Migration" *PLOS Biology* **14** (2), e1002381.

Hohmann, T. and Dehghani, F. (2019): "The Cytoskeleton-A Complex Interacting Meshwork" *Cells* **8** (4), E362.

Horio, T. and Murata, T. (2014): "The role of dynamic instability in microtubule organization" *Frontiers in Plant Science* **5**.

Hostos, E. L. de, Bradtke, B., Lottspeich, F., Guggenheim, R. and Gerisch, G. (1991): "Coronin, an actin binding protein of Dictyostelium discoideum localized to cell surface projections, has sequence similarities to G protein beta subunits." *The EMBO Journal* **10** (13), pp. 4097–4104.

Hostos, E. L. de, Rehfuess, C., Bradtke, B., Waddell, D. R., Albrecht, R., Murphy, J. and Gerisch, G. (1993): "Dictyostelium mutants lacking the cytoskeletal protein coronin are defective in cytokinesis and cell motility" *The Journal of Cell Biology* **120** (1), pp. 163–173.

Huala, E., Dickerman, A. W., Garcia-Hernandez, M., Weems, D., Reiser, L., LaFond, F., Hanley, D., Kiphart, D., Zhuang, M., Huang, W., Mueller, L. A., Bhattacharyya, D., Bhaya, D., Sobral, B. W., Beavis, W., Meinke, D. W., Town, C. D., Somerville, C. and Rhee, S. Y. (2001): "The Arabidopsis Information Resource (TAIR): a comprehensive database and web-based information retrieval, analysis, and visualization system for a model plant" *Nucleic Acids Research* **29** (1), pp. 102–105.

Humphries, C. L., Balcer, H. I., D'Agostino, J. L., Winsor, B., Drubin, D. G., Barnes, G., Andrews, B. J. and Goode, B. L. (2002): "Direct regulation of Arp2/3 complex activity and function by the actin binding protein coronin" *The Journal of Cell Biology* **159** (6), pp. 993–1004.

Iglesias, P. A. (2012): "Biased excitable networks: how cells direct motion in response to gradients" *Current Opinion in Cell Biology*, p. 9.

Ikeda, Y., Men, S., Fischer, U., Stepanova, A. N., Alonso, J. M., Ljung, K. and Grebe, M. (2009): "Local auxin biosynthesis modulates gradient-directed planar polarity in Arabidopsis" *Nature Cell Biology* **11** (6), pp. 731–738.

Inada, N. (2017): "Plant actin depolymerizing factor: actin microfilament disassembly and more" *Journal of Plant Research* **130** (2), pp. 227–238.

Iriki, H., Kawata, T. and Muramoto, T. (2019): "Generation of deletions and precise point mutations in Dictyostelium discoideum using the CRISPR nickase" *PLOS ONE* **14** (10). Ed. by E. Bayer Santos, e0224128.

Ishikawa-Ankerhold, H. C., Daszkiewicz, W., Schleicher, M. and Müller-Taubenberger, A. (2017): "Actin-Interacting Protein 1 Contributes to Intranuclear Rod Assembly in Dictyostelium discoideum" *Scientific Reports* **7**, p. 40310.

Ishikawa-Ankerhold, H. C., Gerisch, G. and Müller-Taubenberger, A. (2010): "Genetic evidence for concerted control of actin dynamics in cytokinesis, endocytic traffic, and cell motility by coronin and Aip1" *Cytoskeleton* **67** (7), pp. 442–455.

Jain, B. P. and Pandey, S. (2018): "WD40 Repeat Proteins: Signalling Scaffold with Diverse Functions" *The Protein Journal* **37** (5), pp. 391–406.

Jaiswal, P., Majithia, A. R., Rosel, D., Liao, X.-H., Khurana, T. and Kimmel, A. R. (2019): "Integrated actions of mTOR complexes 1 and 2 for growth and development of Dictyostelium" *The International Journal of Developmental Biology* **63** (8-9-10), pp. 521–527.

Jiang, H.-L., Hong, J., Jiang, Y.-T., Yu, S.-X., Zhang, Y.-J., Shi, J.-X. and Lin, W.-H. (2020): "Genome-Wide Association Analysis Identifies Candidate Genes Regulating Seed Number per Silique in Arabidopsis thaliana" *Plants* **9** (5), p. 585.

Jose, J., Ghantasala, S. and Roy Choudhury, S. (2020): "Arabidopsis Transmembrane Receptor-Like Kinases (RLKs): A Bridge between Extracellular Signal and Intracellular Regulatory Machinery" *International Journal of Molecular Sciences* **21** (11), p. 4000.

Joseph, J. M., Fey, P., Ramalingam, N., Liu, X. I., Rohlfs, M., Noegel, A. A., Müller-Taubenberger, A., Glöckner, G. and Schleicher, M. (2008): "The Actinome of Dictyostelium discoideum in Comparison to Actins and Actin-Related Proteins from Other Organisms" *PLOS ONE* **3** (7), e2654.

Kammerer, R. A., Kostrewa, D., Progias, P., Honnappa, S., Avila, D., Lustig, A., Winkler, F. K., Pieters, J. and Steinmetz, M. O. (2005): "A conserved trimerization motif controls the topology of short coiled coils" *Proceedings of the National Academy of Sciences* **102** (39), pp. 13891–13896.

Kandasamy, M. K., Gilliland, L. U., McKinney, E. C. and Meagher, R. B. (2001): "One Plant Actin Isovariant, ACT7, Is Induced by Auxin and Required for Normal Callus Formation" *The Plant Cell* **13** (7), pp. 1541–1554.

Kanellos, G. and Frame, M. C. (2016): "Cellular functions of the ADF/cofilin family at a glance" *Journal of Cell Science* **129** (17), pp. 3211–3218.

Karamyshev, A. L. and Karamysheva, Z. N. (2018): "Lost in Translation: Ribosome-Associated mRNA and Protein Quality Controls" *Frontiers in Genetics* **9**, p. 431.

Kato, T., Morita, M. T. and Tasaka, M. (2010): "Defects in Dynamics and Functions of Actin Filament in Arabidopsis Caused by the Dominant-Negative Actin fiz1-Induced Fragmentation of Actin Filament" *Plant and Cell Physiology* **51** (2), pp. 333–338.

Kessin, R. H. and Franke, J. (2001): *Dictyostelium: evolution, cell biology, and the development of multicellularity*. Developmental and cell biology series. Cambridge: Cambridge Univ. Press.

Ketelaar, T., Galway, M. E., Mulder, B. M. and Emons, A. M. C. (2008): "Rates of exocytosis and endocytosis in Arabidopsis root hairs and pollen tubes" *Journal of Microscopy* **231** (2), pp. 265–273.

Ketelaar, T., Allwood, E. G., Anthony, R., Voigt, B., Menzel, D. and Hussey, P. J. (2004): "The Actin-Interacting Protein AIP1 Is Essential for Actin Organization and Plant Development" *Current Biology* **14** (2), pp. 145–149.

Ketelaar, T., Allwood, E. G. and Hussey, P. J. (2007): "Actin organization and root hair development are disrupted by ethanol-induced overexpression of Arabidopsis actin interacting protein 1 (AIP1)" *New Phytologist* **174** (1), pp. 57–62.

Kiefer, C. S., Claes, A. R., Nzayisenga, J.-C., Pietra, S., Stanislas, T., Huser, A., Ikeda, Y. and Grebe, M. (2015): "Arabidopsis AIP1-2 restricted by WER-mediated patterning modulates planar polarity" *Development* **142** (1), pp. 151–161.

Kile, B. T., Panopoulos, A. D., Stirzaker, R. A., Hacking, D. F., Tahtamouni, L. H., Willson, T. A., Mielke, L. A., Henley, K. J., Zhang, J.-G., Wicks, I. P., Stevenson, W. S., Nurden, P., Watowich, S. S. and Justice, M. J. (2007): "Mutations in the cofilin partner Aip1/Wdr1 cause autoinflammatory disease and macrothrombocytopenia" *Blood* **110** (7), pp. 2371–2380.

Kim, J. H., Lee, S.-R., Li, L.-H., Park, H.-J., Park, J.-H., Lee, K. Y., Kim, M.-K., Shin, B. A. and Choi, S.-Y. (2011): "High Cleavage Efficiency of a 2A Peptide Derived from Porcine Teschovirus-1 in Human Cell Lines, Zebrafish and Mice" *PLoS ONE* **6** (4). Ed. by V. Thiel, e18556.

King, J. S. and Insall, R. H. (2009): "Chemotaxis: finding the way forward with Dictyostelium" *Trends in Cell Biology* **19** (10), pp. 523–530.

Konzok, A., Weber, I., Simmeth, E., Hacker, U., Maniak, M. and Müller-Taubenberger, A. (1999): "Daip1, a Dictyostelium Homologue of the Yeast Actin-Interacting Protein 1, Is Involved in Endocytosis, Cytokinesis, and Motility" *Journal of Cell Biology* **146** (2), pp. 453–464.

Krämer, U. (2015): "Planting molecular functions in an ecological context with Arabidopsis thaliana" *eLife* **4**, e06100.

Kueh, H. Y., Charras, G. T., Mitchison, T. J. and Brieher, W. M. (2008): "Actin disassembly by cofilin, coronin, and Aip1 occurs in bursts and is inhibited by barbed-end cappers" *The Journal of Cell Biology* **182** (2), pp. 341–353.

Kuhns, D. B., Fink, D. L., Choi, U., Sweeney, C., Lau, K., Priel, D. L., Riva, D., Mendez, L., Uzel, G., Freeman, A. F., Olivier, K. N., Anderson, V. L., Currens, R., Mackley, V., Kang, A., Al-Adeli, M., Mace, E., Orange, J. S., Kang, E., Lockett, S. J., Chen, D., Steinbach, P. J., Hsu, A. P., Zarember, K. A., Malech, H. L., Gallin, J. I. and Holland, S. M. (2016): "Cytoskeletal abnormalities and neutrophil dysfunction in WDR1 deficiency" *Blood* **128** (17), pp. 2135–2143.

Kuo, C. J., Chung, J., Fiorentino, D. F., Flanagan, W. M., Blenis, J. and Crabtree, G. R. (1992): "Rapamycin selectively inhibits interleukin-2 activation of p70 S6 kinase" *Nature* **358** (6381), pp. 70–73.

Lai, J., Ng, S. K., Liu, F. F., Patkar, R. N., Lu, Y., Chan, J. R., Suresh, A., Naqvi, N. and Jedd, G. (2010): "Marker Fusion Tagging, a New Method for Production of Chromosomally Encoded Fusion Proteins" *Eukaryotic Cell* **9** (5), pp. 827–830.

Li, L., Nørrelykke, S. F. and Cox, E. C. (2008): "Persistent Cell Motion in the Absence of External Signals: A Search Strategy for Eukaryotic Cells" *PLoS ONE* **3** (5). Ed. by M. Hatakeyama, e2093.

Lin, M.-C., Galletta, B. J., Sept, D. and Cooper, J. A. (2010): "Overlapping and distinct functions for cofilin, coronin and Aip1 in actin dynamics in vivo" *Journal of Cell Science* **123** (8), pp. 1329–1342.

Maniak, M., Rauchenberger, R., Albrecht, R., Murphy, J. and Gerisch, G. (1995): "Coronin involved in phagocytosis: dynamics of particle-induced relocalization visualized by a green fluorescent protein Tag" *Cell* **83** (6), pp. 915–924.

Martens, H., Novotny, J., Oberstrass, J., Steck, T. L., Postlethwait, P. and Nellen, W. (2002): "RNAi in *Dictyostelium:* The Role of RNA-directed RNA Polymerases and Double-stranded RNase" *Molecular Biology of the Cell* **13** (2). Ed. by P. N. Devreotes, pp. 445–453.

MBInfo (2018): *What are Rho-GTPases?; https://www.mechanobio.info/what-is-mechanosignaling/what-are-small-gtpases/what-are-rho-gtpases/ ; 2022-09-05*.

McCurdy, D. W., Kovar, D. R. and Staiger, C. J. (2001): "Actin and actin-binding proteins in higher plants" *Protoplasma* **215** (1-4), pp. 89–104.

McDowell, J. M., An, Y., Huang, S., McKinney, E. C. and Meagher, R. B. (1996): "The Arabidopsis ACT7 Actin Gene Is Expressed in Rapidly Developing Tissues and Responds to Several External Stimuli" *Plant Physiology* **111** (3), pp. 699–711.

McWilliam, H., Li, W., Uludag, M., Squizzato, S., Park, Y. M., Buso, N., Cowley, A. P. and Lopez, R. (2013): "Analysis Tool Web Services from the EMBL-EBI" *Nucleic Acids Research* **41** (Web Server issue), W597–600.

Miao, Y., Bhattacharya, S., Edwards, M., Cai, H., Inoue, T., Iglesias, P. A. and Devreotes, P. N. (2017): "Altering the threshold of an excitable signal transduction network changes cell migratory modes" *Nature Cell Biology* **19** (4), pp. 329–340.

Millner, P. and Causier, B. (1996): "G-protein coupled receptors in plant cells" *Journal of Experimental Botany* **47** (8), pp. 983–992.

Molendijk, A. J. (2001): "Arabidopsis thaliana Rop GTPases are localized to tips of root hairs and control polar growth" *The EMBO Journal* **20** (11), pp. 2779–2788.

Muller, W. A. (2013): "Getting Leukocytes to the Site of Inflammation" *Veterinary Pathology* **50** (1), pp. 7–22.

Müller-Taubenberger, A., Kortholt, A. and Eichinger, L. (2013): "Simple system – substantial share: The use of Dictyostelium in cell biology and molecular medicine" *European Journal of Cell Biology* **92** (2), pp. 45–53.

Munk, K. and Bilger, W., eds. (2009): *Botanik*. Taschenlehrbuch Biologie. Stuttgart: Thieme.

Murata, T., Tanahashi, T., Nishiyama, T., Yamaguchi, K. and Hasebe, M. (2007): "How do Plants Organize Microtubules Without a Centrosome?" *Journal of Integrative Plant Biology* **49** (8), pp. 1154–1163.

Nadkarni, A. V. and Brieher, W. M. (2014): "Aip1 destabilizes cofilin-saturated actin filaments by severing and accelerating monomer dissociation from ends" *Current biology : CB* **24** (23), pp. 2749–2757.

Nakamura, M., Claes, A. R., Grebe, T., Hermkes, R., Viotti, C., Ikeda, Y. and Grebe, M. (2018a): "Auxin and ROP GTPase Signaling of Polar Nuclear Migration in Root Epidermal Hair Cells" *Plant Physiology* **176** (1), pp. 378–391.

Nakamura, M. and Grebe, M. (2018b): "Outer, inner and planar polarity in the Arabidopsis root" *Current Opinion in Plant Biology* **41**, pp. 46–53.

Nomura, K., Hayakawa, K., Tatsumi, H. and Ono, S. (2016): "Actin-interacting Protein 1 Promotes Disassembly of Actin-depolymerizing Factor/Cofilin-bound Actin Filaments in a pH-dependent Manner" *The Journal of Biological Chemistry* **291** (10), pp. 5146–5156.

Ogasawara, T., Watanabe, J., Adachi, R., Ono, Y., Kamimura, Y. and Muramoto, T. (2022): "CRISPR/Cas9-based genome-wide screening of Dictyostelium" *Scientific Reports* **12** (1), p. 11215.

Ono, S. (2003): "Regulation of Actin Filament Dynamics by Actin Depolymerizing Factor/Cofilin and Actin-Interacting Protein 1: New Blades for Twisted Filaments" *Biochemistry* **42** (46), pp. 13363–13370.

Ono, S., Nomura, K., Hitosugi, S., Tu, D. K., Lee, J. A., Baillie, D. L. and Ono, K. (2011): "The two actin-interacting protein 1 genes have overlapping and essential function for embryonic development in Caenorhabditis elegans" *Molecular Biology of the Cell* **22** (13), pp. 2258–2269.

Oruganti, V., Toegelová, H., Pečinka, A., Madlung, A. and Schneeberger, K. (2023): "Rapid large-scale genomic introgression in *Arabidopsis suecica* via an autoallohexaploid bridge" *Genetics* **223** (2). Ed. by J. Birchler, iyac132.

Papuga, J., Hoffmann, C., Dieterle, M., Moes, D., Moreau, F., Tholl, S., Steinmetz, A. and Thomas, C. (2010): "Arabidopsis LIM proteins: a family of actin bundlers with distinct expression patterns and modes of regulation" *The Plant Cell* **22** (9), pp. 3034–3052.

Pietra, S., Gustavsson, A., Kiefer, C., Kalmbach, L., Hörstedt, P., Ikeda, Y., Stepanova, A. N., Alonso, J. M. and Grebe, M. (2013): "Arabidopsis SABRE and CLASP interact to stabilize cell division plane orientation and planar polarity" *Nature Communications* **4** (1).

Pollard, T. D. (2016): "Actin and Actin-Binding Proteins" *Cold Spring Harbor Perspectives in Biology* **8** (8), a018226.

Pollard, T. D. and Cooper, J. A. (1986): "Actin and actin-binding proteins. A critical evaluation of mechanisms and functions" *Annual Review of Biochemistry* **55** (1), pp. 987–1035.

Popp, M. W.-L. and Maquat, L. E. (2013): "Organizing Principles of Mammalian Nonsense-Mediated mRNA Decay" *Annual Review of Genetics* **47** (1), pp. 139–165.

Porter, K. and Day, B. (2016): "From filaments to function: The role of the plant actin cytoskeleton in pathogen perception, signaling and immunity" *Journal of Integrative Plant Biology* **58** (4), pp. 299–311.

Prassler, J., Murr, A., Stocker, S., Faix, J., Murphy, J. and Marriott, G. (1998): "DdLIM Is a Cytoskeleton-associated Protein Involved in the Protrusion of Lamellipodia in *Dictyostelium*" *Molecular Biology of the Cell* **9** (3), pp. 545–559.

Premanandan, C. and Jennings, R. (2017): *Veterinary Histology*. Online access: Center for Open Education Open Textbook Library. Ohio State University Libraries.

Provart, N. J., Alonso, J., Assmann, S. M., Bergmann, D., Brady, S. M., Brkljacic, J., Browse, J., Chapple, C., Colot, V., Cutler, S., Dangl, J., Ehrhardt, D., Friesner, J. D., Frommer, W. B., Grotewold, E., Meyerowitz, E., Nemhauser, J., Nordborg, M., Pikaard, C., Shanklin, J., Somerville, C., Stitt, M., Torii, K. U., Waese, J., Wagner, D. and McCourt, P. (2016): "50 years of Arabidopsis research: highlights and future directions" *New Phytologist* **209** (3), pp. 921–944.

Putyrski, M. and Schultz, C. (2012): "Protein translocation as a tool: The current rapamycin story" *FEBS Letters* **586** (15), pp. 2097–2105.

Raper, K. B. (1935): "Dictyostelium discoideum, a new species of slime mold from decaying forest leaves" *J. Agr. Res* **50**, pp. 135–147.

Rasul, F., Gupta, S., Olas, J. J., Gechev, T., Sujeeth, N. and Mueller-Roeber, B. (2021): "Priming with a Seaweed Extract Strongly Improves Drought Tolerance in Arabidopsis" *International Journal of Molecular Sciences* **22** (3), p. 1469.

Ren, N., Charlton, J. and Adler, P. N. (2007): "The flare Gene, Which Encodes the AIP1 Protein of Drosophila, Functions to Regulate F-Actin Disassembly in Pupal Epidermal Cells" *Genetics* **176** (4), pp. 2223–2234.

Ridley, A. J. (2011): "Life at the Leading Edge" *Cell* **145** (7), pp. 1012–1022.

Riedl, J., Crevenna, A. H., Kessenbrock, K., Yu, J. H., Neukirchen, D., Bista, M., Bradke, F., Jenne, D., Holak, T. A., Werb, Z., Sixt, M. and Wedlich-Soldner, R. (2008): "Lifeact: a versatile marker to visualize F-actin" *Nature Methods* **5** (7), pp. 605–607.

Robinson, M. S., Sahlender, D. A. and Foster, S. D. (2010): "Rapid Inactivation of Proteins by Rapamycin-Induced Rerouting to Mitochondria" *Developmental Cell* **18** (2-3), pp. 324–331.

Rosel, D., Khurana, T., Majithia, A., Huang, X., Bhandari, R. and Kimmel, A. R. (2012): "TOR complex 2 (TORC2) in Dictyostelium suppresses phagocytic nutrient capture independently of TORC1-mediated nutrient sensing" *Journal of Cell Science* **125** (1), pp. 37–48.

Ruijter, N. C. A. and Emons, A. M. C. (1999): "Actin-Binding Proteins in Plant Cells" *Plant Biology* **1** (1), pp. 26–35.

Sahoo, S., Das, S. S. and Rakshit, R. (2019): "Codon usage pattern and predicted gene expression in Arabidopsis thaliana" *Gene* **721**, p. 100012.

Salamun, J., Kallio, J. P., Daher, W., Soldati-Favre, D. and Kursula, I. (2014): "Structure of Toxoplasma gondii coronin, an actin-binding protein that relocalizes to the posterior pole of invasive parasites and contributes to invasion and egress" *FASEB journal: official publication of the Federation of American Societies for Experimental Biology* **28** (11), pp. 4729–4747.

Samereier, M., Baumann, O., Meyer, I. and Gräf, R. (2011): "Analysis of Dictyostelium TACC reveals differential interactions with CP224 and unusual dynamics of Dictyostelium microtubules" *Cellular and Molecular Life Sciences* **68** (2), pp. 275–287.

Sameshima, M., Kishi, Y., Osumi, M., Minamikawa-Tachino, R., Mahadeo, D. and Cotter, D. A. (2001): "The Formation of Actin Rods Composed of Actin Tubules in Dictyostelium discoideum Spores" *Journal of Structural Biology* **136** (1), pp. 7–19.

Saran, S., Meima, M. E., Alvarez-Curto, E., Weening, K. E., Rozen, D. E. and Schaap, P. (2002): "cAMP signaling in Dictyostelium" *Journal of Muscle Research & Cell Motility* **23** (7), pp. 793–802.

Schmid, M. W., Heichinger, C., Coman Schmid, D., Guthörl, D., Gagliardini, V., Bruggmann, R., Aluri, S., Aquino, C., Schmid, B., Turnbull, L. A. and Grossniklaus, U. (2018): "Contribution of epigenetic variation to adaptation in Arabidopsis" *Nature Communications* **9** (1), p. 4446.

Sharp, P. M. and Devine, K. M. (1989): "Codon usage and gene expression level in *Dictyosteiium discoidtum* : highly expressed genes do [prefer[optimal codons" *Nucleic Acids Research* **17** (13), pp. 5029–5040.

Shi, M., Xie, Y., Zheng, Y., Wang, J., Su, Y., Yang, Q. and Huang, S. (2013): "*Oryza sativa* actin-interacting protein 1 is required for rice growth by promoting actin turnover" *The Plant Journal* **73** (5), pp. 747–760.

Shina, M. C., Unal, C., Eichinger, L., Müller-Taubenberger, A., Schleicher, M., Steinert, M. and Noegel, A. A. (2010): "A Coronin7 homolog with functions in actin-driven processes" *The Journal of Biological Chemistry* **285** (12), pp. 9249–9261.

Šlajcherová, K., Fišerová, J., Fischer, L. and Schwarzerová, K. (2012): "Multiple Actin Isotypes in Plants: Diverse Genes for Diverse Roles?" *Frontiers in Plant Science* **3**.

Srivastava, R., Prasadareddy Kajuluri, L., Pathak, N., Gupta, C. M. and Sahasrabuddhe, A. A. (2015): "Oligomerization of coronin: Implication on actin filament length in Leishmania" *Cytoskeleton (Hoboken, N.J.)* **72** (12), pp. 621–632.

Staiger, C. J. and Schliwa, M. (1987): "Actin localization and function in higher plants" *Protoplasma* **141** (1), pp. 1–12.

Sussman, M. (1966): "Chapter 14 Biochemical and Genetic Methods in the Study of Cellular Slime Mold Development". In: *Methods in Cell Biology*. Vol. 2. Elsevier, pp. 397–410.

Sussman, R. and Sussman, M. (1967): "Cultivation of Dictyostelium discoideum in axenic medium" *Biochemical and Biophysical Research Communications* **29** (1), pp. 53–55.

Swatzell, L. J., Edelmann, R. E., Makaroff, C. A. and Kiss, J. Z. (1999): "Integrin-Like Proteins are Localized to Plasma Membrane Fractions, not Plastids, in Arabidopsis" *Plant and Cell Physiology* **40** (2), pp. 173–183.

Swer, P. B., Lohia, R. and Saran, S. (2014): "Analysis of rapamycin induced autophagy in Dictyostelium discoideum" *Indian Journal of Experimental Biology* **52** (4), pp. 295–304.

Taiz, L., Zeiger, E., Moller, I. M. and Murphy, A., eds. (2018): *Plant physiology and development*. [International] 6th ed. Sunderland, Massachusetts: Sinauer associates.

Takatsuka, H. and Umeda, M. (2014): "Hormonal control of cell division and elongation along differentiation trajectories in roots" *Journal of Experimental Botany* **65** (10), pp. 2633–2643.

Theriot, J. A. (1997): "Accelerating on a Treadmill: ADF/Cofilin Promotes Rapid Actin Filament Turnover in the Dynamic Cytoskeleton" *The Journal of Cell Biology* **136** (6), pp. 1165–1168.

Timms, R. T. and Koren, I. (2020): "Tying up loose ends: the N-degron and C-degron pathways of protein degradation" *Biochemical Society Transactions* **48** (4), pp. 1557–1567.

Trusov, Y. and Botella, J. R. (2016): "Plant G-Proteins Come of Age: Breaking the Bond with Animal Models" *Frontiers in Chemistry* **4**.

Uetrecht, A. C. and Bear, J. E. (2006): "Coronins: the return of the crown" *Trends in Cell Biology* **16** (8), pp. 421–426.

Untergasser, A. (2008): *Preparation of Chemical Competent Cells*. URL: `http://www.untergasser.de/lab/protocols/competent_cells_chemical_v1_0.htm` (visited on Feb. 23, 2023).

Vantard, M. and Blanchoin, L. (2002): "Actin polymerization processes in plant cells" *Current Opinion in Plant Biology* **5** (6), pp. 502–506.

Vaughn, K. C. and Harper, J. D. (1998): "Microtubule-Organizing Centers and Nucleating Sites in Land Plants" *International Review of Cytology* **181**, pp. 75–149.

Veltman, D. M., Akar, G., Bosgraaf, L. and Van Haastert, P. J. (2009): "A new set of small, extrachromosomal expression vectors for Dictyostelium discoideum" *Plasmid* **61** (2), pp. 110–118.

Wang, G., Zhao, Z., Zheng, X., Shan, W. and Fan, J. (2022): "How a single receptor-like kinase exerts diverse roles: lessons from FERONIA" *Molecular horticulture* **2** (1), p. 25.

Wang, Y., Wang, F., Wang, R., Zhao, P. and Xia, Q. (2015): "2A self-cleaving peptide-based multi-gene expression system in the silkworm Bombyx mori" *Scientific Reports* **5** (1).

Wang, Y.-S., Yoo, C.-M. and Blancaflor, E. B. (2008): "Improved imaging of actin filaments in transgenic Arabidopsis plants expressing a green fluorescent protein fusion to the C- and N-termini of the fimbrin actin-binding domain 2" *The New Phytologist* **177** (2), pp. 525–536.

Wegner, A. (1976): “Head to tail polymerization of actin” *Journal of Molecular Biology* **108** (1), pp. 139–150.

Welch, M. D. (2015): “Cell Migration, Freshly Squeezed” *Cell* **160** (4), pp. 581–582.

Westphal, M., Jungbluth, A., Heidecker, M., Mühlbauer, B., Heizer, C., Schwartz, J.-M., Marriott, G. and Gerisch, G. (1997): “Microfilament dynamics during cell movement and chemotaxis monitored using a GFP–actin fusion protein” *Current Biology* **7** (3), pp. 176–183.

Williams, J. G. (2010): “Dictyostelium Finds New Roles to Model” *Genetics* **185** (3), pp. 717–726.

Williamson, V., Pyke, A., Sridhara, S., Kelley, R. F., Blajchman, M. A. and Clarke, B. J. (2005): “Interspecies exchange mutagenesis of the first epidermal growth factor-like domain of human factor VII” *Journal of Thrombosis and Haemostasis* **3** (6), pp. 1250–1256.

Wullschleger, S., Loewith, R. and Hall, M. N. (2006): “TOR Signaling in Growth and Metabolism” *Cell* **124** (3). Publisher: Elsevier, pp. 471–484.

Xu, W. and Magnani, E. (2023): “An actin starry night regulates seed size” *Nature Plants* **9** (2), pp. 201–202.

Yanagisawa, M., Zhang, C. and Szymanski, D. B. (2013): “ARP2/3-dependent growth in the plant kingdom: SCARs for life” *Frontiers in Plant Science* **4**.

Yang, C., Xing, L. and Zhai, Z. (1992): “Intermediate filaments in higher plant cells and their assembly in a cell-free system” *Protoplasma* **171** (1-2), pp. 44–54.

Yeh, C.-W., Huang, W.-C., Hsu, P.-H., Yeh, K.-H., Wang, L.-C., Hsu, P. W.-C., Lin, H.-C., Chen, Y.-N., Chen, S.-C., Yeang, C.-H. and Yen, H.-C. S. (2021): “The C-degron pathway eliminates mislocalized proteins and products of deubiquitinating enzymes” *The EMBO Journal* **40** (7), e105846.

Yoshida, K. and Soldati, T. (2006): “Dissection of amoeboid movement into two mechanically distinct modes” *Journal of Cell Science* **119** (18), pp. 3833–3844.

Zada-Hames, I. and Ashworth, J. (1978): “The cell cycle during the vegetative stage of Dictyostelium discoideum and its response to temperature change” *Journal of Cell Science* **32** (1), pp. 1–20.

Zhang, Z., Gou, X., Xun, H., Bian, Y., Ma, X., Li, J., Li, N., Gong, L., Feldman, M., Liu, B. and Levy, A. A. (2020): “Homoeologous exchanges occur through intragenic recombination generating novel transcripts and proteins in wheat and other polyploids” *Proceedings of the National Academy of Sciences* **117** (25), pp. 14561–14571.

Supplementary Information

10

10.1 Sequence Comparison of *A. thaliana* and *D. discoideum* Aip1

Fig. 10.1: Predicted protein sequence alignment of D. discoideum Aip1 with the two A. thaliana homologs AIP1-1 and AIP1-2. Comparison of *D. discoideum* Aip1 (upper row), *A. thaliana* AIP1-2 (middle row) and *A. thaliana* AIP1-1 (lower row) amino acid sequences by Clustal Omega Algorithm (McWilliam et al., 2013); Amino acid sequence identity of Aip1 and AIP1-2 is 40% with 59% positives (*/.:); Amino acid sequence identity of Aip1 and AIP1-1 is 37% with 57% positives (*/.:); Amino acid sequence identity of AIP1-1 and AIP1-2 is 68% with 81% positives (*/.:); left: reference numbers and UniProt name (Consortium, 2021); middle: Amino acid sequence in 1 letter code, colors for identification of similar properties; right: position of the amino acid in the protein.

10.2 Primer Sequences for Genotyping

Tab. 10.1: Primer sequences used in *D. discoideum* for genotyping. Primer were designed due to chosen primer binding sites shown below in 10.2 and ordered at Sigma Aldrich (lyophilized, no special purity grade)

Target	Name	Sequence (5'→ 3')
Aip1	Aip1 a (fwd)	CAT ATA TTG CAA CCC ACT TC
	Aip1 b (rev)	TGG TTG GGG TTT TTG TTG TAC
CorA	CorA a (fwd)	CAA ATC AAT TTA ATT AAT CAA CCA C
	CorA b (rev)	GCA GAA TCG ACG ACT TGA GC
Arp2(housekeeping gene)	Arp2 (fwd)	ACC ACC AAT GAA TCC AGT TGC AAA TCG TC
	Arp2 (rev)	TTT CTA GGG TGT GAT GAC TTC AAA ACA C
Blasticidin resistance gene in pDM326	bla (fwd)	CTA GAT CCT GTT GAG AAA TG
pDM326 *E.coli* repl. site	B4BamHI (fwd)	AAG TGC CAC CTG ACG CGC CCT GTA G
CorA 3'UTR	3'UTR (rev)	ATA CAA TTT AAG AAT GAA AAT TAT TA
Geneticin (G418) resistance gene	G418 (rev)	GGT CGG TCT TGA CAA AAA GAA CC
GFP	GFP (rev)	TCC ACT GAC AGA AAA TTT GTG CC

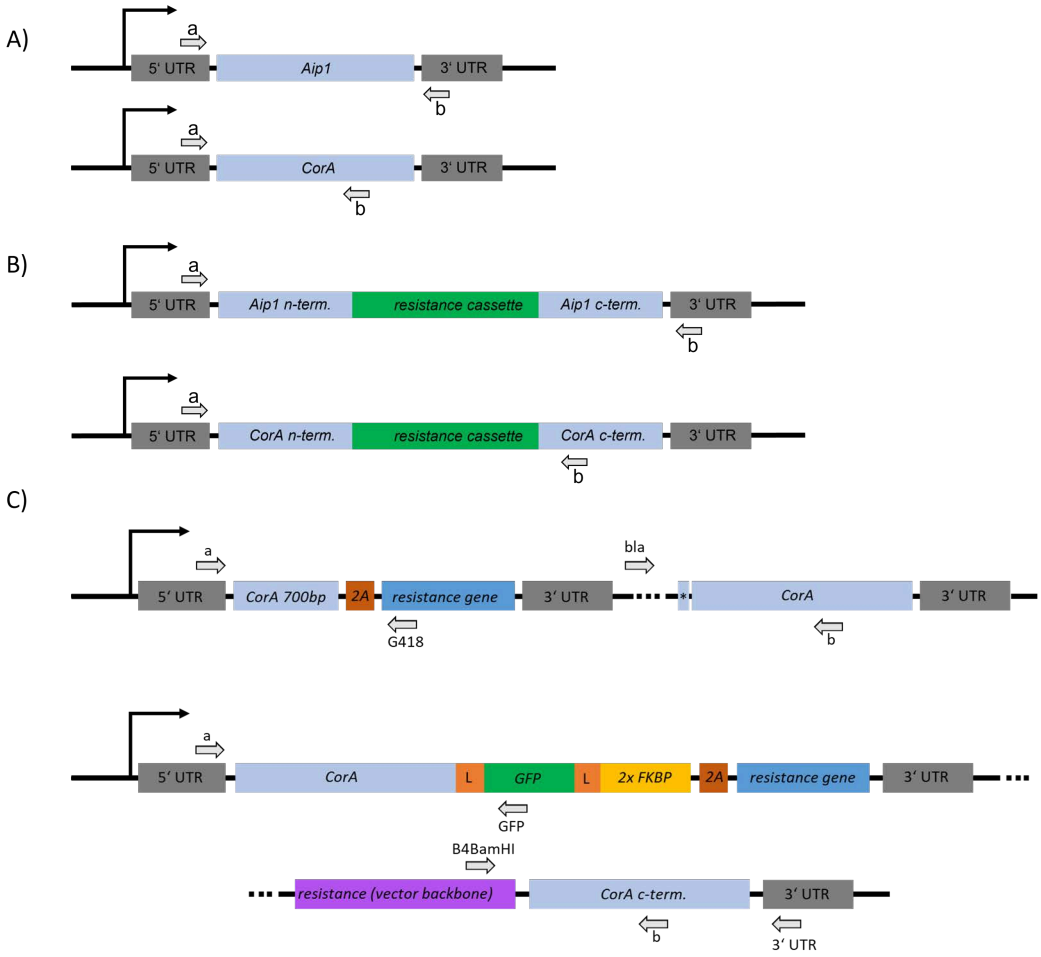

Fig. 10.2: Binding sites of the previously described primers in A) wildtype gene, B) null mutants, and c) SLI knockout and knock sideway. Primer pairs were designed and used in a PCR on whole-cell DNA extract to prove the correct genetic background of the cell line as well as the correct insertion of SLI plasmids into the host genome

Tab. 10.2: Primer sequences used in *A.thaliana* for genotyping. Primer were designed and used as previously described in SI of Kiefer et al., 2015

Target	Name	Sequence (5'→ 3')
act7-6 (SALK_131610)	forward ACT7F0587	CTG CTT CTC GAA TCT TCT GTA TCA TC
	reverse ACT7R114	AAA TCA TGA TCA GTA GTC TTA CAC AT
aip1.2-1 (GK-063F04)	forward AIP2F2871	CAG TGT CTG AAT TTG GTG TTT AGG
	reverse AIP2R3638	GTG TTC CAG ATT CAT GGA GAG ATT C
T-DNA primer	reverse SALK-LBa1	TGG TTC ACG TAG TGG GCC ATC G
	reverse GK-o8760	GGG CTA CAC TGA ATT GGT AGC TC

10.3 Tables of Statistical Tests

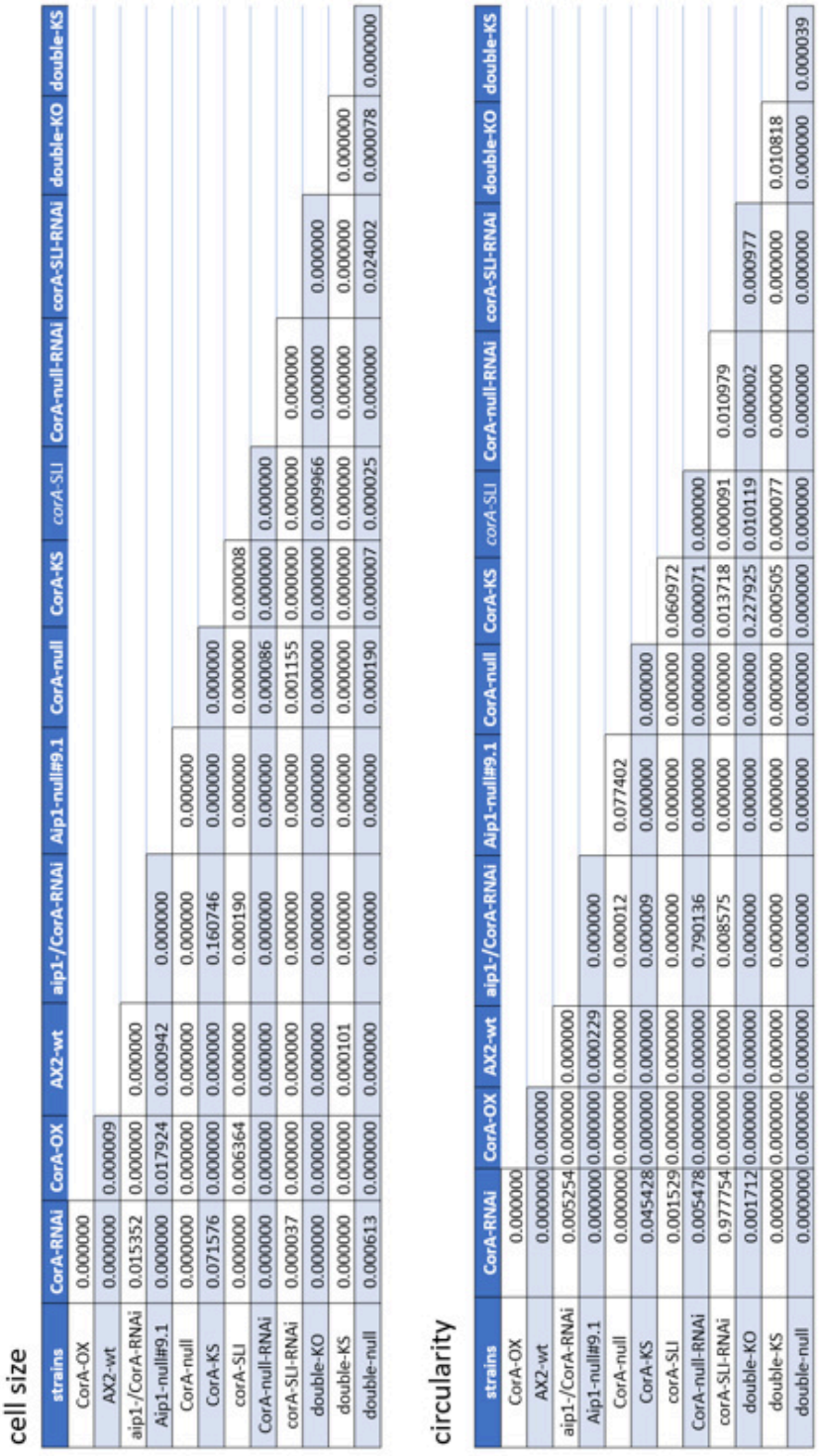

cell size

strains	CorA-RNAi	CorA-OX	AX2-wt	aip1-/CorA-RNAi	Aip1-null#9.1	CorA-null	CorA-KS	corA-SLI	CorA-null-RNAi	corA-SLI-RNAi	double-KO	double-KS
CorA-OX	0.000000											
AX2-wt	0.000000	0.000009										
aip1-/CorA-RNAi	0.015352	0.000000	0.000000									
Aip1-null#9.1	0.000000	0.017924	0.000942	0.000000								
CorA-null	0.000000	0.000000	0.000000	0.000000	0.000000							
CorA-KS	0.071576	0.000000	0.000000	0.160746	0.000000	0.000000						
corA-SLI	0.000000	0.006364	0.000000	0.000190	0.000000	0.000000	0.000008					
CorA-null-RNAi	0.000000	0.000000	0.000000	0.000000	0.000000	0.000086	0.000000	0.000000				
corA-SLI-RNAi	0.000037	0.000000	0.000000	0.000000	0.000000	0.001155	0.000000	0.000000	0.000000			
double-KO	0.000000	0.000000	0.000000	0.000000	0.000000	0.000000	0.000000	0.009966	0.000000	0.000000		
double-KS	0.000000	0.000000	0.000101	0.000000	0.000000	0.000000	0.000000	0.000000	0.000000	0.000000	0.000000	
double-null	0.000613	0.000000	0.000000	0.000000	0.000000	0.000190	0.000007	0.000025	0.000000	0.024002	0.000078	0.000000

circularity

strains	CorA-RNAi	CorA-OX	AX2-wt	aip1-/CorA-RNAi	Aip1-null#9.1	CorA-null	CorA-KS	corA-SLI	CorA-null-RNAi	corA-SLI-RNAi	double-KO	double-KS
CorA-OX	0.000000											
AX2-wt	0.000000	0.000000										
aip1-/CorA-RNAi	0.005254	0.000000	0.000000									
Aip1-null#9.1	0.000000	0.000000	0.000229	0.000000								
CorA-null	0.000000	0.000000	0.000000	0.000012	0.077402							
CorA-KS	0.045428	0.000000	0.000000	0.000009	0.000000	0.000000						
corA-SLI	0.001529	0.000000	0.000000	0.000000	0.000000	0.000000	0.060972					
CorA-null-RNAi	0.005478	0.000000	0.000000	0.790136	0.000000	0.000000	0.000071	0.000000				
corA-SLI-RNAi	0.977754	0.000000	0.000000	0.008575	0.000000	0.000000	0.013718	0.000091	0.010979			
double-KO	0.001712	0.000000	0.000000	0.000000	0.000000	0.000000	0.227925	0.010119	0.000002	0.000977		
double-KS	0.000000	0.000000	0.000000	0.000000	0.000000	0.000000	0.000505	0.000077	0.000000	0.000000	0.010818	
double-null	0.000000	0.000006	0.000000	0.000000	0.000000	0.000000	0.000000	0.000000	0.000000	0.000000	0.000000	0.000039

Fig. 10.3: Table of p-values of the Kolmogorov-Smirnov (KS) test that was performed to compare strains of *D. discoideum* cells in terms of their cell area and cell circularity distributions. KS-test was performed using MATLAB® routine on a minimum of $n > 10^3$ values per strain.

day 1	*aip1.2-1 gAIP1-2-mC*	*aip1.2-1*
Col-0	0.007061402	0.38109433
aip1.2-1	0.029031256	

day 2	*aip1.2-1 gAIP1-2-mC*	*aip1.2-1*
Col-0	0.085327617	0.40525558
aip1.2-1	0.078370087	

day 3	*aip1.2-1 gAIP1-2-mC*	*aip1.2-1*
Col-0	0.001378502	0.02883717
aip1.2-1	1.02107E-08	

Fig. 10.4: Table of p-values of the t-test of root hair growth rate in *A. thaliana aip1.2-1* single mutant, rescue line *aip1.2-1 gAIP1-2-mCherry* (under control of the pAIP1-2 promoter sequence) and wildtype. The t-test was run with Microsoft Excel™with 1-tailed distribution and unpaired test parameters on 3 experiments with each n=10 root hairs per genotype.

t-test (one-sided, unequal variance)

aip1.2-1	0.0486														
act7-6	0.1546	0.0016													
aip1.2-1 act7-6	0.0000	0.0000	0.0000												
+ AIP1-2-mCherry	0.0012	0.0021	0.0025	0.0001											
+ AIP1-1-mCherry line 1	0.0019	0.0023	0.0025	0.0141	0.0041										
+ AIP1-1-mCherry line 2	0.0004	0.0009	0.0009	0.0006	0.0021	0.0545									
+ DdAip1-mCherry line 1	0.0000	0.0000	0.0000	0.1636	0.0002	0.0129	0.0008								
+ DdAip1-mCherry line 2	0.0000	0.0000	0.0000	0.0039	0.0002	0.0086	0.0007	0.0049							
+ mCherry-DdAip1 line 1	0.0008	0.0012	0.0013	0.0108	0.0010	0.2639	0.0137	0.0099	0.0061						
+ mCherry-DdAip1 line 7	0.0000	0.0000	0.0000	0.0113	0.0002	0.0268	0.0010	0.0041	0.0006	0.0254					
+ free-mCherry	0.0000	0.0000	0.0000	0.3660	0.0006	0.0173	0.0017	0.0693	0.0010	0.0148	0.0138				
	Col-0	***aip1.2-1***	***act7-6***	***aip1.2-1 act7-6***	**+ AIP1-2-mCherry**	**+ AIP1-1-mCherry line 1**	**+ AIP1-1-mCherry line 2**	**+ DdAip1-mCherry line 1**	**+DdAip1-mCherry line 2**	**+mCherry-DdAip1 line 1**	**+mCherry-DdAip1 line 7**				

Fig. 10.5: Table of p-values of the t-test of germination rates in *A. thaliana* double mutant rescue lines in comparison to the double mutant line, single mutant lines, and wildtype. The t-test was run with Microsoft Excel™with one-tailed distribution and unpaired test parameters with unequal variance on n=3 experiments with a total of 525 to 1185 seeds per genotype.

day 1

act7-6	aip1.2-1	aip1.2-1 act7-6	+ AIP1-2-mCherry	+ AIP1-1-mCherry line 1	+ AIP1-1-mCherry line 2	+ mCherry-DdAip1 line 1	+ mCherry-DdAip1 line 7	+ DdAip1-mCherry line 1	+ free-mCherry	
0.11845	0.23734	0.00683	0.30361	0.02819	0.00698	0.00145	0.00826	0.00552	0.00335	Col-0
	0.14789	0.00004	0.07119	0.00033	0.00375	0.00009	0.00011	0.00017	0.00146	act7-6
		0.00002	0.26534	0.00009	0.00609	0.00026	0.00002	0.00043	0.00276	aip1.2-1
			0.00007	0.00624	0.21044	0.04672	0.50000	0.50000	0.14661	aip1.2-1 act7-6
				0.00006	0.01578	0.00147	0.00000	0.00239	0.00815	+ AIP1-2-mCherry
					0.11233	0.01227	0.00283	0.06946	0.93029	+ AIP1-1-mCherry line 1
						0.79238	0.41609	0.43744	0.93029	+ AIP1-1-mCherry line 2
							0.12570	0.12570	0.84792	+ mCherry-DdAip1 line 1
								1.00000	0.28827	+ mCherry-DdAip1 line 7
									0.31517	+ DdAip1-mCherry line 1

day 2

act7-6	aip1.2-1	aip1.2-1 act7-6	+ AIP1-2-mCherry	+ AIP1-1-mCherry line 1	+ AIP1-1-mCherry line 2	+ mCherry-DdAip1 line 1	+ mCherry-DdAip1 line 7	+ DdAip1-mCherry line 1	+ free-mCherry	
0.00158	0.02648	0.01349	0.01409	0.00050	0.00073	0.00119	0.00000	0.00000	0.00000	Col-0
	0.18802	0.03047	0.36496	0.00140	0.01671	0.00458	0.00004	0.00000	0.00000	act7-6
		0.02251	0.17058	0.00056	0.00894	0.00206	0.00012	0.00005	0.00002	aip1.2-1
			0.03251	0.44162	0.06926	0.24675	0.36185	0.33498	0.23270	aip1.2-1 act7-6
				0.00132	0.06532	0.00570	0.00110	0.00040	0.00016	+ AIP1-2-mCherry
					0.00536	0.14871	0.31543	0.10151	0.03802	+ AIP1-1-mCherry line 1
						0.02910	0.00165	0.00026	0.00010	+ AIP1-1-mCherry line 2
							0.19987	0.02207	0.00952	+ mCherry-DdAip1 line 1
								0.00638	0.00194	+ mCherry-DdAip1 line 7
									0.09556	+ DdAip1-mCherry line 1

day 3

act7-6	aip1.2-1	aip1.2-1 act7-6	+ AIP1-2-mCherry	+ AIP1-1-mCherry line 1	+ AIP1-1-mCherry line 2	+ mCherry-DdAip1 line 1	+ mCherry-DdAip1 line 7	+ DdAip1-mCherry line 1	+ free-mCherry	
0.10181	0.05647	0.00005	0.01386	0.01955	0.02321	0.00002	0.00100	0.00001	0.00100	Col-0
	0.22221	0.00038	0.01300	0.03757	0.03718	0.00016	0.00322	0.00001	0.00223	act7-6
		0.00018	0.08983	0.04615	0.04318	0.00006	0.00288	0.00000	0.00202	aip1.2-1
			0.00048	0.05680	0.21269	0.25550	0.46332	0.02862	0.03061	aip1.2-1 act7-6
				0.07660	0.06218	0.00017	0.00495	0.00001	0.00283	+ AIP1-2-mCherry
					0.30033	0.03670	0.07314	0.01730	0.00619	+ AIP1-1-mCherry line 1
						0.15114	0.23908	0.07461	0.02578	+ AIP1-1-mCherry line 2
							0.28942	0.06591	0.04603	+ mCherry-DdAip1 line 1
								0.07971	0.03129	+ mCherry-DdAip1 line 7
									0.11168	+ DdAip1-mCherry line 1

Fig. 10.6: Table of p-values of the t-test of stem lengths in *A. thaliana* double mutant rescue lines in comparison to the double mutant line, single mutant lines, and wildtype. The t-test was run with Microsoft Excel™ with 1-tailed distribution and unpaired test parameters on n=3 experiments with each 4 plants per genotype.

10.4 Track Length Distribution for *Dictyostelium discoideum*

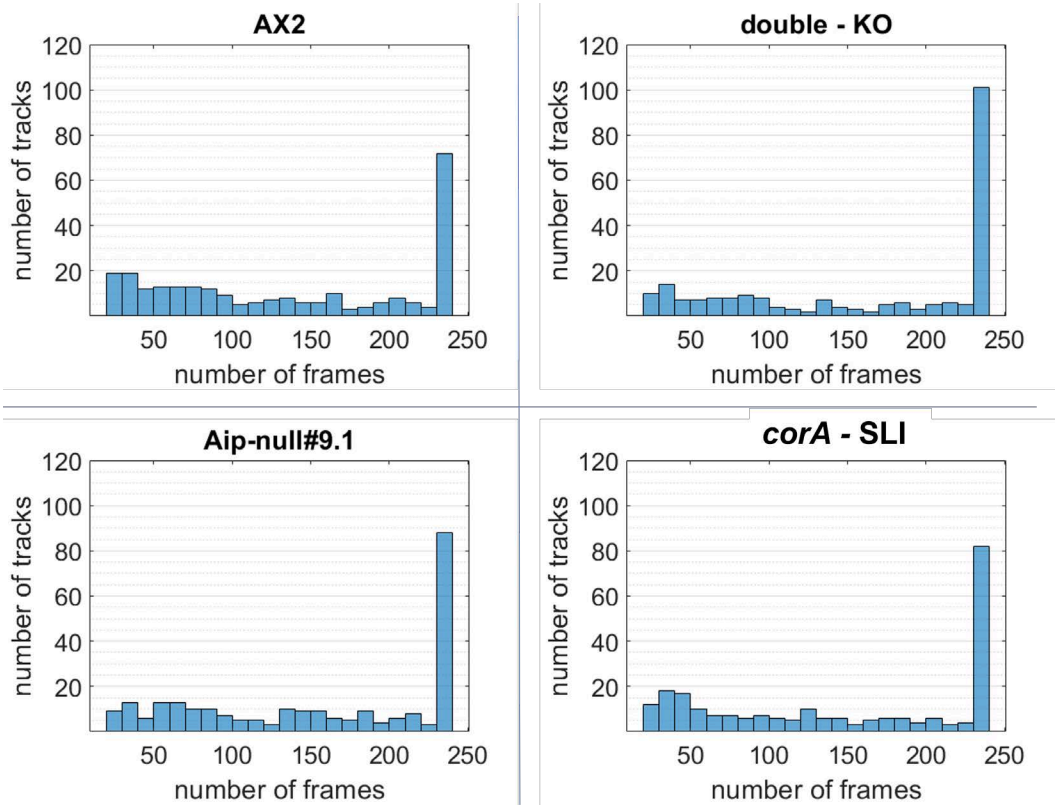

Fig. 10.7: Track Length Distribution for *D. discoideum* AX2 wildtype, Aip-null#9.1, *corA*-SLI and double knockout cell lines. Since all track length distributions have a similar shape, these four important cell lines were chosen as examples to show, whether the tracks were long enough for analysis and comparison; each track resulted from the movement of an individual single cell; tracks shorter than ten minutes were considered too short for reliable statistical analysis and were discarded from the analysis. Notably, tracks with a length of 115-120 min are the most common.

Tab. 10.3: **Table of Track Length Distribution for of the recorded cell trajectories for Motility Assay; (+) with 10 μM rapamycin treatment** the total recording time was two hours; tracks shorter than ten minutes were considered too short for reliable statistical analysis and were discarded from the analysis; tracks with a length of 115-120 min are the most common.

Cell line	Number of total tracks/cells	% of tracks between 230 and 240 frames (last bin)
AX2	261	27.6
AX2 (+)	108	36.1
Aip1-null#9.1 (DAip1-, DBS0252637)	251	35.1
Aip1-null#9.1 (DAip1-, DBS0252637) **(+)**	143	24.5
CorA-null HG1569#1 (DBS0236171)	203	23.6
CorA/Aip1 **double-null** (DBS0350851)	192	38.5
***corA*-SLI**	236	34.7
***corA*-SLI (+)**	101	30.7
double-KO: Aip1-null#9.1/*corA*-SLI	227	44.5
double-KO: Aip1-null#9.1/*corA*-SLI **(+)**	119	38.7
CorA-RNAi	174	32.8
Aip1-null#9.1/**CorA-RNAi**	292	18.8
CorA-null HG1569#1 **/CorA-RNAi**	151	29.1
***corA*-SLI/CorA-RNAi**	218	35.8
CorA-KS	88	42.0
CorA-KS (+)	104	33.7
double-KS: Aip1-null#9.1 + CorA-KS	98	62,2
double-KS (+): Aip1-null#9.1 + CorA-KS	157	39.5
CorA-OX	95	41.1
CorA-OX (+)	99	53.5

Tab. 10.4: Table of Track Length Distribution for of the recorded cell trajectories for Motility Assay in Rescue Lines; The total recording time was two hours; tracks shorter than ten minutes were considered too short for reliable statistical analysis and were discarded from the analysis; tracks with a length of 115-120 min are the most common.

Cell line	Number of total tracks/cells	% of tracks between 230 and 240 frames (last bin)
AX2	261	27.6
Aip1-null#9.1 (DAip1-, DBS0252637)	251	35.1
***corA*-SLI**	236	34.7
double-KO: Aip1-null#9.1/*corA*-SLI	227	44.5
Aip1-null#9.1 **/ mC-DdAip1**	131	30.5
Aip1-null#9.1 **/ mC-AIP1-2**	108	43.5
Aip1-null#9.1 **/ mC-AIP1-1**	108	36.1
Aip1-null#9.1 **/ AIP1-2-mC**	181	26.0
Aip1-null#9.1 **/ AIP1-1-mC**	119	34.5
double-KO / mC-DdAip1	101	40.6
double-KO / mC-AIP1-2	124	32.3
double-KO / mC-AIP1-1	108	50.0
double-KO / AIP1-2-mC	111	48.6
double-KO / AIP1-1-mC	112	34.8

11 List of Abbreviations

(v/v)	Volume per volume
(w/v)	Weight per volume
°C	Degree Celsius
2A	2A self-cleaving peptide
A. thaliana	*Arabidopsis thaliana*
A. tumefaciens	*Agrobacterium tumefaciens*
a.u.	arbitrary units
aa	amino acid(s)
ABP	actin-binding protein
ABD2	actin-binding domain 2 of fimbrin
ADF	actin depolymerizing factor
ADP	adenosine diphosphate
Aip1	Actin-interacting protein 1
AIP1-1	pollen-specific homolog 1 of AIP1 in *A. thaliana*
AIP1-2	constitutiv homolog 2 of AIP1 in *A. thaliana*
Amp	Ampicillin
APS	Ammonium persulfate
Arp	actin-related protein
AS	Acetosyringone
ATP	adenosine triphosphate
AX	axenic strain of *D. discoideum*

BASTA	Phosphinotricine (trade name; Bayer®)
bp	Base pairs
BSA	Bovine serum albumin
cAMP	3',5'-cyclic adenosine monophosphate
cAR1	cAMP receptor 1
CDS / cds	Coding sequence
CID	Chemical-induced dislocation
cm	Centimeter
Col-0	Col-0 accession of *A. thaliana*
CorA	Coronin-A
CorA-null	CorA-null HG1569#1 strain (s.a.)
ct	Cycle threshold
D	Aspartic acid
D. discoideum	*Dictyostelium discoideum*
DAG	Days after germination
Ddaip1	gene coding for Aip1 from *D. discoideum*
DdAip1	Aip1 from *D. discoideum*
coDdaip1	codon-optimized version of *Ddaip1* gene cds for expression in *A. thaliana*
DMSO	Dimethyl sulfoxide
DNA	Desoxyribonucleic acid
dpi	Dots per inch
E. coli	*Escherichia coli*
e.g.	example given
EDTA	Ethylenediaminetetraacetic acid
ER	Endoplasmic reticulum
et al.	et alia (and others)
EtOH	Ethanol
F-actin	Filamentous actin
FKBP12	Immunosuppressant binding cis-trans prolyl isomerase
FRB	FKBP12-Rapamycin Binding (FRB) domain of TOR
g	Gram
g	Gravitational acceleration
G-actin	Globular actin
GFP	Green fluorescent protein
GOI	Gene of interest

GPCR	G-protein coupled receptor
GTP	Guanosine triphosphate
h	Hour
HA	corresponding to amino acids 98-106 from human influenza virus hemagglutinin
HRP	Horseradish peroxidase
Hyg	Hygromycin
Kan	Kanamycin
kDa	Kilo Dalton
KO	knockout
KS	knock sideway
l	Liter
LB	Lysogeny broth / Luria broth
LimE	LIM (LIN-11, Isl-1 and MEC-3) domain-containing protein E
M	Molar
mCherry	Magenta fluorescent protein
mDia	Formin / Rho effector
MES	2-(N-morpholino)ethane sulfonic acid
mg	Milligramm
min	Minute
ml	Milliliter
mm	Millimeter
mM	Millimolar
mRFPmars	enhanced monomeric RFP (Fischer et al., 2004)
mRNA	Messenger RNA
MS	Murashige & Skoog
MTS	Mitochondrial targeting sequence
nm	Nanometer
NP40	Nonyl phenoxypolyethoxylethanol
OX	overexpressor
PBS	Phosphate-buffered saline
PCR	Polymerase chain reaction
pH	Pondus Hydrogenii
Pi	Phosphate
POI	Protein of interest
R	Arginine
rapa	Rapamycin
RFP	Red fluorescent protein

Rho	Signaling G protein family
RNA	Ribonucleic acid
RNAi	RNA interference
ROP	Rho-of-plants
rpm	Rounds per minute
RTK	Receptor tyrosine kinase
S	Serine
SCAR	Alias for WAVE
SD	Standard deviation
SDS	Sodium dodecyl sulfate
SI	Supplementary Information
SLI	Selection-linked integration
SOB	Super optimal broth
TAE	Tris-acetate-EDTA
TAIR	The Arabidopsis Information Resource (database)
T-DNA	Transfer DNA
TE	Tris-EDTA
TEMED	Tetramethylethylenediamine
TOR	Target of rapamycin
tub	Tubulin
Tween	Polyoxyethylene sorbitan monolaurate
UTR	Untranslated region
V	Valin
V	Volt
VASP	Vasodilator-stimulated phosphoprotein
W	Tryptophane
WAVE	Wiskott–Aldrich syndrome protein family member 1
WDR1	WD-repeat protein 1
Y	Tyrosin
Y2H	Yeast two-hybrid
YEB	Yeast Extract Beef
α	alpha
β	beta
μl	Microliter
μm	Micrometer
μM	Micromolar

Declaration

I hereby declare that I have completed the work solely and only with the help of the mentioned references. This manuscript has not been submitted to any other university before.

Potsdam, February 26, 2024

Maike Stange